University of Pretoria

Comparing biochemical and biophysical methodologies for the characterization of induced cell death

by

Karlien le Roux

Student number: 04375068

Submitted in the partial fulfilment of the degree

Philosophiae Doctor Biochemistry

In the Faculty of Natural and Agricultural Sciences

University of Pretoria

Pretoria

South Africa

12 January 2015

Submission Declaration:

I, <u>Karlien le Roux</u> declare that this thesis submitted for the degree Ph.D. Biochemistry at the University of Pretoria is my work. This thesis was not previously submitted for a degree at this or any other tertiary institution.

Signature: _____KleRoux_____   Date: 19-05-2015

Plagiarism declaration

University of Pretoria

Faculty of Natural and Agricultural Sciences

Department of Biochemistry

Full name: Karlien le Roux   **Student number:** 04375068

Title of the work:

Comparing biochemical and biophysical methodologies for the characterization of induced cell death

Declaration:

I understand what plagiarism entails and am aware of the University's policy in this regard.

I declare that this thesis (e.g. essay, report, project, assignment, dissertation, thesis, et cetera) is my own, original work. Where someone else's work was used (whether from a printed source, the internet or any other source) due acknowledgement was given, and a reference was made according to departmental requirements.

I did not make use of another student's previous work and submit it as my own.

I did not allow and will not allow anyone to copy my work with the intention of presenting it as his or her work.

Signature: KleRoux   Date: 19-05-2015

Jeremiah 29:11

"For I know the plans I have for you –

[this is] the Lord's declaration –

"plans for [your] welfare, not for disaster,

To give you a future and a hope.

(The Passion Bible – Holman Christian Standard Bible)

Acknowledgements

1. God for this wonderful grace in my life, I also thank Him for giving me the talent, passion and patience for conducting research.

2. Prof Meyer for teaching me how to be a responsible and determined scientist as well as for all her support throughout my studies.

3. Dr. Prinsloo for teaching me everything she knows about Raman spectroscopy, FTIR spectroscopy and for all of her support throughout the years.

4. The National Research Foundation, the Technology Innovation Agency and the University of Pretoria for their financial support.

5. My parents and family for their love and always supporting me in everything I do.

6. My friends and the HIV research group for always encouraging me to do my best, for sharing all your science knowledge and all the laughing sessions.

7. The Department of Biochemistry and especially Mrs. Van Wyngaardt, who was always available for technical support and a friendly smile.

8. Lungile, Sidhika, Sindi and Sonya, without the four of you my days would have been dull. Thank you for always cheering me on, all the scientific talks and always being available for new perspectives on mind boggling questions.

9. Thank you, Dr Annel Smit, for all the technical support with flow cytometry, for the kind words and encouragement. Thanks as well for all the litres of coffee.

10. Thank you, Mr C. van der Merwe and Ms A. Buys for all the technical support in preparation and cutting of the electron microscopic samples.

Preface

Research done during this investigation have been presented at an international conference and published in peer-reviewed journals. At the end of this document copies of the published manuscripts, are provided

Publications

Le Roux, K., Prinsloo, L.C., Meyer, D., Metallodrug induced apoptotic cell death and survival attempts are characterizable by Raman spectroscopy. *Applied Physics Letters* **105**, 123702 (2014); doi: 10.1063/1.4896616

Le Roux, K., Prinsloo, L.C., Meyer, D., Cellular injury evidenced by impedance technology and infrared microspectroscopy. *Spectrochimica Acta Part A: Molecular and Biomolecular Spectroscopy* **138,** pp.321-330 (2015); doi: 10.1016/j.saa.2014.11.089

International conference

Selected data was presented at the following conference:

SPEC 2012: Shedding new light on disease, held from the 11th to the 16th of November 2012 in Chiang Mai, Thailand.

Poster: K. le Roux, L.C. Prinsloo and D. Meyer (2012) entitled: Vibrational and conventional spectroscopy provide complementary information in drug discovery research.

Awards

➢ University of Pretoria Postgraduate Research Support bursary.

➢ National Research Foundation Innovation scholarship for doctoral research.

➢ National Research Foundation (NRF) Innovation travel bursary to attend the SPEC 2012 conference in November 2012, Chiang Mai, Thailand.

➢ Student bursary from the SPEC 2012 conference committee which covered the registration fee of the conference.

Submitted manuscript

Le Roux, K., Prinsloo, L.C., Meyer, D., Fourier Transform Infrared spectroscopy discloses different types of cell death in flow cytometrically sorted cells, submitted to Biochimica et Biophysica Acta – General subjects on the 12th of January 2015.

Summary

<u>Comparing biochemical and biophysical methodologies for the characterization of induced cell death</u>

Background: In specific circumstances, the induction of cell death can be an appropriate treatment of disease. Cell death can occur because of internal programming or external stress caused by infection, radiation or chemotherapies. There are many ways to investigate cell death and this work utilized vibrational spectroscopy to distinguish viable from dead cells. Cell death was achieved in this study by the addition of chemical stressors.

Methodology: Cervical adenocarcinoma (HeLa) cells and African green monkey kidney (Vero) cells were used. Two organic diphosphino gold complexes designated AE 76 and AE125, auranofin, an extract of *Plectranthus ciliatus,* actinomycin D and methanol were used as external cell death inducers. Biochemical methods used included Sodium 3'-[phenyl amino-carbonyl)-3,4-tetrazolium]-bis-[4-methoxy-6-nitro) benzene sulfonic acid hydrate (XTT) colorimetric assays, Real Time Cell Electronic Sensing (RT-CES), flow cytometry, Transmission Electron Microscopy (TEM) and caspases 3 / 7 assays. The biophysical experiments were Fourier Transform Infrared (FTIR) spectroscopy and single cell Raman microspectroscopy. Multivariate analysis (Principal Component Analysis (PCA)) and one way Analysis Of Variance (ANOVA) was used to determine significantly altered vibrational bands.

Results and discussion: Using XTT, it was found that the cell death inducers were cytotoxic at low concentrations. RT-CES analysis detected that the treatments induced concentration dependent cellular responses (nontoxic or cytostatic to cytotoxic in both cell lines). Early apoptosis was detected after treatment using flow cytometry, with the exception of methanol treated cells being necrotic. Caspase dependent apoptosis was detected in HeLa and Vero cells.

Thirteen FTIR spectral bands associated with cytotoxicity were significantly ($p < 0.05$) altered when HeLa cells were treated with naturally derived products. These bands were related to nucleic acids, proteins and lipids. Two of the bands associated with amide I were also indicative of early stress responses. FTIR microspectroscopy confirmed cytostatic cells were viable and could still recover. Based on significant FTIR changes in both cell lines, flow cytometrically sorted populations (viable, apoptotic and necrotic) could be distinguished. Glycogen and high wavenumber region alterations were distinctly different between viable and necrotic cells while apoptotic cells were mostly altered in the regions of nuclear material. Flow cytometrically sorted cells of different populations (viable and dead) were confirmed using TEM based on morphological characteristics. Raman spectroscopy was utilized in investigating metallodrug induced apoptosis. Vibrational peaks assigned to phosphatidylethaolamine (762 cm^{-1}) and ester bonds significantly increased in intensity which could be a molecular signature of induced apoptosis. Treated cells also had higher intensities for glucose and glycogen, which could be a survival mechanism of cancer cells. Raman spectroscopy detected cell death biomarkers in sorted cells, where dead cells had increased intensities at 762 cm^{-1} and 1578 cm^{-1}.

Conclusion: Investigations of cell death using vibrational spectroscopy initially started around 2000 with limited numbers of articles available on the subject matter. Vibrational spectroscopy proved to be a powerful tool for detecting spectral markers of early cell stress, cytostatic cellular responses, survival mechanisms of cancer cells and cell death. The approach presented here may find application in the (*in vitro*) evaluation of diseases (e.g. HIV / AIDS, TB, malaria and cancer) where induced cell death is part of the pathology. Data produced in this investigation substantially supplemented vibrational spectroscopic knowledge into understanding cellular stress, cell death and potential cell death markers *in vitro*.

Table of Contents

List of Figures

Chapter 2

Chapter 3

Chapter 4

Chapter 5

Chapter 6

Chapter 7

Appendix

List of Tables

Chapter 2

Chapter 3

Chapter 4

Chapter 6

Chapter 7

Appendix

List of important abbreviations

AIDS	Acquired Immunodeficiency Syndrome
ANOVA	Analysis Of Variance
ATCC	American Type Culture Collection
ATP	Adenosine Triphosphate
CC_{50}	Cytotoxic Concentration inhibiting the proliferation of 50% of the cell population
CI	Cell Index
CST	Cytometer Setup and Tracking
DISC	Death Inducing Signalling Complex
DMSO	Dimethylsulfoxide
DNA	Deoxyribonucleic Acid
FACS	Fluorescence Activated Cell Sorter
FBS	Fetal Bovine Serum
FIGO	International Federation of Gynaecology and Obstetrics
FSC	Forward angle light Scatter
FTIR	Fourier Transform Infrared
G1-phase	Gap 1 phase
GLUT 1	Glucose Transporter 1
HIV	Human Immunodeficiency Virus
HPV	Human Papilloma Virus
ICAD	Inhibitors of Caspase Activated DNAse
IgG	Immunoglobulin G
IR	Infrared

LASER	Light Amplification by Stimulated Emission of Radiation
MEM	Minimal Essential Medium
MTS	5-(3-carboxymethoxy-phenyl)-2-(4,5-dimethylthiazolyl)-3-(4-sulphophenyl) tetrazolium
MTT	3-(4,5-dimethylthiazol-2-yl)-2,5-diphenyltetrazolium bromide
MW	Molecular Weight
NADH	Nicotinamide Adenine Dinucleotide
NADP	Nicotinamide Adenine Dinucleotide Phosphate
NCI	National Cancer Institute
Pap	Papanicolaou
PBS	Phosphate Buffered Saline
PC	Principal Component
PCA	Principal Component Analysis
PE	Phosphatidylethanolamine
pH	power of Hydrogen or potential Hydrogen
PI	Propidium Iodide
PMS	Phenazine Methosulfate
pRb	Retinoblastoma Protein
PS	Phosphatidylserine
RNA	Ribonucleic Acids
ROS	Reactive Oxygen Species
RT-CES	Real Time Cell Electronic Sensing
SEM	Standard Error of the Mean
SI	Selectivity Index
S-phase	Synthesis phase

SSC	Side angle light Scatter
STD	Sexually Transmitted Diseases
TB	Tuberculosis
TEM	Transmission Electron Microscopy
TNF	Tumour Necrosis Factor
UV	Ultraviolet
WHO	World Health Organisation
XTT	Sodium 3'-[phenyl amino-carbonyl)-3,4-tetrazolium]-bis-[4-methoxy-6-nitro) benzene sulfonic acid hydrate
$Z_{i/0}$	Impedance at an individual point or start

Chapter 1: Introduction

Cell death detection and characterization plays an important role in the diagnosis and treatment of various diseases. These diseases include, but are not limited to autoimmune diseases, cancer, Human Immunodeficiency Virus (HIV) infection and Acquired Immunodeficiency Syndrome (AIDS), malaria and Tuberculosis (TB) [1,2]. Cell death is either induced by an infection or disease through cellular mechanisms or by the treatment of disease. By the detection of cell death, the disease can be diagnosed, or its progression assessed. It is also possible to measure the effectiveness of treatments by determining the level and type of cell death induced in specific tissues, for example, in the case of different types of cancer.

In order to investigate cell death *in vitro*, cell death must be induced. Cell death can be induced by mechanical (e.g. vigorously pipetting or freeze-thaw cycles), electromagnetic fields (e.g. irradiating the cells with Ultraviolet (UV) light and microwaves producing heat) or chemical stress (e.g. cytotoxins inclusing chemotherapeutics and pure chemicals). Chemical stress can induce cell death directly or indirectly. Highly cytotoxic chemicals cause cells to die or rupture non-specifically while targeted cytotoxins are mechanism driven cell death inducers. The latter (cytotoxins) can bind to specific cellular targets to prevent the cells from proliferating. These substances can also activate cell death initiation molecules. In this study, cells were externally induced to die. Externally induced cell death is defined as cell death induction due to an externally added chemical or chemical mixture.

In this study naturally derived products and gold complexes were used to induce cell death externally. Such diverse treatments were selected because of the two unique areas of drug discovery which are naturally derived products and synthetic chemistry. In our research group, both these fields of drug discovery are being investigated [3,4] and a crude extract of *Plectranthus ciliatus* and two gold complexes found to be extremely cytotoxic and therefore potentially useful inducers of cell death. These compounds were subsequently selected for this project. *Plectranthus ciliatus* is from the mint (Laminacea) family which contains numerous species with excellent medicinal properties [5]. Since Africa is not only rich in

biodiversity, but also in mineral resources, gold complexes have also become potential sources for drug development.

Cancer was chosen as a model disease for this study, in particular, cervical cancer because of its prevalence in our study area. HIV / AIDS is more prevalent in the Sub-Saharan region of Africa than any other part of the world. Infection increases the risk of developing cancers that occur in the event of a depleted immune system [6,7]. Commonly diagnosed cancers in HIV/AIDS patients are Kaposi's sarcomas and cervical carcinomas [8]. Human Papilloma Virus (HPV) infections, specifically subtype 16 and 18 are responsible for most cases of cervical cancer. These viruses are associated with Sexually Transmitted Diseases (STDs) such as HIV infections [6].

HeLa cells were selected as the model system for cervical cancer and the behaviour of these cells compared to that of noncancerous Vero cells in the presence of cell death inducers. Assessing cell death inducers in both cancerous and noncancerous cells allow for the calculation of selectivity indices for the cell death inducers. The selectivity is the ratio of the degree of cytotoxicity in cancerous to healthy cells [9]. Good selectivity supports further investigation in drug discovery process for the inducer (lead) in question. The second reason for selecting Vero cells was due to the primary aim of this project and that was to investigate induced cell death in more than one cell type. Cell death does not only occur in treated cancerous cells but also in healthy cells (for example during human fetal development). Therefore, knowing whether potential biomarkers (indicators) of cell death would differ in cancerous to noncancerous cells, is of value.

When cell death is successfully induced there is a variety of techniques can be used to measure the death of a cell and to distinguish the type of cell death induced. These techniques include well established biochemical and unconventional biophysical measurements with vibrational spectroscopy being investigated here. Conventional biochemical techniques used in the present study were; XTT to assess cell viability, flow cytometry and RT-CES to characterize the type of cell death, and caspase 3 / 7 cleavage for confirmation of apoptosis [10]. A well-known conventional biophysical technique used here

was Transmission Electron Microscopy (TEM) to confirm successful FACS sorting of dead cells. Biophysical techniques investigated for the effective discrimination of cell death types were Raman spectroscopy and Fourier Transform Infrared (FTIR) spectroscopy. The use of these spectroscopic techniques in investigating all aspects of cell death is still in the infancy stages which are why it is viewed as nonconventional biophysical techniques for the purposes of this thesis.

Although most of the above-mentioned techniques have proven to be effective in the discrimination of cell death induction as well as in indicating the type of cell death, room for improvement remains. The stumbling blocks associated with biochemical methods include the long laborious sample preparations and the use of labels (chemical and radioactive) that can produce false positives and false negatives. Harsh chemicals are often used (e.g. hydrochloric acid in the MTT assay) that could lead to distorted results and incorrect data interpretation. In addition, biochemical labelling can sometimes produce doubtful results due to cross reactivity. Some biochemical labels have also been shown to suffer from low levels of reproducibility. The need for innovative, label-free techniques is increasing because the rapid assessment of new drugs as well as the effectiveness of drugs that patients are taking is becoming crucial in the fight against communicable and noncommunicable diseases. Multiple applications of single bench top equipment are also starting to play a role in research where one instrument is used optimally to detect as many parameters as possible in one sample. By using a single instrument for multiple applications, it becomes more cost effective and a more logical option in clinical laboratories with limited space or resources.

Two emerging techniques showing potential to fill the void of such multi-parameter instruments are Raman and FTIR spectroscopy. These two techniques collectively referred to as vibrational spectroscopy can measure vibrations of molecular bonds after the molecules were excited by a laser and light scattered inelastically (Raman spectroscopy) or infrared light absorbed (Infrared spectroscopy). An indication of the type of bonds and even the types of molecules usually detected at a particular wavenumber are due to molecular vibrations. Changes in the vibrational profile of a molecule or mixture give indications of molecular modifications. In the case of biomedical research, mixtures could refer to biofluids and even one cell since the biochemical complexity of even one cell is astonishing. Molecules and

- 3 -

mixtures, therefore, have distinct vibrational (Raman and FTIR) spectra which are as accurate as fingerprints.

Specific peaks are sensitive to particular cellular events such as cell cycle changes, alterations between healthy and diseased cells / tissues and cell death. Previous studies found that changes associated with DNA, protein and lipid alterations were detected in dying cells, but the number of FTIR and Raman spectroscopic studies are limited [11–14]. These two techniques already have an impressive list of applications in biomedical research and show potential for development into useful detectors of different types of cell death which should find the clinical application.

In this thesis, Chapter 2 is a review of the literature on cell death, cancer as a disease model and provides background on commonly used *in vitro* biochemical and biophysical techniques for the investigation of cellular behaviour in the presence of chemicals. The hypothesis, the primary aim and objectives are provided at the end of this chapter. Chapter 3 explored XTT as a conventional cytotoxicity indicator and was also used for the preliminary determination of cytotoxicity. Chapter 4 discusses the importance of distinguishing between cytostatic and cytotoxic cellular responses induced by chemical stress specifically during cancer chemotherapy. The novel application of FTIR spectroscopy to distinguish between cytostatic and cytotoxic cellular responses are explained in detail using the naturally derived chemotherapeutic drug, actinomycin D and the plant extract, *Plectranthus ciliatus* (these data were published in *Spectrochimica Acta Part A: Molecular and Biomolecular Spectroscopy*). In Chapter 5, the molecular vibrations associated with apoptosis were investigated using Raman spectroscopy and the results correlated with the results obtained by flow cytometric analysis. The techniques determined the mechanism of action of metallodrugs and one of cancer's survival strategies, namely excretion of chemotherapeutics was postulated to be due to the influx of glucose for sustained energy (these data were published in *Applied Physics Letters*). In Chapter 6, fluorescence sorted apoptotic and necrotic HeLa and Vero cells were investigated. The accuracy of the sorting was confirmed using TEM. Furthermore, FTIR identified spectral biomarkers were compared to known biomarkers and the novelty of the current findings emphasised. In HeLa and Vero cells commonly shared cell death biomarkers were identified and compared to known biomarkers (these data were submitted for

publication to *Biochimica et Ebiophysica Acta – General subjects*). In <u>Chapter 7</u> caspases 3 / 7 were analysed in HeLa and Vero cells after treatment with the cell death inducers. The cells were also then sorted based on fluorescence and investigated using Raman spectroscopy. Raman bands were identified that in some cases had been previously associated with dead cells while new findings were also discussed. <u>Chapter 8</u> concludes the study and <u>Chapter 9</u> contains all the references. Supporting information and published manuscripts are provided in the <u>Appendix</u>.

Chapter 2: Literature Review

In vitro studies form the starting point for most pre-clinical investigations. In this literature review, the importance of cell death in the regulation of homeostasis and disease states will be described as well as the biochemical and biophysical techniques utilized to investigate cellular status. The development of biochemical and biophysical techniques appear to occur in parallel which means that chemical and physical properties of biological components and systems can be investigated in an integrated manner. Biochemical assays mostly measure the reactivity of biomolecules using specific labels while biophysics techniques use prediction models to identify and classify the physical biomolecular behaviour. Using a combination of these methods should give new insights into disease states by simultaneously looking at biochemical and biophysical properties of particular biological systems such as cell death. Cell death is a vastly researched field influencing a variety of different diseases. The induction of cell death as therapeutic intervention for cancer is the basis of this thesis which is why the types of cell death and the pathways involved will be discussed as well as the pathologies influenced by the up or down regulation of cell death.

2.1 Types of cell death

Cell death is a natural process in which multicellular organisms can maintain a homeostatic equilibrium. Cell death is essential for healthy development (as seen in embryonic stages) and clearance of defective, compromised (e.g. infection, aging) or damaged cells from the system. Apoptosis and necrosis are the most prevalent types of cell death investigated, although many other types are documented [15]. Cell death induction depends on the type of stimuli or the degree of stimuli received by cell. Apoptosis and necrosis can occur independently, at the same time or chronologically [16,17].

2.1.1 *Cell death inducers*

Internal or external stimuli can induce cell death. Cells manage a variety of internal stimuli that can result in cell death, in most cases apoptotic in nature. In this study, only external stimuli were investigated. Induced cell death, therefore, refers to externally added stimuli which caused the cells to die. In this study, the externally added stressors were cytotoxins while many other types of external stressors can also lead to cell death. Other types of

external stressors such as ionizing (for example UV light that can cause DNA damage) and non-ionising radiation (such as microwaves producing heat) can also lead to cell death [15].

i) <u>Apoptosis</u>

Kerr *et al.* (1972) was the first to name programmed cell death "apoptosis". The Greek word "falling off" such as in the case of leaves of trees was used as inspiration. Apoptosis can be recognised by morphological characteristics such as; rounding of cells, retraction of pseudopods (temporary projections of the cytoplasm of cells) and the reduction of cellular volume (pyknosis). Nuclear features of apoptosis include; chromatin condensation, nuclear fragmentation (karyorrhexis) and minor modifications of cytoplasmic organelles. Plasma membrane blebbing (membrane integrity not compromised until the final stages of the process) and engulfment by resident phagocytes in tissues is also characteristic of apoptosis. A majority of these cellular events should take place to classify cell death correctly as apoptotic [17,18]. Apoptosis is one of the most important types of cell death pathways found in eukaryotes and defined as a well-managed process that is activated by external or internal signals. Several steps in human development occur through apoptosis for examples; the fetal tail dies off and the webbing between fingers disappears. Other regulated activations of apoptosis include the apoptotic activation after the detection of damaged or dysfunctional cells within the body. Apoptosis is a super complex process which is energy dependent and involves an intricate series of molecular events [16,17]. Apoptosis can be initiated by three major pathways namely the extrinsic -, the intrinsic - or the perforin / granzyme pathway which involves T-cell mediated cytotoxicity (Fig. 2.1). The perforin pathway is only studied *in vivo* or in more complex *in vitro* studies with the presence of T-cells. All three pathways include the activation of caspase 3, which is the "point of no return" for cell death [16].

The extrinsic pathway, also known as the receptor mediated pathway, is activated upon extracellular receptor binding which is the first step in initiating cell death. The extracellular receptors also contain intracellular "death domains". As soon as one of the various receptors such as the Tumour Necrosis Factor (TNF) super family (TNF, Fas) receives a signal, this pathway will activate. The extracellular receptor is cysteine rich while the intracellular death domain consists of 80 amino acids. Death domains are essential because these domains transmit the extracellular death signal to intracellular signalling pathways. Some of the best-

studied ligand / receptor models include FasL / FasR, TNF-α / TNFR1 and Apo31 / DR3 to name a few. When a ligand binds to a receptor on the cell plasma membrane, it activates the extrinsic pathway. Recruited cytoplasmic adaptor proteins assemble at the death domain. For example, the Fas ligand binds to the Fas' receptor, after which protein adaptors FADD are recruited to the receptor site. At the receptor site, FADD and pro-caspase 8 interacts through dimerization of the death effector domain. This interaction causes the Death-Inducing Signalling Complex (DISC) to assemble. DISC in turn activates pro-caspase 8 to develop the active form of the caspase enzyme. The activation of caspase 8 activates caspase 3. During caspase 8 activity, the release of specific intracellular proteins can prevent the activation of caspase 3, which in turn will prevent the cell from dying, but activated caspase 3 is irreversible [15,16]. Apoptotic death is most prevalent during stages of development and the maintenance of homeostasis.
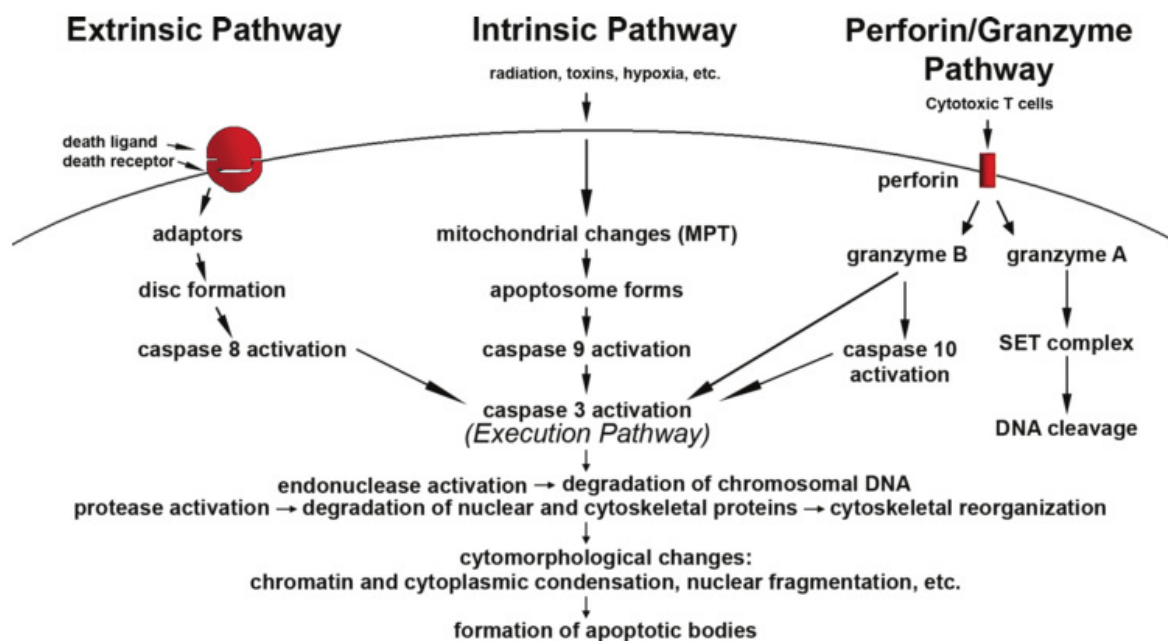
Fig. 2.1. A synopsis of the major apoptotic pathways. The three pathways are; the entrinsic-, intrinsic- and perforin pathway. Specific stimuli are necessary to activate all three pathways. The extrinsic and intrinsic pathways are caspase dependent while the perforin pathway through granszyme A is caspase independent. The caspase dependent pathways lead to the activation of the executioner caspase-3 which leads to induced apoptosis. Taken with permission from [16].

The perforin/granzyme pathway involves sensitized CD8+ cells that destroy antigen presenting cells. This cytotoxic response is similar to type IV hypersensitivity. Cytotoxic T-lymphocytes kill target cells using the extrinsic pathway, where the FasL / FasR is predominantly involved. These cells are also capable of killing tumour and virus infected cells. This pathway involves the secretion of transmembrane pore forming molecules perforin. Perforin releases cytoplasmic granules consisting of serine proteases (granzyme A and B). The functions of granzyme B are to activate pro-caspase 10 and cleave factors such as Inhibitors of Caspase Activated DNAse (ICAD). Granzyme B is also able to amplify the death signals through the mitochondrial pathway. These death signals include the cleavage of Bid and cytochrome c release. Granzyme B is also known to be able to activate caspase 3 directly. By this method, upstream signalling is bypassed, and the executioner phase initiated immediately. Granzyme A, on the other hand, activates caspase independent death pathways. Granzyme A activates intracellular DNAse NM23-H1, which is a tumour suppressor gene. This specific DNAse plays an important role in the prevention of cancer by inducing apoptosis in tumour cells. Granzyme A is also known to interfere with the maintenance of DNA and chromatin and thus once the molecular mechanisms are inactivated; DNA integrity is at risk (Fig. 2.1) [16].

The intrinsic death pathway does not involve any receptors but rather follows the initiation of apoptosis by mitochondrial events. Stimuli received by cell, guide intracellular signals that can trigger a negative or a positive signalling pathway. Negative signals result in the absence of growth factors, hormones and cytokines that can cause the activation of apoptosis. Hypoxia, hyperthermia, viral infections, radiation, free radicals and toxins are positive signals. Both positive and negative signals cause changes in the mitochondria. The inner mitochondrial membrane is affected and results in the opening of the mitochondrial permeability transition (MPT) pore. Other changes also include but are not limited to loss of mitochondrial membrane potential and the release of pro-apoptotic proteins into the cytosol. Pro-apoptotic proteins activate the caspase dependent pathway. Firstly cytochrome c binds to Apaf-1 and procaspase-9 and activates the formed apoptosome. Clustering of the procaspase-9 in the apoptosome leads to the activation of caspase-9. The activation of the execution pathway is carried out by the extrinsic and intrinsic death pathways and leads to apoptotic cell death. During the last stage execution (effector) caspases namely caspase-3; caspase-6 and caspase-7 activates. These caspases cleave various substrates such as; cytokeratins, PARP, the plasma membrane cytoskeleton and nuclear proteins through the activation of

- 9 -

cytoplasmic endonuclease (degrading nuclear material) and proteases (degrading nuclear and cytoplasmic proteins).   In this pathway, caspase-3 is considered one of the principal executioner proteases. Caspase-3 is activated by initiator caspase-8, caspase-9 or caspase-10. Activated caspase-3 degrades chromosomal DNA and causes chromosomal condensation, as well as reorganisation and disintegration of cells into apoptotic bodies (Fig. 2.1) [16].

The classification of apoptosis is multifaceted because of the complexities of the process. Standard biochemical markers include DNA fragmentation and proteolytically active caspases. DNA fragmentatation or laddering of oligonucleotides can be visualized with etridium bromide on electrophoresis gels. The presence of proteolytically active caspases or the products of their substrates can be detected using fluorescence and measured with flow cytometry, bench top assays or fluorescent microscopy. These markers are not always exclusive to apoptosis since apoptotic markers in rare cases can also be present in viable cells (phosphatidylserine on outer membrane of some mammalian cells) [19] or absent during apoptosis (such as caspase-independent apoptosis) [20]. The above mentioned techniques can be used to diagnose and more precisely characterize apoptosis but cannot replace morphological characterization [18,21].

ii) Necrosis

The second type of cell death is necrosis. Necrosis, derived from the Greek word "Nekros" translates to "dead cell". Many years ago pathologists were the first to use the term necrosis as a description of dead cells in tissue samples. Currently, the term necrosis is used with more caution and to describe specific cellular behaviour that lead to the death of cells [22]. Toxins, physical stimuli and ischemia usually cause necrosis. Apoptosis and necrosis can occur together or in a sequence. The extent, to which energy is depleted, is associated with the type of cell death which then depends on the severity and the duration of the cell injury. Necrosis is not dependent on energy and therefore if cells undergo apoptosis due to a particular stressor, the absence of cellular ATP could lead to the induction of necrosis [17]. Necrosis is morphologically defined by an increase in cell volume (oncosis) [23], swelling of organelles and plasma membrane rupture followed by the leakage of cytoplasm. Leakages of cytoplasm lead to an inflammatory response. Nuclear chromatin lysis also occurs but do not result in the formation of internucleosomal fragments [17,22]. Mitochondrial alterations

- 10 -

include the production of reactive oxygen species, nitro-oxidative stress and mitochondrial membrane permeabilization. Necrosis is associated with lipid degradation and an increase in calcium ions in the cytosol which could lead to the activation of "noncaspase" proteases. For necrosis has no dominant biomarker and it is still, therefore, widely determined based on the absence of autophagy or apoptosis [18].

iii) <u>Autophagy</u>

Another type of cell death worth mentioning is autophagy (derived from the Greek word for "eating-self") because it can occur concurrently with apoptosis. Autophagic cell death does not imply that cells died of autophagy but rather that autophagy was present at the time of death [10]. Depending on the conditions autophagy can have two outcomes, either the cells will survive or the cells die. Nutrient deprivation (starvation), some cytotoxins (e.g. actinomycin D and staurosporin) and thermal shock lead to the activation of autophagy [24].

Autophagosomes containing large amounts of cytoplasmic material for degradation by lysosomes and the lack of chromatin condensation are characteristic of autophagy. Autophagosomes are large double membrane organelles which contain defective organelles and cytoplasm. Transmission electron microscopy (TEM) can distinguish these structures from other proteolytic organelles such as lysosomes, peroxisomes, other vesicles such as endosomes and apoptotic bodies. Autophagosomes fuse with lysosomes to form autolysosomes. In the autolysosomes, the autophagosomes inner membrane is digested as well as its contents by acidic lysosomal hydrolases. During autophagy, phagocytes do not remove the dead cells [18]. A useful fusion protein marker found on autophagosomes or autolysosomes known as GFP-LC3 can indicate the presence of autophagic cells although this marker alone is also not sufficient [18]. It is important to remember that autophagy is not a death sentence and that cells can recover when the cell death inducing stimulus is removed [18]. Zhivotovsky and Orrenius (2010) suggested that autophagy could prevent tumour development by at least two different mechanisms. Firstly, the up regulation of protein degradation compared to protein synthesis can reduce cell growth. Secondly, autophagy may aid in the removal of defective mitochondria and other organelles that are potential sources of Reactive Oxygen Species (ROS). The presence of ROS could induce DNA damage and

- 11 -

cause genome instability which will promote carcinogenesis [25]. Figure 2.2 is a schematic illustration of apoptosis, necrosis and autophagy.
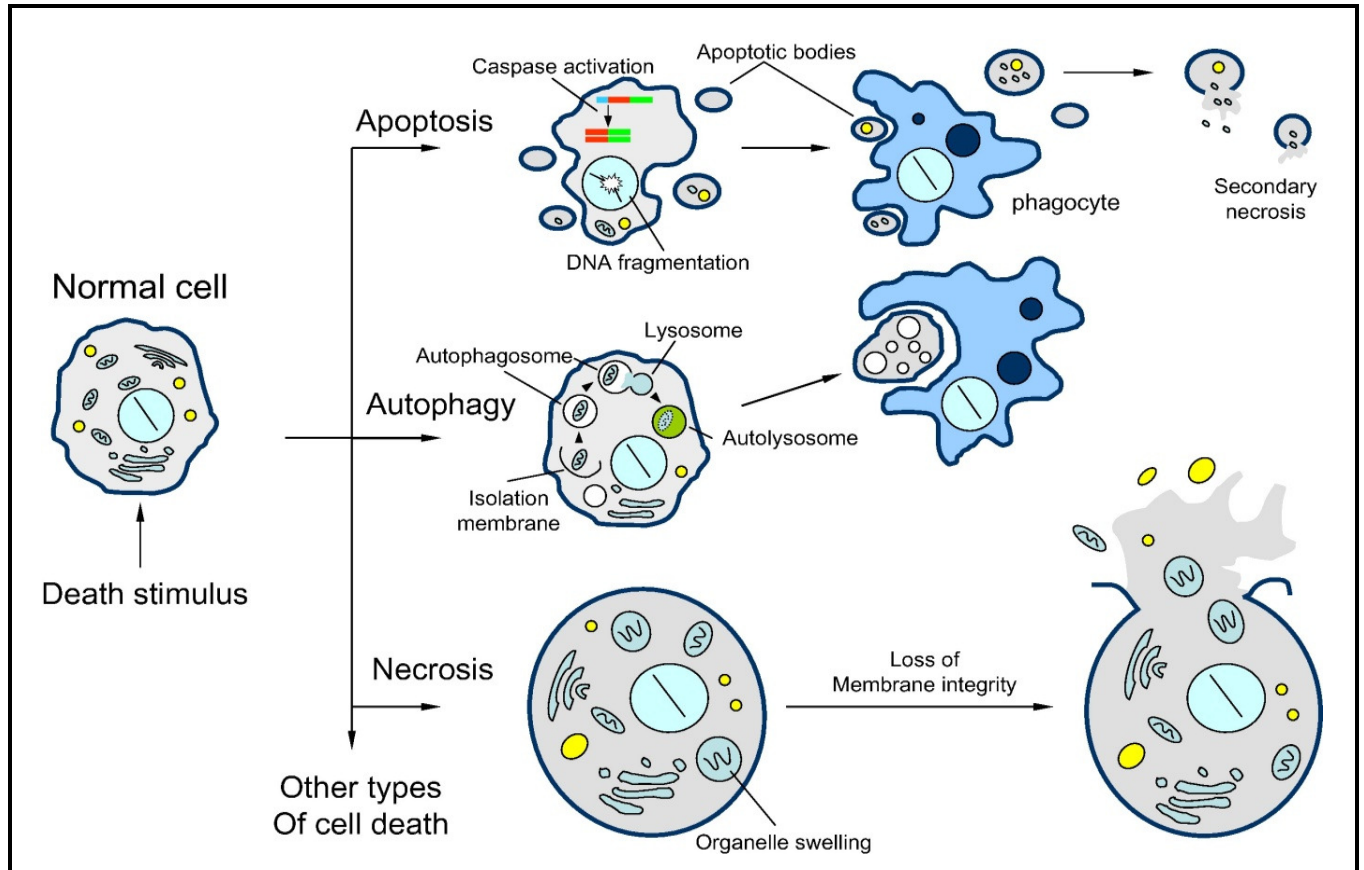
Fig. 2.2. Schematic representation of the two major types of cell death pathways together with autophagy that during prolonged starvation stages could lead to cell death induction. After a death stimulus was received by the cell, a cascade of intracellular events drives the cell to death. Internally or externally stimuli induced apoptosis leads to apoptotic bodies while necrosis lead to cytoplasmic leakage due to lost plasma membrane integrity. Taken with permission from [26].

(iv) Other types of cell death

The term "*anoikis*" is no longer used in the literature but has historical value. The term refers to apoptosis induced due to the loss of attachment to a substrate [18]. *Entosis* is as a form of cellular cannabolism in lymphocytes of patients with Huntington's disease. In this process, one cell would engulf a neighbouring live cell, which then dies in the phagosome. A very popular cell line, MCF-7 (breast cancer cells) routinely used in breast cancer research demonstrated entosis. These cells also lack caspase-3 and beclin-l and are accordingly

apoptosis and autophagy incompetent. Whether entosis is a novel type of cell death is still debatable, since engulfed cells are sometimes released or even undergo mitosis within the phagosome [18].

2.2 How cancer cells bypass cell death mechanisms

When cell death is prevented by various endogenous or exogenous factors, disease could prevail. Cell death is down regulated by diseases such as cancer, viral latency or autoimmune diseases [1]. An up regulation of apoptosis had been linked to neurodegenerative diseases, AIDS, liver disease and ischemic injury (Fig. 2.3) [2]. One of the most widely studied pathologies is cancer and the role of cell death induction in treating cancer. Cancer cells can proliferate indefinitely by escaping the normal cycle of cell maturation and ultimately death after the predetermined amount of cell divisions. Cancer cells can proliferate indefinitely due to alterations in cell physiology. Six of these adaptions have been widely studied namely cancer cells are *(i)* producing their growth signals, *(ii)* insensitive to antigrowth signals, *(iii)* the potential for tissue invasion and metastasis, *(iv)* can replicate indefinitely, *(v)* able to initiate and sustain angiogenesis and *(vi)* able to bypass apoptosis (Fig. 2.4) [27,28].
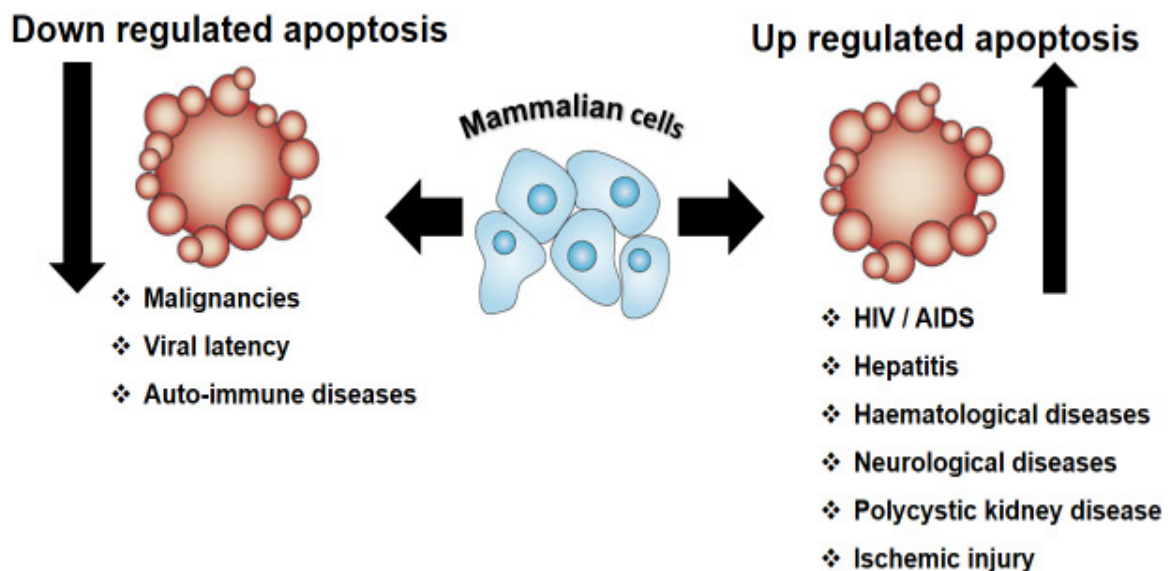
Fig. 2.3. Schematic representation of the two outcomes of deregulated apoptosis [1,2]. Figure adapted from [1] and permission for images was obtained [29].

Cancer cells can produce their *(i) growth signals by autocrine stimulation*. Autocrine stimulation is an adaption of cancer cells that allows the production of growth factors and is not influenced by the microenvironment that may contain healthy cells. Examples of these growth factors are platelet derived growth factor and tumour growth factor α, produced respectively by glioblastomas and sarcomas. In addition, cancer cells can *(ii) ignore antigrowth signals*. Antigrowth signals block proliferation in two ways. Firstly, the signals will force proliferating cells into the dormant Gap 0 phase of the cell cycle for a particular period. Secondly, cells could be forced into postmitotic states permanently. At the molecular level, all antiproliferative signals are channelled through the Retinoblastoma Protein (pRb) and related proteins p107 and p130. When pRb is hypophospharylated, proliferation is blocked by changing the function of E2F transcription factors. The function of E2F transcription factors is controlling expression of genes involved in the progression of cells from the Gap 1 (G1) phase to the Synthesis (S) phase. E2F transcription factors allow the proliferation of cells and the progression through the G1 phase of the cell cycle when the pRb pathway is disrupted. Gene mutations for the pRb protein could also lead to the loss of function. Interestingly, some DNA virus-induced tumours such as cervical carcinomas produced by some strains of the human papilommavirus, cause loss of function of pRb proteins through sequestration by viral oncoproteins.
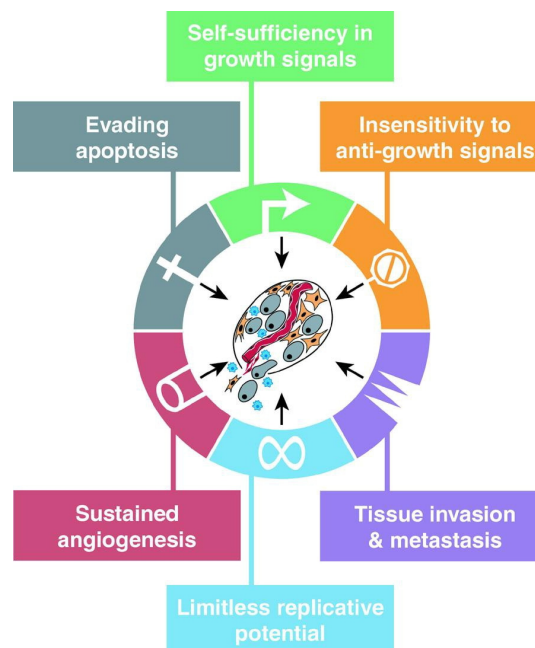
Fig. 2.4. The main characteristics of cancer cells [27,28]. Taken with permission from [27].

- 14 -

During the active proliferation of primary tumours, *(iii) metastasis can occur*. Metastasis is the process of tumour cells traveling to distant tissue, where these cells can in most cases successfully proliferate and start a new colony. Complications of cancer include the spread of the cancer to other tissues and organs which lead to progression of the disease. Metastases are responsible for up to 90% of cancer mortality cases. Cancer cells can *(iv) replicate indefinitely* by sidestepping the natural decay of telomeres. Telomeres on the end of chromosomes consist of six base pairs repeats. During healthy replication cycles, the telomeres will shorten by 50-100 base pairs per cell cycle. Healthy cells have approximately 70 cycles, after which end-to-end chromosomal fusion ultimately leads to cell death. In malignant cells, telomere maintenance is almost always detected and involves either the up regulation of telomerase or recombination-based interchromosomal exchanges of telomere sequence information. For primary and secondary tumour colonies, to expand in size, *(v) angiogenesis is necessary*. In the early and middle stages of solid tumour formation angiogenesis occurs. Angiogenesis is initiated and sustained by a complex system of overexpression of angiogenesis inducers and down regulation of inhibitors. Tumour angiogenesis has also become an attractive therapeutic target since all solid tumours form these vascular networks [27,28]. The last trademark of tumours is the ability to *(vi) escape apoptosis*. It is also this trademark characterized by this project. Two different strategies are known to prevail namely acquired resistance (the treatment was effective in the beginning but becomes less effective with time) and intrinsic resistance (when the treatment was ineffective from the start). A variety of strategies is used to acquire resistance to apoptosis. One of the most commonly found strategies is the loss of pro-apoptotic regulators after p53 tumour suppressor gene mutations. The inactivation of p53 proteins leads to the removal of an essential component of the DNA damage sensor. The malfunctioning of this sensor causes the lack of functional apoptotic effector cascades. In 50% of cancers, mutations are found in the gene of p53. A well-studied case of resistance involves cisplatin. Those resistance strategies involved increased drug excresion, decreased the concentration of the intracellular drug, increased cellular thiols leading to drug inactivation and enhanced drug induced damage to DNA [27,30].

2.2.1 *Emerging trademarks of cancer cells*

New trademarks of cancer cells are *(i) reprogramming of cellular energy metabolism* and cancer cells *(ii) avoiding immune destruction*.

*(i) **Reprogramming the energy metabolism*** of cancer cells is necessary to fuel the uncontrolled proliferation of cancer cells. Otto Warburg first observed the phenomenon that cancer cells can reprogram glucose metabolism [31]. Cancer cells (even in the presence of oxygen) can limit their energy metabolism to glycolysis (aerobic glycolysis). Cancer cells import high concentrations of glucose to compensate for the 18 fold loss of ATP compared to mitochondrial oxidative phosphorylation. This efficient import of glucose is achieved by up regulation of Glucose Transporter 1 (GLUT 1). The increased import of glucose in cancer cells was confirmed noninvasively in patients by using positron emission tomography. The instrument detects a radiolabeled analog of glucose, ^{18}F – fluorodeoxyglucose that is ingested by the patient. A possible reason for cancer cells favouring glycolysis could be because glycolytic intermediates can be used to generate nucleosides and amino acids. The nucleosides and amino acids in turn fuels biosynthesis of macromolecules and organelles for the assembly of new cells [28].

The second emerging trademark of cancer cells is the phenomenon of *(ii) **evading immune destruction***. The immune system is always on alert to detect any changes in cells and tissues that could indicate the onset of disease. The occurrence of solid tumours suggests that the immune system cannot always detect the formation of tumour cells and some tumour cells have evolved to evade the surveillance of the immune system. The increased prevalence of cancer in immunocompromised patients also specifies that the role of the immune systems is essential. Most of those cancer formations in immunocompromised individuals are virus induced. The prevalence of that class of cancers is dependent on reducing the viral burden of the patient. It can, therefore, be said that the immune system is able, in immunocompetent patients, to eradicate up to 80% of cancers not induced by viruses [28]. Through many different experiments using carcinogens, it was found that solid tumours form in healthy subjects when the immune system eradicates potent immunogenic cells while weak immunogenic cells remain in the body. The weak immunogenic cells can grow and generate solid tumours. On the other hand, the immune system of immunocompromised patients was unable to eliminate highly immunogenic cells or weaker counterparts, leading to the formation of solid tumours [28].

2.3 The prevalence and treatment options for cervical cancer

There are many types of cancer. This work will use a cancer cell line as a model system which is why background information on cervical cancer is essential here. Newly recorded cancer cases in 2012 were 14 million and 8.2 million deaths occurred worldwide due to various types of cancer [32]. In 2012, more than 32 million people were living with cancer. The most prevalent types of cancers were lung, liver, stomach, colorectal and breast cancers. Africa, Asia and Central / South America contribute to more than 60% of the world's new cancer cases. These areas also account for 70% of all deaths due to cancer. Cancer is predicted to rise from 14 million in 2012 to 22 million within the next 20 years [32]. Worldwide, breast cancer is the most prevalent cancer diagnosed in women while cervical cancer is the second most commonly diagnosed cancer, with an estimated 530 000 new cases reported annually. Approximately 270 000 women die annually of cervical cancer, with > 85% of recorded fatalities found in low- and middle income countries [33]. Statistics reported by the World Health Organisation indicated that up to 31 females per 100 000 were diagnosed with cervical cancer in Southern Africa (Fig. 2.5). The regions, where incidences were the highest, were also the regions where more than half of the diagnoses were fatal (Fig. 2.6).
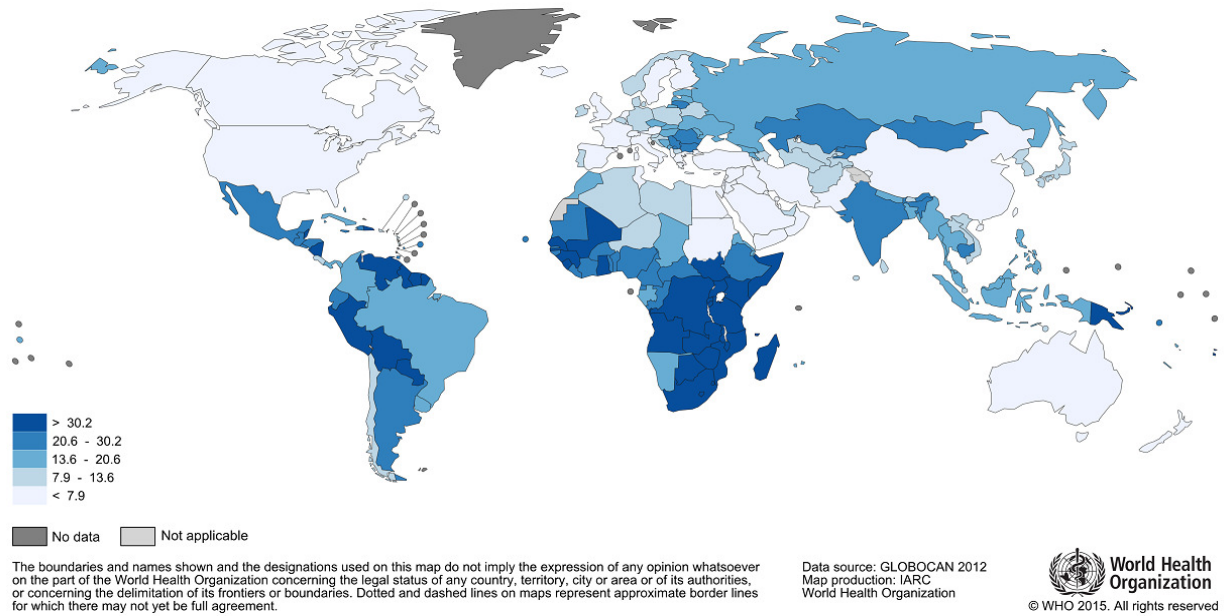
Fig. 2.5. World map indicating the incidence of cervix-uteri cancer, the highest frequency is among South American, African and Asian women. Sub-Saharan- and Eastern Africa has the highest occurrences of cervix-uteri cancer. The incidences are the lowest in countries such as Australia, North America and parts of North Africa and Europe [34]. No permission needed to reproduce.
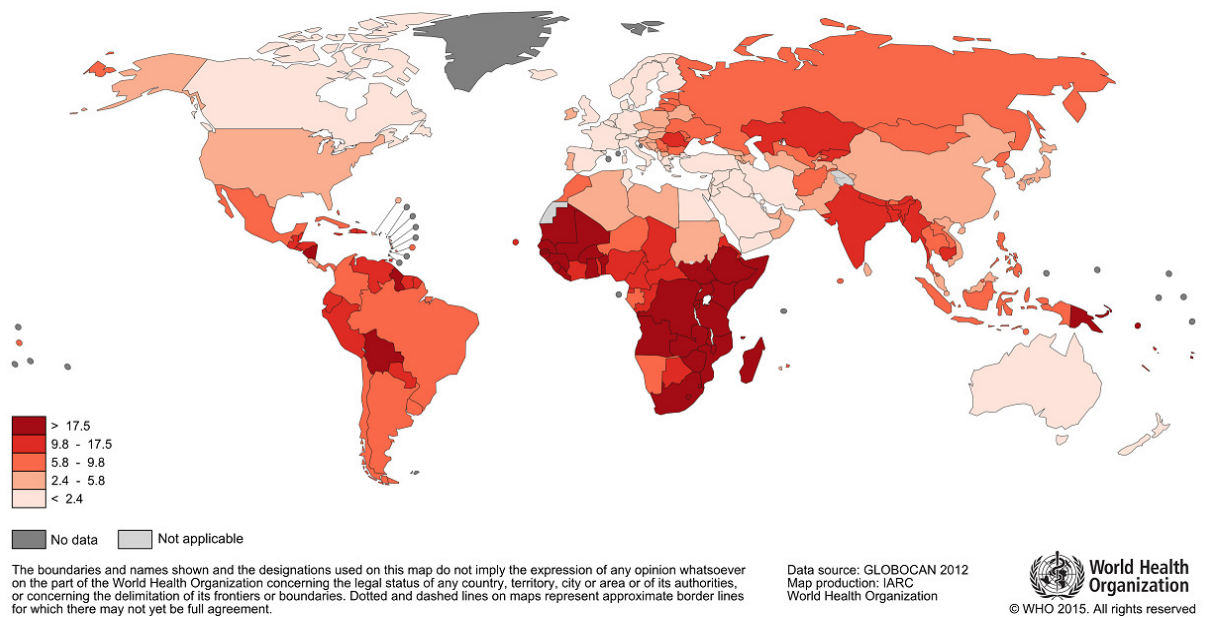
Fig. 2.6. World map indicating the mortality rates of women diagnosed with cervix-uteri cancer in 2012. Africa is the continent with the highest mortality rate due to cervix-uteri cancer. High mortality rates are also reported in South America and Asia. The lowest mortality rates were found in Australia and North America [34]. No permission needed to reproduce.

Cervical cancer is in most cases caused by different strains of the human papillomavirus (HPV). Ninety percent of cervical cancer contains HPV DNA. The virus spreads through sexual activity. Risk factors include sexual activity at very young ages (< 16 years) and multiple sexual partners. Patients receiving immunosuppressive agents and patients that are HIV positive have a higher risk of HPV infections leading to the development of cervical cancer [6,7]. The strains responsible for the most invasive cancers are types 16, 18, 31, 35, 39, 45, 51, 52, 56, and 58. The two most studied strains HPV 16 and HPV 18 have transcriptional units termed E6 and E7. These units are essential for encoding proteins playing a role in viral replication. The E6 oncoprotein binds to and inactivates TP53, which ultimately disrupts a cell cycle check point. The E7 oncoprotein binds to and inactivates the retinoblastoma gene, pRb. This inactivation allows cells to progress through the cell cycle and proliferate indefinitely [35]. In South Africa, cervical cancer is one of the biggest health problems women faces. The disease affects at least one out of 41 South African women. Approximately eight women die of cervical cancer each day while the prediction for 2025 is approximately 12 women daily. Cervical cancer is a preventable disease and if diagnosed early can be successfully treated. In South Africa, the screening coverage is only 13%, leaving most of the women unaware of the disease and its implications. The HIV endemic has had devastating effects on the country with HIV positive women being at a very high risk for secondary infections of HPV, which leads to premalignant lesions and cervical cancer. Advances in HIV diagnoses and the success of highly active antiretroviral therapy together with the small screening coverage in South Africa resulted in HIV patients being diagnosed up to ten years earlier with advanced stages of cervical cancer [36].

Cervical cancer is primarily preventable by getting a prophylactic vaccine such as Cervarix (GlaxoSmithKline Biologicals, Belgium) or Gardacil (Merck and Company, United States of America). The vaccine Cervarix offers protection against HPV 16 and 18 while Gardasil protects against HPV 6, 11, 16 and 18. The vaccines use recombinant HPV major capsid (L1) proteins (type specific) that can self-assemble into virus like particles. Both vaccines induce neutralising serum antibodies (IgG). High concentrations of IgG is then found in the cervical epithelium binding to virus particles and preventing infection [37]. Vaccination has been widely practiced in the last few years, mostly vaccinating school girls from as young as nine years old. Boys are also now eligible for vaccination with Gardasil. The vaccine also

- 19 -

protects women from developing genital warts and anal cancers associated with HPV infections [38,39].

Diagnoses of cervical cancer are possible with either a Pap (Papanicolaou) smear or after visual investigation of lesions on the cervix. Biopsies are mostly taken from lesions to determine the aggressiveness of the cancer. Staging occurs at the time of the primary diagnosis and never change even if the recurrence or discovering the disease is more extensive during surgery. The FIGO staging system is used clinically to determine the severity and progress of pathogenesis based on the size of the tumour and consists of five stages starting from stage 0. In high income countries, cervical cancers are often discovered in the first stages of development / disease progression (tumour size < 4 cm). Patients in middle- and low income countries are sometimes diagnosed with the third or fourth stage of the cancer which is wide spread into the pelvic area while metastases occur [35].

A variety of treatment options are available and the treatment chosen in terms of the cancer stage. In the early stages of the disease, treatment usually relies on whether the patient desires fertility. If the patient still wants to conceive children, conisation of the cervix is performed while if the patient does not want to remain fertile a hysterectomy is performed. When surgery seems to be futile especially as the stages of the disease progress, more aggressive treatments are carried out. These treatments include radiotherapy (radiation), chemoradiotherapy (combination of chemotherapy and radiation) or chemotherapy. Patients diagnosed with Stage IV cancer (most severe stage of the disease), have a prognosis of 12 months since diagnosis, with only 20% of patients surviving for more than two years [35].

Radiotherapy becomes an important treatment for patients diagnosed with later stages of the disease. In 1997, radiotherapy was not available in 32 African countries (total of 47 countries) while this number had improved to 15 countries in 2003 [40]. Chemotherapy is another option in advanced stages or recurrence of cervical cancer. The drug deemed best at the moment is cisplatin either alone or in combination with other drugs or radiation (Fig. 2.8) [35]. Cisplatin is not always efficient in treating cancers since resistance is well documented [30]. Other disadvantages of cisplatin are that the treatment is extremely toxic leading to severe side effects and this toxicity could also result in secondary malignancies [41,42].

- 20 -
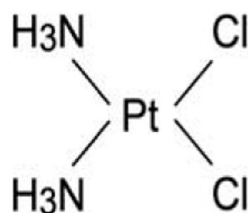
Fig. 2.7. The chemical structure of cisplatin. Taken with permission from [43].

2.4 Continuing chemotherapeutic research

The search for drugs that show selective toxicities towards cancerous cells with minimal side effects includes synthetic compounds as well as plant-, marine and microbially derived compounds. *(i) Gold compounds* and *(ii) naturally derived products* are the two types of external cell death inducers used in this study and will be introduced next.

The success of cisplatin paved the way for investigating medicinal qualities of other metal based compounds such as palladium, ruthenium, copper, silver and gold to name a few [44]. In ancient Egypt, the pharaohs placed gold in tombs because of the belief in *(i) gold's life giving properties*. For the middle class, Egyptians wearing gold jewellery served as a vehicle for magic spells and incarnations. From ancient Egypt to India until now, wearing gold is considered to protect the wearers from evil spirits and spells that might cause illness. In the first century, Pliny stated that gold could be used to cure fistulas, haemorrhoids and warts by rubbing gold onto these. Years later the properties of gold are still being investigated; in the 19th century, interesting claims were made that gold compounds could cure syphilis, tuberculosis and alcoholism. Later on most of the claims were found to not be true, or severe side effects accompanied treatments [45]. Only in the 1930s was real evidence obtained for the value of gold in medicine. An effective treatment and cure for rheumatoid arthritis namely auranofin or (triethylphosphine (2,3,4,6-tetra-O-acetyl-b-1-Dthiopyranosato-S) gold(I)) was discovered. Auranofin is an Au(I) thiolate-triethylphosphine complex (Fig. 2.9). Since the introduction of auranofin into the pharmaceutical market in 1985 no other gold compound has been evaluated in clinical trials for rheumatoid arthritis or any other disease. Auranofin is moderately toxic but was also found to have an anticancer activity that was similar to that of cisplatin [44].
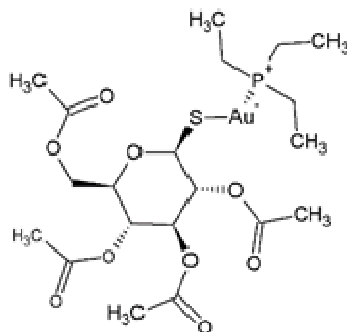
Fig. 2.8. The chemical structure of auranofin used for the treatment of rheumatoid arthritis. Redrawn with permission from [46].

Many different derivatives of auranofin have been synthesized containing up to three atoms of gold. Major issues during the synthesis of Au(I) complexes were the chemical instability of the compounds in solution. Improvements were made using diphosphine ligands, but these also led to higher cardiotoxicities. Compounds such as Au(I) phosphine-dithiocarbamate were found to be effective against a variety of different cancers, with the effectiveness depending mostly on the nature of the phosphine ligand. A variety of other Au(I) complexes include; bis(phosphine)Au(I), phosphine-gold-halides and phosphine-gold-alkynyl complexes. These compounds' mechanism of action had been found to be associated with the inhibition of thioredoxin. Phosphine complexes containing coligands of pyrazolates and imidazolates are more soluble in polar solutions and have been shown to have superb antiproliferative activity of up to 70 times better than cisplatin. Substituents on the phosphorous atom of diphosphine Au(I) complexes attributed to its cytotoxicity. The highest activity was for a phenyl group and the lowest activity for a methyl group. The nature of the linker between the two phosphorous atoms (as noted earlier) also plays a role in the activity. The steric and electronic nature of molecules are, therefore, important when designing efficient gold complexes [44].

The mechanism of action of Au(I) complexes against cancer have been studied in great detail. One of the theories was that apoptosis is induced independently of DNA damage since the affinity of gold complexes to react with DNA was improbable. It was confirmed that the theory by the ability of gold complexes to treat cisplatin (high affinity for DNA binding) resistant cancers. Gold (I) complexes have a high affinity for interacting and accumulating within mitochondria. This is attributed to cationic interactions with the mitochondrial

membrane as well as the lipophilic character of many of these compounds. Thioredoxin reductase is commonly inhibited by gold (I) complexes such as auranofin, although this cannot be seen as the primary mechanism of action. Other enzymatic inhibitions are seen such as inhibition of protein tyrosine phosphatases which plays a critical role in cancer, diabetes and obesity. Measurements of cancer metabolism were done using morphology, cell respiration assays, measurement of glycolysis and the cleavage of caspase 3 [47].

Except for Au(I) complexes being relevant candidates for anticancer treatments, Au(III) complexes had also shown excellent anticancer activity. Unfortunately, Au(III) complexes share a variety of side-effects with cisplatin such as; high toxicity, poor selectivity (cytotoxic to cancer and healthy cells), induced drug resistance and limited bioavailability. Other bioactivities of Au(I) and Au(III) complexes include promising data in terms of treatment potential for leishmaniasis, malaria, TB and HIV. Anti-inflammatory properties are also being investigated for newly synthesized Au(I) compounds [44]. In the present study, three gold (I) complexes were investigated namely auranofin and two diphenyl phosphine gold compounds. The synthesis and characterization of the compounds were done by A. Elkhir in Prof. Darkwar's laboratory (Department of Chemistry, University of Johannesburg, South Africa) [48]. The compounds showed promising anticancer (inducing cell death) activity in our laboratory [4,48].

(ii) Naturally derived products include but are not limited to; microbes, marine organisms and plants. Plants have formed part of sophisticated traditional medicine systems since as early as the 26th century before Christ. Plants still form an important part of health care systems in some cultures such as Chinese, Indian and African communities. In high income countries, the use of plants for medicine is more indirect with the use of supplements. A survey done by the World Health Organisation (WHO) found that of 94 traditionally used plants, 122 compounds were isolated that had related bioactivities. Some examples of traditionally used plants include; *Papaver somniferum* (treatment for hypertension: isolated compound – papaverine, and pain: isolated compounds - morphine and codeine), *Cinchona officinalis* (antimalarial, isolated compound: quinine) and *Artemisia annua* (antimalarial, isolated compound: artemisinin) [49].

Plants have also been used for a very long time to treat cancers, although cancer is not entirely defined by traditional medicine. Well-known cancer treatments derived from plants include; vinca alkaloids, vinblastine and vincristine. Semisynthetic derivatives of epipodophyllotoxin used clinally are etoposide and teniposide. The Taxus genus delivered the potent compound, paclitaxel (taxol®) that has been employed in the early nineties against ovarian and breast cancer (Fig. 2.10). Many derivatives of taxol are now being used such as taxorere®, abraxane® and cabazitaxel®.
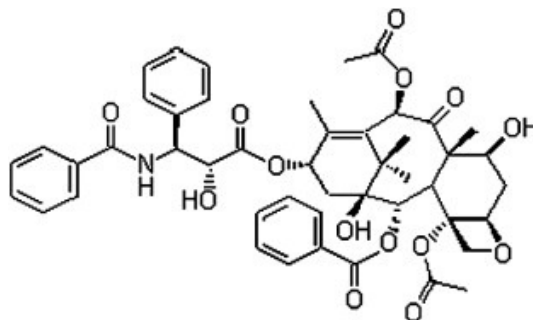
Fig. 2.9. The chemical structure of Taxol, naturally derived chemotherapeutic drug. Taken with permission from [50].

With so many success stories in the quest to find effective treatments for cancer, ethnobotanical studies are widely conducted in countries with diverse cultural heritages. One of the plant families known to have numerous species being used medicinally is Lamiaceae, which includes genera such as *Salvia* (sage), *Ocimum* (basil), *Mentha* (mint) and *Plectranthus*. The *Plectranthus* genus contains around 300 species and is located in Australia, Asia and Africa. The documented ethnobotanical uses of the plants are; medicine, digestive-, skin-, respiratory conditions, infections and fever, genito-urinary- and muscular-skeletal conditions [5]. *Plectranthus termifolius* exhibited cytotoxic and anticancer properties against nasopharanx carcinoma *in vitro* and *in vivo* lymphocytic leukaemia in mouse models [51]. *Plectranthus amboinicus* exhibited not only cytotoxic effects (< 30 µg/mL) against the proliferation of liver - and breast cancer cells, but also showed anti-inflammatory, analgesic, diuretic and antimicrobial activities [52]. Eighteen species of the Lamiaceae family was previously tested for bioactivity, of which *P. ciliatus* was one that showed potential anticancer activity (Fig. 2.11) [3]. *P. ciliatus* is known to be an ornamental plant in gardens and also widely used as ground cover. New Zealand has placed this plant on the list of "pest plants" in Auckland, which is indicative of the robustness of the plant [5,53]. *P. ciliatus* does

not have many ethnobotanical uses, except for using the plant for personal hygiene and washing of clothes [5,53]. Phytochemical analysis has detected that the species has high concentrations of essential oils and also contains diterpenoids [54,55]. Essential oils consist of mixtures of 20 - 60 terpenoids and aromatic compounds. Since the mixture of essential oils are so complex, the mechanism of cell death induction in eukaryotic cells are not unique, although some reports suggested that essential oils cause depolarization of mitochondrial membranes, disrupt ion pumps, coagulate cytoplasm and damages the plasma membrane [56]. Terpenoids and in particular diterpenoids have been studied for their anticancer potential and was found to be cytotoxic in a variety of different cancers by the induction of apoptosis and the production of ROS [57]. In this study, the crude extract of the plant was used to induce cell death, instead of purifying the extract to find the active constituents. The reason for this was that many traditional medicines have recently been proven to contain a mixture of compounds that work synergistically together. With mixtures of compounds, the resistance of cancer cells can be overcome. Different constituents in the crude extract target various parts of cellular pathways that ultimately lead to cell death induction, enhance pharmacological potency and decrease side effects experienced with pure compounds [58–60]. It can, therefore, be expected based on phytochemical information that the crude extract used in this study has the potential to induce cell death, most likely apoptosis. The National Cancer Institute of America recommends that a crude extract should be further evaluated for its anticancer activity when the CC_{50} value against cancerous cells is less than 20 µg/mL [61].

Fig. 2.10. *Plectranthus ciliatus* grown as ground cover in Kirstenbosch botanical garden, Cape Town, South Africa. Photo used with permission from S. Hariparsad (2014).

Microbial sources have played a crucial role in antibiotics and the discovery of cancer-fighting antibiotics such as anthracyclines. Many compounds are isolated from *Streptomyces* species and include; bleomycin, mitomycin, enediynes and staurosporines, doxorubicin [49] and actinomycin D (cosmegen®) [62]. Actinomycin D (Fig. 2.12) is used for the treatment of testicular cancer, melanoma, uterine sarcomas, Kaposi's sarcoma and soft tissue sarcoma [62]. Actinomycin D induces apoptosis *in vitro* and in *in vivo* cancerous cells, by intercalating into DNA, inhibiting RNA and protein synthesis. At high doses (> 1 µg/mL) transcription of all RNA occurs, while at very low concentrations (< 100 ng/mL) only inhibition of ribosomal RNA synthesis occurs [63]. In HeLa cells, it was found that when the cells were treated with 1-10 µg/mL actinomycin D, the treatment was cytotoxic [64]. Treating cells with concentrations higher than 0.1 µg/mL led to the cells detaching and ~ 75-80% death. When cells were continuously treated with concentrations between 0.1-0.01 µg/mL, the cytotoxic responses were delayed. Sawicki and Godman (1971) found that HeLa cells were more susceptible to the effects of actinomycin D as compared to cells such as Vero, W138 and mouse L cells. Therefore, at lethal concentrations of actinomycin D, HeLa cells would show cytotoxic responses quicker as compared to Vero cells where the cytotoxic response would be detected at small percentages and only after longer treatment times. During the treatment, RNA synthesis is inhibited in treated cells. With high concentrations, where > 85% RNA inhibition occurs; cells will have a cytotoxic response after at least two hours. Such high inhibition % can also be reached with lower actinomycin D concentrations but during much longer incubation times [64]. It was also found with other ribosomal RNA inhibitors that autophagy is induced which could ultimately lead to cell death in prolonged exposure times [65].
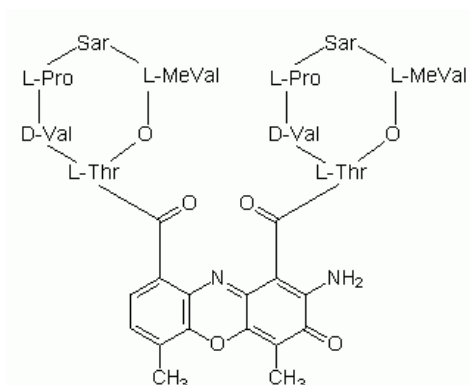
Fig. 2. 11 Chemical structure of actinomycin D. Taken with permission from [66].

2.5 Cytotoxic or cytostatic drugs

Chemotherapeutic drugs are classified as cytostatic or cytotoxic depending on the outcome during and after treatment. Cytostatic drugs are drugs that target intracellular proteins and the tissues supporting tumours to inhibit metastasis. Therefore, the cancer cells will not die of the treatment but rather be prevented from proliferating. Cells are not killed and thus will not have an effect on the size of tumours. Clinically, patients being treated with cytostatic drugs have a stable disease state and a better survival rate compared to patients receiving cytotoxic drugs. Cytotoxic drugs, on the other hand, lead to the death of cancer cells (mostly apoptosis) and a decrease in tumour size. Cytotoxic drugs cause side effects that in most cases do not distinguish between fast growing healthy cells (such as hair follicles and the lining of the colon) and cancer cells. The mechanism of action of cytotoxic drugs is associated with DNA damage that leads to the induction of cell death while the mechanism of action of cytostatic drugs is not confined to DNA damage. Cytostatic compounds also have different cellular targets such as microtubules that results in a mitotic arrest. In the case of mitotic arrest, cells being trapped too long in this predicament, would eventually die [67].

Most conventional drugs are cytostatic and cytotoxic. Whether the treatments are classified as cytotoxic or cytostatic depends on the concentration of the treatment and the variable effects recorded at the different concentrations. This was proven with a variety of treatments such as; topotecan (topoisomerase I inhibitor), norubicin (topoisomerase II inhibitor) eliciting cytostatic responses at low concentrations and cytotoxicity at high concentrations. On the other hand, vincristine and paclitaxel bind to microtubules and are both inherently cytostatic. With prolonged mitotic arrest, cells have to either escape or ultimately die, hence the cytotoxic property of cytostatic drugs. It has been shown that in *in vitro* models, cytostasis can occur with almost all conventional drugs although there is no enough evidence currently to confirm this in *in vivo* models. In preclinical studies, it was found that in some cytotoxic drug treatments there was a delay in tumour growth, which is a characteristic of cytostasis. Theoretical differences between cytostatic and cytotoxic drugs have been postulated. Cytostatic drugs are molecular targeted therapies with high selectivity while cytotoxic drugs are the conventional chemotherapy drugs that are less sensitive as compared to cytostatic drugs. Cytostatic drugs are currently being administered as a monotherapy or in combination with cytotoxins on a continuous basis while chemotherapy is administered in cycles of a

- 27 -

monotherapy or a combination with other cytotoxins or radiotherapy. Drug resistance has not been identified with cytostatic drugs while cancer cells have built up resistance against some cytotoxins [67].

2.6 Background on cell lines important to this study

In this thesis, cell death was investigated using cervical adenocarcinoma (HeLa) and African green monkey kidney (Vero) cells. Historically, *(i) HeLa cells* were harvested from an adult black female, Henrietta Lacks, who died in 1951 of a very aggressive cervical adenocarcinoma (Fig. 2.13 (a)). During a biopsy at the John Hopkins hospital for diagnosis of the disease, extra tissue was given to Dr. G. Gey's tissue culture laboratory. In this laboratory, the cells were successfully propagated and so became the first human cell line. The name of the cell line was derived from the first two letters of the patient's first and last names. HeLa cells were distributed worldwide to researchers interested in investigating carcinomas [68]. A deposit of the cells were made at the American tissue culture collection (ATCC) and is listed under the number: CCL-2 (Fig. 2.13 (b)) [69]. To date, more than 90 000 documents have been published using HeLa cells with an average of between 4000 and 5 000 manuscripts being published using HeLa cells annually. HeLa cells are mostly used for research in biochemistry, genetics & molecular biology (65.3%) and medicine (24.8%) (Fig. 2.13 (c)).

(a)

(b)

©ATCC
High Density
Scale Bar = 100µm

(c)

Other (11.3%)
Undefined (0.3%)
Chemical Engine... (3.0%)
Materials Scien... (3.2%)
Agricultural an... (4.5%)
Multidisciplina... (4.7%)
Chemistry (8.6%)
Pharmacology, T... (9.5%)
Immunology and ... (16.0%)
Medicine (24.8%)
Biochemistry, G... (65.3%)
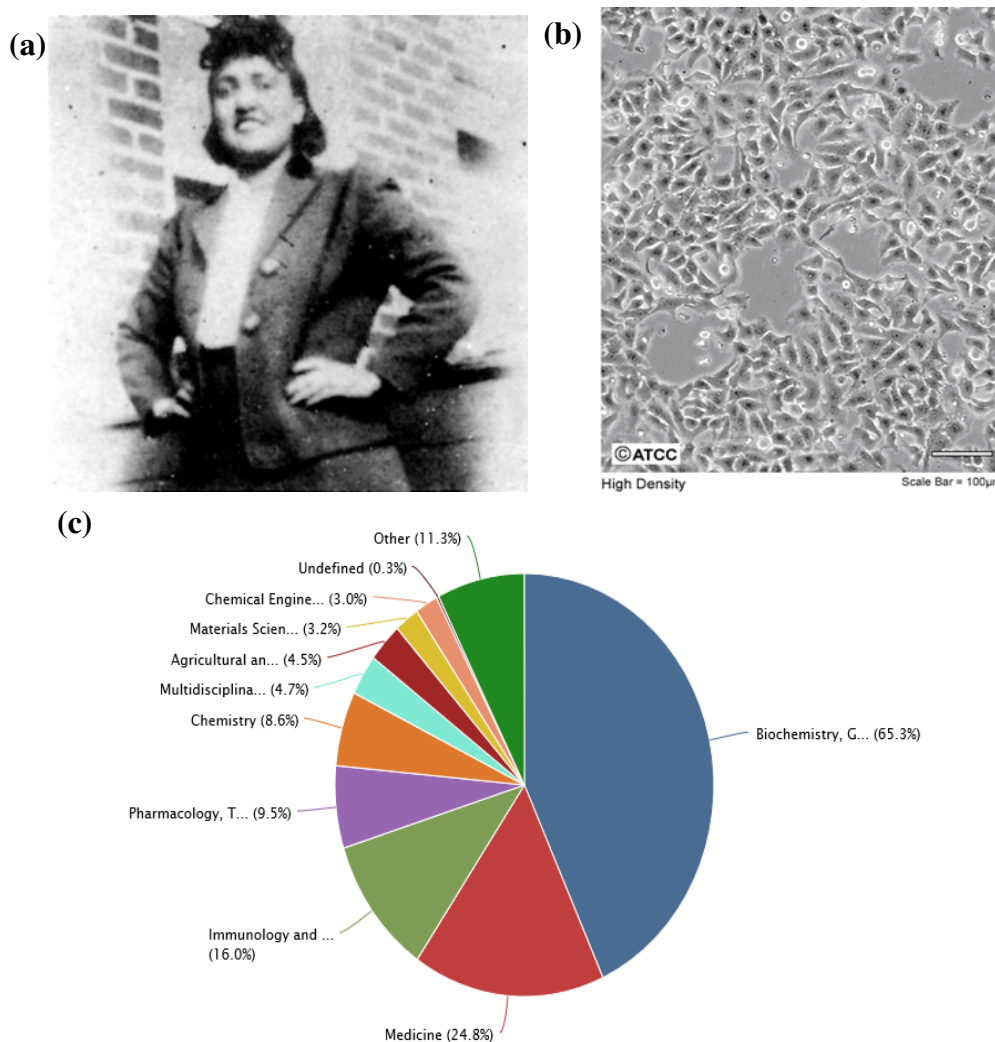
Fig. 2.12. (a) Henrietta Lacks, taken with permission from [70] **(b) HeLa cells** from her biopsy [69] and **(c) Most of the research using HeLa cells** are published is in the fields of biochemistry, genetics and molecular biology (65.3%), medicine (24.8%) and immunology and microbiology (16%) [71].

(ii) Vero cells are the second cell line used in this study and were originally harvested from the kidney of a healthy adult African green monkey (*Cercopithecus aethiops* L.) in 1962 by Y. Yasumura and Y. Kawakita at the Chiba University of Japan (Fig. 2.14 (a)). The cells are used to investigate virus host interactions since the cells are sensitive to infection with a variety of pathogens. Vaccines are also being produced using Vero cells including; rotavirus, smallpox, Japanese encephalitis, influenza, poliomyelitis and rabies (http://www.actip.org/ pages/vaccinestable.html). A deposit of the cells was made at ATCC and is listed under the number: CCL-81 (Fig. 2.14 (b)). This cell line was selected for this investigation to represent a group of cells with noncancerous characteristics. Vero cells are one of the few cell lines available from ATCC, which was not harvested from a diseased individual.[69]

Approximately 17900 documents were published on research based on these cells with between 500 and 900 annually. Most of the research subjects covered in the manuscripts was of immunology and microbiology (53.6%), medicine (33.8%) and biochemistry (30.2%) (Fig. 2.14 (c)).

(a)

(b)

(c)
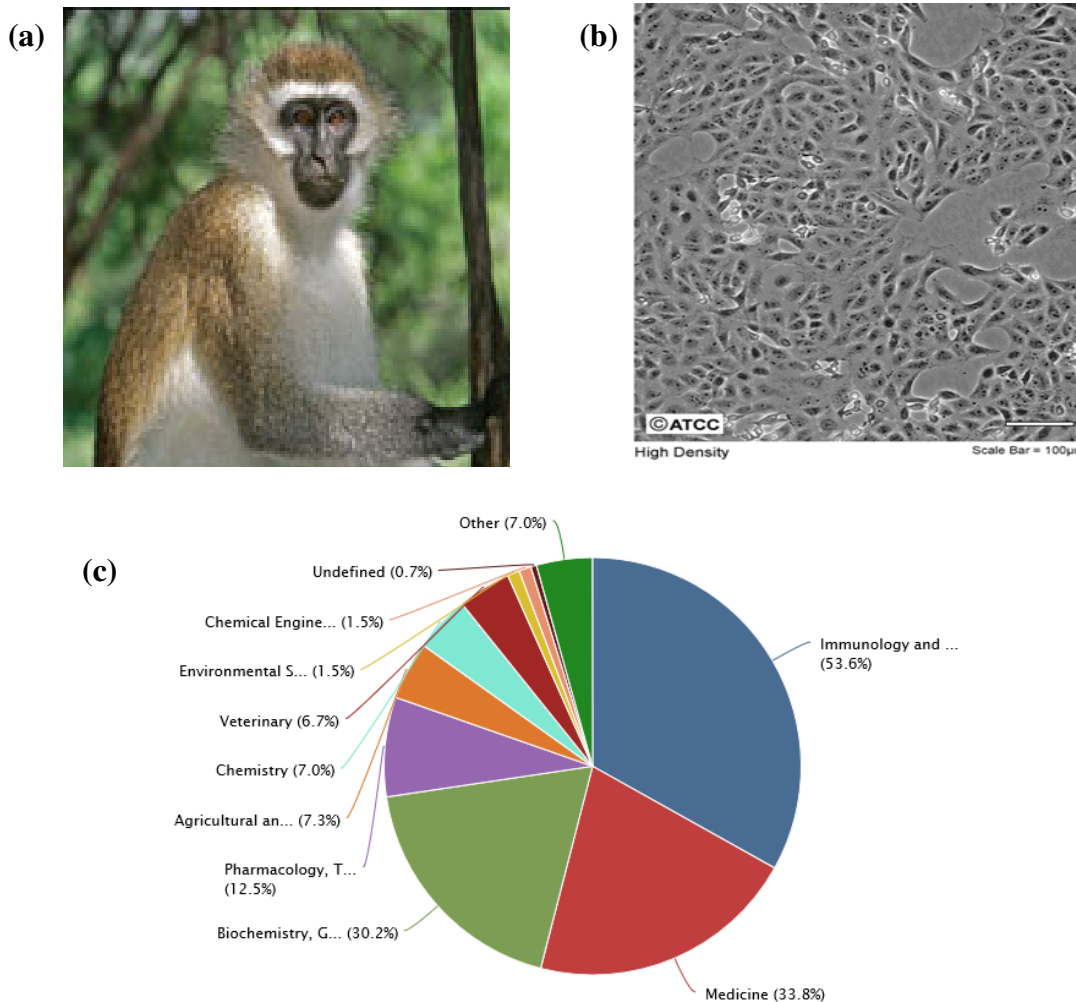
Fig. 2.13. (a) An African green monkey, adapted with permission from [72] **(b) Vero cells** [69] **and (c) research fields in which Vero cells are used** [71]**.**

2.7 Conventional biochemical methods for detecting cell status

Cell status can be defined as living (proliferating / viable) or dead (apoptotic / necrotic and can be detected using labels or dyes.

Cytotoxicity is usually determined by popular *(i) colorimetric assays* such as 3-(4,5-dimethylthiazol-2-yl)-2,5-diphenyltetrazolium bromide (MTT), 5-(3-carboxymethoxy-phenyl)-2-(4,5-dimethylthiazolyl)-3-(4-sulphophenyl) tetrazolium (MTS) or sodium 3′-[1-[(phenylamino) carbonyl]-3,4-tetrazolium]bis(4-methoxy-6-nitro) benzensulphonic acid hydrate (XTT). Other assays include crystal violet staining, which is proportional to the protein content of the treated cells and neutral red staining [73]. Older biochemical assays include trypan blue exclusion assay which is time-consuming and mostly not reproducible. The assay that will be used during this study is the XTT tetrazolium salt viability assay. This tetrazolium salt is used as a non-radioactive marker for quantification of cell proliferation and viability. The assay is based on the cleavage of a yellow tetrazolium salt. This salt forms an intense orange formazan dye in metabolically active (viable) cells *via* mitochondrial dehydrogenase (Fig. 2.15). Therefore, XTT assay only measures the activity of one enzyme and how the enzyme is affected by the treatments.
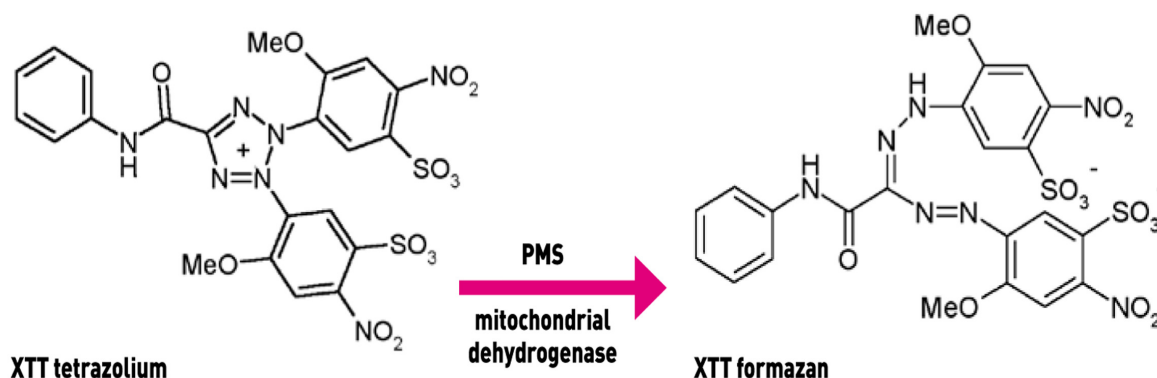
Fig. 2. 14: The tetrazolium salt, XTT is cleaved by mitochondrial dehydrogenase in the presence of phenazine methosulfate (PMS), an electron coupling reagent to form orange XTT formazan salt. Permission for the image was requested.

The formazan dye is soluble in aqueous solutions (whereas MTT needs solubilisation) and is directly quantified using a microtitre plate reader. The increase in the number of living cells results in an increase in the overall activity of mitochondrial succinate dehydrogenase in the cells. This increased activity directly correlates to the amount of orange formazan detected. XTT salt is part of tetrazolium salt family who is metabolically reduced to intensely coloured end products. The bio-reduction of the salts is still poorly understood despite the long historical use in viability assays. According to Berridge *et al.* (1996), it was found that XTT

- 31 -

in the absence of cell extract was reduced by NADH and NADPH. It was also evident that the NADH-dependent reduction of XTT was inhibited by mitochondria.[74] On the other hand, succinate-dependent reduction of XTT was dependent on mitochondria. If the reduction took more than an hour, it was likely to have been either NAD(P)H dependent reduction or succinate-dependent reduction of the salt. It was also found that superoxide was involved in a reduction of XTT by NAD(P)H and NADH. The results of XTT are usually expressed as the Cytotoxic Concentration inhibiting the proliferation of 50% of the cell population (CC_{50}). Calculated CC_{50} values of the same treatment on cancerous and noncancerous cells can be used to work out the selective cytotoxicity of a treatment. The selectivity index (SI) of a treatment is defined as the ratio of cytotoxicity against normal healthy cells to cancerous cells. In general, it is considered that the biological efficacy is not due to cytotoxicity when the SI value is $\geq$ 10.[9] XTT has been used in a variety of experiments to determine the cytotoxicity of natural products [75–78]. A relatively new system is also available that measure cell behaviour in the environment of cytotoxic compounds in real time, which makes the technique highly informative with the continuous monitoring of cells.

This system is called *(ii) the Real Time Cell Electronic System (RT-CES).* The RT-CES system consists of four components mainly the analyser, station, computer with integrated software and disposable E-plates. The RT-CES station fits inside a standard tissue-culture incubator while an analyser and laptop computer with software are outside of the incubator. Cells are seeded in E-plates, which are microtitre plates with gold cell sensor arrays at the bottom of the plates. These cell sensors allow the cells to be monitored continuously. The gold electrodes form a layer covering approximately 80% of each well. The electric impedance is measured to give indications of the physiological conditions of the treated cells. The voltage that is applied during measurements is not higher than 20 mV and was found not to cell growth or viability. The impedance that is read depends on the ion concentration in the aqueous medium and the concentration of cells attached. When cells attach to the bottom of the wells, the ion balance compared to 'no cells', will change. The change that took place when cells attached to the electrode surface was due to the insulating nature of the cells, which will increase the impedance. Thus, when more cells are growing on the electrodes, the value of electrode impedance will increase [79]. Measurements are based on the unit less cell index (CI) which is based on the differences of the impedance measured when cells are

attached or detached from the electrodes. The formula used to calculate impedance is as follows: $CI = (Z_i - Z_0)/15$. The abbreviation Z_i is the impedance at an individual point of time during the experiment and Z_0 is the impedance at the start of the experiment (Fig. 2.16). Two theories are postulated when the impedance of cells changes during treatments [79]. When no cells are attached to the electrodes at the bottom of the well, no change in impedance will be measured. When more cells attach to the electrodes, the impedance will increase and thus the CI will also increase. The CI is influenced by the cells starting to attach directly after cells were seeded, as well as cell proliferation. During the treatment of cells with cytotoxic samples, the cells will die and thus detach from the electrode surface. A detachment of cells will cause the CI to decrease [79]. During different treatments, the cells might change morphologically, which could lead to increased cell adhesion or spread of the cells. This behaviour will cause an increase in the CI. The addition of samples can cause cells to clump together and even spread out while the treatment is taken up by the cells, thus leading to higher CI values. Cytotoxicity of treatments can cause the CI to decrease when cells shrink and detach [79]. RT-CES measures the adherence of the cells to the electrodes and, therefore, the adherence proteins found in the plasma membrane.
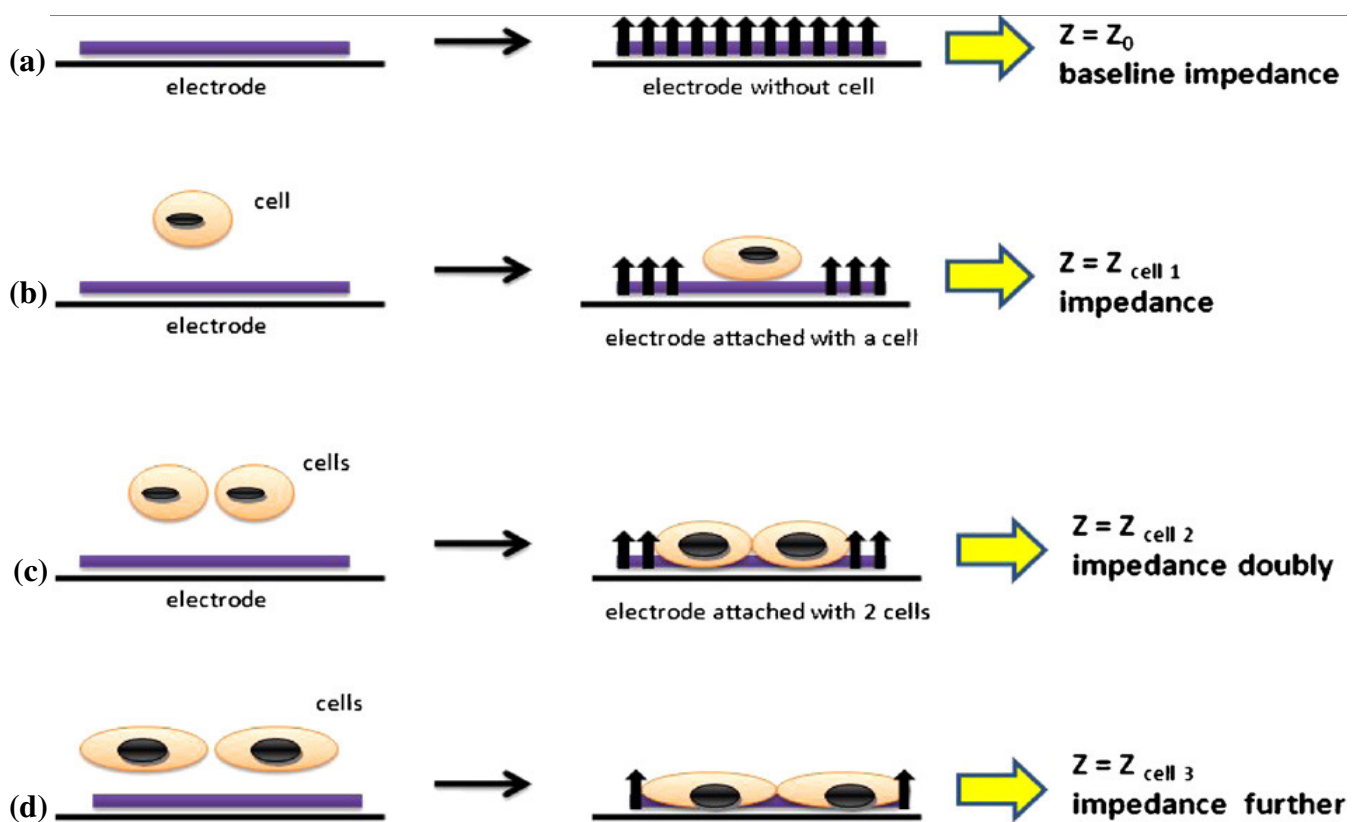
Fig. 2.15: Impedance based on the number of cells attached to the bottom of the well using RT-CES. (a) When no cells are in the wells and only media is added, the baseline impedance will be equal to zero, (b) while as soon as the cells start attaching there will be an increase in the impedance, (c) that will be equal to the number

of cells attaching to the electrodes, (d) until cell confluence is reached and the cell index is high. Taken with permission from [79].

Recent publications show RT-CES able to distinguish cytotoxic from cytostatic treatments. Fonteh *et al.* (2011) investigated the anti-HIV activity of four bis (thiosemicarbazonate) gold (III) complexes using auranofin as a positive control. With RT-CES Fonteh *et al.* (2011) found that these compounds were cytostatic and not cytotoxic as was predicted by very small CC_{50} values determined using MTT. It was concluded that the end-point measurement of MTT was less reliable in determining precisely what type of cellular response was triggered during and after the treatment [80] because viability was only measured in terms of the behaviour of one enzyme. In another study, in which the researchers compared XTT CC_{50} values to CC_{50} values calculated with RT-CES, it was found that the two assays complemented each other. Urcan *et al.* (2010) found that the CC_{50} values of different dental composite components showed similar toxicities on gingivital fibroblasts. The main findings were that although the two assays were comparable, some of the results indicated that RT-CES was more sensitive to cellular behaviour [79]. Ehlers and colleagues (2010) studied the embryo toxic effects of a marine biotoxin okadiac acid on murine embryonic stem cells and found again that RT-CES was more sensitive compared to the MTT assay. The researchers concluded that RT-CES gave real time data which was easy to use and more informative of cell behaviour [81]. Kapewangolo *et al.* (2013) used RT-CES to confirm MTT data that a medicinal plant extract, Plectranthus barbatus, was not toxic at concentrations where HIV reverse transcriptase activity was evident [82]. No comparisons of RT-CES with other less conventional techniques have been done and therefore in this investigation RT-CES data was compared to an unconventional cell death detection technique such as Fourier Transform infrared spectroscopy (Chapter 4).

(iii) Flow cytometry is a quantitative analysis which can be used for studying the mechanisms of cell death, usually discriminating between early apoptosis, late apoptosis and necrosis. Functional attributes of cells, such as mitochondrial metabolism, oxidative stress, intracellular pH and other variables closely associated with mechanisms regulating cell sensitivity to apoptosis can also be explored [83]. Flow cytometry is based on forward-angle light scattering (FSC) which is an indication of the cell size, while side-angle light scattering gives an indication of the complexity of the cells based on the intracellular components [84]. Fluorochromes can be used to bind specifically to cells to differentiate between different

stages of cell death. During this investigation, annexin-V and propidium iodide were used. Annexin-V is a fluorescent protein which in the presence of calcium ions can bind to phosphatidylserine which is externalized during apoptosis when plasma membrane proteins are rearranged. Propidium iodide (PI) is a DNA intercalator which is only able to bind to DNA when the cells undergo necrosis or when cells have damaged plasma membranes through which PI can enter (Fig. 2.17). Flow cytometry using annexin-V and propidium iodide is still a very traditional assay conducted by researchers worldwide for the assessment of cell death. Annexin-V detects phosphatidylserine molecules on the surface of apoptotic cells while PI detects DNA molecules and indirectly the loss of plasma membrane integrity.
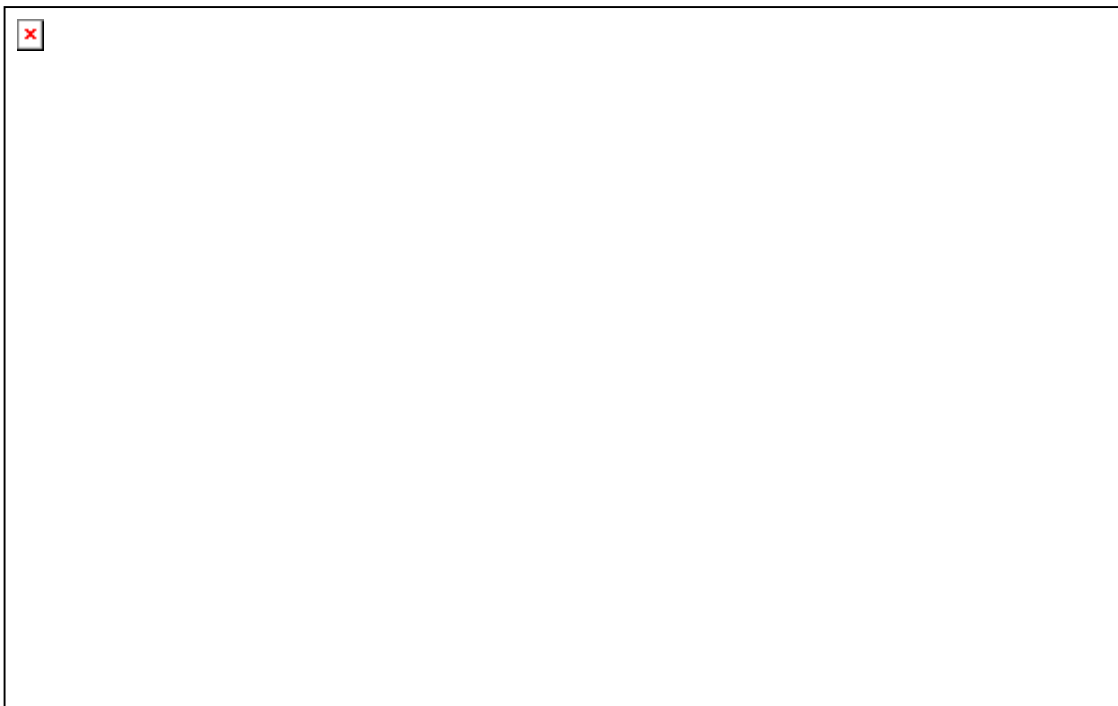
Fig. 2.16. Binding of annexin-V and propidium iodide in viable cells versus early and late apoptotic cells. On the right hand, a typical dot plot of cells, where viable, early and late apoptotic cells are detected. Permission requested from [85].

Flow cytometry is not only a quantitative technique to indicate what type of cell death was induced by treatments, but the distinct populations of cells can also be separated by sorting the cells based on fluorescence [86]. Fluorescence Activated Cell Sorter (FACS) systems use the principle of electrostatic deflection of charged droplets to sort mixed populations of cells. Firstly cells are ejected in the sheath fluid and passed through a nozzle tip that oscillates the sample at high frequency. This oscillation breaks the stream into tiny droplets. The droplets

- 35 -

are interrogated by the lasers and the information sent to the processing software. The operator then selects the population(s) of interest, for example, viable, early apoptotic or necrotic cells. The fluorescently tagged cells are then charged in the drop as they pass through the laser beams. The drops pass through two electrostatic platinum plates that are charged, one negatively and the other plate positively. The positive droplets are then deflected towards the negative plate while the negative droplets are deflected towards the positive plate. Uncharged cells are collected in the waste drawer. Up to four populations can be sorted into flow tubes simultaneously (Fig. 2.17) [87]. Sorting of labelled cells are employed successfully, but cross reactivity of the fluorochrome can occur, and, therefore, sorted cells need to be confirmed in the population of interest [86]. In Chapter 6, the cells were confirmed to have died either by apoptosis or necrosis by employing Transmission Electron Microscopy (TEM).
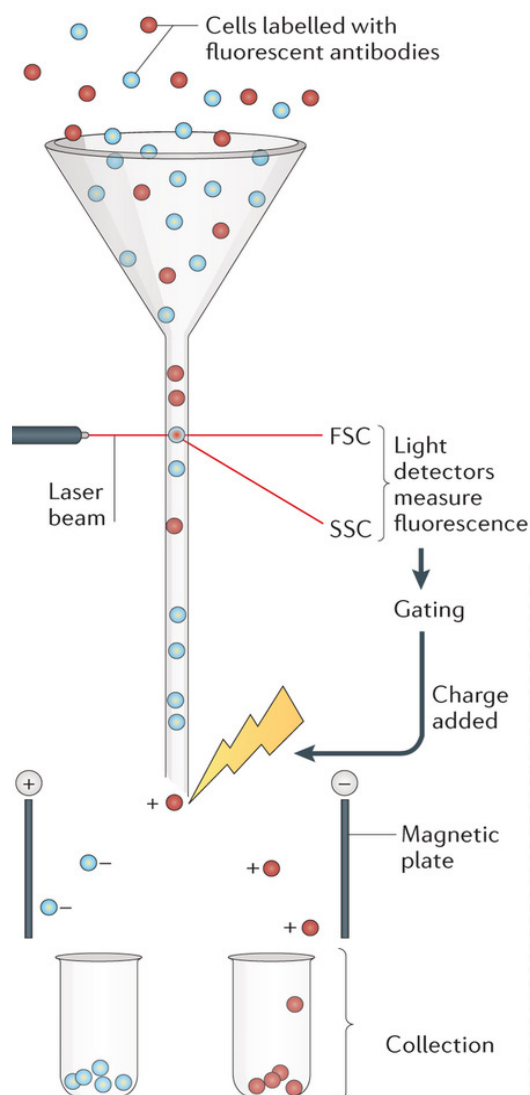
Fig. 2.17. Principles of flow cytometrically sorting of labelled cells. Image was taken with permission from [88].

(iv) Transmission Electron Microscopy (TEM) is a golden standard in identifying and distinguishing different types of cell death in cells and tissues. The technique is known as a traditional biophysical technique because electrons are directly involved in imaging of the sample. In this investigation, it was categorized as a conventional biochemical technique due to its long history being used as a tool in ultrastructural studies in biochemistry and related research fields. The sections are also stained with different heavy metals to obtain better contrast in the micrographs and, therefore, contains strong features of biochemical interactions of the metals with the biomolecules. After fixation, dehydration, embedding and

obtaining a ultrathin section of the samples the sections are viewed using a TEM [23]. The TEM system consists of three major components. These components are; the electron gun and condenser (to focus the electrons on the sample), the image producing system (objective lens, movable stage, intermediate and projector lenses to focus the electrons passing through) and an image recording system (Fig. 2.19) [89]. Electrons are accelerated from the source on their way to the sample. When the electrons reach the sample, the electrons are collected and the image constructed on the projection screen using electron optics. When the electrons first reach the samples, the electrons are scattered, diffracted and absorbed by the specimen. The image is produced when electrons are deflected within specific angular ranges (determined by the aperture of the imaging lens) [90]. TEM can visualize morphological changes in nuclear material, cytoplasm density, organelle, and plasma membrane changes.

© 2008 Encyclopædia Britannica, Inc.
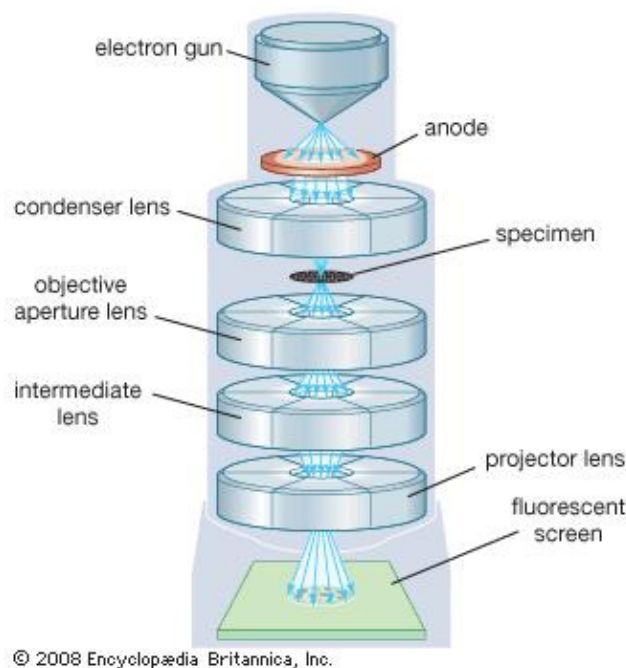
Fig. 2.18. A typical TEM with the major components indicated. The electron gun produces electrons, which are focused on the sample by a condenser lens. When the electrons pass through the specimen, a series of lenses are used to produce an image on a fluorescent screen and permission for the image from [89].

Essential ultrastructure characteristics are associated with particular types of cell death. In the case of necrosis, the plasma membranes are ruptured, mitochondria are swollen with disruption of the cistae and nuclear dispersion is visible. Ultrastructural characteristics of apoptosis are associated with plasma membrane blebbing, chromatin aggregation, detection

of mitochondrial changes (including fission and mitoptosis) while autophagy is characterized by double membrane vacuoles [91]. Some of the disadvantages of using TEM for studying cell death is that; apoptotic cells are detected at a terminal stage of apoptosis and thus TEM cannot be used to distinguish between different stages of apoptosis, condensed chromatin does not necessarily indicate nuclear fragmentary DNA and to cut ultrathin sections of the samples can be tedious and require a high level of skill. Although some disadvantages are evident, it still remains crucial to use TEM to investigate cell death in the samples to confirm the type of cell death for example detected by flow cytometry of a specific cell death induer [92].

(v) Caspases 3 / 7 assay is based on the principle that when apoptosis is initiated, then caspase activity increases. Caspases are endoproteases found within a variety of cells. These enzymes hydrolyse peptide bonds. The active site contains catalytic cysteine residues which react with aspartic acid residues in substrates. Caspases are also involved in the release of signalling molecules that partake in apoptosis and inflammation. Caspases involved in apoptosis are broadly classified into two categories namely initiator caspases and executioner caspases. Initiator caspases consist of caspase 8 and 9 while executioner caspases have been identified as caspases 3, 6 and 7 [93]. The initiator caspases are highly specific and only cleaves a few proteins while it had been established that executioner caspases carry out the bulk of the proteolysis. Caspase 3 and 7 share very similar specificity and their proteolytic activities are practically indistinguishable. Caspase 3 and 7 also have other functions that will not be discussed here [94]. In terms of apoptosis, the activation of caspase 3 and 7 results in the degradation of the nuclear material and cytoplasmic proteins. Initiation of apoptotis to the completion of the process can occur as quickly as 3 hours. Therefore, the timing of experiments is crucial since the experiment might deliver false positive or negatives when the reaction is missed, or detection is assayed before the reaction takes place. Various assays can be used to detect caspase activities such as western blotting, immunoprecipitation and immunohistochemistry or fluorescence using flow cytometry or benchtop assays [16]. In this investigation, the fluorescent R110 product was detected to measure caspase 3 and 7 activity. The principle of the assay is that lysed cells contain caspase 3 and 7, which then cleaves the added substrate DEVD peptide-rhodamine 100. The fluorescence is measured (485 nm excitation, 527 nm emission) with a fluorescence plate reader. Considerations to keep in

mind is that the time of the experiment needs to be optimised extensively since the activity of caspase 3 and 7 passes quickly [95].
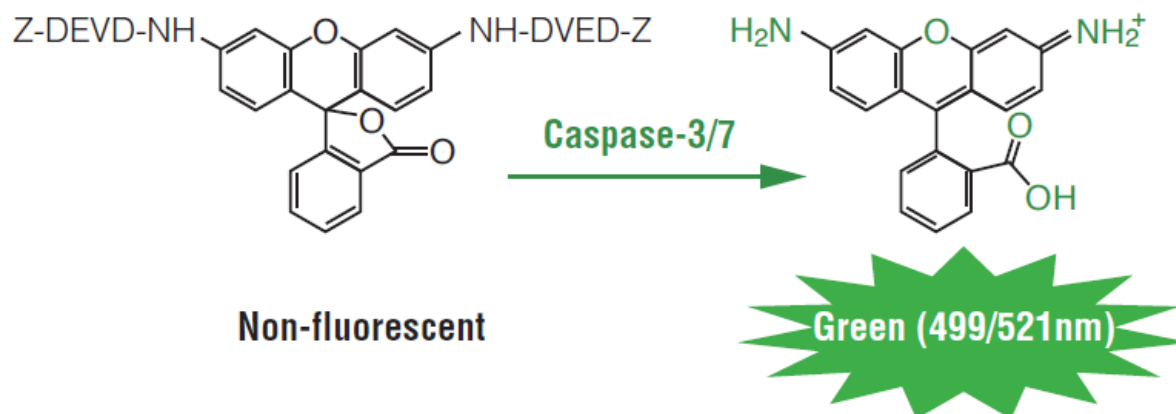
Fig. 2.19. Cleavage of caspase substrate Z-DEVD-R110 by caspase 3 / 7 creating a fluorescent rhodamine 110. Fluorescence is measured at 521 nm. Permission requested from Promega.com [96].

2.8 Advantages and disadvantages of conventional assays

In vitro assays involve the use of tissues, cells, cell lines or cell components isolated from animals or humans, maintained in an aqueous medium and tested outside of the body of the donor. *In vitro* assays hold the advantage that all variables can be controlled and that a specific end-point can be measured. The experiments are easy to set up, inexpensive, less time consuming than *in vivo* studies and permit replications in the same setup. Because human tissues and cells can be isolated, there is no need to extrapolate the animal data obtained in the laboratory to compare it to humans. It has also been established that adequate drug concentrations *in vitro* corresponds very closely with free plasma concentrations *in vivo*. Using *in vitro* assays also allow high throughput analysis of many samples in a short time frames compared to *in vivo* studies [97].

There are only some disadvantages involved using *in vitro* assays. These disadvantages include the fact that due to all variables being controlled except the one or a few variable being tested, scientists are unable to predict the response to the treatment in living organisms. *In vitro* assays are also more aim driven to determine very specific responses of isolated

enzymes and cells, thus ignoring any other possible interactions taking place in a particular response. Secondary cell lines are indefinitely growing cells isolated from humans as well as a variety of animals. These cells may not necessarily represent wild type cancers. Fortunately, when activity is seen against secondary cell lines, it can be predicted that the activity might be similar in clinical samples [10].

Although most of the techniques discussed in the previous section have been used successfully for decades, some serious disadvantages are still obvious. The disadvantages include that most readings are end-point analyses which are dependent on specific markers (labels) that may not be stable over long time periods. In addition, these labels may cross react with other markers or cell components. Specifically, *(i) tetrazolium salts* represent a rapid and user-friendly method, but these salts are toxic to cells preventing the assessment of cells over a long time period. Also, the end-point analysis can only give one reading per analysis and only a few variables are measured, for example, the viability and proliferation of cells as well as dead cells. Another disadvantage of tetrazolium salts are that the presence of antioxidants in the treatment (as found in crude plant extracts) can cause misleading results due to the interaction between the antioxidants and the tetrazolium salts. Tetrazolium salt data must generally be confirmed by more sensitive reproducible means. On the other hand, this assay has been optimized in such a way that it is being used as a high throughput assay for the assessment of cytotoxicity.

To confirm the results of the tetrazolium salt (XTT) used in this study, *(ii) RT-CES* was performed. RT-CES is the dynamic measurement of cell behaviour in the presence and absence of chemical stressors without the aid of labels. Due to the continuous monitoring of the cells through impendence readings, the data obtained is rich in information which can tell the researcher exactly if the cells were proliferating optimally, what the initial and long term effects are of the chemical stressors were as well as CC_{50} values at particular time points. The instrument was originally designed for the analysis of adherent cells, but recently suspension cells were successfully monitored by coating the E-plate wells with polyethyleneimine [98]. The disadvantages include the cost of the instrument and the E-plates.

(iii) Flow cytometry, on the other hand, can produce label free and labelled data. The label free data is based on the information obtained when investigating the forward scatter and side scatter of the sample, in this case, cells. Forward scatter gives an indication of the size of particles being analysed, for example, the size of apoptotic bodies is smaller than viable cells. Side scatter is indicative of the granularity of the cells [23]. Light scatter is not a good marker for the detection of cell death, since mechanically broken cells, cell debris and apoptotic cells display decreased light scattering properties [99]. Therefore, labels are required for accurate measurements and identification of cell death. Flow cytometry is a very sensitive technique which can measure multiple fluorochromes simultaneously (up to 17 flourochromes). The disadvantage is that the fluorochromes or kits can be very expensive and the fluorochromes are often unstable (measurements should be taken immediately after staining) and light sensitive too. Another disadvantage is that the fluorochromes could bind to the wrong markers (cross-reactivity). The running cost of a flow cytometer is also quite expensive. However, the protocols and parameters used for preparing and measuring cells are optimized and working optimally. *(iv) Sorting* of specific subpopulations is possible with some of the flow cytometers such as the FACS Aria used in this study. The advantage of sorting cells is that small populations of cells with specific characteristics (determined by the binding of fluorochromes) can be isolated from a heterogeneous population of cells. Sorting is also extremely accurate, but some disadvantages have been identified.   These disadvantages could lead to decreased viability and include expulsion by high velocity into collection tubes, long time periods required for sorting and the field pulse applied for cell deflection [86]. Some of the disadvantages can be optimised for specific cell lines / clinical samples as was done in this study. Firstly the collection tubes were coated in Fetal Bovine Serum (FBS) to assist the cells to slide down the sides of the tubes and then to stay in suspension. The serum also provided nutrients for the cells to limit cell deterioration during the long sorting time. Viability of untreated (viable) cells was also assessed with trypan blue and light microscopic investigation.

(v) Transmission electron microscopy has the advantage of having magnificent resolution and thus even the smallest detail inside of the cells can be seen. On the other hand, cutting of the samples into ultrathin sections requires experienced technicians and is extremely time-consuming. Various hours sitting at the microscope are necessary to take adequate amounts of micrographs for quantitative data. Institutions also usually one have one microscope that

caters for all the disciplines making the TEM not readily available. Due to some pitfalls in most conventional assays, there is always room for new methodologies for the monitoring of cell death.

(vi) Fluorescence caspases 3 / 7 detection is a convenient assay which can be easily conducted in any lab that has a fluorescence plate scanner. The disadvantage remains that apoptosis cannot be definite by only detecting caspase activity, since different scenarios exist where cells might have higher baseline caspase activities or where caspase activity is absent in the presence of apoptosis. The time of measurements is also very difficult to determine and sufficient time should be made to optimize the time for each treatment and in different cell lines [95].

2.9 New methodologies for monitoring cell death

New methodologies for monitoring cell death should ideally not use labels, be inexpensive, user-friendly and rapid. Another advantage of developing new methodologies could be the detection of more than one biomarker or macromolecule. The simultaneous detection of changes in DNA, protein and lipid concentrations and conformations will be superior to the conventional methods where only specifically labelled molecules can be measured. The techniques that are promising in becoming new methodologies for the detection of cell death are Fourier Transform Infrared (FTIR) spectroscopy and Raman spectroscopy, collectively called vibrational spectroscopy.

Vibrational spectroscopy is relatively straight forward, reproducible, non-destructive to the samples, label free and very small amounts of samples are required for analysis. Data obtained give molecular information which allows investigations of functional groups, bonding types and molecular confirmations. Spectral bands in vibrational spectroscopy are molecule specific and provide direct information on the biochemical composition of the sample. FTIR and Raman's spectra produce complementary data while some differences are evident in the techniques [100]. Raman and infrared spectroscopy are usually needed to completely measure the vibrational modes of a molecule. Although some molecules may be Raman and Infrared active, these two forms of spectroscopy arise from very different

processes and selection rules. Raman spectroscopy interrogates symmetric vibrations of non-polar groups while infrared spectroscopy is used to investigate asymmetric vibrations of polar groups. Both techniques study the interaction of radiation with molecular vibrations but the manner in which the photon energy is transferred to a molecule by changing its vibrational state. Infrared spectroscopy measures transitions (electric dipole mediated) between vibrational energy as a result of the absorption of mid-IR radiation. Raman spectroscopy is a two photon inelastic light scattering event. The incident photon has much more energy compared to the vibrational energy due to losing part of the energy to the molecular vibration (interaction due to Raman polarizability of the molecule). The remaining energy is scattered as a photon with reduced frequency. Vibrational bands are characterized by their frequency, intensity and band shape. Their frequency is linked to energy, the intensity of the band to the polar character or polarizability of the molecule while the band shape is indicative of the environment of the bonds. Vibrational energy levels are unique to each molecule and, therefore, the vibrational spectrum is a fingerprint of the specific molecule. Frequencies of molecular vibrations are dependent on the masses of the atoms, their geometric arrangement and the strength of the chemical bonds. The vibrational spectrum is characterized by the following regions: X-H stretch (3700-2500 cm^{-1}), XΞY stretch, X=Y=Z asymmetric stretch (2500-2000 cm^{-1}), X=Y stretch (2000-1500 cm^{-1}), X-H deformation (1500-1000 cm^{-1}) and X-Y stretch (1300-600 cm^{-1}) [214]. A simple comparison of the two techniques is provided in Table 2.1.

Table 2.1. Comparison of Raman and FTIR spectroscopy [100]

Raman spectroscopy	FTIR spectroscopy
Aqueous and non-aqueous samples	Non-aqueous samples
Emission of scattered light	Absorption of infrared
Changing of polarizability of covalent bonds like C=C, C-S, S-S and aromatics	Detects dipole and ionic bonds such as O-H, N-H, C=O

2.9.1 *FTIR spectroscopy*

FTIR spectroscopy is a well-established method that can be used for high-throughput experiments that do not destroy samples [101]. The components of an FTIR spectrometer

consist of the infrared source, the interferometer, the detector, calibrating laser and computer (Fig. 2.20). The infrared beam from the source enters the interferometer where an energy diagram pattern is produced called the interferogram. Depending on the type of analysis conducted the beam is transmitted through the sample (or reflected off the sample). Functional groups of molecules within the sample will absorb the infrared radiation. The radiation then passes through to the detector, which continuously monitors the wavenumber range of infrared radiation. Finally, a computer converts the interferogram to an absorption spectrum using a Fourier Transform technique for transformation. The absorption or vibrations of the functional groups can be directly correlated to species found in the sample [101,102]. Samples are usually analysed using the mid-infrared region ($4000 - 600$ cm^{-1}) because the peaks produced in this region are sharp and extremely rich in information. Nucleic acids, carbohydrates, proteins, amino acids and lipids can be detected [101]. FTIR spectroscopy has been successfully used to investigate a variety of questions associated with cells, such as whether different cell types could be distinguished, if the cell cycle stage could be classified and if diseased tissues could be distinguished from healthy tissues. Chemotherapeutic drugs mechanism of action has also been investigated using this type of vibrational spectroscopy [103–108]. Although the procedure is not as specific or sensitive as gas chromatography time of flight mass spectroscopy, the reproducibility and rapid analysis of FTIR cannot be dismissed, since the instrument is more available, user-friendly and more cost effective. The technique is also holistic in the sense that carbohydrates, amino acids, fatty acids, lipids, proteins and polysaccharides can be detected simultaneously. The only major disadvantage is that the absorption of water is intense and can interfere in the regions of interest. This disadvantage is easily overcome by dehydration of samples or subtracting water signals [101].
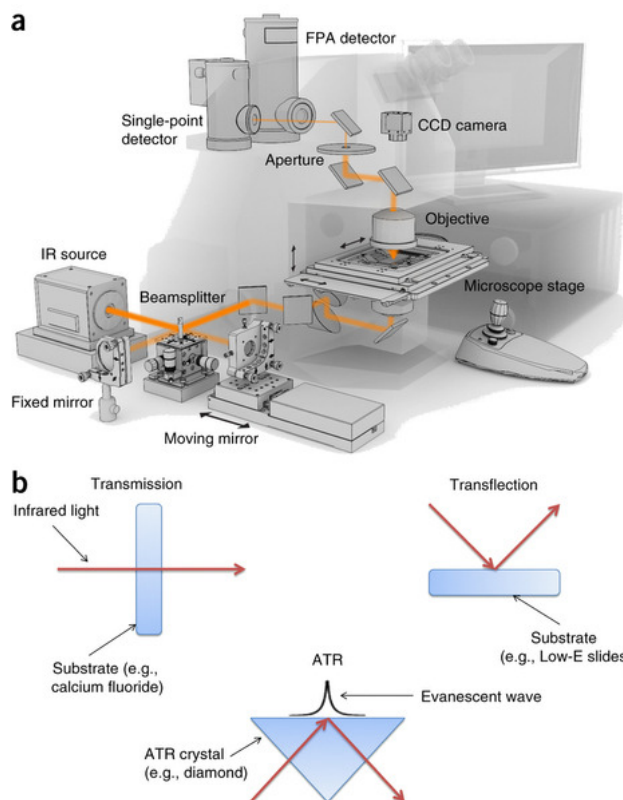
Fig. 2. 20. (a) The different components of an FTIR spectrometer. (b) Different modes of recording FTIR spectra. Taken with permission from [109]**.**

A brief review of cell death analysis using FTIR spectroscopy

A summary of all the literature on cell death detection using FTIR spectroscopy is given in Table 2.2. The treatments of leukemic CEM cells with etopside lead to apoptosis and was assessed using flow cytometry (propidium iodide staining) and infrared spectroscopy by Liu *et al.* (2001). Liu *et al.* found that the vibrational band at amide I (C=O) found in all proteins, shifted from 1635 cm^{-1} to 1657 cm^{-1} in treated cells. Bands associated with DNA such as 968 cm^{-1}, 1087 cm^{-1} and 1240 cm^{-1} (symmetric and antisymmetric PO$_2^-$) and 1713 cm^{-1} (base paired DNA) decreased in absorbance. Apoptosis was also characterized by an increase in lipid associated bands such as the band at 1740 cm^{-1} and between 2800-3000 cm^{-1}. The correlation between the percentage change in protein peaks and caspase activity was reported to be linear, as the protein changes increased so did the caspase activity [110].

Table 2.2. Summary of FTIR bands and assignments associated with cell death induced by various treatments in different cell lines.

Cells	Treatment	Band (cm^{-1})	Assignment	↑/↓[1]	Status	Additional experiments	Ref
CEM	Etopside	968	DNA	↓	Apoptotic	Flow cytometry (PI)	[110]
		1087 & 1240	Symmetric & asymmetric PO$_2^-$	↓			
		1635 and 1657	β-sheets of Amide I to unordered conformation	↓ and ↑			
		1713	Base paired DNA	↓			
		1740	C=O phospholipids	↑			
		2800-3000	Lipid C-H stretching	↑			
LS 102.9/ Jurkat	Jo2 anti-mouse Fas mAb / DX2 anti-human Fas mAb	966	Phosphodiester main chain of DNA/RNA	↑	Apoptotic	Fluorescent microscopy (annexin-V and PI)	[14]
		1054	C-O stretching modes of ribose sugars	↑			
		1084	Symmetric phosphate stretching	↓			
		1177	C-O, C-C, C-O-H, C-O-C deformations of oligo- and polysaccharides or symmetric / asymmetric stretching of CO-O-C groups of phospholipids / cholesterol esters	↑			
		1222	Asymmetric phosphate stretching fully H-bonded(indicative of fragmentation)	↑			
		1234	Asymmetric phosphate stretching	↓			
		1044	C-O, C-C, C-O-H, C-O-C deformations of	↑			
		2850-		↑ (early apoptosis)			

[1] ↑ Increase in absorbance ↓ Decrease in absorbance

		2950	oligo- and polysaccharides or symmetric / asymmetric stretching of CO-O-C groups of phospholipids / cholesterol esters Phospholipids	and ↓ (late apoptosis)			
		1739	C=O ester bond of lipids	↑ (early apoptosis) and ↓ (late apoptosis)			
		1222	Same as in apoptotic				
LS 102.9	Nutrient deprivation	1044	Same as in apoptotic		Necrotic		
		1222					
		< 1657	Amide I band appeared at lower wavenumber	↑[2]			
Jurkat cells	Actinomycin D	2960	CH$_3$ methyl asymmetric stretch of membrane phopholipids	↑	Apoptosis	Flow cytometry	[111]
		2928	CH$_2$ methylene asymmetric stretch of membrane phospholipids	↑		Band correlated linearly with percentage of PS	
		2856	CH$_2$ methylene symmetric stretch of membrane phospholipids	↑			
	1 M HCl in media (pH 4.2)				Necrosis		
HL 60	0.2% Tween 20	1548	Amide II	↑	Necrosis	Light microscopy and trypan blue assay	[112]
		1655	Amide I				
U-937 and CCRF -CEM	Ara-C and doxorubicin	2852	Lipid	↑	Apoptosis	Subcellular fractionation for the determination of proteins Western blot Fluorescent microscopy	[13]
		2923	Lipid				
		966	C-O / C-C stretching of DNA	↓			
		780	DNA	↓			
		1627	B-sheets of	↑			

[2] No wavenumber was given

- 48 -

			Amide I				
U-937	Freeze-thaw / 0.2 mg/mL saponin / KCN	2852	Lipid	↑	Necrosis		
		29231	Lipid	↑			
		966	DNA	↑			
		780	DNA	↑			
U-97 MG	Hypericin combined with radiation	1622	B-sheets of Amide I	↑	Apoptosis	Flow cytometry	[113]
Jurkat	UV light	1122	Lactic acid	↓	Apoptotic	Flow cytometry	[114]
		1397	Amino acid side chains and fatty acids				
	Heat shock	1621	Nucleic acids	↑	Necrotic		

Jamin *et al.* (2003) conducted experiments on mouse hybridoma B cells and Jurkat cells for the induction of apoptosis using antibodies, while late apoptosis (secondary necrosis) was induced by depriving the cells of nutrients. Fluorescent microscopy and synchrotron based IR microscopy was simultaneously conducted on a modified IR microscope. Jurkat cells were stained with annexin-V and propidium iodide. Using the modified IR microscope, cells in different states of cell death were identified. Unstained cells were classified as viable, while early apoptotic cells were classified by only the fluorescence of annexin-V, late apoptotic cells by both the fluorescence of annexin-V and prodpidium iodide and necrotic cells by the fluorescence of propidium iodide. Apoptotic cells had decreased absorbances at 1054 cm^{-1} (C-O vibrations of ribose sugars) and 966 cm^{-1} (phosphodiester bonds of DNA / RNA). Apoptotic cells also showed similar ratios between DNA (1080 cm^{-1} and 1234 cm^{-1}) band areas corresponding to proteins (amide I) as compared to control (viable) cells. Both in early and late apoptotic cells, it was observed that asymmetric and symmetric phosphate stretching vibrations (1234 cm^{-1} and 1084 cm^{-1}) decreased while bands at 1222 cm^{-1}, 1177 cm^{-1} and 1044cm^{-1} increased. The increase at 1222 cm^{-1} was postulated to be due to full hydrogen bonded PO$_2^-$ group which could be related to DNA fragmentation during apoptosis. Late apoptosis was characterized by an increase in the bands 1044 cm^{-1} and 1177 cm^{-1} relative to amide I. In early and late stages the amide I bond shifted upwards by approximately 7 cm^{-1}, that meant an increase in α-helices in relation to β-sheet conformation. Absorbance corresponding to phospholipid vibrations (2850-2950 cm^{-1} and 1739 cm^{-1}) was found to be the highest for cells classified as early apoptotic as compared to late apoptotic

cells which had very low absorbencies. It was postulated that this occurrence could be due to differences of lipids around the nucleus. Symmetric and asymmetric stretching of methylene vibrations (2854 cm^{-1} and 2924 cm^{-1}) relative to symmetric and asymmetric stretching of methyl groups was highest for early apoptotic cells and lowest for late apoptotic cells. When mouse hybridoma B-cells were analysed in the same manner Liu *et al.* (2001) found that the same results were obtained as was found in Jurkat cells. Heterogeneity between cells was also detected by Jamin *et al.* (2003) that showed that the cells were in different stages of cell death when analysed. No statistical analysis was performed, which is crucial to derive significant changes from the data. In many cases, major changes are observed in spectral data, but these results are not always significantly different [110].

Gaudenzi *et al.* (2004) reported on an apoptotic specific marker after Jurkat cells were treated with 50 µM actinomycin D. Necrosis was also investigated that was induced by lowering the pH of cell culture media with 1 M hydrochloric acid to a pH 4.2. The 2800 – 3000 cm-1 region was investigated which after actinomycin D treatment showed absorbance increased for the bands at 2960 cm^{-1} (CH$_3$ methyl asymmetric stretch of membrane phospholipids), 2928 cm^{-1} (CH$_2$ methylene asymmetric stretch of membrane phospholipids) and 2856 cm^{-1} (CH$_2$ symmetric stretch of methylene of membrane phospholipids). The band at 2928 cm-1 was found to be linearly correlated with the % apoptosis in the sample. The authors explained that an increase in CH$_2$ vibrations showed a conformational disorder that was directly related to the number of molecular groups vibrating at the same wavenumber. The bands corresponding to methyl and methylene groups of membrane phospholipids disappeared after treatment.

Yamaguchi *et al.* (2007) developed a method to measure cell death induction in real time using FTIR spectroscopy. Leukemic HL 60 cells were treated with 0.2% Tween 20 that led to rapid cell lysis (therefore necrotic cell death). The amide II band absorbance increased up to 1 hour of incubation after which a plateau was reached [112]. Zelig *et al.* (2009) also investigated externally induced cell death in human leukemic U-937 cells and T lymphoblastic leukemic CCRF-CEM cells. Apoptosis inducers were Ara-C and doxorubicin while necrosis was induced in U-937 cells using the freeze-thaw procedure, 0.2 mg/mL saponin or incubated with KCN. It was found that in apoptotic cells there were an increase in

lipid absorbance at (2852 cm^{-1} and 2923 cm^{-1}) and a decrease in DNA absorbance at 966 cm^{-1} (C-C / C-O stretching of DNA vibrations) and 780 cm^{-1} as well as an increase in β-sheet proteins (1627 cm^{-1}). Saponin, freeze-thawed and KCN necrotic cells had increased lipid absorbance at 2852 cm^{-1} and 2923 cm^{-1} as well as increased DNA absorbance at 966 cm^{-1} and 780 cm^{-1}.

Buriankova *et al.* (2010) treated human glioma U-97 MG cells with hypericin, a photosensitizing pigment isolated from the genus Hypericum species. After cells had been treated with radiation for the activation of hypericin, apoptosis was confirmed by flow cytometry and investigated using FTIR. The most severe changes were identified in the amide I region. Untreated cells had only one band in the second derivatives at 1652 cm^{-1} assigned to α-helices while apoptotic cells had another band appearing at 1622 cm^{-1} assigned to β-sheets. The β-sheets band shifted to 1643 cm^{-1} after 24 hours which was due to the unfolding of proteins into unstructured coils, this was also proven by other researchers.[113]

Di Giambattista *et al.* (2011) induced cell death in Jurkat cells by ultraviolet light (apoptotic cells) and heat shock treatment (necrotic cells). Necrotic cells had an absorbance band at 1621 cm^{-1} (nucleic acids) that was not found in any other apoptotic samples and it was suggested that the band could be used as an indicator of the % necrosis in a heterogenic population. In apoptotic cells, it was found that 1397 cm-1 (amino acid side chains and fatty acids) and 1122 cm^{-1} (lactic acid) was specifically found. The 1397 cm^{-1} protein band was weaker due to methylation processes during cancerogenesis (the initiation of cancer) and a decrease in lactic acid due to its efficient scavenging of reactive oxygen species [114]. To investigate cell death, many of the researchers used suspension cells and only one or two cell death experiments were used with no or minimal statistical analyses. The Proper statistical analysis is needed in such studies because to estimate visually that bands increased or decreased without sufficient reproducibility or statistical evidence, make the results futile.

2.9.2 *Raman spectroscopy*

Raman spectroscopy has been used in industry and engineering since its development as a laboratory technique during the 1970s. Raman spectroscopy characterizes materials

according to their vibrational spectra, which is unique for each material. A Light Amplification by Stimulated Emission of Radiation (LASER) source which emits irradiation that leads to light scattering of an elastic and inelastic nature. The energy spectrum of inelastically scattered light is directly related to vibrational, rotational and other low energy modes specific to the biochemical composition of the substance investigated (Fig. 2.21). These energy modes serve as very specific molecular fingerprints and can be rapidly translated into unique spectral signatures using minute amounts of sample [115]. Raman spectroscopy is complementary to FTIR spectroscopy because similar vibrational groups are detected. Raman spectroscopy has the advantage over FTIR spectroscopy that water does not interfere with the scattering of photons. On the other hand, only approximately one in every 10^6 photons is scattered in an inelastic manner. Weak scattering can be overcome by resonance Raman spectroscopy or surface enhanced Raman spectroscopy [101]. Light scattering is a two photon event where one photon is absorbed and the other photon is emitted. Usually, photons are emitted at the same frequency as the incident photon. This is known as Rayleigh scattering. But photons sometimes loose or gain energy due to molecular interactions and are shifted in frequency. In contrast with Rayleigh scattering, inelastic scattering is categorised as Stokes or anti-Stokes inelastic scattering. During this type of scattering the photon oscillates in response to the photon excitation. The emitted photon is shifted in frequency and the previous electronic ground state is distinctly different [117] (Fig. 2.21 (b)).

(a)

(b)
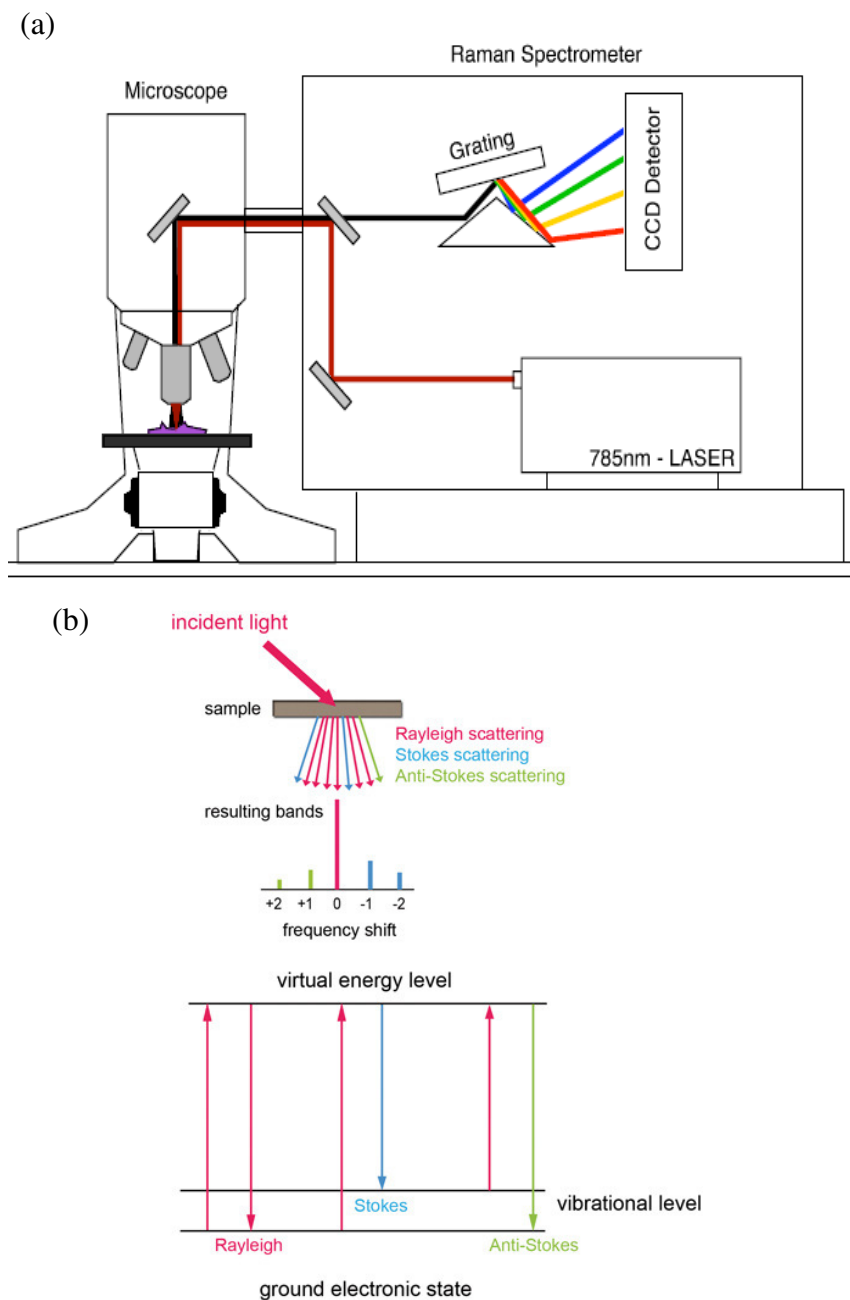
Fig. 2.21.   **The micro-Raman spectrometer and the basic principle of Raman spectroscopy**.   (a) A microscope coupled to the Raman spectrometer focuses the laser through the objective onto the sample. The scattered photons are collected by the same objective to travel to the Raman spectrometer. (b) Types of light scattering, Rayleigh, stokes and anti-stokes scattering and the resulting frequency shifts. Molecular energy levels in relation to the virtual energy level and the ground state. Taken with permission from [116,117].

All diseases and pathological conditions have biochemical and biophysical intracellular characteristics.   Commonly used methods for studying diseases have been electron microscopy, immunocytochemistry and fluorescence microscopy.   All these methods take

time to perform, a large number of cells is required and mostly cells need to be fixated and labelled. Raman spectroscopy on the other hand can be a rapid and non-destructive technique that can be used to study cells and tissues [118], for the identification of bacterial species, diagnoses of different types of cancers based on differences in diseased and healthy cells / tissues and diabetes [101,119].

A brief review of cell death analysis using Raman spectroscopy

Raman spectroscopy has also been employed to investigate cell death induction. Notingher *et al.* (2003) investigated human lung adenocaricoma (A549) cells that naturally perished during cell culture. One of the most prominent cell death indicators was the peak at 788 cm^{-1} assigned to phosphodiester bonds of DNA. The peak decreased dramatically if the cell was dead and that was most likely due to DNA fragmentation. This was also seen in another phosphodiester bond peak at 823 cm^{-1}. Cytosine and thymine (782 cm^{-1}), adenine (1342 cm^{-1}) and guanine (1320 cm^{-1}) assigned together with proteins, decreased, Phenylalanine (1005 cm^{-1}) also dramatically decreased indicating that the amino acid was degraded, or phenyl groups were degraded. It was suggested that the decrease in the intensity of 1231 cm^{-1} assigned to random coils was an indication that cell death was associated with α-helices and β-sheets. Decreases in 1324 cm^{-1} and 1005 cm^{-1} were associated with caspase activation. An increase in the peak at 1743 cm^{-1} (C=O of lipids) was also suggested as being related to induced cell death.[11,12] Findings on the secondary structure of amide I was contradictory to the findings of FTIR spectroscopy where most researchers found that random coils and β-sheets were associated with apoptosis, but in this case, it was still apoptosis. Human gastric carcinoma cells were treated by Yao *et al.* (2009) with the apoptosis inducer, 5-fluorouracil. After microscopy, the cells were analysed using Raman spectroscopy. It was found that apoptotic cells had lower Raman intensities for several peaks associated with DNA such as; 782 cm^{-1}, 1092 cm^{-1}, 1320 cm^{-1}, 1340 cm^{-1} and 1576 cm^{-1}. Decreased intensities for 1655 cm^{-1} (amide I) was also recorded [120].

Ong *et al.* (2012) induced apoptosis and necrosis in human chronic myelogenous leukemia (K562) cells. Apoptosis was induced by treating the cells with 300 µM cytosine arabinoside and necrosis by treating the cells with 100 µM triton X-100. An increase in the peak at 734 cm^{-1} (choline group of phospholipids) was observed in apoptotic cells while the peak

decreased in necrotic cells. An increase showed that membrane lipids increased while a decrease in necrotic cells were related to a decrease in the number of membrane lipids. In apoptotic cells DNA related peaks at 794 cm^{-1} (O-P-O) and 1098 cm-1 (PO$_2^-$ nucleic acids backbone) decreased in intentsity while necrotic cells also additionally had a decrease in 1356 cm^{-1} (purine bonds of polynucleotides) peak. The phenylalanine peak decreased in necrotic cells while no apparent changes were observed in apoptotic cells.

Table 2.3. Summary of Raman spectroscopic investigations of cell death in different cell lines due to a variety of cellular stressors.

Cell	Treatment	Peak (cm^{-1})	Assignment	Intensity [3]	Status	Additional experiments	Ref
A549	Naturally perished in culture	788	Phosphodiester bonds of DNA	↓	Apoptosis		[12]
		823	Phosphodiester bonds of DNA	↓			
		782	Cytosine and Thymine	↓			
		1342	Adenine	↓			
		1320	Guanine	↓			
		1005	Phenylalanine	↓			
		1231	Random coils (protein)	↓			
		1743	C=O (lipids)	↓			
SGC-7901	5-Fluorouracil	782	DNA related	↓	Apoptosis	Fluorescent microscopy	[120]
		1092					
		1320					
		1340					
		1576					
		1655	Amide I				
K562	Cytosine arabinoside	734	Choline group phospholipids	↑	Apoptosis	Fluorescent microscopy / trypan blue	[121]
		794	O-P-O	↓			
		1098	PO$_2^-$ nucleic acids	↓			
		1462	CH2 (lipids and protein)	↑			

---

[3] ³ ↑ Increase in intensity ↓ Decrease in intensity

Cell	Treatment	Peak (cm^{-1})	Assignment	Intensity[3]	Status	Additional experiments	Ref
		1672		↑			
	Triton X-100	734	Choline group phospholipids	↓	Necrosis		
		794 / 1098 / 1356	Purine bonds				
		1005	Phenylalanine	↓			
		1462	CH2 (lipids and protein)	↑			
		1672		↑			
Breast and prostate cancer	Starved	718	Phospholipids	↑	Autophagy		[122]
		937 / 1005	Proteins / Phenylalanine	↓			
Saos-2 and SW-1353	Room temp for 7 days	1375	Progression of nuclear condensation	↑	Apoptosis		[123]
		1003	Phenylalanine	↓			
		1450		↓			
		1658		↓			
	Heat shock	1375	Progression of nuclear condensation	↑	Necrosis		
Jurkat		2850	CH3 symmetric stretching lipids	↓	Cell death (necrosis)	Trypan blue	[124]
		2875	CH2 asymmetric stretching of lipids	↓			
MDA-MB-231	Etopside	788	DNA	↑	Apoptosis	Immunohistochemical staining and fluorescence microscopy	[125]
		1659	C=C stretching of lipids	↑			
A549	Etopside	1158	CC stretching of lipids	↑	Apoptosis	MTT and western blot	[126]
		720	Symmetric stretching of choline group in phosphatidylserine	↑			
		788	O-P-O backbone of DNA	↓			
Jurkat	Doxorubicin	1266, 1303, 1445, 1656, 1740	Lipid related	↑	Initial apoptotic signals (24 hours incubation		[127]

Cell	Treatment	Peak (cm^{-1})	Assignment	Intensity [3]	Status	Additional experiments	Ref
					with drug)		
		785, 1092, 1340, 1578	DNA related signals	↓	Early apoptosis (incubation with the drug for 48 hours)		
		785, 1094, 1215, 1378, 1578	DNA related	↑	Apoptosis - 72 hours incubation		
		1004	Phenylalanine	↑			
DU 145	Irradiation	784	Uracil, Cytosine, Thymine, O-P-O backbone	↑	Apoptosis	Cell cycle analysis and viability using PI	[128]
		811	O-P-O of RNA	↑			
		1421	CH$_2$ backbone of DNA	↓			
		1486 ——— 1577	Adenine and guanine	↑			
		759 / 853	Tyr ring	↓			
		936	C-C stretching (protein)	↓			
		1003	Phenylalanine	↓			
		1032	C-H Phenylalanine	↓			
		1127	C-N	↓			
		1230	Amide III random coil	↑			
		1267	Amide III α-helix	↑			
		1660	Amide I α-helix	↑			
		719	Choline	↑			
		811	O-P-O stretching	↑			
		975	Head C-C stretching (lipids)	↑			
		1127	Chain C-C stretching (lipids)	↑			
		1300, 1438, 1460	CH2 vibrational modes	↓			

The CH_2 bending vibrations of lipids and proteins (1462 cm^{-1}) and the peak at 1672 cm^{-1} decreased in necrotic cells and increased in apoptotic cells. No reduction in glycogen was observed for apoptotic cells and a reduction in glycogen was found in necrotic cells. Ong *et al*. (2012) summarized the finding as; protein decreased significantly in necrotic cells compared to viable cells and apoptotic cells, the phosphate backbone increased significantly in apoptotic cells and decreased significantly in necrotic cells compared to viable cells, DNA peaks decreased significantly in apoptotic cells compared to viable cells while necrotic cells had an even lower intensity as compared to apoptotic cells [121].

In general, autophagy associated cell death had not been extensively investigated. Isabelle *et al.* (2013) reported in a review article that autophagy is commonly induced by metabolic stressors, which might be an adaption of cancer cells to survive in suboptimal microenvironments. Those suboptimal microenvironments include hypoxic conditions, starvation and the cytotoxic insults of chemotherapeutics. Autophagy in starved breast and prostate cancer cells was characterized by an increase of the peak at 718 cm^{-1} associated with phospholipids. The reason for this could be the formation of autophagosomes. A decrease in the phenylalanine peak and 937 cm^{-1} could be related to autophagic degradation of proteins [122].

Brauchle *et al.* (2014) investigated apoptotic and necrotic cells by using a modified Raman microscope that was also capable of fluorescence microscopy. Two different adherent cell lines were used in the study namely Saos-2 and SW-1353. Apoptosis was induced by leaving the cells at room temperature for up to 7 days and the cells then harvested from the supernatant. Heat shock induced necrosis. In Saos-2 and SW-1353 cells, a new Raman band featured at 1375 cm^{-1} in early apoptotic cells and became more prominent in late apoptotic cells. This peak was also increased in necrotic cells. Late apoptotic Saos-2 cells had decreased intensities as compared to viable cells at 1003 cm^{-1} and 1450 cm^{-1} which were also prominent in SW-1353 cells together with a decrease in the 1658 cm^{-1} peak. Necrotic Saos-2 cells had an increased intensity for phenylalanine; a shift also occurred in the amide I as well as an intensity increase. Glycogen (1052 cm^{-1}) peaks were not detected in any of the necrotic cells of both cell lines. All of the peaks that were detected by Brauchle *et al.* were known for the particular types of cell death, except for the peak at 1375 cm^{-1} which was identified in

apoptotic and necrotic cells. It was postulated that an increase in the peak was due to progression in nuclear condensation. The peak had not been previously identified to be associated with cell death, but rather found in peripheral blood cells and isolated chromosomes [123].

Heterogeneity of cells in a cell population is one of the major problems of investigating single cells. Heterogeneity between cells could be due to the different areas being interrogated by the laser and / or even the cell cycle stage and the cell culture confluency in which the cells are being grown in before the investigation [128]. On the other hand, cancer cells are also heterogeneous in their response to cytotoxins which depends on the sensitivity of individual cells to the treatments. It has been found that cancer cells would undergo apoptosis at different time points in one population, even if the cells were all treated at the same time [10,95,127]. Adequate numbers of cells should be investigated to decrease the variability of the measurements of individual cells while biochemical assessment could also help in determining how heterogeneous a population is for specific markers / processes.

2.10   Statistical analysis of vibrational spectroscopy data

Both FTIR and Raman spectroscopy produce spectra that contain a complex array of information. Many of the visible bands are combinations of multiple overlapping bands and thus data interpretation cannot always rely on the visual inspection. Multivariate data are generated from infrared and Raman experiments that consist of numerous different variables (wavenumbers) for a number of treatments. Multivariate data analysis aims to simplify huge data sets. This data reduction can be done in two ways; unsupervised or supervised learning algorithms. Unsupervised methods such as Principal Component Analysis (PCA) and hierarchical cluster analysis visualises the differences and similarities in the data. Most FTIR and Raman experiments contain tiny amounts of sample numbers as compared to the variables (wavenumbers) and thus PCA and hierarchical cluster analysis is most suited. Supervised methods can only be used when some sample information is known [101]. PCA is built on the assumption that variation implies information: It replaces the original several hundred wavenumbers with just a very few major new variables or principal components (PCs). PCs are automatically listed in order, according to how much of the original data variance is accounted for by each one. For each spectrum obtained, each of the many

readings (one for each wavenumber) is replaced by a ''score,'' one for each PC. Thus in a scores plot, each set of measurements (spectrum) appears as a single point in a dimensional space. PCAs allow one to identify the wavenumbers that contribute to inter-spectral variation; plots are showing the extent to which each wavenumber contributes to a given PC provide the necessary pseudo-spectrum or loadings plot.[129]

2.11   Hypothesis

The work undertaken here sought to investigate the hypothesis that vibrational spectroscopic assessment of cell death associated molecules should identify complementary markers as those reached using conventional biochemical methods.

2.12   Primary objective

- To compare conventional cell death detection assays (XTT, RT-CES and flow cytometry) to vibrational spectroscopy, during cell death analysis.

2.13 Aims

- To determine the degree of cytotoxicity of the selected cell death inducers (metallodrugs and naturally derived crude extract and compound) and to determine the selectivity of the treatments in HeLa and Vero cells.

- To determine whether FTIR microspectroscopy could successfully distinguish between different types of cellular injury induced by a potentially anticancerous plant extract, *P. ciliatus.*

- To determine whether Raman spectroscopy could be used for the characterization of metallodrug-induced cell death.

- To determine whether detected apoptosis was caspase-dependent.

- To determine whether FTIR- and Raman spectroscopy could distinguish between

viable and dead FACS sorted cells using two different cell lines and a variety of cell death inducers.

◆ To determine whether the cell sorting was successful using TEM analysis.

2.14 Workflow
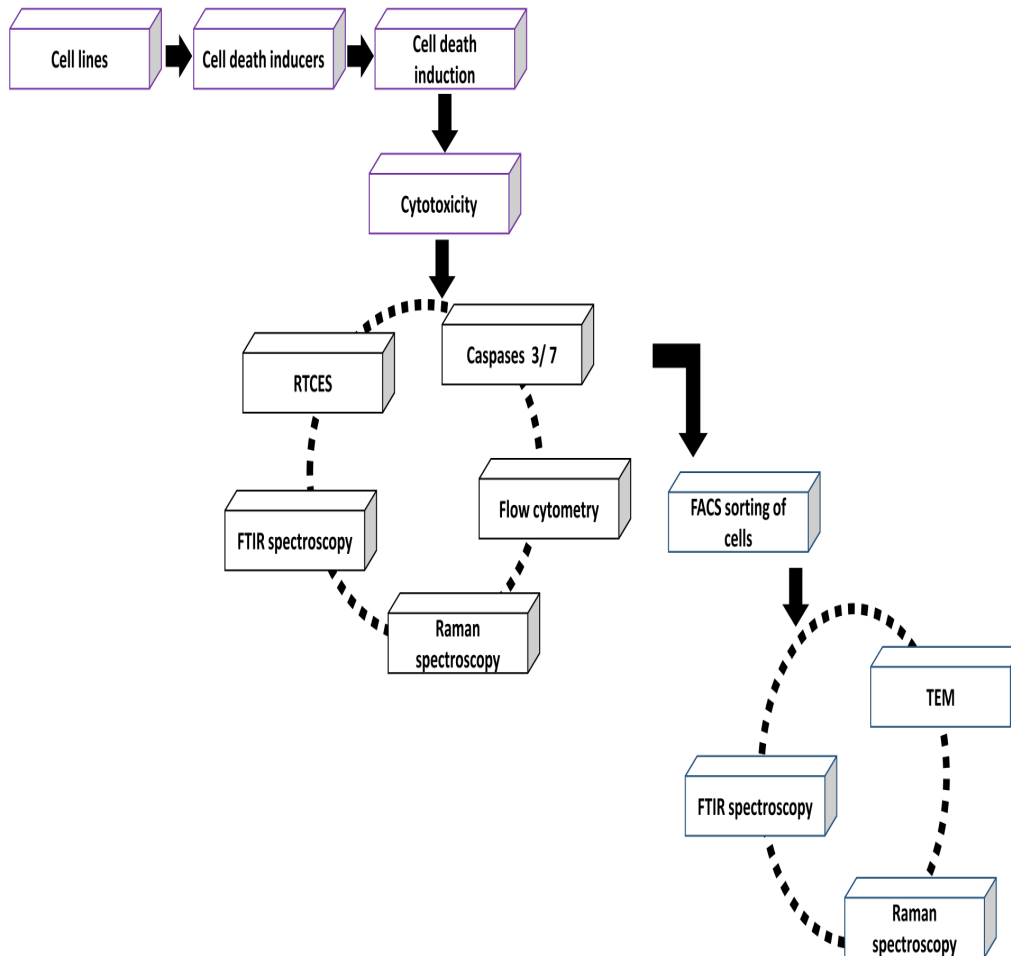
Chapter 3: Cytotoxicity of selected cell death inducers

Abstract

Chemotherapeutic research for different cancers involves an investigation of the cytotoxicity of the proposed drug in comparison to known cell death inducers. The experimental treatments in this case were inorganic (two gold complexes) and organic (an ethanolic extract of *Plectranthus ciliatus*). Also included were the following positive controls auranofin and actinomycin D. Auranofin is a known rheumatoid arthritis treatment known to be very cytotoxic while actinomycin D is a known cancer drug used in *in vitro* studies. The aim of the study was to quantify and determine the selectivity of the treatments in terms of cytotoxicity against cancerous cervical carcinoma (HeLa) – and noncancerous African monkey kidney (Vero) cells. Cytotoxicty was assessed using a tetrazolium salt assay, sodium 3'-[phenyl amino-carbonyl)-3,4-tetrazolium]-bis-[4-methoxy-6-nitro) benzene sulfonic acid hydrate (XTT). Viability dyes usually serve as a preliminary screening methodology for cytotoxicity but because of its reproducibility and cross-reactivity limitations, data sets collected in this manner are later confirmed by more sensitive analysis (e.g. Real Time Cell Electronic Sensing (RT-CES) and Fluorescence Activated Cell Sorter (FACS)). Noteworthy cytotoxicities were detected with all of the treatments with the Cytotoxic Concentration inhibiting the proliferation of 50% of the cell population (CC_{50}) values for the metallodrugs being < 11 µM in HeLa cells (auranofin = 2.79 ± 0.89 µM, AE 76 = 10.39 ± 0.25 µM and AE 125 = 8.94 ± 1.36 µM) and < 7 µM in Vero cells (auranofin = 1.45 ± 0.05 µM, AE 76 = 6.62 ± 0.22 µM and AE 125 = 6.93 ± 0.43 µM). The natural derived (plant extract and positive control derived from *Streptomyces* species) treatments also showed good cytotoxicities with CC_{50} values < 10 µg/mL (acinomycin D = 0.02 ± 0.005 µg/mL and *P. ciliatus* = 9.23 ± 0.17 µg/mL) in HeLa cells and < 20 µg/mL (acinomycin D = 0.11 ± 0.02 µg/mL and *P. ciliatus* = 19.85 ± 1.52 µg/mL) in Vero cells. Because the selected cytotoxicity inducers were being developed as potential anti-cancer agents, the National Cancer Institute (NCI) guidelines for active crude extracts (CC_{50} < 20 µg/mL) and pure compounds (CC_{50} < 10 µM) were used to define activities as potential anticancer drug candidates. The selectivity indices of all treatments were below 6, which indicated that cancer cells were more sensitive to the

treatments and, therefore, died more readily as compared to healthy cells. Actinomycin D had the highest selective index (SI = 5.5) while auranofin had the lowest (SI = 0.5). The data collected was used as a guideline in more sensitive assays.

3.1 Introduction

To investigate cell death, it was necessary to determine the degree of toxicity of the selected cell death inducers. If the cell death inducers are eventually to become cancer treatments the Selectivity Index (SI) of the compounds must be assessed as well. The SI is defined as the ratio of cytotoxicity of noncancerous cells to the cytotoxicity of cancerous cells for a particular treatment [9,61].

The cell death inducers that were chosen for this study were categorized into synthetic metallodrugs and naturally derived treatments. These two categories are part of the major classes of compounds used for drug discovery in cancer treatments. Metallodrugs are derivatives of bioactive parent molecules and include a variety of different metals, including platinum, silver and gold [47]. In this investigation, two gold compounds were investigated for their ability to induce cell death. Metallodrugs sparked the interest of cancer researchers when a breakthrough was reached in 1978 when cisplatin (Fig. 3.1 (a)), a platinum drug was successfully used to treat a number of malignancies including testicular, head, neck and bladder cancers [130]. Gold have been used for centuries for the treatment of different ailments, but the investigation of gold based compounds as potential cancer treatments only started in 1980 [41,131]. Derivatives containing the linear P – Au – S structure, as found in auranofin (Fig. 3.1 (b)) demonstrated the potential for treating cancer. Auranofin was originally developed for the treatment of rheuthatoid arthritis but was then also part of the inspiration for investigating gold (I) complexes for their anti-cancer potential. It was found that gold (I) complexes had anti-inflammatory and immunosuppressive activities which not only made them useful for the treatment of arthritis but also cancer [131]. Auranofin was a positive control for comparison to two diphenylphosphino complexes (experimental samples).

(a)   **(b)**
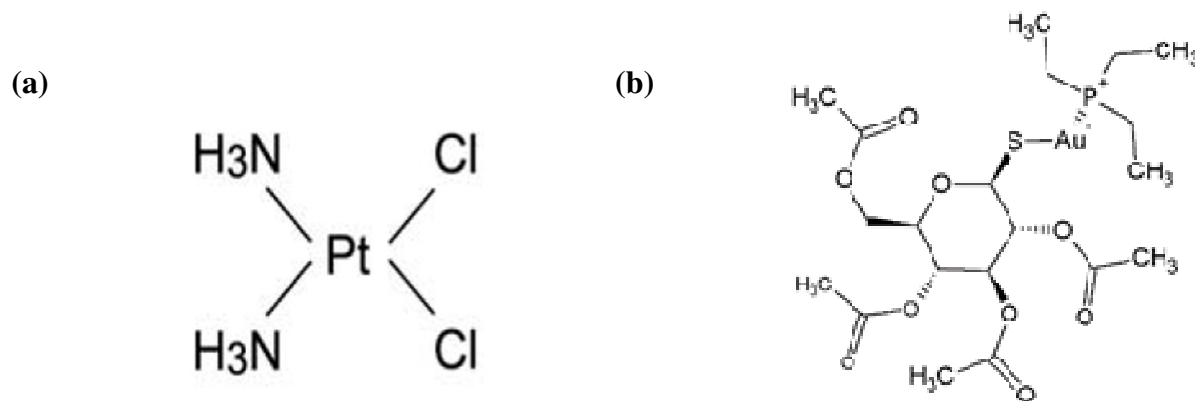
Fig. 3.1. The chemical structures of (a) cisplatin and (b) auranofin. Taken with permission from [43,46].

Organic drug discovery research is flourishing since western scientists started acknowledging the importance of traditional medicine. Traditional medicine has been practiced worldwide for centuries, for example, the well-known practices of Chinese traditional medicine, auyrveda (Indian traditional medicine) as well as African traditional medicine. These medicines are now scientifically evaluated to determine the bioactive compounds in the traditionally used crude extracts and to determine the safety and efficacy of such products. In this study, the plant being evaluated was *Plectranthus ciliatus* a herbaceous plant from the family Lamiaceae (Fig. 3.2 (a)). The plant's anti-neoplastic activity was previously demonstrated by our group [3]. In traditional medicine plants of this genus are used to treat ailments of the digestive tract, respiratory system, muscular skeletal and nervous systems, inflammation, cancers, infections and pain [5]. Actinomycin D was used as a positive control for naturally derived products since it is isolated from *Streptomyces* species and used for treating a variety of cancers (Fig. 3.2 (b)) [49,62]. The aim of this study was to determine the degree of cytotoxicity of the selected metallodrugs and naturally derived treatments and to determine the selectivity of the treatments against the proliferation of HeLa and Vero cells.
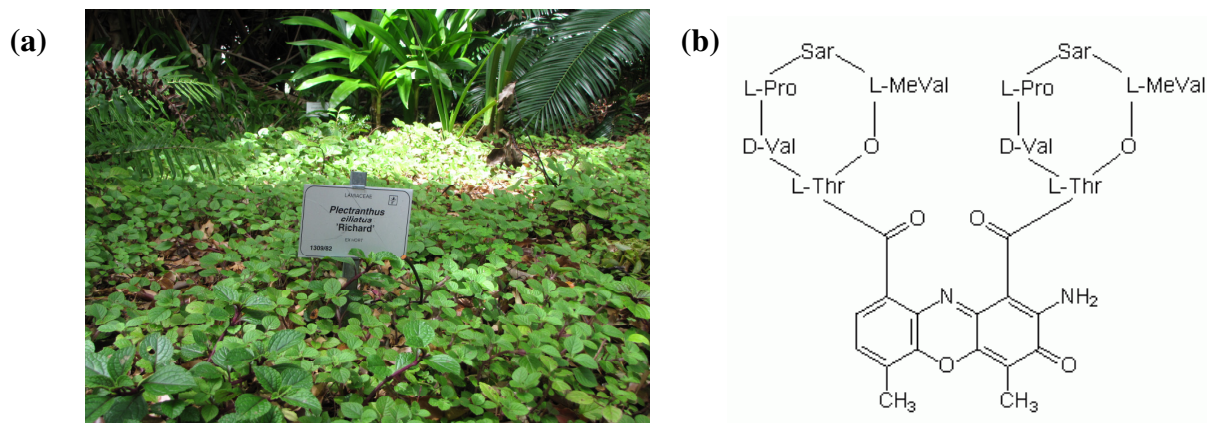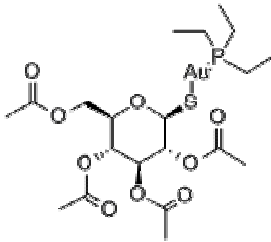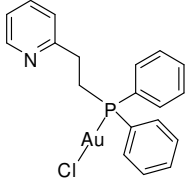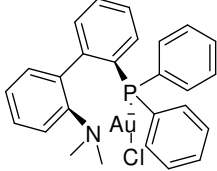
Fig. 3.2. **Photo of *Plectranthus ciliatus* and the chemical structure of actinomycin D.** Taken with permission from S. Hariparsad and [66].

3.2 Methodology

Cell death inducers utilized here were developed for other projects in the group and is described in detail elsewhere [3,4,48]. These materials were selected based on severe toxicity on a variety of different primary and secondary cell lines. Prof. Darkwa kindly donated the two gold (I) complexes, Department of Chemisty, University of Johannesburg, South Africa having been synthesised and characterized by A. Elkhadir [48]. The positive control, auranofin was obtained from Sigma Aldrich (Germany) (Table 3.1). *Plectranthus ciliatus* leaves were collected in Pretoria, South Africa during April 2011. The plant material was identified by Ms. M. Nel at the Department of Plant Science, University of Pretoria and a voucher specimen was deposited in the Schweickerdt Herbarium, Pretoria, South Africa. The crude extract was kindly donated by Ms. P. Kapewangolo, Department of Biochemistry, University of Pretoria.[3] Briefly, fresh leaves of *P. ciliatus* were homogenised and extracted with distilled ethanol. The menstruum was filtered and concentrated under reduced pressure with a vacuum rotary evaporator (Buchi, Germany). The crude extract was stored at 4°C. The crude extract stock solution was freshly prepared by dissolving it in dimethyl sulfoxide (DMSO) (Sigma, Germany) before each experiment.

Table 3.1. List of metallodrugs with full names, molecular weights and the chemical structures.

Metallodrug	Full Name	MW (g/mol)	Structure
Auranofin	1-Thio-β-D-glucopyranosatotriethylphosphine gold-2,3,4,6-tetraacetate, 3,4,5-Triacetyloxy-6-(acetyloxymethyl) oxane-2-thiolate triethylphosphanium	678.48	
AE 76	2-(2-(diphenylphosphino)ethyl)pyridyl-gold(I) chloride	523.7462	
AE 125	2-(diphenylphosphino)-2'-(N,N-dimethylamino)biphenylgold(I) chloride	613.8688	

HeLa cells were maintained in culture flasks in Minimum Essential Medium (MEM), supplemented with 5% heat-inactivated foetal bovine serum (FBS) and antibiotic cocktail (100 U/mL penicillin, 100 µg/mL streptomycin and 250 µg/L fungizone). Cells were grown and maintained in a humidified incubator at 37°C and 5% CO_2. Cytotoxicity was measured with XTT - Cell Proliferation Kit II (Roche Diagnostics GmbH, Germany) as previously described [61]. Briefly cells (100 µL) were seeded (105 cells/mL) into the wells of a 96 well microtitre plate and incubated for 24 hours to allow the cells to adhere. Dilution series were prepared of the plant extract (0.625-80 µg/mL) and 100 µL were added to the microtitre plate and incubated for 72 hours. All controls such as actinomycin D (apoptotic cell death inducer), untreated cells and vehicle (DMSO – tested at 0.09%) controls were included. After the cells had been incubated for 72 hours, XTT reagent (50 µL) was added to a final concentration of 0.3 mg/mL and the plates incubated for one hour. After incubation, the absorbance of the formazan colour was spectrophotometrically quantified, which measured the absorbance at 450 nm with a reference wavelength of 690 nm. The assay was carried out in triplicate and done three times independently. The results were statistically analysed with GraphPad Prism 5 software (GraphPad Sotfware Incorporated, United States of America) to determine the CC_{50} values. The absorbance values of vehicle treated cells were used as a 100% cell viability parameter. The CC_{50} values were expressed as the mean of three

independent assays and the variability as the standard error of the means (SEM). The SI value was calculated based on the ratio of noncancerous (Vero) cells CC_{50} value to the CC_{50} value of cancerous (HeLa cells) [9].

3.3 Results and discussion

The tetrazolium salt, XTT was used to determine the level of cytotoxicity of the selected treatments. Concentration dependent cellular responses were detected and are depicted in Fig 3.2 and Fig. 3.3 for all the cell death inducers for HeLa and Vero cells respectively. The metallodrugs had very similar trends in the concentration dependent responses while the naturally derived products had a more predictable trend which also deviated in some concentrations.

(i) <u>HeLa cells:</u> It was found that the two positive cell death inducers, auranofin and actinomycin D had superb bioactivity against the proliferation of HeLa cells (Table 3.2). These superb bioactivities were expected since auranofin is known to be extremely toxic because of its known side effects in patients treated with rheumatoid arthritis while actinomycin D is a known clinical cancer chemotherapeutic. The metallodrugs also decreased proliferation of the HeLa cells, although the cytotoxicity of the compounds was approximately fourfold (AE 125) and fivefold (AE 76) lower compared to auranofin. On the other hand the crude extract of *P. ciliatus* had an CC_{50} value of 9.23 ± 0.17 µg/mL against the proliferation of HeLa cells, which is considered noteworthy by the National Cancer Institute of America which recommends that a crude extract should be further evaluated for its anticancer activity when the CC_{50} value against cancerous cells is less than 20 µg/mL [61]. Actinomycin D had a CC_{50} value that was much lower than all the other treatments.
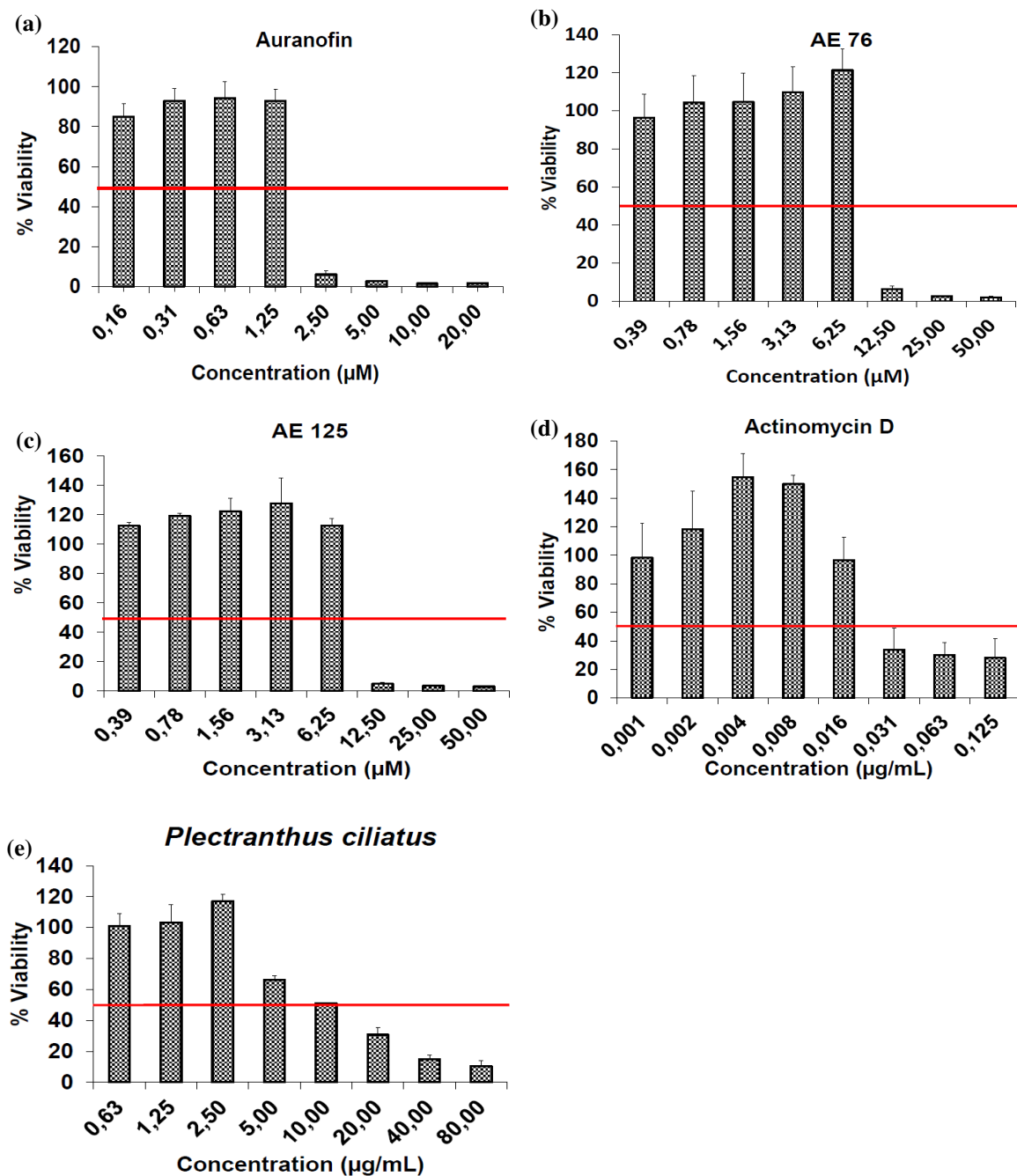
Fig. 3.3. The effect of the selected cell death inducers on the viability of HeLa cells after 72 hours treatment. The viability assay was firstly optimised (results of various concentrations per treatment) and quantified using the XTT assay and it was found that the treatments had a concentration-dependent response on the viability of the cells. The red lines indicate where 50% of the cells were viable. Similar concentration dependent trends are observed for the metallodrugs (a-c) while the naturally derived products (d-e) show a moderate decline in viability as the concentration of the cell death inducer increased. The % viability over a 100% was indicative of proliferation of the cells at low concentrations tested, which is a well known effect of minor stress on a biological system.

(ii) <u>Vero cells</u> were selected as a representative noncancerous cell line. Reasons for selecting this cell line included its similarity to HeLa cells in respect of morphology and growth characteristics (example adherence to tissue culture flask surfaces). Another important aspect of Vero cells is the fact that the cells were derived from the kidneys, which are involved in essential physiological processes such as purifying the blood. The cells responded differently to the various treatments, with the metallodrugs showing higher cytotoxicity as compared to the naturally derived treatments.
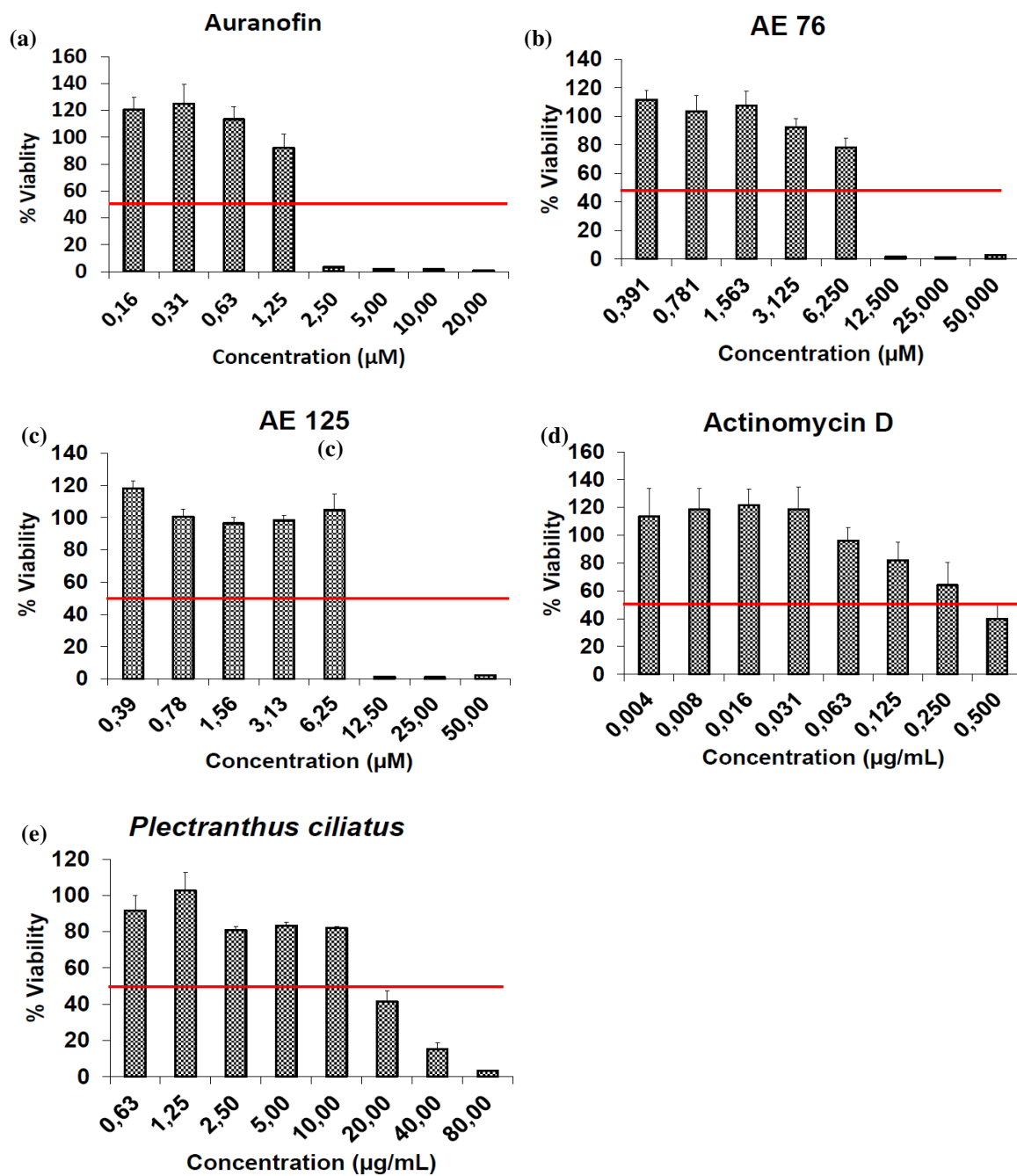
Fig. 3.4. The effect of the selected cell death inducers on the viability of Vero cells after 72 hours treatment. Viability assay was optimised and quantified using the XTT assay. It was found that the treatments had a concentration-dependent response on the viability of the cells. The red lines indicate where 50% of the cells were viable. The metallodrugs elicited a sudden drop in viability at a concentration of 2.5 uM for auranofin (a) and 12.5 uM for AE 76 (b) and AE 125 (c). The naturally derived products (d-e) had a moderate decline in viability as the concentration of the cell death inducer increased.

(iii) **Selectivity Index (SI):**   The naturally derived treatments showed some selectivity with actinomycin D demonstrating the highest SI value. According to Mena-Rejon *et al.* (2009) when the SI value is lower than 10, a cytotoxic cellular response was induced, while if the SI value was 10 or higher, the mechanism of action of the treatments would have been due to another type of mechanism unrelated to cytotoxicity [9]. The best SI value was obtained when the cells were treated with actinomycin D with an SI value of 5.5. This result was in agreement with the finding of Sawicki and Godman (1971) who found that actinomycin D showed good selectivity for HeLa cells compared to Vero cells [64]. It could be concluded that all of the selected treatments were cytotoxic and that the degree of selectivity was best for naturally derived treatments as compared to the metallodrugs. Because auranofin had been successfully used for the treatment of arthritis and showed good anticancer potential [131], it was retained as part of the study. The synthesized AE 76 and AE 125 was more selective than auranofin and, even though, the selectivity was not optimal, these complexes remained part of the study because they were successful in inducing cell death

Table 3.2. The CC_{50} values of the treatments against the proliferation of HeLa cells and Vero cells, as well as the treatments respective SI values.

Cell death inducers	HeLa cells	Vero cells	Selectivity index
Auranofin	$2.79 \pm 0.89\ \mu M$	$1.45 \pm 0.05\ \mu M$	0.5
AE 76	$10.39 \pm 0.25\ \mu M$	$6.62 \pm 0.22\ \mu M$	0.6
AE 125	$8.94 \pm 1.36\ \mu M$	$6.93 \pm 0.43\ \mu M$	0.8
Actinomycin D	$0.02 \pm 0.005\ \mu g/mL$	$0.11 \pm 0.02\ \mu g/mL$	5.5
Plectranthus ciliatus	$9.23 \pm 0.17\ \mu g/mL$	$19.85 \pm 1.52\ \mu g/mL$	2.2

It can be concluded that the selected treatments had noteworthy cytotoxicities and were suitable for further study in terms of cell death induction. The rest of the research was carried out using all of the cell death inducers. The data collected here served as a guideline for the concentrations of cell death inducers to use in more sensitive assays. These sensitive assays included RT-CES and flow cytometry. In Chapter 4, a comparison of the type of cellular injury induced by naturally derived treatments is investigated by comparing the data obtained with RT-CES with FTIR spectroscopic data. In Chapter 5, cell death induced by metallodrugs is investigated using flow cytometry and Raman spectroscopy. In Chapter 6 and 7, all treatments (metallodrugs and naturally derived compounds) investigated in these chapters are used to induce cell death that was investigated by Transmission Electron

Microscopy (TEM) and vibrational (FTIR and Raman) spectroscopy to find new biomarkers of cell death.

Chapter 4: Cellular injury evidenced by impedance technology and infrared microspectroscopy

Published in:

Spectrochimica Acta Part A: Molecular and Biomolecular Spectroscopy

Abstract

Fourier Transform Infrared (FTIR) spectroscopy is finding increasing biological application, for example in the analysis of diseased tissues and cells, cell cycle studies and investigating the mechanisms of action of anticancer drugs. Cancer treatment studies routinely define the types of cell-drug responses as either total cell destruction by the drug (all cells die), moderate damage (cell deterioration where some cells survive) or reversible cell cycle arrest (cytostasis). In this study the loss of viability and related chemical stress experienced by cells treated with the medicinal plant, *Plectranthus ciliatus,* was investigated using real time cell electronic sensing (RT-CES) technology and FTIR microspectroscopy. The use of plants as medicines is well established and ethnobotany has proven that crude extracts can serve as treatments for various ailments. The aim of this study was to determine whether FTIR microspectroscopy would successfully distinguish between different types of cellular injury induced by a potentially anticancerous plant extract. Cervical adenocarcinoma (HeLa) cells were treated with a crude extract of *Plectranthus ciliatus* and cells monitored using RT-CES to characterize the type of cellular responses induced. Cell populations were then investigated using FTIR microspectroscopy and statistically analysed using One-way Analysis of Variance (ANOVA) and Principal Component Analysis (PCA). The plant extract and a cancer drug control (actinomycin D) induced concentration dependent cellular responses ranging from nontoxic, cytostatic or cytotoxic. Thirteen spectral peaks (915 cm^{-1}, 933 cm^{-1}, 989 cm^{-1}, 1192 cm^{-1}, 1369 cm^{-1}, 1437 cm^{-1}, 1450 cm^{-1}, 1546 cm^{-1}, 1634 cm^{-1}, 1679

cm^{-1} 1772 cm^{-1}, 2874 cm^{-1} and 2962 cm^{-1}) associated with cytotoxicity were significantly (p value < 0.05, one way ANOVA, Tukey test, Bonferroni) altered, while two of the bands were also indicative of early stress related responses. In PCA, poor separation between nontoxic and cytostatic responses was evident while clear separation was linked to cytotoxicity. RT-CES detected morphological changes as indicators of cell injury and could distinguish between viable, cytostatic and cytotoxic responses. FTIR microspectroscopy confirmed that cytostatic cells were viable and could still recover while also describing early cellular stress related responses on a molecular level.

4.1 Introduction

Fourier Transform Infrared spectroscopy is a label free, non-destructive, high throughput method which is growing in popularity as the applications increase. The applications of the technique include structure elucidation of compounds [132] and peptides [133,134], identification of different bacterial strains [135,136] and antimicrobial compounds affecting bacterial viability [137], the discrimination of diseased and healthy tissues or cells [103,104,129], cell cycle analysis [105], the effects of known toxins on cells [138] and the identification of molecular targets of natural and synthetic anticancer drugs [106–108,139].

Anticancer drugs under development are generally tested *in vitro* to determine whether they can be classified as non-toxic (no or limited cell death caused), cytostatic (arrest of cell proliferation but the cells are essentially still alive) or cytotoxic (considerable cell death induced by the treatment). Cytostatic responses are usually employed to stop uncontrolled tumour growth while cytotoxic responses lead to cell death caused by apoptosis, necrosis or cell lysis [140]. Cytostatic and cytotoxic behaviour plays an important role in the progression of a drug into preclinical and clinical studies. Cytostatic drugs have been found to be metastases preventative and increase the survival rates of patients by delaying the time to disease progression [67]. Cytotoxic drugs, on the other hand, are less selective and the induced cell death could be more detrimental to the patient in terms of side effects. Rixe and Fojo (2007) found that a drug elicited either cytostatic or cytotoxic cellular responses depending on its active concentration [67].

Classifications of cytostasis / cytotoxicity are usually decided following a spectrophotometric assessment of cell viability in the presence of the drug and a labelling agent, but the use of spectroscopy in the absence of labels is gaining momentum. Conventionally, biochemical labels such as trypan blue, tetrazolium salts and fluorochromes are used to measure a single parameter such as; membrane integrity, enzymatic reactions and intra- or extracellular markers. The major disadvantage of labels is that the experiment becomes an end point analysis measuring only one or a few parameters at a particular time point after which the cells are destroyed. Biochemical labels are also very expensive and can sometimes crossreact with other molecules. Accordingly, new label free methodologies that are less time-consuming and more comprehensive in evaluating multiple cellular components should be developed.

One of the popular label free assays currently in use is RT-CES. The principle of the instrument is based on the growth of adherent cells on gold electrodes. Impedance changes associated with the cells behaviour is measured continuously. When cells initially attach to the electrodes the impedance (electrical resistance) increases, causing an increase in the unit less Cell Index (CI). The CI will increase as the resistance increases, which are due to the cells proliferating or spreading out within the culture well. When a toxin is added to the wells, the cellular response can be measured continuously. Thus, any change in cell size and shape is monitored by changes in the CI. Generally a decrease in CI values could be due to cell volume decreasing, cells rounding up during the activation of cell death or the detachment of cells which leads to a decrease in resistance measured by the electrodes [79]. This technique successfully characterized the type of cellular responses of importance in our research group [80,82] as well as others [98,140–142].

In a previous study, we found that Raman micro-spectroscopy could be used to pre-screen a plant extract for its anticancer activity against the proliferation of leukemic U-937 cells [143]. Since FTIR spectroscopy is complementary to Raman spectroscopy and Raman spectroscopy only interrogates one cell at a time, we set out to determine whether FTIR could distinguish viable from cytostatic and cytotoxic responses in a given cell population following exposure to a cell death inducer. Many publications focus on the cytotoxic drugs and plant extracts or compounds affecting FTIR spectra of treated cells [107,108,138,144,145] while little research had been done on cytostatic responses [139].

In the evaluation of FTIR spectroscopy as a tool for the screening of anticancer drug responses, a cell death inducer is required. In this case, a South African traditional medicinal plant was selected. Medicinal plants have long been studied for their effectiveness in treating cancer. Crude extracts of medicinal plants are more potent cytotoxins because of the synergy of the many phytochemicals found in the mixture [143]. The cell death inducer in this investigation was a leaves extract of *Plectranthus ciliatus*. In traditional medicine, plants from this genus are used to treat ailments of the digestive tract, respiratory system, nervous system, inflammation, infections, pain and different types of cancers [5]. The plant's anticancer activity was previously demonstrated by our group [3]. The aim of this study was to determine whether FTIR microspectroscopy could successfully distinguish between different types of cellular injury induced by a potentially anticancerous plant extract.

4.2 Methods

4.2.1 *Plant material and extraction*

Plectranthus ciliatus leaves were harvested in the Manie van der Schijff botanical garden, Pretoria, South Africa. The leaves were authenticated and a voucher specimen deposited in the Schweickerdt Herbarium, Pretoria, South Africa. The crude extract of the leaves was prepared and kindly donated by Dr. T.P. Kapewangolo, Department of Biochemistry, University of Pretoria. The plant extraction procedure was done as previously described [82]. The crude extract was stored at 4°C until use. Stock solutions were freshly prepared before each experiment by dissolving the plant extract in cell culture tested dimethyl sulfoxide (DMSO) (Sigma, Germany).

4.2.2 *Cell culture*

Human cervix adenocarcinoma (HeLa) cells were purchased from Highveld Biological (Pty) Ltd. (Johannesburg, South Africa) and grown in standard culture flasks in a humidified incubator at 37°C and 5% CO_2. The growth media was Minimum Essential Medium (MEM), supplemented with 5% heat-inactivated foetal bovine serum (FBS) (Hyclone, Separations, Johannesburg, South Africa) and antimicrobial cocktail (100 U/mL penicillin, 100 µg/mL streptomycin and 250 µg/L fungizone) (Hyclone, Separations, Johannesburg, South Africa). The cells were maintained by sub-culturing the cells when 80-90% confluence was reached.

4.2.3 *Real time cell analysis of plant extract treated HeLa cells*

An RT-CES device (Roche Diagnostics, Mannheim, Germany) in a humidified incubator was used to observe the proliferation of the cells in the absence and presence of the selected plant extract. Cell titrations (5 000 – 60 000 cells / well) were done to determine the optimal cell number for the experiments. The specific concentration (1 x 10^5 cells/well) where the optimal exponential growth curve was found, was used for further studies as recommended by Fonteh *et al.* (2011) [80]. Three different concentrations (0.5 x cytotoxic concentration of a treatment affecting 50% of the cell population tested (CC_{50}), CC_{50} and 2 x CC_{50} – determined by the tetrazolium dye XTT, Table 4.1) of the treatments were tested alongside the positive control (actinomycin D). The plant extract was dissolved in DMSO (ensure that all components were solubilized) to a stock solution of 20 mg/mL, while actinomycin D was completely dissolved in only sterile distilled water to a stock solution of 1 mg/mL. Further dilutions were made in complete media before the assays were conducted. Controls; a background (media only, no cells), untreated cells (cells and media) and a vehicle control (DMSO at 0.09%) were included every time. Electronic impedance increases as cells attach to the electrodes and is known as the Cell Index (CI). The cells were incubated in a humidified incubator for approximately 18 hours where the unit less CI ≈ 1, after which the treatments were added to the E-plates, final volume 250 μL. Cells were monitored for a total of 90 hours. Data sets were normalized at the point where cells were treated. The Cell Index was normalized using a build in function of the Roche xCelligence Software 1.2.1. The normalized CI is calculated automatically for each well as the CI at a given time point, divided by the CI at the normalized time point (Normalized $CI_{time} = CI_{time} / CI_{normalized\_time}$). Therefore, the Normalized Cell Index for all wells must be equal one (1) at the normalization time point. Cells exhibited varying response patterns represented by CI changes that either indicated the cells as growing (increasing CI), dying (decreasing CI) or experiencing proliferation arrest (unchanging CI). Three independent experiments were conducted.

Table 4. 1. Concentrations of the cell death inducers used in the RT-CES experiment.

Cytotoxic concentration ratios	*Plectranthus ciliatus*	Actinomycin D
0.5 x CC_{50}	4.5μg/mL	0.01μg/mL
CC_{50} [a]	9μg/mL	0.02μg/mL
2 x CC_{50}	18μg/mL	0.04μg/mL

[a] **Determined by XTT**

Cytotoxic concentrations of the treatment affecting 50% of the cell population tested (CC_{50}) based on RT-CES data were calculated using Roche xCelligence Software 1.2.1. The CC_{50} values were expressed as the mean of three independent assays and the variability between repeats as the standard error of the mean (SEM). RT-CES graphs were used to determine whether the responses to treatment were cytotoxic or cytostatic by using guidelines published by Kustermann *et al.* (2013) [140]. The line at CI = 1 divided the graphs into viable / proliferating cells (CI > 1) and nonproliferating / dying cells (CI < 1) from each other (Fig. 4.1). Three typical graphs were described in Kustermann *et al.* (2013), where the response of cells in the absence or presence of treatments was described. Where the CI was more than 1, the cells were viable / proliferated indicative of cells under no stress. Where the CI < 1 the cells experienced toxicity. Lastly, when the growth curve moved from CI > 1 to a CI < 1 during the observation time the cells could be defined as experiencing cytostatic responses [140].

For the FTIR investigation, methods published by Zelig *et al.* (2009) and Machana *et al.* (2012) were used as a guideline during the optimization of the experiments [13,108]. Exponentially growing HeLa cells were seeded (1 x 10^5 cells) and incubated in 12-well plates. After 24 hours incubation, the cells were exposed to two different concentrations (CC_{50} and 2 x CC_{50}) of the plant extract and actinomycin D respectively (Table 1). Vehicle (0.09% DMSO) and negative control (untreated) cells were included in the analyses. Cells were incubated for 72 hours, after which all the cells were collected from each well. Cells were centrifuged for 10 minutes, the supernatant discarded and the pellets washed twice with 1 mL phosphate buffered saline (PBS) to remove all traces of the culture media. The cells were incubated at room temperature in 1 mL 10% formalin (in PBS) for 10 minutes to fixate the cells. The cells were centrifuged for five minutes and the supernatant discarded. The cells were washed twice with 1 mL of sterile distilled water and centrifuged for three minutes to remove all traces of formalin and PBS, which could influence the spectra. The supernatant was removed and the cells suspended in 10 µL sterile distilled water. The cell suspensions (3 µL) were dried in the biosafety flow hood for one hour on sterile CaF_2 discs (Crystran, UK).

The FTIR spectra were acquired using a Bruker V70x spectrometer equipped with a Hyperion 15x IR objective (Bruker, Germany). Using a liquid nitrogen cooled detector

attached to the microscope, ten areas were analysed containing a lawn of cells (approximately 400 cells / area). Spectra in the range of 850-4000 cm^{-1} were recorded. Data were collected in transmission mode and spectra (4 cm^{-1} spectral resolution, 2 cm^{-1} interval, co-added for 100 scans) recorded using Bruker OPUS software. Three independent experiments were conducted. All the spectra were pre-processed using OPUS 7 software. Atmospheric contributions (water vapour and CO_2) were subtracted and the spectra vector normalized. Baseline correction was done using the rubber band function. Second derivatives were calculated (17 smoothing points using the built in Savitzky-Golay algorithm to improve the signal-to-noise ratio) and used for interpretation and statistical analysis [13]. Second derivatives were analysed to assign accurately and visually maximize differences [13,108].

Average spectra of the treatment groups were constructed and One-way Analysis of Variance (ANOVA) calculated. A $p < 0.05$ was considered significant. Bonferroni multiple comparison tests in conjunction with Tukey post-hoc testing were done in SPSS 20 to determine which variances were significant. An unsupervised method, principal component analysis (PCA) was used to identify trends in the spectra. The data sets were reduced by five principal components and mean centred. The PCA plot was constructed in OPUS 7 while Principal Component (PC) variances were calculated in SPSS 20.

4.3 Results and discussion

In the current study, the effects of a crude extract (*Plectranthus ciliatus* leaves) against HeLa cells proliferation were investigated using FTIR microspectroscopy to distinguish between cytostatic and cytotoxic cellular responses. RT-CES, a well-established technique used for making these distinctions (among others) served as a reference point for the FTIR spectroscopic data.

4.3.1 *Real Time Cell Electronic Sensing of treated HeLa cells*

Distinctions between cytotoxic and cytostatic responses were determined using Kustermann and colleagues (2013) manuscript as a guideline [140] who found the area under the curve to be indicative of the type of cellular response. The analysis model created by Kustermann *et al*. [140] was constructed following on assessment of the behaviour of T3T fibroblast cells

when exposed to three different compounds; Indocine (anti-inflammatory drug, nontoxic), Vandetanib (tyrosine kinase inhibitor, cytotoxic) and Dasatinib (kinase inhibitor, cytostatic affecting cell cycle). The analysis model was then tested by that same research group with 40 known compounds inducing well documented cellular responses *in vivo* and was confirmed to have good correlation with known records.

Graphs were analysed and indicated in Fig. 4.2. The line at CI = 1 divided the graphs into viable / proliferating cells (CI > 1) and nonproliferating / dying cells (CI < 1) from each other (Fig. 4.1). Three typical graphs were described in Kustermann *et al.* (2013), where the response of cells in the absence or presence of treatments was described. Where the CI was more than 1, the cells were viable / proliferated indicative of cells under no stress. Where the CI < 1 the cells experienced toxicity. Lastly, when the growth curve moved from CI > 1 to a CI < 1 during the observation time the cells could be defined as experiencing cytostatic responses [140].
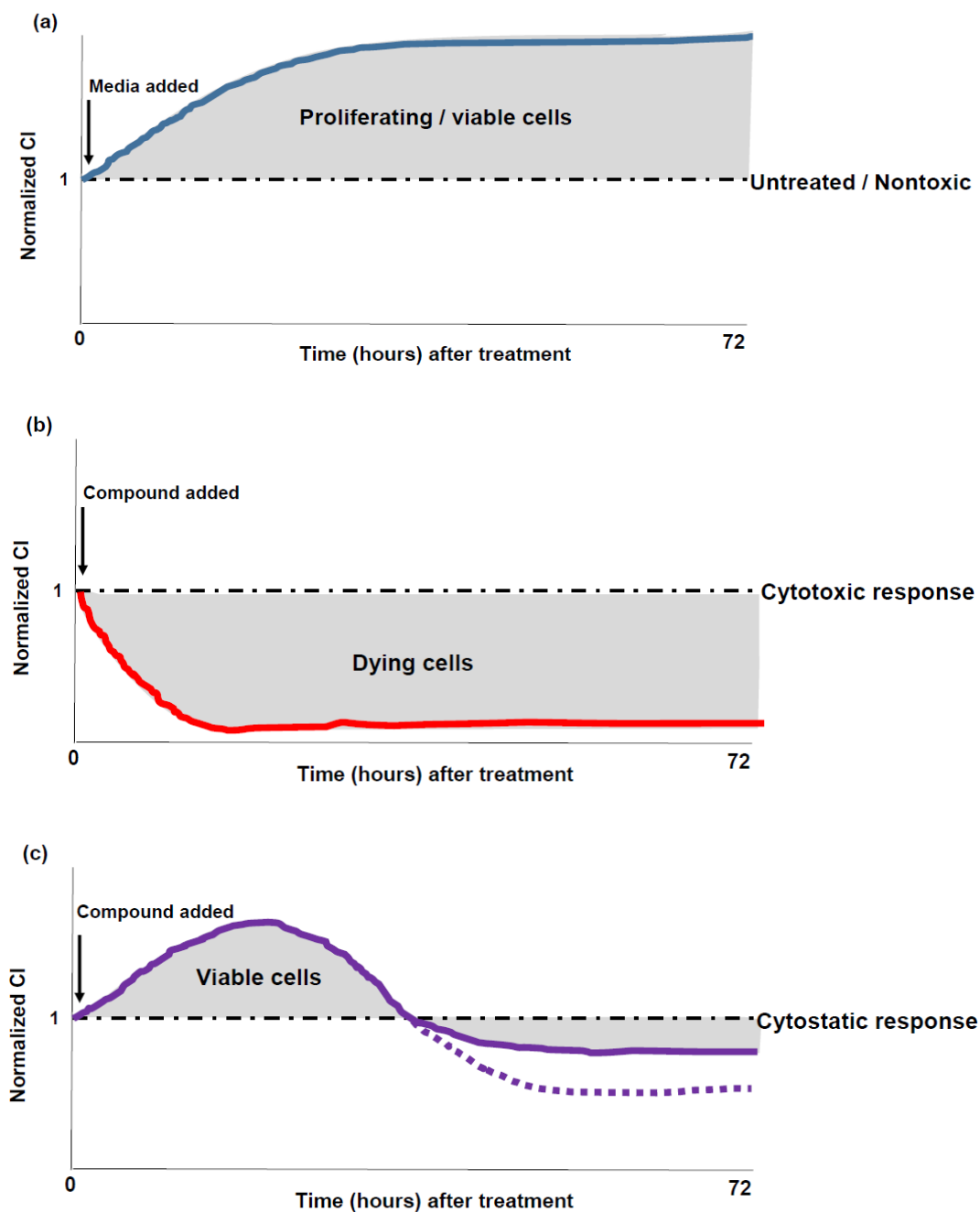
Fig. 4.1. **Representative graphs of cellular responses monitored with RT-CES, where the data is normalized from compound addition until the experiment is stopped approximately 72 hours after the addition of the treatment.** Data is normalized to CI = 1 and a line at 1 is indicated in each of the graphs. Untreated or vehicle treated cells where cells grow normally / as expected (CI > 1), the graph appears as shown in (a) where nontoxic responses have similar graph trends as compared to untreated and treated cells, (b) is a representation of a cytotoxic compound where the CI < 1 and finally (c) represents a cytostatic response where the cells firstly has a CI > 1 and as time progress has a CI < 1 in the observation time.

Preliminary screening of the plant extract using XTT gave a CC_{50} value of 9 µg/mL while actinomycin D (positive control) produced a CC_{50} value of 0.02 µg/mL (Table 4.1). Three concentrations based on these CC_{50} values were investigated using the RT-CES system. The RT-CES system established the crude extract and actinomycin D as having CC_{50} values of 15 ± 1.8 µg/mL and 0.015 ± 0.003 µg/mL respectively (Fig. 4.2). The difference in CC_{50} determined by the two approaches is a testament to the improved sensitivity of RT-CES compared to conventional viability assays.

RT-CES graphs were compared to the graphs in Fig. 4.1 that distinguished the type of cellular responses observed (Fig. 4.2 and Table 4.2). Actinomycin D was dissolved in sterile distilled water while the plant extract was dissolved in DMSO to ensure that the mixture of components dissolved. Untreated cells were thus used as the control cells for actinomycin D treated cells while DMSO treated cells were used for plant extract treated cells. Vehicle (DMSO) treated HeLa cells had a very similar graph and proliferation profile as untreated cells and, therefore, nontoxic. When HeLa cells were treated with the crude extract at a concentration of 18 µg/mL (2 x CC_{50} determined by XTT), there was a sudden and severe cell response within the first 10 hours after the addition of the treatment. The cell response observed included the size of the cells decreasing as well as cell detachment that led to a CI below 0.5 that remained constant (Fig. 4.2 (a)). Cells treated with 18 µg/mL crude extract had a typical graph associated with cytotoxicity. Treatment of the cells with lower concentrations of the crude extract of *Plectranthus ciliatus* (4.5 µg/mL and 9 µg/mL) caused a minor decrease in CI values with similar growth trends as untreated cells (where the CI values remain similar to the CI values of treated cells, then the treatment was nontoxic). The cells treated with 9 µg/mL (the CC_{50}) showed a decrease of 20% in viability when comparing the CI values of DMSO treated cells. The areas were also not meaningfully different from the untreated- and DMSO cells and thus the cellular response small. The plants extract elicited nontoxic and cytotoxic cellular responses which depended upon the concentrations of the plant extract. Cytotoxicity of the extract can be traced back to the phytochemicals (including diterpenes) documented for this plant in the literature. Diterpenes isolated from the Plectranthus genus had been identified as having anti- neoplastic activity [146]. One of the speculated compounds which might have caused inhibition of cell proliferation as well as detachment of cells is rosmarinic acid which is found only in the subfamily of Nepetoideae of which *Plectranthus ciliatus* is a member [54,147].

Actinomycin D treated HeLa cells exhibited an entirely different cellular response when compared to the crude extract treated cells (Fig. 4.2 (b)). When the cells were treated with higher concentrations of actinomycin D, the CI decreased more dramatically compared to the lower concentrations. The RT-CES graphs indicated that lower concentrations of actinomycin D induced minor changes and were, therefore, nontoxic. After the cells were treated with 0.04 µg/mL actinomycin D (2 x CC_{50}), the drug significantly changed the cellular response. In this case, actinomycin D elicited a cytostatic cellular response. Sawicki & Godman (1971) observed that the induction of apoptosis in HeLa cells were evident at concentrations between 1 – 10 µg/mL actinomycin D, while cell deterioration was delayed when the cells were treated with lower concentrations (0.1 - 0.01 µg/mL). During the S- and G2-phase, actinomycin D is incorporated into DNA causing the cells to have cytostatic characteristics [64,148] as seen here as well.
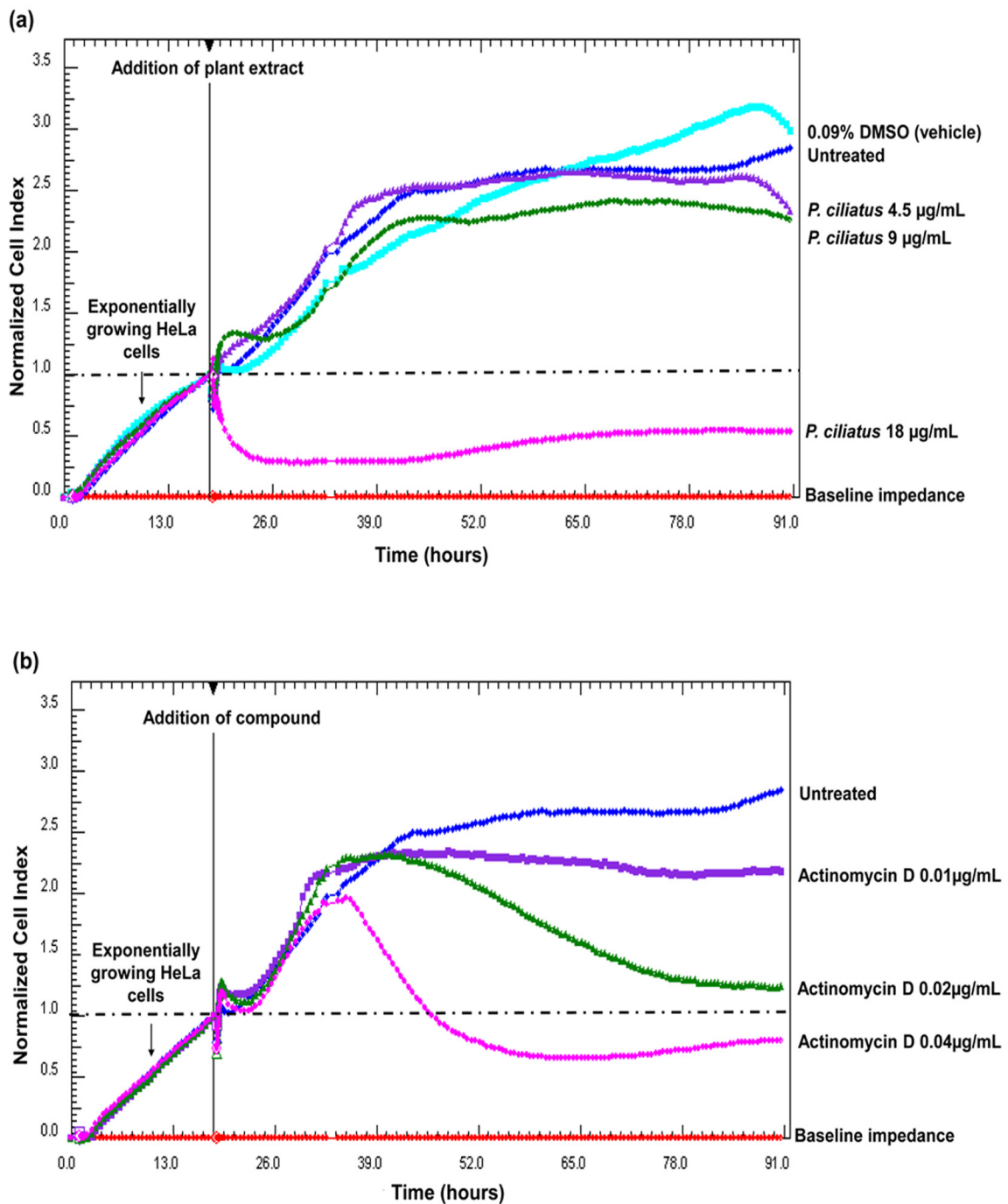
Fig. 4.2. Representative graphs of the effect on the proliferation of (a) *Plectranthus ciliatus* **extract and (b) actinomycin D (cell death inducer) treated HeLa cells using RT-CES.** Cells were incubated for approximately 18 hours after which the treatments at three different concentrations of the treatments were performed. In (a), the vehicle (DMSO) and media-only cells show minimal CI changes. The plant extract treated cells were severely affected by 18 µg/mL which led to a sudden decrease in the CI values. In (b) the effects were also more severe as compared to actinomycin D treated cells (0.04 µg/mL).

Table 4.2. Summary of the treatments and cellular responses after treatment.

Treatment	Cellular response
Untreated	-
DMSO	Nontoxic
Plectranthus ciliatus **4.5 µg /mL**	Nontoxic
Plectranthus ciliatus **9 µg /mL**	Nontoxic
Plectranthus ciliatus **18 µg /mL**	Cytotoxic
Actinomycin D 0.01 µg/mL	Nontoxic
Actinomycin D 0.02 µg/mL	Nontoxic
Actinomycin D 0.04µg/mL	Cytostatic

4.3.2 *FTIR spectral analysis of HeLa cells treated with actinomycin D and Plecthrantus ciliatus*

RT-CES demonstrated a cytostatic response for actinomycin D (0.04 µg/mL) while the effects of *P. ciliatus* (18 µg/mL) was cytotoxic. The sensitivity of FTIR microspectroscopy was evaluated to assess whether similar observations would be evident. Spectra were recorded for untreated and treated cells in the region of 4000-850 cm^{-1} (Fig. 4.3) and exhibited bands originating from lipids, proteins and carbohydrates (Table 4.3). Increasing signal to noise levels originated when the cells were treated with the crude extract of *P. ciliatus*. The increase in noise was concentration dependent as can be seen in Fig. 4.3. The noise was likely due to the crude extract containing numerous compounds causing noise in the region between 1800 and 2000 cm^{-1}. The presence of the noise in the region between 1800 and 2000 cm^{-1} did not lead to any spectral shift since shifts were not apparent in the averaged spectra nor the second derivatives (Fig. S4.1). In Table 4.3, the mid infrared band assignments common to biological samples were summarized. Major vibrational bands of untreated HeLa cells in the fingerprint region were similar to proliferating HeLa cells investigated previously [105,149]. No major spectral differences were observed between vehicle control (0.09% DMSO) and untreated cells.
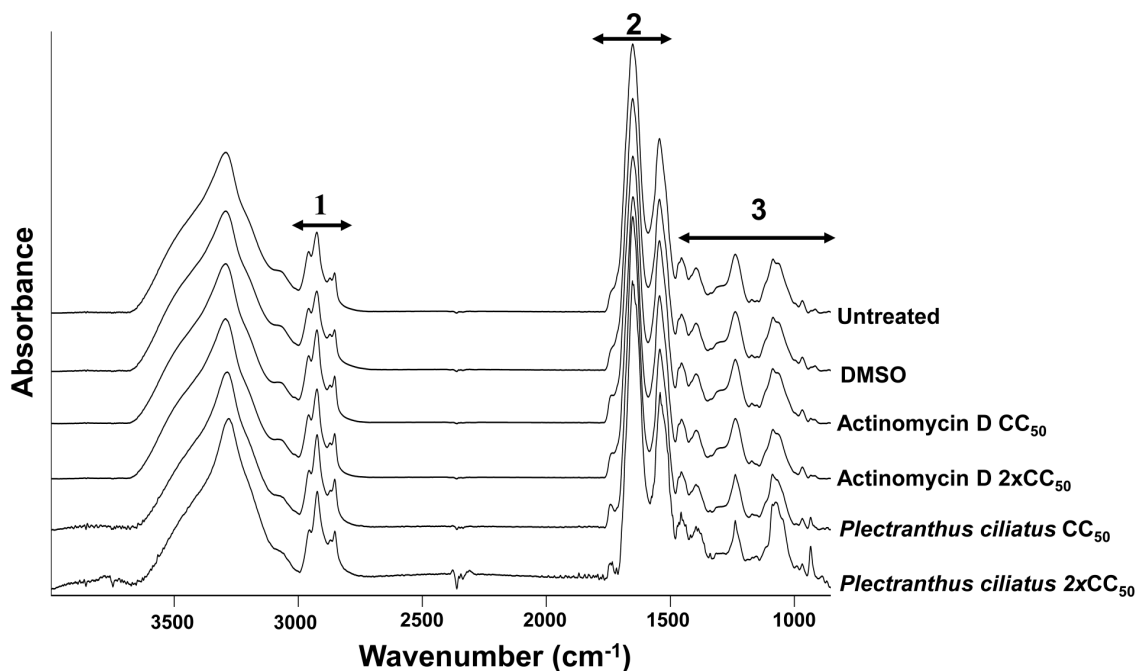
Fig. 4.3. Average spectra of FTIR spectral features in the regions between 850-4000 cm^{-1} of untreated and treated HeLa cells. The interaction between HeLa cells and the treatments P*lectranthus ciliatus* and actinomycin D at two different concentrations. The average spectrum of Actinomycin D 2xCC$_{50}$ treated cells showed some noise between 1800-2000 cm^{-1} which could have been due to plant extract components or relatively more atmospheric moisture in the laboratory during measurements. Major vibrations assigned to biological molecules are indicated.

Table 4.3. Major mid infrared spectral ranges in cells

Region	Spectral range	Assignment
1	3000 – 2800 cm^{-1}	Stretching vibrations of CH$_2$ and CH$_3$ contained mainly in the lipid acyl chains and to a lesser extent proteins [106,150]
2	1800 – 1300 cm^{-1}	Absorptions were due to proteins, the shoulder band around 1738-1745 cm^{-1} was assigned to C=O stretching mode of phospholipids. Protein amide C=O stretching took place around 1655 cm^{-1} (amide I) and the amide N-H bond (amide II) appears at 1546 cm^{-1}. Bands around 1480-1300 cm^{-1} were caused by amino acids side chains and fatty acids [106,107,133]
3	1300-850 cm^{-1}	The absorptions were from carbohydrates and phosphates associated with nucleic acids. The vibrational bands at 1238 cm^{-1} and 1088 cm^{-1} were associated with asymmetric and symmetric phosphodiester vibrations of nucleic acids. Various glycogen bands were superimposed between 1153 cm^{-1} and 1022 cm^{-1} while a small peak appearing at 966 cm^{-1} was assigned to C-O phosphodiester moieties [106,151]

In this investigation the vector normalized second derivatives were analysed to accurately assign and visually maximize differences [13,108] in the spectral regions (850 - 1800 cm^{-1} and 2800 – 3000 cm^{-1}) of untreated and treated HeLa cells (Fig. 4.4).
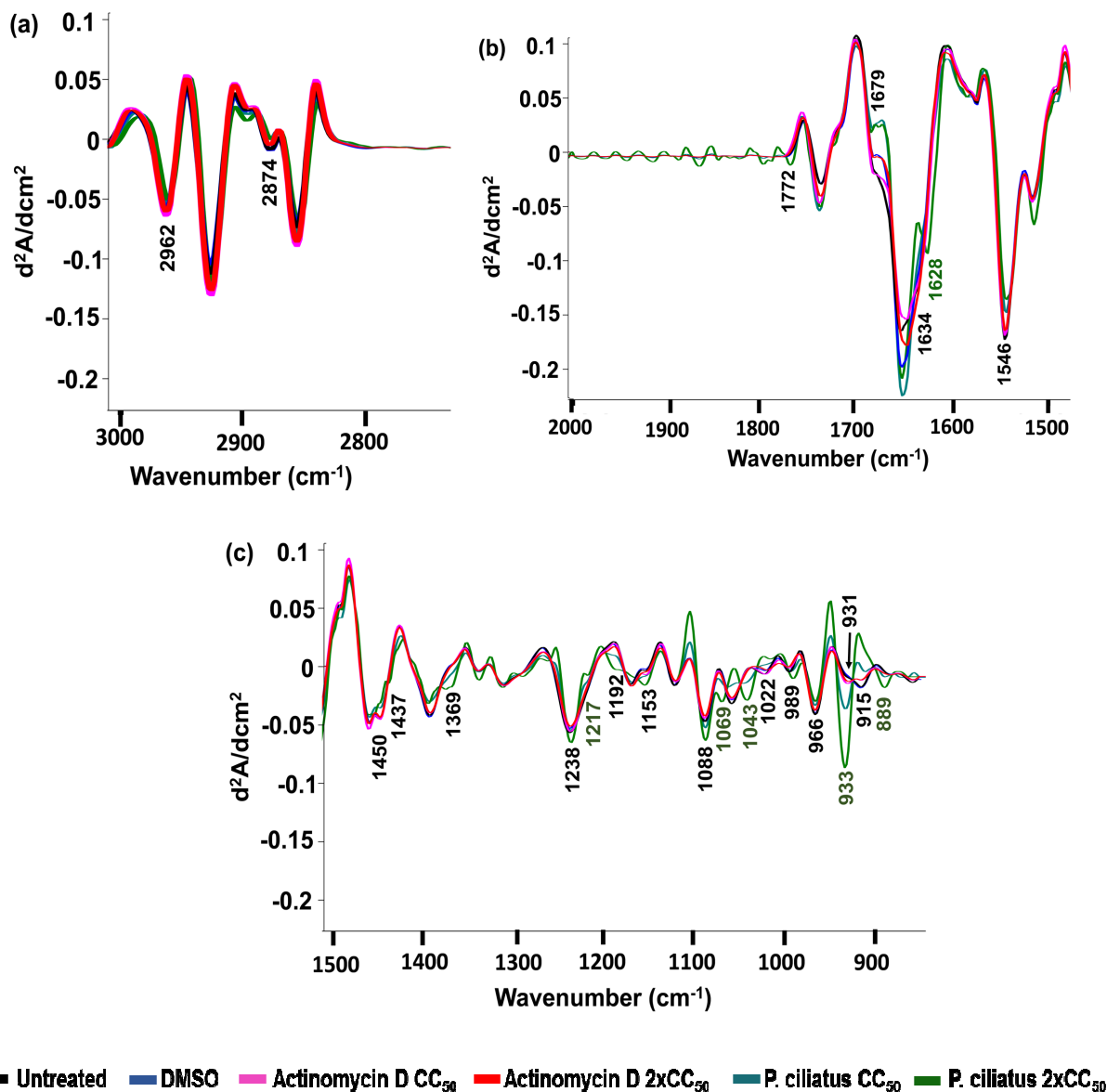
Fig. 4.4. The average second derivative spectra of untreated and treated HeLa cells in the regions of (a) 3000 - 2800 cm^{-1} (b) 2000 - 1500 cm^{-1} and (c) 1500 - 850 cm^{-1}. The y-axis is defined as the second derivative of Absorbance. Actinomycin D treated cells had very small variances in most spectral regions. When the cells were treated with the plant extract more severe vibrational band changes occurred as compared to lower concentrations of the plant extract.

i)   <u>**Significantly altered vibrational bands associated with cellular injury**</u>

All the wavenumbers of the spectra between 850 - 1800 cm^{-1} and 2800 - 3000 cm^{-1} were evaluated because this is where the treatments under investigation appeared to have had the strongest impact.

ii) <u>**Cytostatic and nontoxic responses**</u>

Nontoxic responses were identified when the cells were treated with DMSO (negative control) and actinomycin D (0.02 µg/mL) using RT-CES. Actinomycin D of higher concentrations (0.04 µg/mL) was defined as inducing a cytostatic response, but none of the vibrational bands was found to be significantly altered. FTIR microspectroscopy was unable to distinguish viable (untreated HeLa cells) from cells treated with DMSO and actinomycin D at 0.02 µg/mL nor could vibrational spectroscopy distinguish healthy from cytostatic cells treated with actinomycin D (0.04 µg/mL). Cytostatic drugs encourage cells not to proliferate and cause cell cycle arrest. During cytostasis, the cells remain viable with very low energy consumption and thus remain in the cell cycle stage in which the cytostatic drug inhibits further growth. Cells remain morphologically intact with limited expansion and movement. FTIR spectroscopy was able to confirm the data of RT-CES and literature that cytostatic cells on a molecular level were still viable and not committed to death since the cells can still recover. Spectra were similar to untreated / viable cells and / or vehicle treated cells.

iii) <u>**Early stress related responses and cytotoxicity**</u>

P. ciliatus (9 µg/mL) was defined as being non-toxic using RT-CES while significant vibrational band alterations were identified after statistical analysis compared with viable, non-toxic and cytostatic responses. It was postulated that RT-CES could not detect early stress related responses since those responses were based on vibrations of the molecules. Two vibrational bands were identified as significantly altered after the treatment. Those bands were assigned to amide I vibrations (1634 cm^{-1} and 1679 cm^{-1}). It was found that antiparallel β-sheets and β-sheets of amide I could be used to distinguish *P. ciliatus* (9 µg/mL and 18 µg/mL) from nontoxic and cytostatic responses (Table 4.4). Therefore, 1634 cm^{-1} and 1679 cm^{-1} could be used as indicators of early stress related responses that remain evident during cytotoxic responses. The dynamic biochemical reaction towards cytotoxins could, therefore, be seen in the conformational changes in the amide I with the increase in β-sheets and a noteworthy increase in α-helices (1655 cm^{-1}). The change in conformation of amide I

could also be due to different proteins being expressed. Zelig *et al.* (2009) found that this scenario to be associated with apoptotic cells [13].

Table 4.4. Significantly (One-way ANOVA post hoc tests: Tukey test, Bonferroni) different bands in the second derivative spectra.

Wavenumber (cm^{-1})	One-way ANOVA p-value	Multiple comparison outcomes	Assignment
915	0.03	Nontoxic vs. Cytotoxic	Ribose – phosphate main chain vibrations associated with nucleic acids [152,153]
931-933	0.007	Nontoxic vs. Cytotoxic Cytostatic vs. Cytotoxic	C-O-C ring of deoxyribose in Z-form DNA [151,154]
989	0.002	Nontoxic vs. Cytotoxic Cytostatic vs. Cytotoxic	PO_3^{2-} vibrations of nucleotides [155,156]
1192	0.021	Nontoxic vs. Cytotoxic	Deoxyribose - phosphate backbone with high contribution from the C3' endo sugar moiety [151]
1369	0.009	Nontoxic vs. Cytotoxic Cytostatic vs. Cytotoxic	Stretching C-N of cytosine and guanine [151]
1437	0	Nontoxic vs. Cytotoxic Cytostatic vs. Cytotoxic	CH_2 bending of proteins (amide II) [157]
1450	0.012	Nontoxic vs. Cytotoxic	Hydrogen bonded Aspartic acids and Glutamic acid (CH_3COOH) [133] Methylenes of biomolecules [158]
1546	0.008	Nontoxic vs. Cytotoxic	Metastable phase of Amide II [159]
1634	0.001	Nontoxic vs. Cytotoxic Cytostatic vs. Cytotoxic PC vs. Cytostatic	Antiparallel β-sheets of Amide I [150,160]
1679	0.006	Nontoxic vs. Cytotoxic Nontoxic vs. PC	β-sheets of Amide I [133,150]
1772	0.001	Nontoxic vs. Cytotoxic Cytostatic vs. Cytotoxic Cytotoxic vs. PC	Glycerol bound fatty acids, triacylglycerides [161]
2874	0.037	Nontoxic vs. Cytotoxic	C-H stretching of lipids and proteins of CH_3 [162]
2962	0.016	Nontoxic vs. Cytotoxic	C-H stretching of lipids and proteins [163]

Other vibrational bands associated with cytotoxicity were also detected in the cells treated with 18 µg/mL (Fig. 4.4, Table 4.4). Those bands were associated to nucleic acids (915 cm^{-1}, 933 cm^{-1}, 989 cm^{-1}, 1192 cm^{-1}, 1369 cm^{-1}), proteins (1437 cm^{-1} and 1546 cm^{-1}), lipids and proteins (1450 cm^{-1}, 1772 cm^{-1}, 2874 cm^{-1}, 2962 cm^{-1}). The 933 cm^{-1} band was assigned to the vibrational mode of the C-O-C ring of deoxyribose in Z-form DNA [151,152,158]. The region of 1069-1044 cm^{-1} was assigned to C-O vibrations of furanose and is documented to be enhanced in Z-DNA [151]. After the treatment of the cells with *P. ciliatus,* the peak broke up into two new peaks ~1069 and ~1043 cm^{-1}. Other bands associated with Z-DNA was also apparent in the same spectra around 1438 cm^{-1} (shoulder peak not present in the other treated cells) assigned to adenine in Z-DNA, the main Z-DNA marker at 1216 cm^{-1} as well as the band at 1264 cm^{-1} assigned to guanine-cytosine helices in Z-form DNA [151]. The 915 cm^{-1} band became less intense as the treatment increased and the band significantly decreased after 18 µg/mL plant extract treatment. The band was assigned to ribose – phosphate main chain vibrations associated with nucleic acids [152,153,163–166].

The transformation of B-DNA to Z-DNA can occur under physiological conditions but also due to increased salt concentrations or dehydration of the cells [167]. In this investigation, it is unlikely that the severity of Z-DNA formation seen in the cytotoxicity response was only due to dehydration since the control cells showed less severe changes. Lampronti *et al.* (2006) found that when different plant extracts were incubated with oligonucleotides isolated from cancer cells, an inhibition of transcription factors were evident [168]. Nucleosome formation and placement, as well as the organisation of chromosomes, are affected by the formation of Z-DNA [169], which could have caused the increased absorption of the FTIR peak. Increased salt concentration could be due to additional salts found in the stomata to help with the opening and closing during respiration of the plant. During the day (when the leaves were harvested) the stomata are open which requires a high concentration of potassium. Eukaryotic muscle cells have a concentration of 30 mM potassium and a slight increase to 50 mM could induce detectable transformation of B-DNA to Z-DNA [170,171]. Conformational changes in the amide II band could indicate at a glance that biochemical processes involved in chemical stress and cell death induction, such as protein expression related to chemical stress had taken place.

An increase in triacylglycerides and glycerol bound free fatty acids (1772 cm^{-1}) increased during the cytotoxic response. An increase in the absorbance was likely due to increased lipid

content within the cells such as the formation of lipid droplets [172]. Lipid droplets formed in T-lymphoblastoid (Jurkat) cells when apoptosis was induced by anthracyclins and other cancer drug controls [173]. The reason for the occurrence of the lipid droplets are still not clear, although the degradation of lipids, due to inhibition of the mitochondrial fatty acid β-oxidation pathway during apoptosis could be a possible reason [172,174]. The increase of high wavenumber peaks at 2874 cm^{-1} and 2962 cm^{-1} could be indicative of plasma membrane modifications caused by the cytotoxic treatment [13,14].

4.3.3 *Principal component analysis*

The analysis is an unsupervised data reduction method used to identify trends within data based on similarities and differences within the data [101]. Untreated and treated cells at different concentrations of actinomycin D and *P. ciliatus* showed spectral variance which could be described by the first two principal components (PC). The total percentage variance per PC was indicated in brackets (Fig. 4.5). A total of 59 % of the spectral variance were explained by the data reported. It was seen that PC 1 separated the plant extract treated cells from the untreated and actinomycin D treated cells. FTIR spectra caused clustering of *P. ciliatus* treated cells although the cellular injury was concentration dependent using RT-CES. A possible reason for the clustering could be due to significant alterations of amide I (as found in ANOVA). Clustering of actinomycin D treated cells with untreated cells and DMSO (vehicle) cells confirms that only small spectral changes occurred and it can be assumed that minimal cellular injury was caused by the addition of actinomycin D (0.02 μg/mL). These cells treated with actinomycin D or DMSO were classified as nontoxic. Cells treated with 0.04 μg/mL had a cytostatic RT-CES curve which could not be distinguished from the non-toxic responses using PCA. The cells were reversibly inhibited to proliferate, but still being able to maintain cellular functions for survival. It was postulated that RT-CES could measure the after-effects of cytotoxicity while FTIR could measure the molecular changes using vibrational differences before any morphological effects may become evident.
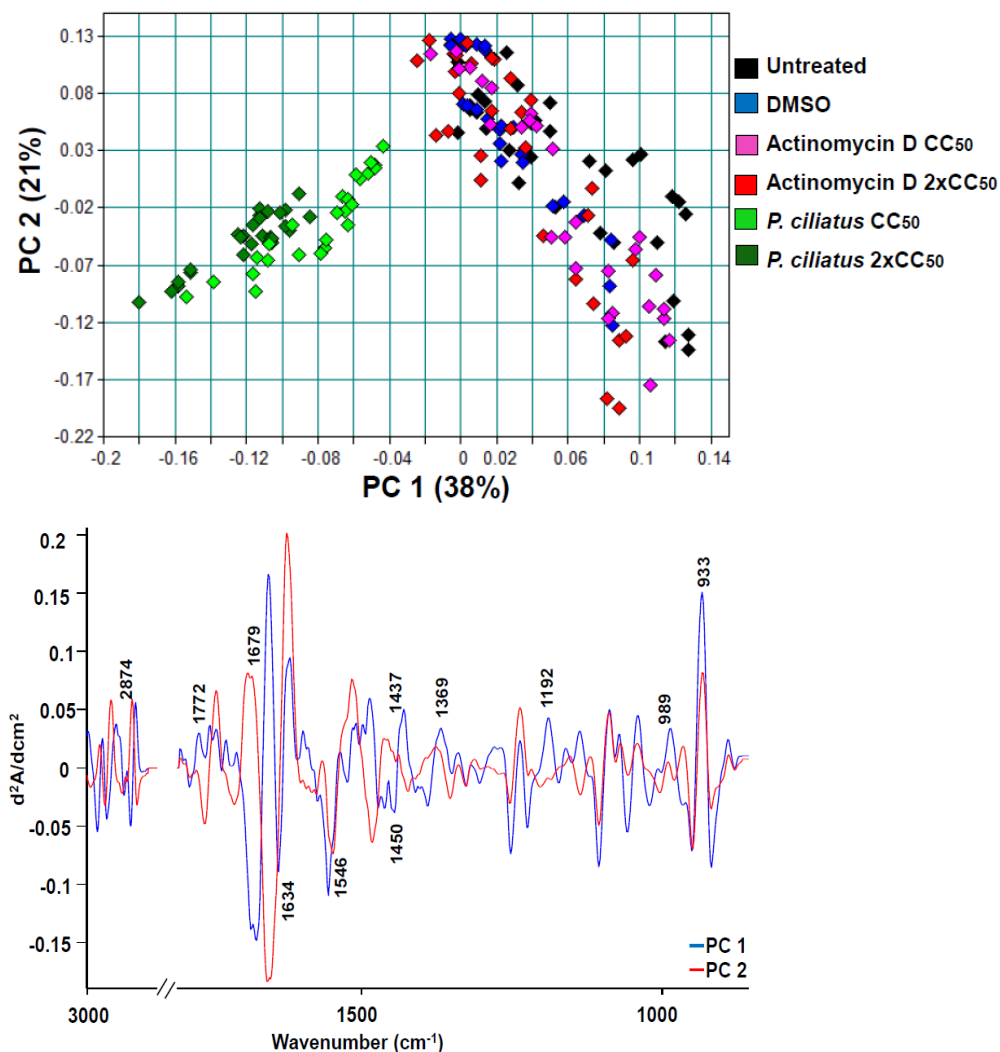
Fig. 4.5. **(a) Principal component analysis of the spectral variance of the treated samples in the regions of 850 -1800 cm^{-1} and 2800 - 3000 cm^{-1}.** A degree of linearity was seen in the score plot which could have been due to a concentration dependent effect. **(b) Loading plots of the PCA analysis**. Major bands that contributed to the separation of the treatment groups were indicated and those bands were also found to be significantly different.

RT-CES classified cellular injury based on changed morphology of the cells and the ability to attach to the electrodes. Detachment is characteristic of cell death induced by cytotoxins. It was concluded that 18 μg/mL *P. ciliatus* treated HeLa cells induced a cytotoxic response while the other treatments had less severe effects on the cells. RT-CES is an established technique for distinguishing non-toxic, cytostatic and cytotoxic responses which cannot be distinguished by conventional viability assays. FTIR microspectroscopy is widely used to distinguish between different cell types; cell cycle stages as well as cytotoxic treatments. FTIR microspectroscopy confirmed the reversible nature of cytostatic cellular status by

detecting that the cells were still viable. Additionally, FTIR detected changes in the molecular vibrations initiated by 9 µg/mL *P. ciliatus* treatment of cells which was associated with the early cellular stress responses.

In conclusion, RT-CES and FTIR microspectroscopy complemented each other by RT-CES detecting morphological changes as indicators of cell injury and could distinguish between viable, cytostatic and cytotoxic responses[§]. FTIR microspectroscopy confirmed that cytostatic cells were not committed to death and could still recover while also describing early cellular stress related responses on a molecular level. Using FTIR microspectroscopy, it can be determined whether a treatment were inducing cytostatic responses, early stress related responses or cytotoxic responses.

[§] Supportive data analysis on metallodrug induced cellular responses are found in the Appendix

Chapter 5: Metallodrug induced apoptotic cell death and survival attempts are characterizable by Raman spectroscopy

Published in:

Applied Physics Letters

Abstract

Chrysotherapeutics are under investigation as new or additional treatments for different types of cancers. In this study, gold complexes were investigated for their anticancer potential using Raman spectroscopy. The aim of the study was to determine whether Raman spectroscopy could be used for the characterization of metallodrug-induced cell death. Symptoms of cell death such as decreased peak intensities of proteins- and phosphodiester bonds found in deoxyribose nucleic acids (DNA) were evident in the principal component analysis (PCA) of the spectra. Vibrational bands around 761 cm^{-1} and 1300 cm^{-1} (tryptophan, ethanolamine group and phosphatidylethanolamine) and 1720 cm^{-1} (ester bonds associated with phospholipids) appeared in the Raman spectra of cervical adenocarcinoma (HeLa) cells after metallodrug treatment. The significantly ($p < 0.05$, one way analysis of variance – ANOVA) increased intensity of phosphatidylethanolamine after metallodrug treatment could be a molecular signature of induced apoptosis since both the co-regulated phosphatidylserine and phosphatidylethanolamine are externalized during cell death. Treated cells had significantly higher levels of glucose and glycogen vibrational peaks, indicative of a survival mechanism of cancer cells under chemical stress. Cancer cells excrete chemotherapeutics to improve their chances of survival and utilize glucose to achieve this. Raman spectroscopy was able to monitor a survival strategy of cancer cells in the form of glucose uptake to alleviate chemical stress. Raman spectroscopy was invaluable in obtaining molecular information generated by biomolecules affected by anticancer metallodrug treatments and presents an alternative to less reproducible, conventional biochemical assays for cytotoxicity analyses.

5.1 Introduction

Cervical cancer is the second most commonly diagnosed cancer worldwide among women, with an estimated 530 000 new cases reported annually. Every year approximately 270 000 women die of cervical cancer and > 85% of recorded fatalities are found in low- and middle income countries [33]. Cervical cancer is one of the biggest health problems among South African women, affecting one out of every 41 women and mortalities associated with this disease are estimated at eight South African women per day [36]. The co-infection of human immunodeficiency virus (HIV) and human papillomavirus is well documented [6,175]. Advances in diagnoses / success of highly active antiretroviral therapy, lead to HIV positive patients being diagnosed up to 10 years earlier with advanced stages of cervical cancer. With these staggering statistics in mind, new chemotherapeutic treatments are under investigation [36].

Research into gold based compounds as potential cancer treatments started in 1980 [131], but this metal had been used centuries prior for the treatment of other ailments [41]. During the early phases of metallodrug research, it was found that derivatives containing the linear P – Au – S structure found in auranofin (a known rheumatoid arthritis drug) had potential for treating cancer [131].

Successful cancer treatments are expected to selectively kill diseased cells only and the cytotoxic effects of the drugs are routinely monitored by conventional biochemical assays such as 3-(4,5-Dimethylthiazol-2-yl)-2,5-diphenyltetrazolium bromide (MTT) reduction assays [176], microscopy, flow cytometric techniques [177] and real time cell electronic sensing (RT-CES) [80]. The disadvantages of some of these techniques are that expensive reagents are needed and specialised instruments to measure absorbance, impedance, fluorescence or luminescence of labelled biosensors. An alternative to these techniques could be Raman spectroscopy where samples can be investigated in a label free manner, with minimal preparation and analyses in relatively short time periods.

In this investigation, gold (I) complexes were investigated for their cytotoxic effect on a cancer cell line. We suggest Raman spectroscopy as a practical tool for the characterization of chemically induced cell death in a population.

5.2 Methods

Two organic gold complexes designated 2-(2-(diphenylphosphino)ethyl)pyridyl-gold(I) chloride (AE 76) and 2-(diphenylphosphino)-2'-(N,N-dimethylamino)biphenylgold(I) chloride (AE125) were synthesized and characterized [178,179] by the laboratory of Prof. Darkwa in the Chemistry Department of the University of Johannesburg, South Africa. Details of the synthesis and characterization can be found in the PhD thesis of A.Elkhadir (2014) [48]. Auranofin (Sigma, Germany) was used as a positive control drug for the induction of apoptosis [180, Appendix].

5.2.1 *Flow cytometry for the detection of induced cell death*

Apoptotic cell death induction by the metallodrugs was determined using flow cytometry. Exponentially growing HeLa cells were seeded (10^5 cells/mL) and incubated for 24 hours (37°C, 5% CO_2) after which the cells were exposed to the metallodrugs (auranofin = 5.6 µM, AE76 = 20.8 µM, AE125 = 17.8 µM) for 72 hours. After treatment, detached cells were collected and the wells washed with 500 µL phosphate buffered saline (PBS). The cells were rinsed with 200 µL trypsin (Hyclone) and incubated for five minutes. Trypsinized cells were washed twice with the respectively collected media, thus pooling detached and adherent cells. Pooling cells was capable in this case because the cells were in various stages of cell death. Samples were prepared for annexin-V and propidium iodide staining as prescribed by the manufactures (BD Biosciences, California, USA) and analysed using a Fluorescence Activated Cell Sorter (FACS) Aria. Four independent experiments were performed and expressed as % cell events with a standard error of the mean. Data was analysed statistically using one way ANOVA where $p < 0.05$ was documented as significant.

5.2.2 *Raman spectroscopic investigation of untreated and treated cells*

After the quantification of apoptosis (with flow cytometry), a qualitative Raman spectroscopic study was done to determine the molecular changes. The method published by Matthaus *et al.* (2007) [149] was used as a guideline. Cells were prepared in the same manner as for flow cytometry and pooling cells which were centrifuged for 10 minutes at 1200 reps per minute. The supernatant was discarded, the pellets loosened and the cells washed twice with 1 mL PBS. The cells were incubated at room temperature in 1 mL 10% formalin for 10 minutes and then centrifuged for five minutes. The cells were washed with 1

mL sterile distilled water and centrifuged to remove all traces of formalin. The cells were suspended in 10 µL sterile distilled water. Three microliters cell suspension was dried in the biosafety flow hood for one hour on sterile CaF_2 discs. Raman microspectroscopy was performed with a T64000 micro-Raman spectrometer from HORIBA Scientific. The 514.5 nm line of an Innova 70v argon-krypton mixed gas laser was used as the excitation source. The 50x objective of an Olympus microscope was used to focus the laser beam (spot size ~ 2 µm) in the middle of single air-dried cells, where the nuclei is most likely situated as is the norm [11,123,182,183]. The laser power at the sample was kept constant at 10 mW. Three independent experiments were carried out of which a total of seven cells per treatment were analysed. All the spectra were recorded with a 150 seconds acquisition time for two accumulations. The Labspec 6.0 software was used to fit and subtract a fourth order polynomial function to obtain a zero baseline. A 5 degree linear Savitsky-Golay smoothing procedure was applied to all the spectra. Second derivatives of the spectra (vector normalized) were used for final interpretations (generated in OPUS 7). Principal component analysis was carried out using Quant 2 OPUS software. Vibrational peaks of interest involving phospholipid and glucose metabolism were validated with one way ANOVA followed by Tukey's multiple comparison tests using GraphPad Prism 5. Changes in vibrational peaks were significant if $p < 0.05$.

5.3 Results and discussion

The metallodrugs were evaluated using conventional biochemical methodologies to determine the degree of cytotoxicity and the type of cell death induction. Raman spectroscopy was then used to identify molecular targets of the metallodrugs and the drug induced effects on phospholipid and glucose metabolism. Flow cytometric analysis detected that early apoptosis was significantly ($p < 0.05$) induced by the metallodrugs (Fig. 5.1, Fig S5.1) [Appendix]. Less than 14% of the cells were viable, confirming light microscopic evidence which indicated that all cells treated with AE 76 and auranofin experienced severe chemical distress after treatment.
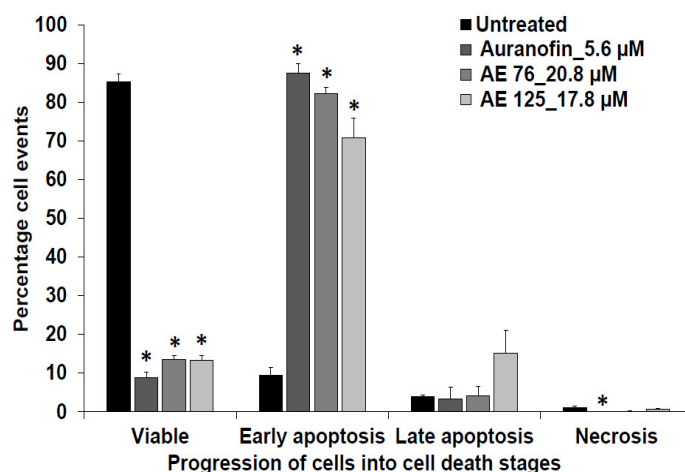
Fig. 5.1. Flow cytometry: The percentages viable and dead HeLa cells after treatment with different concentrations of metallodrugs. The induction of early apoptosis was significant (*$p < 0.05$) for all treatments. Necrotic events were negligible and late apoptosis minimal (n=4).

Further insight into the mechanism of action of the three metallodrugs was determined by studying the molecular vibrations of the chemically stressed cells. The investigation was focused on the centre of the HeLa cells. This area of cells are known to be rich in nuclear material such as proteins, lipids, nucleic acids, nuclear- and plasma membranes [11,123,184]. The hallmarks of apoptosis involve the nucleus (chromatin condensation and DNA fragmentation, etc. [16]) and are well documented. The raw spectra of the cells analysed in this study [Appendix] had vibrational peaks for proteins, lipids, nucleic acids and carbohydrates and were comparable to previously reported spectra obtained for HeLa cells including Raman spectra of the nucleus [149,183]. Since only small variances were seen in the raw spectra of untreated and metallodrug treated spectra, second derivatives were used for further discussion (Fig. 5.2 and Fig. S5.2). The most prominent peaks in the spectra belonged to protein vibrations, namely methyl (CH_3) stretch vibrations (2927 cm^{-1}) , amide I at 1657 cm^{-1} (overlapping with peaks originating from fatty acids including triglycerides), amide III overlapping with asymmetric phosphate stretching modes (1224 cm^{-1}), phenylalanine (1006 cm^{-1}) and tyrosine (1165 cm^{-1}) [119]. The intensity of CH_2 symmetric stretch vibrations (2862 cm^{-1}) of lipids / proteins [119] and carbon-hydrogen (CH) and CH_2 vibrations [119] at 1449 cm^{-1} were also prominent. Cellular responses to treatment were heterogeneous, probably due to different degrees of sensitivity [127] of individual cells to the treatments. Heterogeneity of the spectra could also be due to the spectra only being recorded for the centre of the cell, where nuclear material could be showing different stages of apoptotic progression (chromatin condensation would be presented by increased DNA intensities

compared to decreased DNA intensities due to DNA fragmentation [12,122]). The cell number was sufficient for this study [11,12,125,185] since it was qualitative and was carried out on well-defined populations of viable and apoptotic cells as determined by flow cytometry.
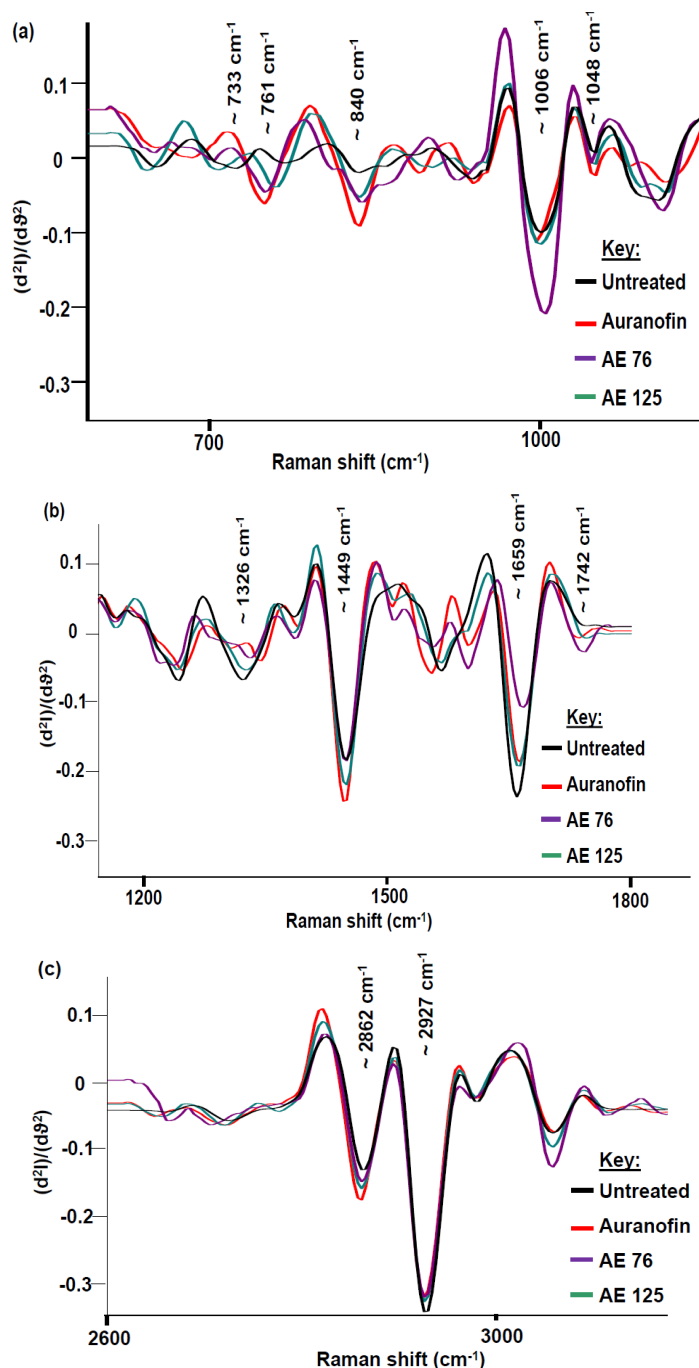
Fig. 5.2. The second derivatives of untreated and metallodrug treated HeLa cells in the regions between (a) 600 – 1150 cm^{-1}, (b) 1150 cm^{-1} – 1800 cm^{-1} and (c) 2600 – 3200 cm^{-1}. Major spectral differences are visible which indicate aspects of the mechanism of action of these metallodrugs and also induction of apoptotic cell death. The y-axis is defined as the second derivative of intensity.

Focusing on single peaks is not sufficient when describing the major peak shifts seen in this study which is why PCA was used for further analysis [123]. Cells were not deliberately synchronized, but our data (Fig. 5.3) showed that intercellular variations were low. The occurrence can be explained by the study of Matthews *et al.* (2010) [128] where cells were mostly in one (Gap 1) phase. Score plots were used to identify significant changes between untreated and treated HeLa cells. It was found that most of the spectral variance was within the first principal component (PC) between the 600-1800 cm^{-1} regions. In the case of PC 1, the untreated cells clustered separately from the treated cells, with the exception of some of the spectra of AE 125 treated cells (Fig.5.3 (a)). This clustering is explained by the different stages of cellular responses after treatment. Although all cells were exposed to AE 125 simultaneously, the exact amount absorbed may differ so that individual cells are at different stages of early apoptosis allowing some to behave as if unaffected by treatment (as if untreated), while others present a more severe response. Flow cytometry showed a population of seemingly healthy cells migrating towards early apoptosis after cells were treated with AE 125 (Fig. S5.1) [Appendix]. These trends in cellular responses were also prominent in the study conducted by Brauchle *et al.* (2014), which found that Saos-2 and SW-1353 apoptotic cells (exposure to room temperature for four days) also showed poor separation on PCA score plots [123]. In the AE 76 treated cells, the spectra showed a higher degree of spectral variance between samples, but all cells behaved as if apoptotic. The differences in response between treatments are explained by their structural differences. The many bulky aromatic rings of AE 125 certainly affect its cellular absorption.
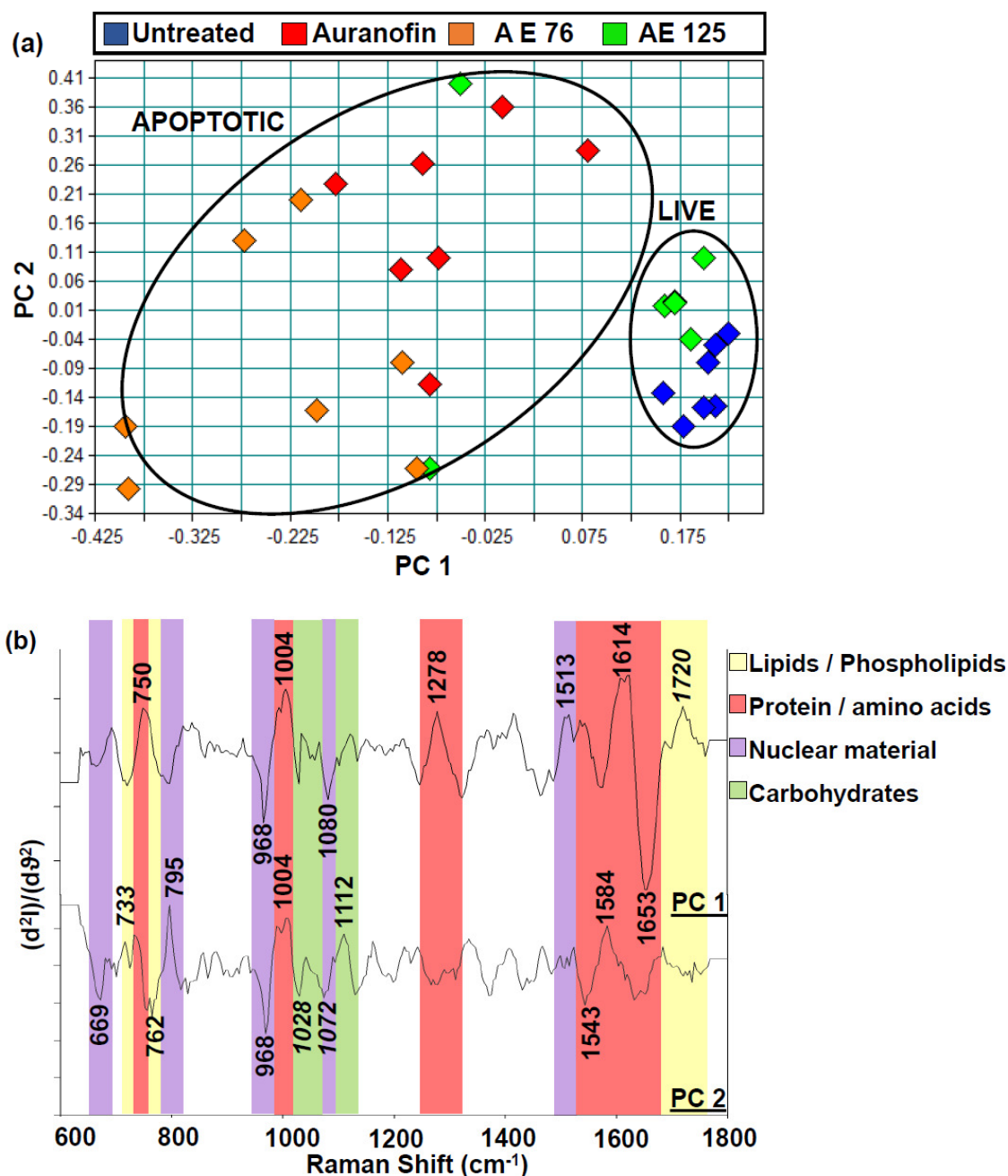
Fig. 5.3. Principal Component Analysis (PCA) score plots comparing the second derivatives of the Raman spectra of (a) the region of 600 – 1800 cm^{-1}, "live" and less damaged cells, while all others clustered together (dead). Spectral variance were best described in the first two Principal Components (PC) and (b) corresponding loading spectra leading to the clustering in the PCA plot. Assigned components were identified as major contributors of separation.

Clustering of untreated and treated HeLa cells showed strong separation along PC 1. Spectra obtained from metallodrug treated cells were associated with negative scores in the score plot. Since the PCA was performed on second derivatives, a negative score was associated

with a positive loading [138]. The positive loadings in PC 1 corresponded to a decrease in tryptophan (750 cm^{-1}) phenylalanine (1004 cm^{-1}), amide III (1275 cm^{-1}), cytosine (1513 cm^{-1}) and a combination of tyrosine, tryptophan and C=C protein vibrations (1614 cm^{-1}) [119] and was associated with treated HeLa cells. The positive loadings were packed with amino acid and protein vibrations decreasing as compared to untreated HeLa cells. The negative loadings in PC 1 corresponded to lipid vibration (968 cm^{-1}), phospholipids and phosphodiester groups of nucleic acids (1080 cm^{-1}) and C=C, carbonyl (C=O) (lipids) and amide I (1653 cm^{-1}) [119] (Fig 5.3.(b)). The negative loadings were associated with untreated and some AE125 cells therefore indicative of the other treated cells having lower intensities in some proteins, phospholipids and other lipids as well as phosphodiester groups associated with nucleic acids as compared to viable cells. These findings were in agreement with other researchers [11,12,120]. PC 1 explained the highest variance within the spectra while some clustering could be seen due to PC 2 loadings. Negative loadings of PC 2 corresponded to cytosine (669 cm^{-1}), phosphatidyletanolamine (761 cm^{-1}), lipids (968 cm^{-1}) and amide II (1543 cm^{-1}) [119]. Positive loadings of PC 2 were DNA (795 cm-1), phenylalanine (1004 cm^{-1}), carbohydrates (1112 cm^{-1}) and phenylalanine (1586 cm^{-1}). The decrease of a band at 795 cm^{-1} had been suggested by previous researchers to be related to internucleosomal DNA cleavage [11,123,127]. Negative loadings of PC 2 was associated with increases in of glucose (1072 cm^{-1}) and glycogen (1028 cm^{-1}) indicated noteworthy changes in the metabolism of treated cells, which were further investigated to determine the significance of the metabolites.

Changes in carbohydrate vibrational peaks could give more insight into the metabolic functions of the treated cells. Peaks assigned to glycogen was identified in the PCA loadings around 853 cm^{-1}, 918 cm^{-1}, 935 cm^{-1}, 1028 cm^{-1}, 1155 cm^{-1} and 1335 cm^{-1} [104,119,120,186]. The bands at 1028 cm^{-1} and 1155 cm^{-1} significantly ($p < 0.05$) [Appendix] increased in intensity. Together with the peak at 1072 cm^{-1} identified in the PCA, other glucose and polysaccharides related peaks, 898 cm^{-1} and 920 cm^{-1} were also identified [119]. The peak at 1072 cm^{-1} significantly increased. Changes in the intensities of glycogen or glucose could be indicative of a survival mechanism of chemically stressed cancer cells. Higher concentrations of glucose within the cells could be due to the active up take of glucose from the nutrient rich culture media while the surplus glucose within the cells were stored as glycogen. Although the apoptotic process had already started as detected by flow cytometry and Raman spectroscopy, it's generally known that cancer cells do not die easily and thus

will try to excrete any of the drugs taken up. Energy to sustain the excretion of the metallodrugs could come from glucose.

In the PCA analysis, loading plots indicated spectral changes in phospholipids. Spectral peaks associated with the plasma membrane were identified and further analysed to determine significant changes which could be linked to flow cytometry results. The laser pathway through the cell interrogates the plasma membrane, cytoplasm, nuclear membranes and nuclear material. The peaks at 733 cm^{-1} and 787 cm^{-1} in spectra of the untreated cells were assigned to phosphatidylserine [119,187]. Phosphatidylserine forms part of the inner leaflet of the plasma membrane and make up 2-10% of all the phospholipids found in the plasma membrane [188]. During apoptosis, a conformational change takes place within the bilayer of the plasma membrane. This conformational change occurs when phosphatidylserine is externalized on the cellular surface. It was found that the peaks changed significantly [Appendix] in intensity after treatment. Phosphatidylethanolamine (761 cm^{-1} and 1300 cm^{-1})[119,187] is also located in healthy cells on the inner leaflet of the plasma membrane and forms between 20-50% of the membrane composition [188]. This peak was evident after the HeLa cells were treated with auranofin and AE76 (Fig. 5.2). Phosphatidylethanolamine is co-regulated with phosphatidylserine and externalized during apoptosis [189,190]. This existing relationship between these two phospholipids could potentially be used for the detection of apoptosis using Raman spectroscopy. The band at 1720 cm^{-1} was assigned to carbonyl and ester groups associated with phospholipids [119], an increase in phospholipids could be due to the formation of lipid rich vesicles which forms during apoptosis [122]. The decrease in the peak at 733 cm^{-1} together with the prominent appearance of the peak at 761 cm^{-1} and a significant increase in 1720 cm^{-1} appears to be indicative of induced apoptosis.

To summarize; the interpretations of Raman spectroscopy data allowed for a detailed description of the mechanism of action of the metallodrugs tested (some metallodrug were superior at inducing apoptosis quicker). Changes in vibrational bands assigned to phosphatidylethanolamine were indicative of apoptosis[**]. Confirmatory experiments using other methodologies are needed to validate this finding; e.g. the detection of fluorescent anti-phosphatidylethanolamine antibodies using enzyme-linked immunosorbent assay, fluorescent

---

[**] Supportive data were conducted on the naturally derived products and can be found in the Appendix

microscopy or flow cytometry [189,191]. Correlations between flow cytometric data and Raman spectra were evident in the detection of indicators of apoptosis. The increase of glucose peak intensities was also unmistakeable and knowing the important role this metabolite plays during cancer cell survival (high levels of glucose consumption involved in excreting chemotherapy), supports this observation.

Chapter 6: Fourier Transform Infrared spectroscopy discloses different types of cell death in flow cytometrically sorted cells

Submitted to:

Biochimica et Biophysica Acta – General subjects

Abstract

Fourier Transform Infrared (FTIR) spectroscopy is a label free methodology showing promise in characterizing different types of cell death. Cell death induction has application in targeted treatment of diseases like cancer where successful intervention relies on the death of abnormal cells. Cervical adenocarcinoma (HeLa) and African monkey kidney (Vero) cells were treated with a necrosis inducer (methanol), novel apoptotic cell death inducers (diphenylphosphino gold (I) complexes and an extract of *Plectranthus ciliatus*) as well as positive controls of cell death auranofin and actinomycin D. Following treatment, cells stained with annexin-V and propidium iodide were sorted using a Fluorescence Activated Cell Sorter (FACS Aria) to obtain pure populations consisting of either viable, necrotic or apoptotic cells. FACS parameters and Transmission Electron Microscopy (TEM) confirmed successful sorting of all three populations. Four FTIR bands were identified which could significantly ($p < 0.05$) discriminate between viable and necrotic cells namely 1022 cm^{-1} (glycogen), 2852 cm^{-1} (lipids), 2875 cm^{-1} (lipids and proteins)and 2923 cm^{-1} (lipids). Significantly ($p < 0.05$) altered bands were identified in both cell lines which distinguished viable from apoptotic, viable from necrotic and apoptotic from necrotic cells. Principal Component Analysis showed good separation between the different types of cell death and the loadings plots indicated an increase in an additional band at 1623 cm^{-1} (β-sheet protein-protein interactions) in dead cells. FTIR spectroscopy can there for be developed into an invaluable tool for the assessment of specific types of chemically induced cell death. This is the first report where pure populations of fluorescence sorted cells were analysed by FTIR to identify biomarkers of cell death.

6.1 Introduction

Cervical cancer, which is primarily caused by a sexually transmitted human papilloma virus (strains 16 and 18), is increasingly becoming a threat in low income countries. The stage, in which the disease is diagnosed, determines the type of treatment as well as the prognosis [35]. In low income countries, women are generally uninformed of the dangers of sexually transmitted diseases and the associated complications. Screening for cervical cancer is also not widely available, which leads to the disease only being diagnosed at very late stages [36]. Cervical cancer is treated by surgery, radiation, chemotherapy or a combination of these. Since surgery is only effective in early stages of the disease, radiation and chemotherapy is generally used for treatment of the demand for the latter being the highest [40]. The most successfully used drug for the treatment of cervical cancer is cisplatin, but resistant cancers support the development of improved alternatives [30].

New chemotherapeutics derived from natural sources or through synthesis must be able to kill cancerous cells with the least amount of damage to neighbouring healthy cells and tissues. The assessment of new drug leads *in vitro* uses label-based biochemical assays which assess the viability or death of cells by measuring different enzyme activities, biomarkers and cell morphologies during and after treatments [61,73]. Flow cytometry and transmission electron microscopy are routinely used for the assessment of cellular responses including cell death. In flow cytometry, cells are labelled with fluorescent markers, such as annexin-V and propidium iodide. Annexin-V binds to phosphatidylserine that is externalized on the plasma membrane during apoptosis while propidium iodide intercalates into deoxyribonucleic acid (DNA) when plasma membrane integrity is lost as in the case of necrosis. When apoptosis is induced, phosphatidylserine is externalized during the early stages of the process [84]. Transmission electron microscopy (TEM) on the other hand is seen as the golden standard of characterizing the type of cell death induced. Using TEM cells are classified as apoptotic (with the presence or absence of autophagy) or necrotic based on morphological characteristics. In the case of necrosis, the plasma membranes are ruptured, mitochondria swollen with disruption of the cistae and nuclear dispersion visible. Characteristics of apoptosis, as seen with TEM, are associated with; plasma membrane blebbing, chromatin aggregation and detection of mitochondrial changes [91]. Autophagic cell death is characterized by the lack of chromatin condensation and the presence of large

autophagosomes. Autophagic cell death does not imply that cells died of autophagy but rather that autophagy was present at the time of death [18].

The above-mentioned conventional biochemical assays require labels, costly instrumentation and can also be very labour intensive. New methods are under investigation for effectiveness in measuring cell death without the need for labels that are expensive and that can cross react with other molecules. Two of those techniques are FTIR - and Raman spectroscopy. FTIR- and Raman spectroscopy have demonstrated biomedical applications in cancer research [136,192] including the ability to differentiate between healthy and cancerous cells / tissues, spectral differences between different tissues and types of cancers, grading of the stage of cancer progression and drug discovery where new drug leads were tested against the proliferation of cancerous cells as well as investigations on the molecular mechanism of action of known chemotherapeutics. Some spectral regions have been identified where cell death induction led to spectral differences in FTIR data [12,14,111,138,193]. In this study, two cell lines were investigated; cervical carcinoma cells (HeLa) and Vero cells (as noncancer control). Using both cell lines allows for the calculation of the selective index which is used to determine whether drug leads are specifically targeting cancer cells or cytotoxicity in general. In this investigation, we set out to determine whether FTIR microspectroscopy could successfully distinguish between viable, apoptotic and necrotic cells which are confirmed as such by supporting conventional (FACS, TEM) methodologies.

6.2 Methodology

6.2.1 *Cell death inducers and treatment of HeLa and Vero cells*

Cell death induction was facilitated by three different types of treatments previously confirmed to induce cytotoxic responses in Chapter 4, Chapter 5 and elsewhere [3,194,195]. Two synthetic gold compounds namely; 2-(2-(diphenylphosphino) ethyl)pyridyl-gold(I) chloride (AE 76) and 2-(diphenylphosphino)-20-(N,N-dimethylamino) biphenylgold(I) chloride (AE125) were synthesized [178,179] and characterized by Elkhadir (2014) [48] under the supervision of Prof. Darkwa at the Department of Chemistry, University of Johannesburg, South Africa. Auranofin, a well-known gold compound notorious to be cytotoxic against cancer cells and used for the treatment of rheumatoid arthritis was included as a positive control [44]. Two different types of naturally derived products were also

investigated in this study namely; an antineoplastic antibiotic, actinomycin D, which is an antibiotic polypeptide isolated from Streptomycin *spp*. used for the treatment of several types of cancers [63,196] and used as a positive control. A crude plant extract of *Plectranthus ciliatus* that comes from a genus that are widely used for its medicinal properties [5] was also included. Necrosis was induced by mechanical and chemical stress simultaneously through the use of ice cold methanol. Methanol is known to be extremely toxic to cells and when the cells (1.5×10^6 cells/mL) were exposed to ice cold methanol (2 mL), minuscule crystals caused poration of the plasma membranes. Cytotoxicity was measured with tetrazolium dye and confirmed with Real Time Cell Electronic Sensing (RT-CES) which indicated a decrease in cell viability within the first few hours after treatment for all apoptotic inducers (Chapter 4) [195].

Cervical carcinoma (HeLa) and African monkey kidney (Vero) cells (Highveld Biological, Johannesburg, South Africa) were used in this investigation. The selection of the cells were based on including both diseased (HeLa) and healthy (Vero) cells in this study because apoptosis and necrosis are universal processes that do not discriminate based on pathogenesis. The two cell lines are also morphologically similar. Propagation of the two cell lines was done as previously described [61]. When the cells reached 80-90% confluency, the cells were briefly trypsinized (Hyclone, Separations, Johannesburg) and counted. HeLa - and Vero cells were seeded in 10 mL complete media at 1.5×10^6 cells / 25 cm^2 flask and for the untreated control 0.2×10^6 cells / 25 cm^2 flask were plated. For downstream analysis of the cell, a minimum of 1.5×10^6 cells were essential and, therefore since sudden cytotoxic responses were seen with the treatments, 1.5×10^6 cells were plated initially. Due to the treatment time the cells doubled to ~ 1.5×10^6 cells/mL when 0.2×10^6 cells were plated. After 24 hours following cellular adherence to the cell culture flasks, the cells were exposed to the treatments (Table 6.1) and incubated for 72 hours. The treatments were dissolved in cell culture tested dimethyl sulfoxide (DMSO) to assure that all natural derived and gold complexes dissolved completely. The final % DMSO exposure for the cells was 0.09 % for HeLa cells and 0.2% for Vero cells. It was found that since the untreated cells were left to grow optimally for 96 hours in total, the cells reached approximately 1.5×10^6 cells in the flasks. To obtain a positive control for necrosis, cells were treated with 2 mL ice cold methanol (100%), for up to 10 minutes. After 72 hours, cells were harvested and suspended in complete media so the membranes could recover from trypsinization. The cells were then

incubated for 1 hour in a humidified incubator at 37°C to allow the plasma membrane to recover. Cells (3×10^6) were centrifuged for 5 minutes at 1200 rpm. The supernatants were discarded and the cells washed with 2 mL binding buffer (BD Biosciences, Johannesburg, South Africa). The cells were then resuspended in 100 µL binding buffer and stained with 5 µL annexin-V and 5 µL propidium iodide (Apoptosis Detection Kit II, BDBioSciences, Johannesburg, South Africa). The cells were incubated for 15 minutes in the dark and washed with 500 µL binding buffer. The stained cells were suspended in 500 µL before flow cytometric analysis.

Table 6.1. Treatments used to induce maximum cell death in HeLa and Vero cells

Treatment	HeLa cells[a]	Vero cells[a]
Auranofin	5.6 µM	2.9 µM
AE 76	20.8 µM	13.2 µM
AE 125	17.8 µM	13.9 µM
Actinomycin D	0.04 µg/mL	0.22 µg/mL
Plectranthus ciliatus extract	18.5 µg/mL	39.7 µg/mL
Ice cold methanol	100%	100%

[a] The concentrations used were determined by XTT to induce maximal cell death

6.2.2 *FACS staining and sorting for further analyses*

Before sorting, standard protocols, as advised by BD Biosciences (Germany, Europe), were conducted. Those protocols included the calibration of the stream using the Accudrop delay function. After the stream had been calibrated, a test sort was done to determine the accuracy of the FACS sorting. The accuracy was tested using cytometer setup and tracking (CST) beads which gave three distinct populations of beads when interrogated. The beads were sorted in a two way sort using the purity function. Approximately 40,000 beads per population were sorted before it was measured again. It was found that the sorting was always 99.99% accurate. The cells could not be analysed with the flow cytometer after sorting because the cells were photo bleached and thus had no fluorescent signal.

Annexin-V and propidium iodide fluorescence were measured using a BD FACS Aria flow cytometer (BD Biosciences) equipped with an air-cooled argon laser (excitation 488 nm). The annexin-V signal was detected using the FitC channel and the propidium iodide signal

using the PE-Texas Red channel. The parameters of the FACS Aria (BDBiosciences, South Africa) were optimized for cell death analysis. Data of 10,000 cells were analysed with the BD FACS Diva Software Version 6.1 (BD Biosciences) before the sorting started. The population of interest (annexin-V negative, propidium iodide negative: viable cells or annexin-V positive, propidium iodide negative: early apoptotic cells or annexin-V negative, propidium iodide positive: necrotic cells) was sorted continuously until ~1.2 x 10^6 cells were sorted per population group of interest.

6.2.3 *Transmission electron microscopy*

After 3 x 10^6 cells were sorted, the cells were centrifuged for 5 minutes at 1200 rpm and resuspended in phosphate buffered saline (PBS). The supernatants were discarded without disruption of the pellets and the cells fixated in TEM fixative (2.5% gluteraldehyde, 2.5% formaldehyde in 0.075 M PBS, pH 7.4) for 1 hour. The samples were rinsed with 0.075 M PBS twice for 10 minutes each and then fixed in 0.5% aqueous osmium tetroxide for 30 minutes. After incubation, the samples were rinsed twice with distilled water. The samples were then dehydrated stepwise with ethanol (30%, 50%, 70%, 90%, 100%, 100%, 100% each for 10 minutes) and stored at 4°C for a few days until all the samples were sorted and dehydrated. The dehydrated samples were infiltrated with 50% Quetol for 30 minutes, followed by 100% Quetol for 3 hours. After infiltration, the samples were polymerized at 60°C for 40 hours. Ultrathin sections of the samples were cut with a Reichert-Jung Ultracut E microtome with a Diatome diamond knife and transferred on to copper mesh grids. The sections were contrasted by staining the samples with 4% uranyl acetate for 5 minutes, followed by staining the samples with Reynold's lead citrate for 2 minutes [197]. The sections were then examined using a multipurpose transmission electron microscope (Phillips, 301) at the Laboratory of Microscopy and Microanalysis (University of Pretoria, South Africa) [198].

6.2.4 *FTIR microspectroscopy analyses of sorted cells*

Sorted cells were incubated at room temperature in 1 mL 10% formalin (in PBS) for 10 minutes. The supernatant was discarded and the cells washed twice with 1 mL sterile distilled water to remove all traces of formalin and PBS, which could influence the spectra. The supernatant was removed and the cells suspended in 10 µL sterile distilled water. The cell

suspensions (3 µL) were dried in the biosafety hood for one hour on sterile CaF_2 discs. The FTIR spectra were obtained with a 15x IR objective of Hyperion microscope attached to a Bruker V70x spectrometer equipped (Bruker, Germany). Using a liquid nitrogen cooled detector attached to the microscope, 30 areas were analysed containing a lawn of cells (~ 400 cells per area). Spectra in the range of 850-4000 cm^{-1} were recorded. Data were collected in transmission mode and spectra (4 cm^{-1} spectral resolution, co-added for 100 scans) recorded using Bruker OPUS software. All the spectra were pre-processed using OPUS 7 software. Atmospheric contributions (water vapour and CO_2) were subtracted and the spectra vector normalized. Baseline correction was done using the rubber band function. Second derivatives were calculated (17 smoothing points) and used for interpretation and statistical analysis in the same manner as in Chapter 4 and published elsewhere [13,108,195]. An unsupervised method, hierarchical cluster analysis was performed to identify trends in the spectra. One way ANOVA was calculated for all bands together with the Tukey and Bonferroni posthoc test to identify significantly different ($p < 0.05$) bands. HeLa cells were analysed and trends were observed with natural product induced or gold complex induced apoptosis and necrosis. The trends were noted when the positive control, as well as the experimental treatments, were significantly altered. After the bands had been identified in HeLa cells, the bands were also investigated for Vero cells to determine if there were any shared cell death marker bands.

6.3 Results and discussion

HeLa and Vero cells were sorted to obtain pure populations of cells that were either viable, apoptotic or necrotic. To confirm the staining and sorting, the cells were investigated using transmission electron microscopy before further analyses with FTIR spectroscopy. With flow cytometry, it was observed that untreated cells were viable and thus remained unstained (Fig. 6.1 and Fig 6.2). The percentages DMSO did not show any detrimental effects on the cells and viability was similar to that of untreated HeLa and Vero cells (Appendix). It was found that separating the cells based on fluorescence was an easy and convenient method to obtain large numbers of the desired cell populations. The FACS Aria was able to sort cells with an accuracy of 99.99%.
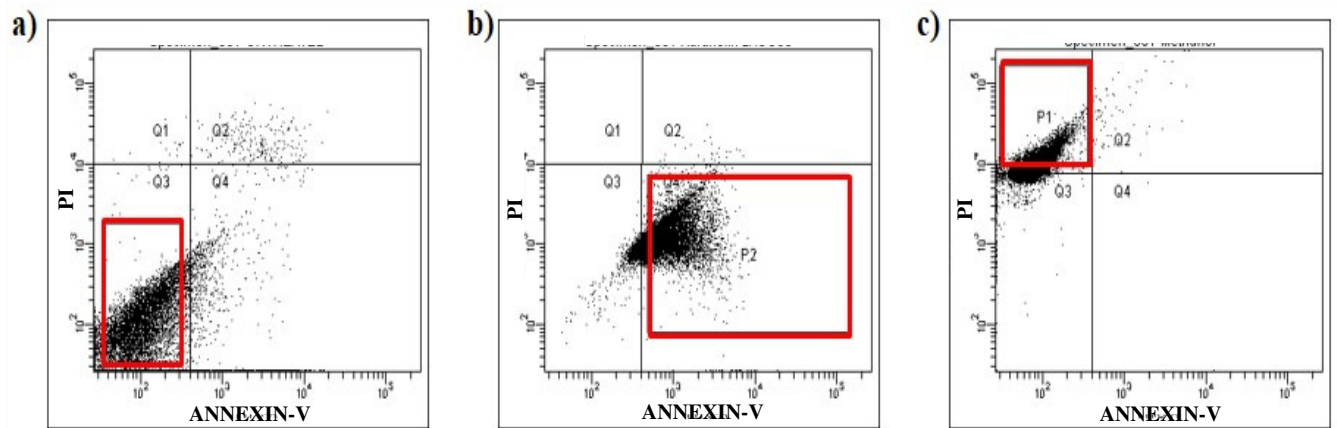
Fig. 6.1. Representative dot plots used to select an area of interest within the cell population (HeLa cells) to be sorted. Typical dot plots for sorting (a) viable cells (annexin-V negative, propidium iodide negative), (b) apoptotic cells (annexin-V positive, propidium iodide negative) or (c) necrotic cells (annexin-V negative, propidium iodide positive).
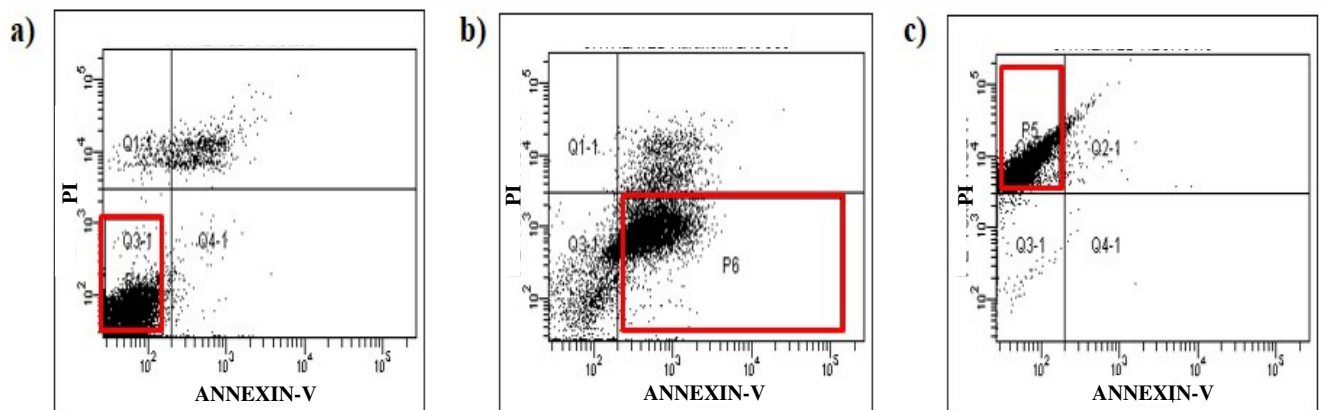
Fig. 6.2. Representative dot plots used to sort Vero cells into pure populations based on fluorescence. Typical dot plots for sorting (a) viable cells (bottom left quadrant) (b) apoptotic cells (bottom right quadrant) or (c) necrotic cells (top left quadrant).

To confirm that the sorting process could effectively separate populations of interest, transmission electron microscopy was performed on collected populations. It was found that untreated viable cells (annexin-V negative, propidium iodide negative) had average nuclear material distribution within the nucleus and a clearly defined nucleolus while the nuclear envelope was intact and clearly visible. The organelles were plentiful and cytoplasm densities were similar between the two cell lines. The plasma membranes were intact with normally distributed protrusions seen, usually used for adherence (Fig. 6.3 (a) and Fig. 6.4

- 112 -

(a)). Necrotic sorted cells were achieved by treating the cells with ice cold methanol; small ice crystals porated the plasma membranes, causing the cell contents to leak. It was quite clear that the sorted cells had damaged plasma membranes and aggregated cellular components. Severely damaged mitochondria were observed which included swollen mitochondria with disrupted cistae. The nuclear material was also dispersed and granular (Fig. 6.3 (b) and Fig. 6.4 (b)). Cells that were sorted as early apoptotic mostly showed signs of condensed chromatin which in most cases were fragmented and marginalized on the inside of the nuclear envelop (Fig. 6.3 (c) to 6.3 (g) and Fig. 6.4 (c) to 6.4 (g)). Big clear vacuoles were present in most apoptotic cells, with the exception of actinomycin D treated Vero cells that had prominent autophagic vacuoles containing cytoplasmic material. In the case of actinomycin D treated Vero cells, apoptosis in the presence of autophagy were induced due to the presence of autophagic vacuoles and plasma membrane blebbing (Fig. 6.4 (f)). Sorted cells had features of the specifically sorted group of cells. Different severities of apoptosis were identified. Since apoptosis is a dynamic process, the morphological characteristics differed between the treatments depending on the onset time of cell death induction. The probability of interrogating the correct type of induced cell death, using FTIR spectroscopy was high because of the accuracy of sorting.
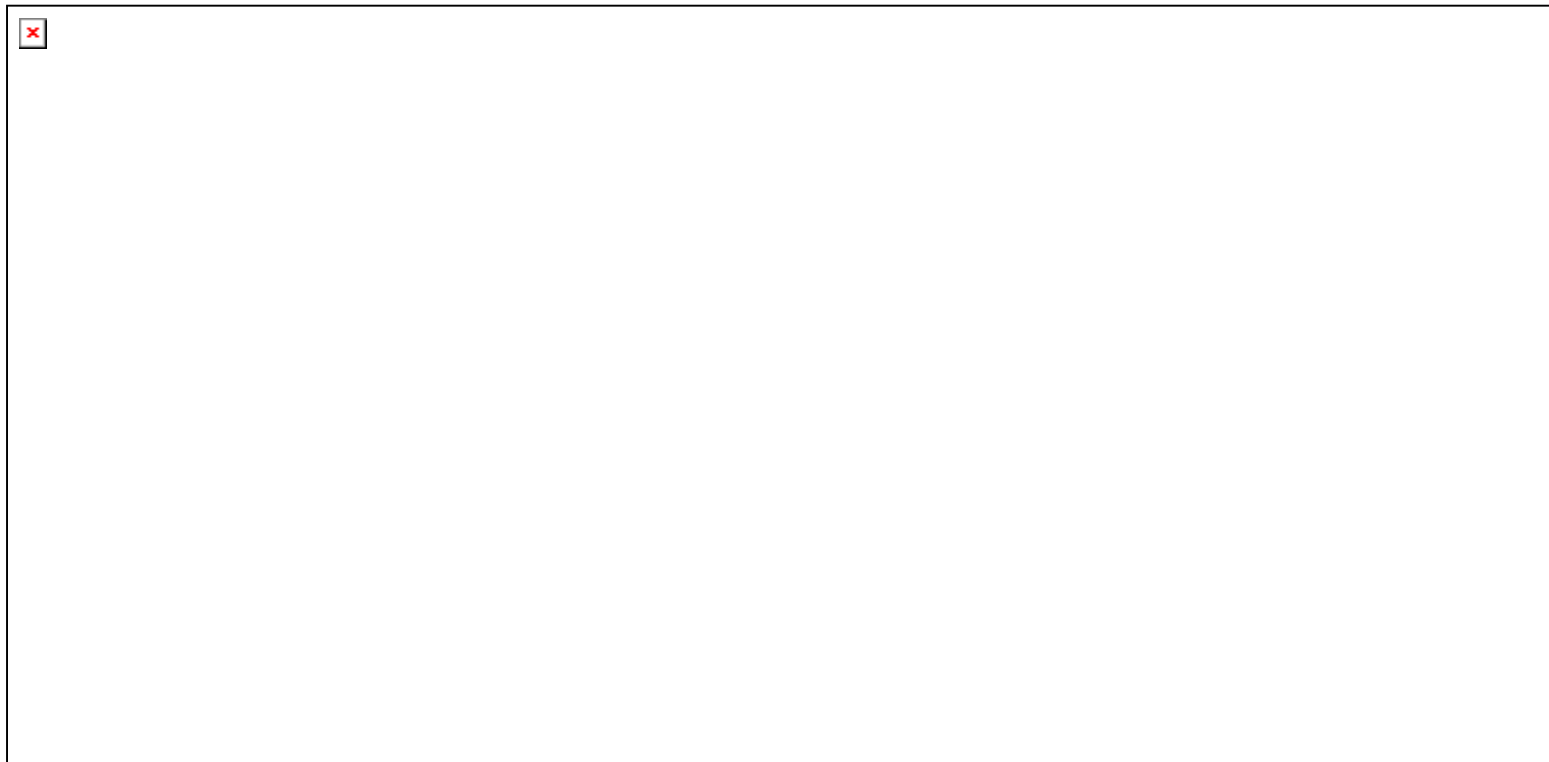
Fig. 6.3. Electron micrographs of the sorted HeLa cells based on annexin-V and propidium iodide staining. (a) Untreated viable cell with a large nucleus (red arrow) and intact plasma membrane (purple arrow), (b) the methanol treated nectrotic cell had a ruptured plasma membrane (purple arrow), dispersed granular nuclear material (red arrow) and swollen mitochondria (green arrow) in the cytoplasm associated with necrosis, (c) auranofin treated cell showed signs of apoptosis, which includes a nucleus with condensed chromatin (red arrow), membrane bledbbing (purple arrow), big vacuoles (blue arrow) and apoptotic bodies (black arrow), (d) AE76 treated cell showed signs of nuclear membrane folds (red arrow), vacuoles (blue arrow) and plasma membrane blebbing (purple arrow) with apoptotic bodies (black arrow), (e) AE 125 treated cell has nuclear membrane folds (red arrow), plasma membrane blebbing (purple arrow) with apoptotic bodies (black arrow), (f) actinomycin D treated cells shows signs of condensed nuclear material (red arrow), significant vacuole formation (blue arrow), (g) *Plectranthus ciliatus* treated apoptotic cells had fragmented nuclear material (red arrow), vacuole (blue arrow) and apoptotic bodies (black arrow). Different stages of early apoptotic cell death were detected with the synthetic gold compounds and naturally derived products.
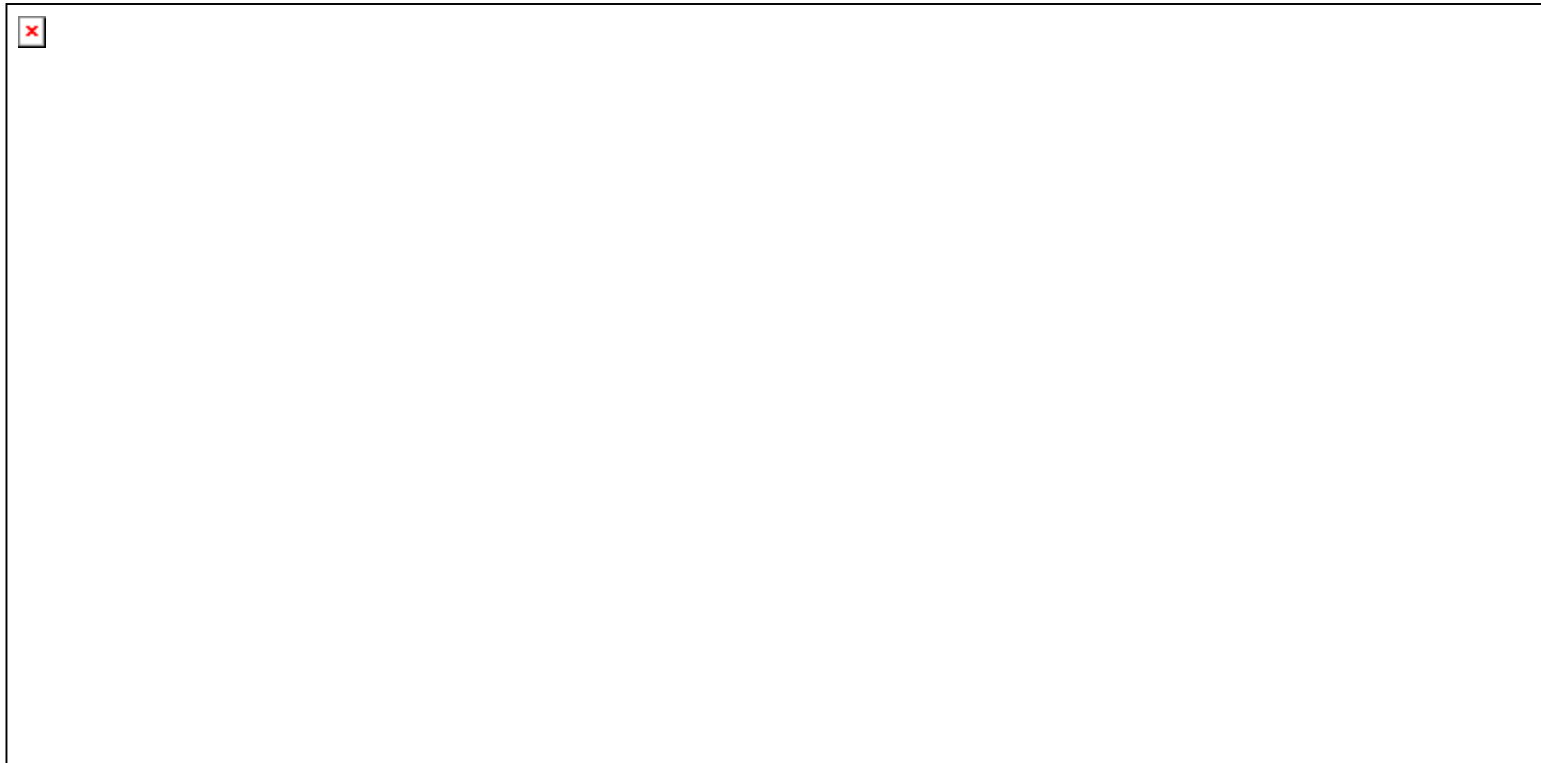
Fig. 6.4. Electron micrographs of flow cytometrically sorted Vero cells based on fluorescence. (a) Untreated viable cell with intact plasma membrane (purple arrow) and nucleus (red arrow) and with a vacuole (blue arrow), b) methanol treated nectrotic cell showed severe morphological damage due to chemical stress like ruptured plasma membrane (purple arrow) and a nucleus containing aggregated dispersed chromatin. Mitochondria were swollen and contained disrupted cistae. (c) Auranofin treated cell had marginalised nuclear material (red arrow) with apoptotic bodies being released from the blebbing plasma membrane (black arrow). (d) AE76 treated cells had fragmented condensed chromatin (red arrow) with vacuoles present in the cytoplasm (blue arrow) and visible apoptotic bodies (black arrow), while (e) AE 125 treated cells has similar apoptotic features as AE 76 treated cells. The features include fragmented DNA and apoptotic bodies. (f) Actinomycin D treated cell had visible autophagosomes (navy arrows) that is indicative of autophagy, while apoptotic characteristics included condensed mitochondria (blue arrow) and blebbing plasma membranes (purple arrows) with apoptotic bodies (black arrow). (g) *Plectranthus ciliatus* treated cell had condensed chromatin (red arrow) and blebbing cell membranes with apoptotic bodies (black arrow).

6.3.1 *FTIR spectroscopy measurements for the detection of cell death specific vibrational bands*

After the confirmation that the cells were successfully sorted into viable, apoptotic and necrotic cell death groups, FTIR spectroscopy was used to investigate if the same vibrational bands of apoptosis and necrosis were evident when using different cell death inducers and different cell lines. The second derivatives of FTIR spectra were used for the interpretation of the results since second derivatives are known to emphasize small spectral differences [13,108]. After the data had been analysed, it was found that a definite trend existed in most of the spectral bands. The trend was based on the fact that viable cells' spectra were significantly different when compared to naturally derived product treated cells or synthetic gold compound treated and necrotic cells' spectra. Significantly ($p < 0.05$, one way ANOVA, post hoc tests) altered bands were identified and the similarities and differences between the cell lines discussed (Fig. 6.5, Fig. 6.6 and Table 6.2).
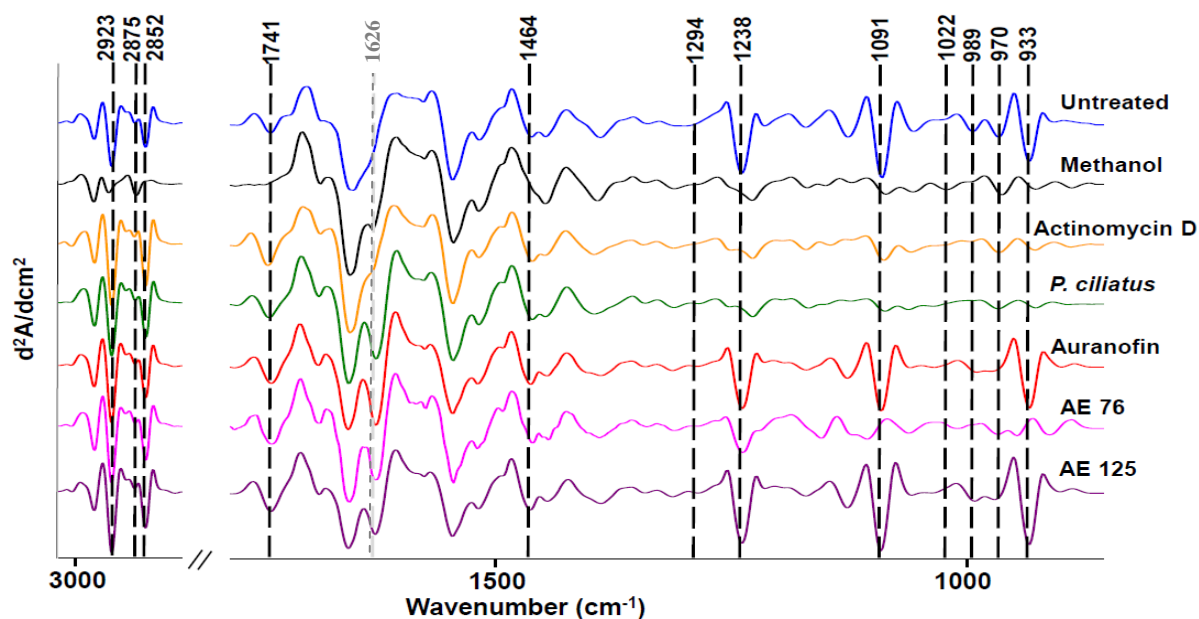
Fig. 6.5. The average second derivatives of untreated (viable) – and treated HeLa cells. Viable cells were compared to methanol treated cells (necrotic) as well as to synthetic (auranofin, AE 76 and AE 125) gold compounds treated cells and natural derived (actinomycin D and *P. ciliatus*) treated cells. Although some of the spectral trends were visible to the naked eye, statistical analyses were conducted to determine significantly altered bands. Significantly different bands (ANOVA one way, posthoc Tukey and Bonferonni, $p < 0.05$) are indicated in black while the band indicated in grey showed visible evidence of cell death which was not significant.

Firstly in HeLa cells, significantly altered nucleic acid associated bands were identified at 933 cm^{-1}, 970 cm^{-1}, 989 cm^{-1}, 1091 cm^{-1} and 1238 cm^{-1}. A strong band at 933 cm^{-1} was detected in viable, auranofin and AE 125 treated HeLa cells. This vibrational band decreased significantly ($p < 0.001$) with all other treatments. The band at 933 cm^{-1} was assigned to the vibrational mode of the C-O-C ring of deoxyribose in Z-form DNA [151,154,158]. The bands at 989 cm^{-1}, 1238 cm^{-1} and 1091 cm^{-1} were assigned to PO_4^{2-} (nucleic acids), antisymmetric and symmetric stretching modes of phosphates (PO_2^-) found in DNA [155,156,199]. The presence of the five above mentioned bands in viable cells were indicative that the nuclei were associated with metabolically active cells.

The high absorbance at 933 cm^{-1} could be indicative of active transcription in which case Z-DNA could be prominent [200] while, on the other hand, the cells might have been moderately stressed due to the sorting process which could also have increased the peak absorbance or dehydration of the cells. In a previous study it was found that viable unsorted HeLa cells only had a very small shoulder band at 933 cm^{-1}, while chemically stressed cells had a prominent band at 933 cm^{-1}, therefore supporting the statement that the cells in this study might have been experiencing some minor mechanical / electrical stress due to the sorting process. Dehydration of the cells was also not likely to have caused in increase in this peak, since drying time of the cells remained the same in this and the previous study (Chapter 4) [195]. On the other hand the TEM micrographs of sorted viable HeLa cells did not indicate any visible signs of the cells experiencing possible fatal stress and therefore the cells were prone to be more metabolically active due to the small amount of cellular stress (Chapter 4) [86,195]. Strong DNA signals are usually detected in metabolically active cells or in cells that are in late stages of apoptosis when the cell's DNA became fragmented. The detection of DNA signals is very low when the DNA is condensed and tightly packed [199]. In the case of auranofin and AE 125 treated HeLa cells, the prominent bands at 933 cm^{-1}, 1091 cm^{-1} and 1238 cm^{-1} could be indicative of DNA fragmentation that was also evident in the TEM micrographs. Actinomycin D, *P. ciliatus* and AE 76 treated apoptotic cells had low absorbencies for 933 cm^{-1}, 989 cm^{-1}, 1091 cm^{-1} and 1238 cm^{-1} compared to viable cells, which could be due to later stages of apoptosis, where the nucleus membranes become affected and starts blebbing, while the formation of apoptotic bodies could also lead to lower concentrations of DNA in the cell. Necrotic HeLa cells displayed faint bands at 933 cm^{-1},

989 cm^{-1}, 1091 cm^{-1} and 1238 cm^{-1} which was as expected due to the dispersion of DNA in the nucleus and lysis of the nuclear membrane (karyolysis).

Table 6.2. A summary of the significantly (p < 0.05, One way ANOVA and post hoc tests) altered FTIR bands and the description of the alterations in terms of viability and cell death.

Wavenumber	p-value (HeLa)	Post hoc	p-value (Vero)	Post hoc
933	0.00003	Viable versus apoptosis (NP)[6]	NS[7]	
		Viable versus necrosis		
970	0.004	Viable versus necrosis	NS	
989	0	Viable versus apoptosis (NP)	NS	
		Viable versus necrosis		
1022	0.009	Viable versus necrosis	0.003	Viable versus necrotic
				Necrosis versus apoptosis (NP)
				Necrosis versus apoptosis (GC)[8]
1091	0.0002	Viable versus apoptosis (NP)	NS	
		Viable versus necrosis		
1238	0.001	Viable versus apoptosis (NP)	NS	
		Viable versus necrosis		
1294	0.004	Viable versus apoptosis (GC)	NS	
1315			0.01	Viable versus necrotic
1346			0.03	Viable versus necrotic
1464	0.005	Necrosis versus apoptosis (NP)	0.0004	Necrosis versus apoptosis (GC)
1626			0.0008	Viable versus apoptosis (GC)
1718	NS		0.0006	Viable versus necrosis
				Necrosis versus apoptosis (GC & NP)
1741	0.0007	Necrosis versus apoptosis (NP)	0.00001	Viable versus necrosis
		Necrosis versus apoptosis (GC)		Viable versus apoptosis (GC)
				Necrosis versus apoptosis (GC & NP)
2852	0.0004	Viable versus necrosis	< 0.0001	Viable versus necrosis
		Necrosis versus apoptosis (NP)		Viable versus apoptosis (GC)
		Necrosis versus apoptosis (GC)		Necrosis versus apoptosis (GC & NP)
2875	0.00003	Viable versus necrosis	0.00009	Viable versus necrosis
		Necrosis versus apoptosis (NP)		Necrosis versus apoptosis (GC & NP)
		Necrosis versus apoptosis (GC)		
2896			0.0001	Viable versus necrosis
				Necrosis versus apoptosis (GC)
2923	0.0001	Viable versus necrosis	< 0.0001	Viable versus necrosis
		Necrosis versus apoptosis (GC &NP)		Viable versus apoptosis (GC & NP)
				Necrosis versus apoptosis (GC & NP)

---

[6] NP refers to naturally derived products, actinomycin D (positive control) and *P. ciliatus*
[7] NS indicates to Not Significant
[8] GC refers to gold complexes; auranofin (positive control), AE 76 and AE 125.

Another DNA related band that changed significantly in HeLa cells was 1294 cm^{-1} assigned to N-H vibrations of cytosine [158]. The vibrational band increased significantly when the cells were treated with gold compounds. This increase in absorbance could be due to interactions with the gold compounds or the mechanism elicited with this type of compounds such as DNA fragmentation or an interaction of nucleic acids exposing cytosine. An increase in phosphorylated proteins and DNA (970 cm^{-1}) were detected in all treated HeLa cells but were only found be significantly increased in necrotic cells, which could be due to a survival mechanism of cells containing DNA breaks [201] in which case repair proteins were phosphorylated before trying to fix the breaks [202]. None of the above-mentioned vibrational bands were significantly altered in Vero cells after treatment, although similar trends between the treatments were seen in this region (Fig. 6.6).
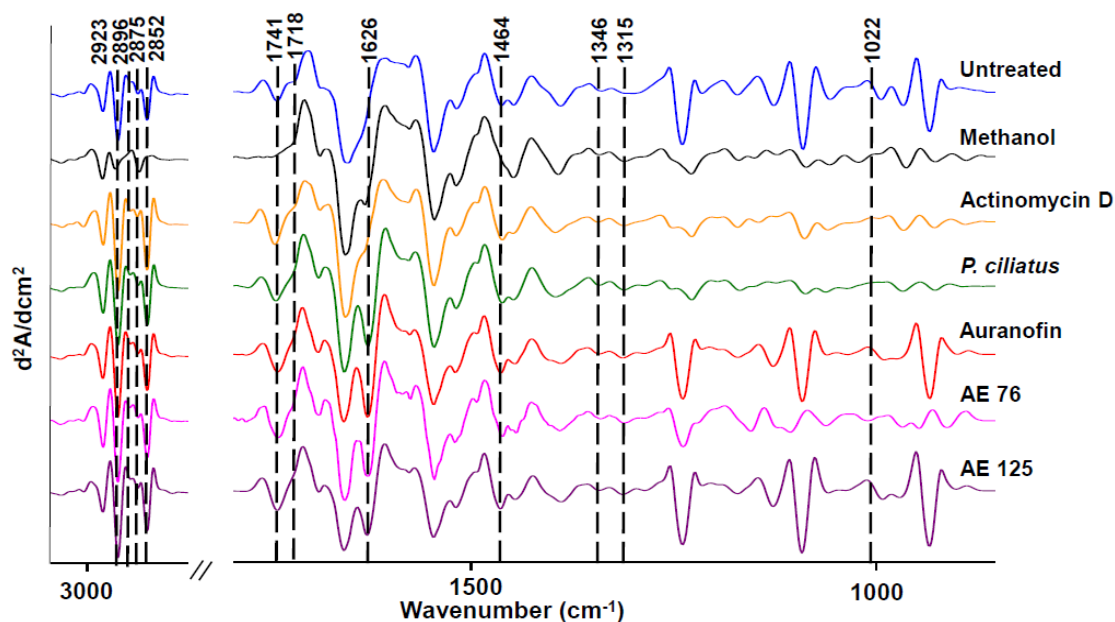
Fig. 6.6. The average second derivatives of untreated (viable) – and treated flow cytometrically sorted Vero cells. Viable cells, methanol treated cells (necrotic), synthetic (auranofin, AE 76 and AE 125) gold compounds treated cells and natural derived (actinomycin D and *P. ciliatus*) treated cells spectra were compared to each other. Statistical analyses were conducted to determine altered bands using ANOVA one way, posthoc Tukey and Bonferonni and the bands indicated in black.

Glycogen (1022 cm-1) was significantly decreased in necrotic HeLa cells. The glycogen band was also significantly decreased in Vero necrotic cells. Necrosis is a passive process and thus does not need energy for progress, but since the plasma membranes were ruptured

due to the treatment, it was most likely that the metabolites leaked out of the cells. In Vero cells, the vibrational bands at 1315 cm^{-1} and 1346 cm^{-1} were altered in necrotic cells that led to an increase in the intensity of the bands. The bands were assigned to CH vibrations and protein bound tryptophan respectively. Due to the harsh methanol treatment that the cells underwent many of the proteins could have denatured. One of the vibrational bands visibly altered in both dead HeLa - and Vero cells (but only significantly altered in Vero cells) was the appearance of the band at 1623 cm^{-1}. This band was assigned to intermolecular β-sheet protein-protein interactions suggestive of protein compactness and the degree of protein aggregation [203]. Zelig *et al.* (2009) found that a decrease in α-helices and an increase in β-sheets were indicative of apoptosis and that the degree of β-sheets could be linked to the stage of apoptosis [13]. In the present study, it was observed that all apoptotic HeLa and Vero cells had similar trends in the presence of β-sheets, although actinomycin D was different. The presence of autophagy could have resulted in much lower detection of the β-sheets. Recently, Yadav *et al.* (2014) found that mitochondrial proteins were favourably in β-sheets as compared to α-helices during apoptosis [204], which may partly explain the detection of β-sheets in some apoptotic cells. Necrotic HeLa and Vero cells also had a detectable conformational changes in amide I region, with an increase in β-sheets, although not as prominent as found with apoptotic cells. The β-sheet formation could be due to the severity of the necrosis inducer used in the present study and, therefore, the possibility of detecting this band after other types of necrotic induction should be investigated. In this study, the detection of β-sheets was indicative of cell death.

A very small shoulder band was identified as 1717 cm^{-1} and assigned to guanine and thymine (C=O) [205] as well as glutamine and asparagine in Vero cells. This band was detected as significantly altered only in Vero cells. It was seen that the small band decreased in necrotic cells. The change in the peak suggests changes within DNA and RNA most likely due to the dispersion of nuclear material. The vibrational bands at 1464 cm^{-1} (CH_2 vibration of acyl chain of lipids), 1741 cm^{-1} (C=O ester vibration of phospholipids), 2852 cm^{-1} (symmetric CH_2 vibration of lipids), 2875 cm^{-1} (C-H stretching of lipids and proteins of CH_3) and 2923cm^{-1} (antisymmetric CH_2 vibrations of lipids) [13,138,158,162] were altered in both cell lines. The vibrational bands of necrotic cells at 1464 cm^{-1} and 1741 cm^{-1} were significantly lower in absorbencies as compared to apoptotic cells but not compared to viable cells. This decrease in lipid absorbencies could be due to some of the lipid components (lipophilic) of

the cells having dissolved / extracted in the methanol during treatment. In the case of 1464 cm^{-1} necrosis could be distinguished from apoptotic cells, while the phospholipid C=O band could distinguish between necrotic and apoptotic HeLa and Vero cells; viable from necrotic (Vero) and apoptotic from viable (Vero). The vibrational bands 2852 cm^{-1}, 2875 cm^{-1} and 2923 cm^{-1} were significantly affected by the induction of necrosis; with necrotic cells being significantly different from viable and apoptotic cells.

A possible reason why viable and apoptotic cells were not significantly different may be due to the fact that when cells undergo apoptosis (as seen in Fig 6.3, where metallodrugs and naturally derived products induced apoptosis), the plasma membranes remain intact [10], while with chemically induced necrosis (methanol treated cells), the plasma membrane structural integrity is compromised, causing some lipids to dissolve in the methanol. Similar trends such as the disappearance of the peaks at 2925 cm^{-1} and 2852 cm^{-1} were seen when Vero cells were fixed using acetone [206]. Gaudenzi *et al.* (2004) found a positive correlation between the vibrational band of ~2928 cm^{-1} increasing in intensity and the detection of the % apoptosis using annexin-V. Annexin-V binds to phosphatidylserine, which is a phospholipid externalized during apoptosis. It was speculated by Gaudenzi *et al.* (2004) that the vibrational band could be directly attributed to phosphatidylserine [111]. These authors used Jurkat cells treated with actinomycin D while, in the current study, various treatments tested on different cell lines showed highly variable spectral intensities of 2928 cm^{-1} with no significant differences observed for this band. The region of 2800 – 3000 cm^{-1} could be useful in distinguishing necrotic cells from viable cells or necrotic cells from apoptotic cells. A vibrational band around 1742 cm^{-1} assigned to C=O (ester linkage) of membrane phospholipids was identified with major spectral changes accompanied by different types of induced cell death. Under normal conditions, when cells are proliferating, only a shoulder of this peak can be seen [138,183]. Munro *et al.* (2010) investigated the cytotoxicity of arsenic trioxide against the proliferation of leukemic HL60 cells and tried to characterize the changes in the 1740 cm^{-1} band to apoptosis with little success, since trypan blue enters dead cells and does not discriminate between apoptotic and necrotic cells. Holman *et al.* (2000) acknowledged the potential of the phospholipid peak as a potential molecular marker for dead cells [193]. On the other hand, other researchers concluded that lipid content in terms of relative absorbance cannot be used for the distinction between types of cell deaths [13,14].

Summary of ANOVA data

Based on significant changes in both cell lines four bands were identified which could discriminate between viable and necrotic cells namely 1022 cm^{-1}, 2852 cm^{-1}, 2875 cm^{-1} and 2923 cm^{-1} (Table 6.2). None of these or any other bands could distinguish between viable and apoptotic cells for positive controls or experimental treatments. Four bands could distinguish necrotic cells from apoptotic cells in both cell lines these were; 1741 cm^{-1}, 2852 cm^{-1}, 2875 cm^{-1} and 2923 cm^{-1}. Four bands detected in HeLa cells could distinguish between viable and naturally derived product induced apoptosis (933 cm^{-1}, 989 cm^{-1}, 1091 cm^{-1} and 1238 cm^{-1}), while only one band could distinguish between viable and gold complex induced apoptosis (1294 cm^{-1}). Nine bands were identified as able to distinguish between viable and necrotic HeLa cells. Those bands were 933 cm^{-1}, 970 cm^{-1}, 989 cm^{-1}, 1022 cm^{-1}, 1091 cm^{-1}, 1238 cm^{-1}, 2852 cm^{-1}, 2875 cm^{-1}, 2923 cm^{-1}. Nine bands could also distinguish between viable and necrotic Vero cells (1022 cm^{-1}, 1315 cm^{-1}, 1346 cm^{-1}, 1718 cm^{-1}, 2852 cm^{-1}, 2875 cm^{-1}, 2896 cm^{-1} and 2923 cm^{-1}). Only one band was significantly different to distinguish between viable and natural product induced apoptosis. The band was at 2923 cm^{-1} while three bands were identified to be significantly different from viable and gold complex induced apoptosis namely; 1626 cm^{-1}, 1741 cm^{-1} and 2852 cm^{-1}. Significantly altered bands that could discriminate between necrotic and apoptotic cells were; 1022 cm^{-1}, 1718 cm^{-1}, 1741 cm^{-1}, 2852 cm^{-1}, 2875 cm^{-1} and 2923 cm^{-1}.

6.3.2 *Principal component analysis of FTIR spectra*

Principal component analysis (PCA) was also carried out for the treatments to determine the patterns in the spectral data based on similarities and differences within the data. This analysis is an unsupervised method used for data reduction [101]. It was found that when all of the HeLa cells' data were analysed in one PCA, there was poor separation between the types of cell death groups, better separation was found when natural products and metal based compounds were not analysed together. Significant band alterations were also found to be extremely variant between cell lines and between the different types of apoptosis inducers (natural derived products and gold complexes) that also supported the reasoning why not all the treatments and positive controls were analysed in one PCA plot per cell line. Since the PCA was performed on second derivatives, a negative score was associated with a positive loading [138]. When viable, natural derived product induced apoptosis and necrotic HeLa

cells were analysed, it was found that the spectral variance could be described by the first two Principal Components (PC) (Fig. 6.7 (a)). Major bands identified in the loading plot describing the PCA plot are illustrated in Fig. 6.7. (b). It was found that apoptotic and necrotic cells had decreased absorbencies at 933 cm^{-1}, 1091 cm^{-1} and 1238 cm^{-1}. In the PC 1 loading plot, a definite increase in the absorbance at the band 1623 cm^{-1} was also seen in dead cells. In the PC 2 loading plot, there was an increase in the absorbencies at 2852 cm^{-1} and 2923 cm^{-1} which were associated with apoptotic cells. These findings were in agreement with the statistical analysis discussed in the previous section.
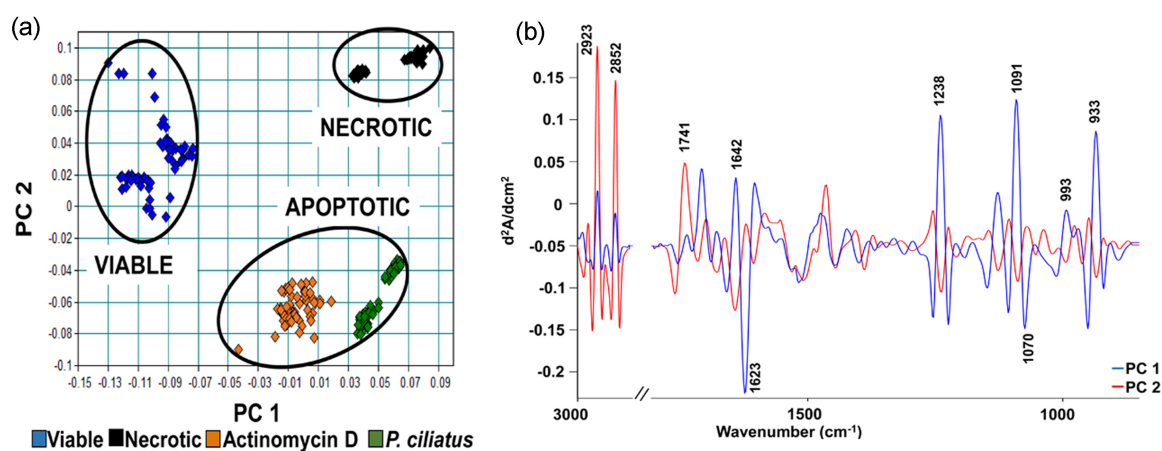
Fig. 6.7. (a) The PCA plot of viable, necrotic and naturally derived product induced apoptosis. Clear separation was seen between viable and dead HeLa cells in PC 1 while PC 2 separated the viable and necrotic cells from the apoptotic cells. **(b) The loading plots of the PCA.** The major differences indicated were also determined to be in most cases significantly different (p < 0.05).

When the HeLa cells were treated with metallodrugs, some separation could also be observed which signifies that FTIR spectroscopy can distinguish between different types of cell death induction. The first two PCs explained the total variance within the spectra (Fig. 6.8 (a)). Better separation was seen along PC 2, where viable cells were separated from the dead (necrotic and apoptotic cells). The most prominent band was identified as an increase in β-sheets in the amide I band which was associated with dead cells. In the loading plot, it was confirmed that significantly altered bands (Table 6.2) were mostly responsible for the separation seen in Fig. 6.8 (b).
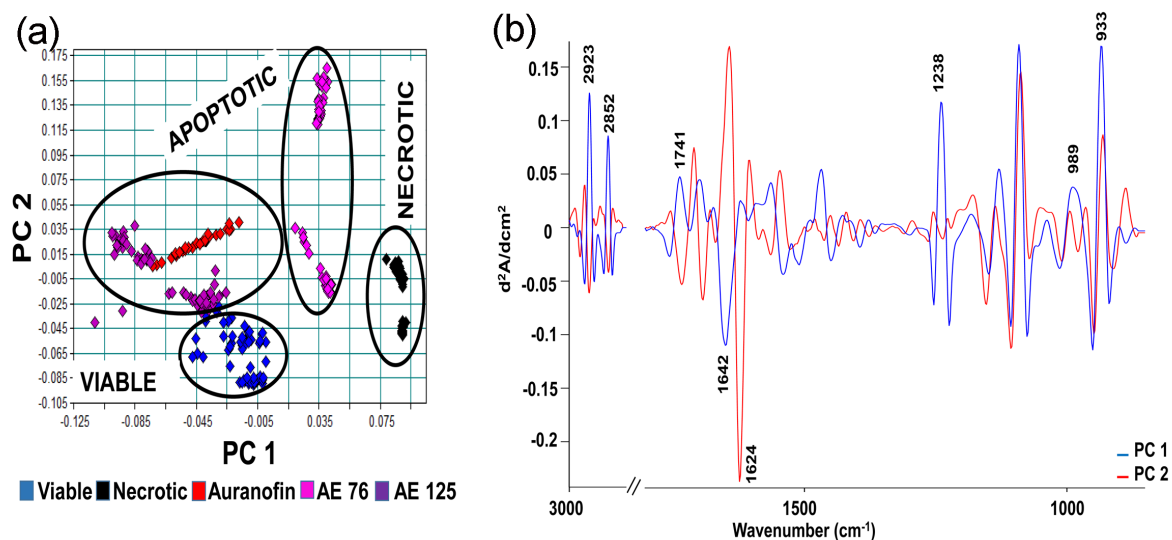
Fig. 6.8. **(a) The PCA plot of viable, necrotic and metallodrug induced apoptosis of HeLa cells.** Separation was seen between viable / apoptotic and necrotic HeLa cells in PC 1 while PC 2 moderately separated the viable cells from apoptotic- and necrotic cells. It was observed that AE 125 treated cells were situated very closely to the viable cells. **(b)** **The loading plots of the PCA.** The major differences indicated were also determined to be in most cases significantly different.

Good separations were also obtained when Vero cell spectra were investigated. The total variance in the spectra of viable, necrotic and natural derived product induced apoptotic Vero cells were best explained using PC 2 and PC 3 (Fig. 6.9 (a)). The most prominent band was again, as found in HeLa cells, the band at 1623 cm^{-1} that was of a higher intensity in dead cells. When the Vero cells treated with metallodrugs were investigated, it was found that the first two components could explain the most variance in the data. In PC 1 as well as PC 2, the band at 1623 cm^{-1} was prominent and, therefore, played an important role in the separation of the different groups. It was confirmed as previously in HeLa cells that an increase in the peak at 1623 cm-1 was indicative of dead cells. Although that band was not found to be significantly altered, it was seen with PCA that the band and, therefore, the presence of β-sheets in Amide I conformation could give important leads in the identification of dead cells.
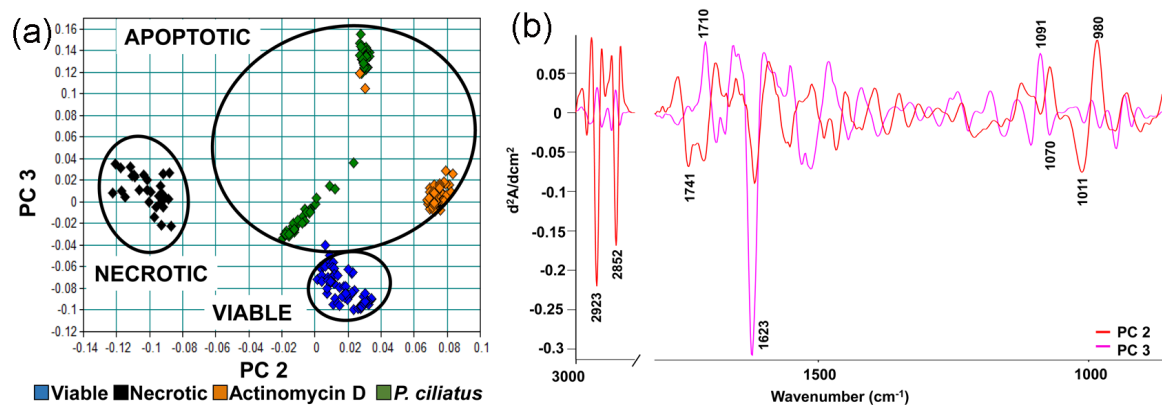
Fig. 6.9. (a) The PCA plot of viable and dead (necrotic and naturally derived products induced apoptosis) Vero cells. Separation was seen between viable / apoptotic and necrotic Vero cells in PC3 while PC2 separated the viable / apoptotic cells and necrotic cells. It was observed that there were variances in the spectra of *P. ciliatus* treated cells most likely due to heterogeneity in the cells due to apoptosis that is a dynamic process. **(b) The loading plots of the PCA that was constructed**. The major differences were also determined to be in most cases significantly altered. Some bands were not further investigated since the significantly altered bands were identified in HeLa cells and those bands were then investigated further in relation to changes in Vero cells.
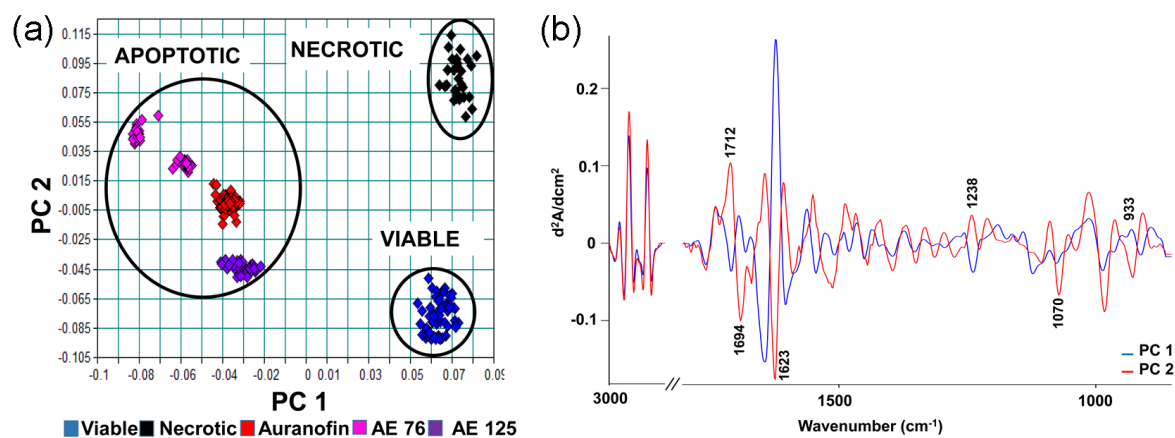
Fig. 6.10. (a) The PCA plot of viable, necrotic and metallodrug induced apoptosis in Vero cells. Clear separation was seen between viable / necrotic and apoptotic cells in PC 1 while PC2 separated the viable cells from apoptotic- and necrotic cells. **(b) The loading plots of the PCA.** The major differences indicated were also determined to be in most cases significantly different.

To summarize, in this investigation pure populations (viable, apoptotic and necrotic) were obtained by FACS. Successful sorting was confirmed by TEM after which populations were investigated using FTIR microspectroscopy. Several bands were found to be useful in distinguishing between necrotic and viable cells in different cell lines. This study

- 126 -

demonstrated the importance of investigating cancer cells in parallel with noncancerous cells when assessing the specific type of cell death induced by a drug lead. The conformational change in amide I, with a definite increase in β-sheets, is of importance and could be developed into a biomarker of cell death, although the exact origin of the band should still be further analysed. Lipid rich regions were also detected as potential parameters for cell death detection. DNA rich regions of the FTIR spectra were found to be of interest in cancerous cells, with many bands changing significantly when cell death was induced. FTIR spectroscopy can be developed into an invaluable tool to investigate new drug leads and to study the repurposing of drugs conventionally used to treat other diseases (for example auranofin).

Chapter 7: Fluorescent activated sorting of dead cells to determine spectral characteristics by Raman spectroscopy

To be submitted to the Biophysical Chemistry Journal

Abstract

Raman spectroscopy has been used for various biomedical applications in the past few years. Here Raman spectroscopy was used to investigate whether chemically induced apoptosis and necrosis in two different cell lines would be able to produce altered peaks able to characterize cell death status. Apoptotic cell death was induced with metallodrugs and naturally derived products while necrotic cell death was induced by treating the cells with ice cold methanol. Apoptosis was firstly assessed by detecting caspase 3 / 7 activity using a bench top assay. The cells were then flow cytometrically sorted (annexin-V and propidium iodide) into particular populations of cells namely; viable, early apoptotic and necrotic and directly afterwards investigated using Raman spectroscopy. Caspase dependent apoptosis was detected in HeLa and Vero cells with up to five fold increase in activity for the cell death inducers (excluding necrotic inducer). *P. ciliatus* induced caspase activity of up to 40 fold increased activity, although the activity was weak in actinomycin D treated cells. Flow cytometric sorting of apoptotic and necrotic cells were an easy and rapid method for accurately purifying cell populations. Raman spectroscopy detected cell death biomarkers, some that were previously identified and also new bands that can be used to distinguish between viable and dead cells. Necrotic cells had increased band absorbance at 762 cm^{-1} and an increase in the intensity of phosphodiester bond vibrations. Necrotic cells were also associated with decreased absorbance bands for phosphatidylcholine and phosphatidylserine. Apoptotic cells had increased bands at 762 cm^{-1} assigned to phosphatidylethanolamine which was also detected previously. A known apoptotic biomarker, 785 cm^{-1} was also prominent in this study, which also validated the sorting of the cells. A band at 1572 cm^{-1} was identified in apoptotic and some necrotic cells which had not been previously been described in necrotic cells.

7.1 Introduction

The quantification of cell death plays an important role in the investigation of potential cancer treatments induced by radiation, immunotherapy and chemotherapeutics. The two major cell death processes are apoptosis and necrosis, although other forms also exist [18]. Apoptotic cell death is known as programmed cell death in which case cells die and are cleared by phagocytic cells. When cell death is caused by ruptures of the cell membrane which leads to cytoplasm leaking from the cells, the cell death is called necrosis. Necrosis is mostly unwanted clinically since the leakage of the cells causes local inflammation. Apoptosis is detected with a range of assays which includes caspases 3/ 7, flow cytometry for the detection of phophatidylserine exposure, western blotting, DNA fragmentation electrophoresis and microscopy [10,16].

In vitro and *ex vivo* detection of drug induced cell death can be determined with biochemically labelled molecules such as annexin-v (binding to phosphatidylserine which is externalized during apoptosis) and propidium iodide (intercalates in between DNA bases and indicative of cellular membrane integrity loss associated with necrotic cells). Flow cytometric analysis can quantitatively distinguish between the stage of apoptosis and whether necrosis took place in one run. The assay is based on the principle that phosphatidylserine is exposed on the outer membrane of cells when apoptosis is initiated. Annexin-V binds to phosphatidylserine which is then indicative of early apoptotic cells. When the cells are more deteriorated such as in the case of not being phagocytised the cells membranes will start to disintegrate, which then gives the opportunity for propidium iodide (in dual staining with annexin-V) to intercalate with cell DNA. The cells will thus have a positive signal for both annexin-v and propidium iodide, which is then revealing of late apoptosis or secondary necrosis. Necrotic cells have ruptured plasma membranes that allow propidium iodide to inter the cells, but not annexin-V to bind to phosphatidylserine, since it is not exposed on the outside membrane. A positive signal of only propidium iodide is suggestive of necrosis [83,84].

Although biochemical and morphological assessment is widely used and accepted practice, the potential applications of label free methods are continually being investigated. Label, free methods in the long run, could be more cost effective, more sensitive and the results

- 129 -

more reproducible. Scientists are now moving into operating theatres to assists surgeons in removing solid cancers from healthy tissues. Where pathologists are used to making sure the borders of cancerous tissues are completely removed, Raman spectroscopy potentially does the same chemical mapping the area before and after surgery.

In the previous study done in our lab, we identified biomarkers of chemically induced apoptosis using Raman spectroscopy (Chapter 5) [194]. The cell populations consisted of cells containing 70 – 90% early apoptotic cells, 5-15% late apoptotic cells and less than 5% necrotic cells. Of the cells investigated, the bands around 761 cm^{-1} assigned to tryptophan, ethanolamine and phosphatidylethanolamine together with the carbonyl / ester bond vibration of phospholipids could be seen as potential markers for plasma membrane alterations indorsing apoptosis. Those peaks needed to be confirmed with other types of cell death induction and thus this research was carried out (Chapter 5) [194]. The aim of the study was to expand our previous study to find potential markers that could detect apoptotic and necrotic cells independent of the cell line. Two cell lines (cancerous and healthy) were used to determine if any feasible vibrational bands could be identified in different tissues.

7.2 Methodology

To investigate cell death markers using Raman spectroscopy, the cells had first to be treated with cell death inducers that were tested previously to determine the concentration for maximal cell death. The cells were then analysed to determine the initiation and execution of apoptosis using a caspases 3 / 7 assay before the cells were ultimately sorted and investigated using Raman spectroscopy.

7.2.1 *Cell death inducers*

Cell death induction was facilitated by two different types of treatments. Firstly, natural derived products, *P. ciliatus* ethanolic extract (kindly donated by P. Kapewangolo, Department of Biochemistry, University of Pretoria, South Africa) and actinomycin D (positive control), was used in this study because *P. ciliatus* is a member of the genus Plectranthus that is notorious for medicinal properties [5], while actinomycin D is an antibiotic isolated from *Streptomyces* species and used for the treatment of a variety of

cancers.[63]   Secondly, metal based compounds 2-(2-(diphenylphosphino)ethyl)pyridyl-gold(I) chloride (AE 76) and 2-(diphenylphosphino)-20-(N,N-dimethylamino)biphenylgold (I)chloride (AE125) were synthesised [178,179] and characterization by Elkhadir (2014) [48] under the supervision of Prof. Darkwa at the Department of Chemistry, University of Johannesburg, South Africa. The positive control, auranofin (gold compound known to be cytotoxic against cancerous cells and used for the treatment of rheumatoid arthritis[131]) was also included.

7.2.2 *Cell lines and treatment concentrations*

Cervical carcinoma (HeLa) cells and monkey kidney (Vero) cells (Highveld Biological, Johannesburg, South Africa) were used in this investigation. The cell lines were grown under conditions previously described.[61] When the cells reached 80-90% confluency, the cells were briefly trypsinized (Hyclone, Separations, Johannesburg) and counted.

Table 7.1. Concentrations used to induce cell death in HeLa and Vero cells[a]

Treatment	HeLa cells	Vero cells
Auranofin (CC_{50})	2.8 µM	1.45 µM
Auranofin (2 x CC_{50})	**5.6 µM**	**2.9 µM**
AE 76 (CC_{50})	10.4 µM	6.62 µM
AE 76 (2 x CC_{50})	**20.8 µM**	**13.2 µM**
AE 125 (CC_{50})	8.94 µM	6.93 µM
AE 125 (2 x CC_{50})	**17.8 µM**	**13.9 µM**
Actinomycin D (CC_{50})	0.02 µg/mL	0.11 µg/mL
Actinomycin D (2 x CC_{50})	**0.04 µg/mL**	**0.22 µg/mL**
***Plectranthus ciliatus* extract (CC_{50})**	9.23 µg/mL	19.85 µg/mL
***Plectranthus ciliatus* extract (2 x CC_{50})**	**18.5 µg/mL**	**39.7 µg/mL**
Ice cold methanol	**100%**	**100%**

[a] The concentrations used were determined by XTT (Chapter 3)

7.2.3 *Caspases 3 / 7 activity of treated cells*

Caspase-3/7 activities were measured using the Apo-ONE Homogeneous Caspase-3/7 Assay kit (Promega, Madison, USA) according to the manufacturer's suggestions. HeLa and Vero cells were plated in 96 well plates (1 x 10^5 cells/well) and incubated 24 hours before

treatments were added. Treatments at two different concentrations (Table 7.1) were added and the cells incubated for six hours. After the six hours had elapsed, the cells were frozen in lysis buffer that contained caspase substrate Z-DEVD-R100 at -80 °C and left overnight. Caspase substrate Z-DEVD-R100 was added to the wells and incubated in the dark at room temperature for 18 hours. Caspase-3/7 activities were measured as fluorescence released from Z-DEVD- R100 at 485/538 nm (excitation/emission) using a fluorescence microplate reader. Three independent experiments were conducted.

7.2.4 *Flow cytometric analysis of the cells with annexin-V and propidium iodide*

HeLa - and Vero cells were seeded at 1.5×10^6 cells per 25 cm^2 flask and for untreated cells control 0.2×10^6 cells were plated. Since a large number of cells are needed for sorting, the experiments were conducted in 25 cm^2 flasks, since the cell death inducers were previously found to induce apoptosis within the first few hours, a large number of cells could be treated. On the other hand, untreated cells double within 24 hours and therefore the amount of cells plated were optimized to get around ~ 3×10^6 cells / mL before sorting which was then similar to the amount of treated cells. After 24 hours, to allow for attachment of the cells, the cells were exposed to the treatments and incubated for 72 hours. The treatment concentrations were determined using a tetrazolium salt viability (XTT) assay and the highest concentrations were used to produce maximal cell death induction (Table 7.1, concentrations in bold).

To obtain a control for necrosis, cells were also treated with ice-cold methanol (100%), for up to 10 minutes on ice. After 72 hours, detached cells were pooled with trypsinized cells and resuspended in 2 mL growth medium. The cells were then incubated for 1 hour in a humidified incubator at 37°C to allow the plasma membranes to recover after trypsinization. Cells (~ 3×10^6) were centrifuged for 5 minutes at 1200 rpm. The supernatants were discarded and the cells washed with 2 mL binding buffer (BD Biosciences, Johannesburg, South Africa). The cells were resuspended in 100 µL binding buffer and stained with 5 µL annexin-V and 5 µL propidium iodide (Apoptosis Detection Kit II, BDBiosciences, Johannesburg, South Africa). The cells were incubated for 15 minutes in the dark and

washed with 500 µL binding buffer. The stained cells were suspended in 500 µL before analysis.

7.2.5 *FACS sorting for further analyses*

Before sorting, standard protocols as advised by BD Biosciences (Germany, Europe) were conducted. Those protocols included the calibration of the stream using the Accudrop delay function. After the stream had been calibrated, a test sort was done to determine the accuracy of the FACS sorting. The accuracy was tested using cytometer setup and tracking (CST) beads which gave three distinct populations of beads when interrogated. The beads were sorted in a two way sort using the purity function. Approximately 40,000 beads per population were sorted before it was measured again. It was found that the sorting was always 99.99% accurate. The cells could not be analysed with the flow cytometer after sorting because the cells were photo-bleached and thus had no fluorescent signal.

Annexin-V and propidium iodide fluorescence were measured using a BD FACS Aria flow cytometer (BD Biosciences) equipped with an air-cooled argon laser (excitation 488 nm). The annexin-V signal was detected using the FitC channel and the propidium iodide signal using the PE-Texas Red channel. The parameters of the FACS Aria (BDBiosciences, South Africa) were optimized for cell death analysis. Data of 10,000 cells were analysed with the BD FACS Diva Software Version 6.1 (BD Biosciences) before the sorting started. The population of interest (annexin-V negative, propidium iodide negative: viable cells or annexin-V positive, propidium iodide negative: early apoptotic cells or annexin-V negative, propidium iodide positive: necrotic cells) was sorted continuously until ~1.2 x 10^6 cells were sorted per population group of interest.

7.2.6 *Raman microspectroscopic investigation of sorted viable and dead HeLa and Vero cells*

The measurements and analysis were carried out as previously published (Chapter 5) [194]. Briefly, the 50x objective of an Olympus microscope (attached to T64000 micro-Raman spectrometer from HORIBA Scientific) was used to focus the 514.5 nm laser beam (spot size ~ 2 µm) in the middle of air-dried individual cells. The center of the cell is where the nucleus

- 133 -

is situated [11,123,182]. The laser power was kept constant at 10 mW. Three independent experiments were carried out and 20 - 30 cells per treatment were analysed. All the spectra were recorded with a 150 seconds acquisition time for two accumulations. The Labspec 6.0 software was used to fit and subtract a fourth order polynomial function to obtain a zero baseline. A 5 degree linear Savitsky-Golay smoothing procedure was applied to all the spectra. Second derivatives of the spectra (vector normalized) were used for final interpretations (generated in OPUS 7). PCA analysis was carried out on the second derivatives in the Quant 2 function (OPUS 7, Bruker, Germany).

7.3 Results and discussion

Apoptosis was firstly detected by measuring caspase 3 / 7 activity of treated cells, after which flow cytometry confirmed the presence of apoptosis and necrosis induced by methanol. Cells were then sorted and interrogated using Raman spectroscopy.

7.3.1 *Caspases 3 / 7 activity as indicator of apoptosis*

To determine whether the caspase-dependent apoptotic activity was modulated by the treatments, HeLa and Vero cells were treated with two different concentrations for 6 hours. Six hours of incubation with the treatments were selected based on previous RT-CES results (Chapter 4 and Appendix A3). Previously it had been found that caspase 3 activity is involved in the detachment of cells during apoptosis [207–210]. It was found that in both cell lines that the highest concentrations tested, an immediate decrease in the CI value occurred, which indicated that the cells are already dying and, therefore, the caspase activity will most probably be detected in the first few hours after treatment. At the lower concentrations tested a variety of different responses were measured.

Caspase activity in viable cells was found to be approximately five Relative Fluorescence Units (RFU) (Fig. 7.1). After the cells were treated with auranofin, the fluorescence and therefore caspase 3 / 7 activity increased three fold, with only a two fold increase when the cells were treated with 5.6 μM. HeLa cells treated with AE 76 and AE 125 also displayed similar trends in activity as auranofin. Caspase activity for cells treated with AE 76 were slightly higher when the cells were treated with 10.4 μM (CC_{50}) than when the cells were

treated with 20.8 µM (2 x CC$_{50}$). A major increase in caspase activity was observed when the cells were treated with 8.9 µM (CC$_{50}$), a five fold increase compared to untreated counterparts while lower activity was observed at higher concentrations. When caspase 3 / 7 activity was measured after cells were treated with naturally derived products, an opposite trend was observed. Actinomycin D treated cells did not produce well detectable levels of caspase activity while 18.5 µg/mL *P. ciliatus* treated cells had an increase of 40 fold in the activity. Cells treated with 9.2 µg/mL *P. ciliatus* produced approximately ten fold increase.
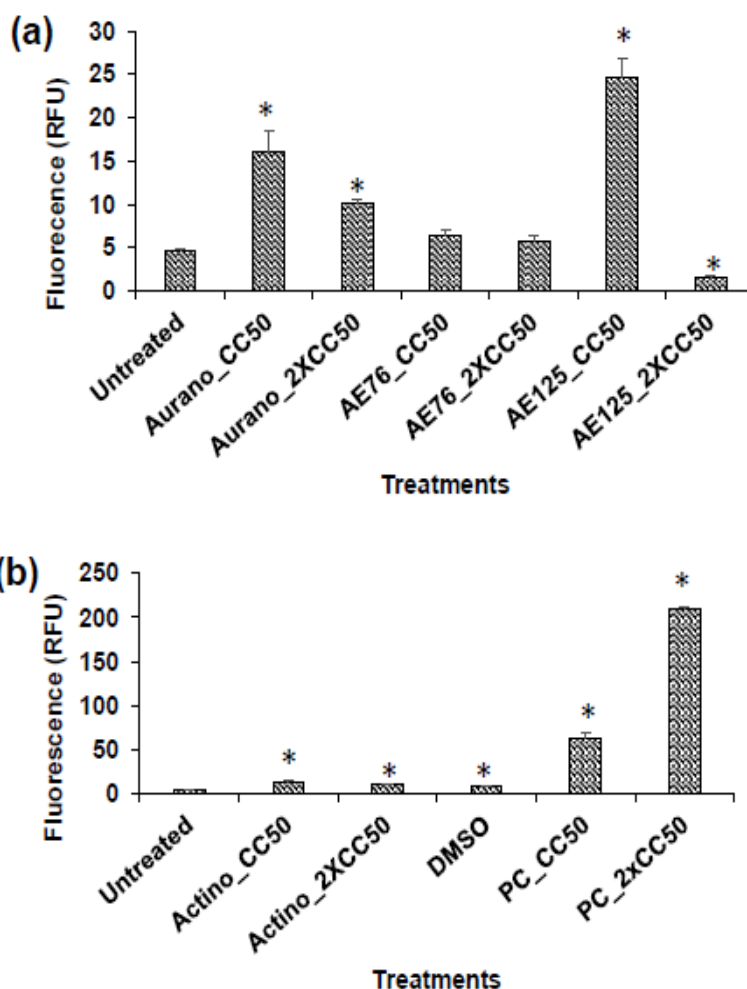
Fig. 7.1. Bar graphs illustrating the percentages fluorescent Rhodamine 110 detected in Relative Fluorescence Units (RFU) after the HeLa cells are treated with different concentrations cell death inducers. (a) Caspase 3 / 7 activities after the cells were treated with (a) metallodrugs, auranofin (aurano), AE 76, AE 125, (b) naturally derived products, actinomycin D (Actino) and *P. ciliatus* (PC). An increase in caspase activity is detected in most treatments, although not all caspase activities are increased significantly (*p < 0.05 compared to untreated cells, # *P. ciliatus* is compared to DMSO treated cells) (n=3).

In Vero cells, a different trend was observed in caspase activity (Fig. 7.2). When the cells were treated with auranofin, the caspase activity increased three fold irrespective of the concentration of the treatment (although the RT-CES curves were not comparable). Vero cells treated with AE 76 and AE 125 had higher caspase activity when the cells were treated with higher concentrations of AE 76 and AE 125. The activities were five and three fold higher respectively. When the cells were treated with 6.6 µM AE 76, a fourfold increase was detected while no changes were observed when the cells were treated with 6.9 µM of AE 125. Actinomycin D treated Vero cells also showed poor caspase activity while *P. ciliatus* (PC) treated cells had an approximate 32 fold increase in caspase activity irrespective of the concentration.
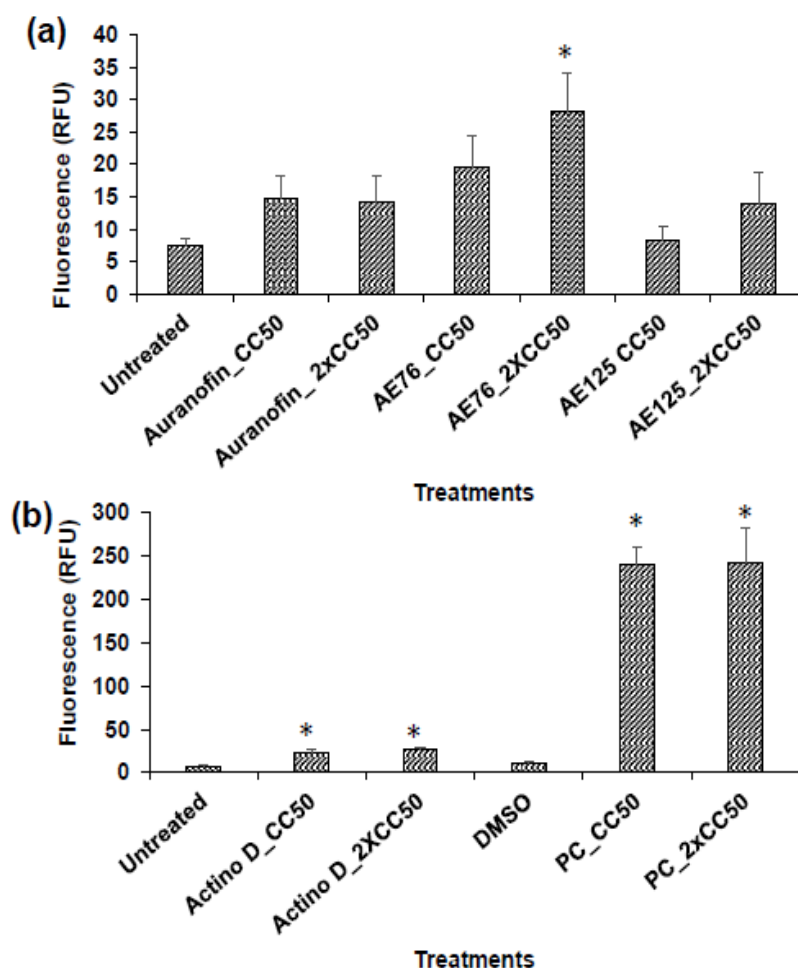
Fig. 7.2. Bar graphs illustrating the percentages fluorescent Rhodamine 110 detected in RFU after the Vero cells are treated with different concentrations cell death inducers. (a) Caspase 3 / 7 activities after the cells are treated with (a) metallodrugs, auranofin (aurano), AE 76, AE 125, (b) naturally derived products, actinomycin D (Actino) and *P. ciliatus* (PC). An increase in caspase activity is detected in most treatments, although not all caspase activities are increased significantly (One way ANOVA, *$p < 0.05$, # *P. ciliatus* is

compared to DMSO treated cells) for all treatments (n=3). The best caspase activity was detected in cells after been treated with *P. ciliatus*. All activities were measured after 6 hours treament.

Even though, the RT-CES curves for all the treatments at the highest concentrations tested had very similar curves, the activity of caspase 3 / 7 varied immensely. After most of the treatments, there was a significant increase in caspase 3 / 7 activity, which indicate that apoptosis is induced and caspase dependent. Different mechanism of actions of the treatments, as well as differences in the cell lines, made it difficult to find an optimal time to take measurements. Actinomycin D had very low caspase activity in both cell lines, but this could be expected since actinomycin D is known to inhibit the protein synthesis and autophagic mediated cell death which could take longer to initiate (Chapter 6). For further analysis, 72 hours incubation was used to ensure that enough time was granted for apoptosis to occur.

7.3.2 *FACS for the collection of pure viable, apoptotic and necrotic cells based on fluorescence*

Cells were investigated using flow cytometry to quantify the percentage dead cells (Appendix: Section A3). Large percentages dead cells were identified as early apoptotic after treatment and qualified for downstream experiments. Dot plots were constructed during the FACS experiments and representative zebra plots illustrated in Fig. 7.3 and Fig. 7.4. Blocks in the figures indicated the areas of interest that were selected for sorting. Cells were classified and sorted based on the ability to bind either annexin-V or propidium iodide or none of the above. HeLa and Vero cells were treated with two concentrations for each treatment, but only one concentration, the highest concentration (2 x CC50) was used for further analysis and sorting of the cells. It was observed that the higher the concentration of the treatment, the larger the population of cells that could be sorted. Only one treatment gave very small percentages dead cells in both cell lines. That treatment was actinomycin D. As found in previous chapters (chapter 4 and chapter 6); actinomycin D was not as potent in inducing apoptosis as the rest of the cell death inducers. A small percentage cell death was induced, which ranged between 5% and 45% (Appendix, Section A5 for average percentages). During cell sorting the fluorescence of the fluorochromes were quenched and

- 137 -

thus reanalysis of the sorted cells to check the accuracy of the sorting procedure could not be confirmed by flow cytometry[9].

---

[9] FACS sorting was validated using TEM as discussed in Chapter 6.
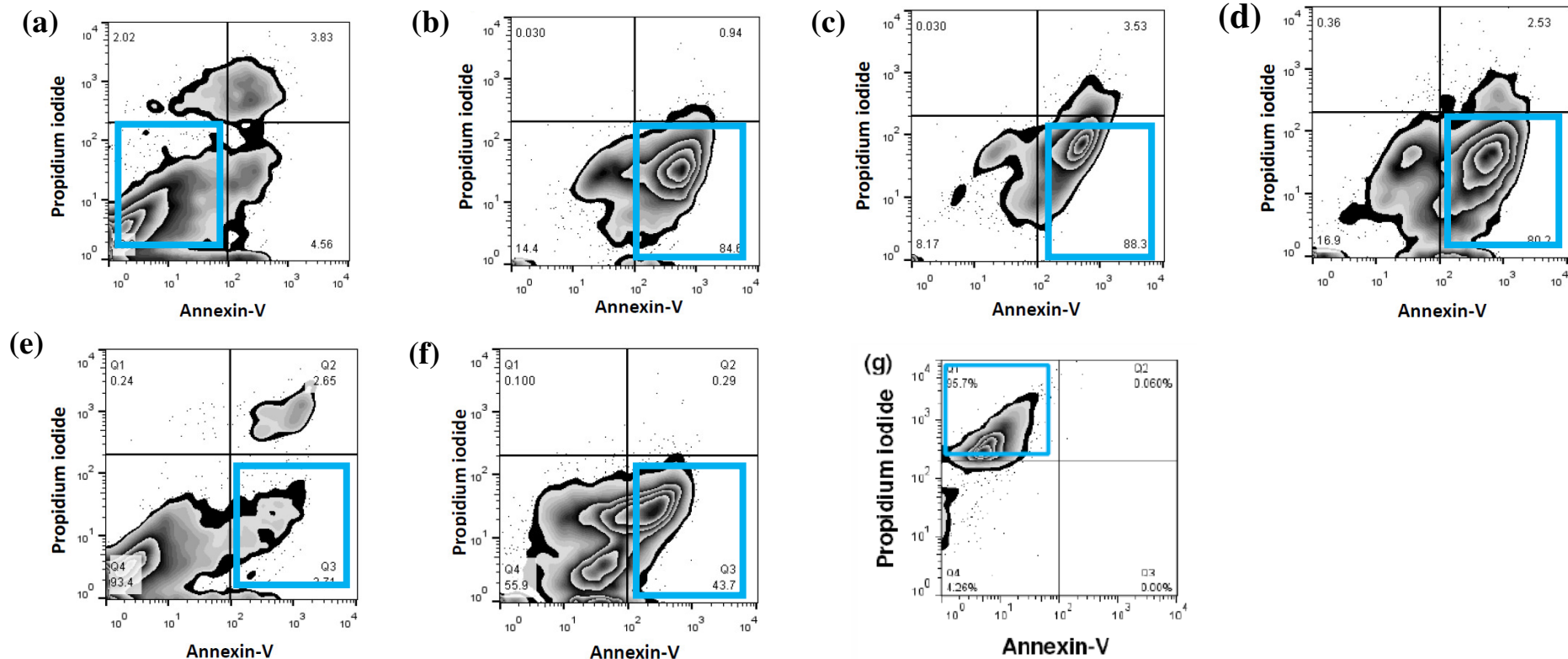
Fig. 7.3. Flow cytometry representative zebra plots for viable and dead HeLa cells: Treatments induced cell death of HeLa cells and measured with annexin-V and propidium iodide. Metallodrugs and naturally derived products are used as cell death inducers. (a) Untreated HeLa cells are viable with the cells not staining (annexin-V negative, propidium iodide negative). Each treatment's effect is measured at a concentration that was determined with an XTT viability assay for maximal cell death. (b) Auranofin 2 x CC_{50} displays one population that consisted of 85% apoptotic cells. A similar trend is seen when the cells were treated with (c) AE 76 2 x CC_{50} where an apoptotic population of cells was 88%. (d) AE 125 2 x CC_{50} treatment lead to 80% apoptosis. The naturally derived products in this experiment did not show very good results for (e) actinomycin D treated cells. Less than 10% apoptosis is induced, although in some of the other repeats up to 30% apoptosis was induced. When the cells were treated with the crude extract, (f) *Plectranthus ciliatus*, 44% apoptotic cells were detected. Quadrant Q4 was selected for sorting unstained viable cells while Q3 was used to sort apoptotic cells. Q1 was selected to sort necrotic cells. (g) Q1 was selected to sort necrotic cells.
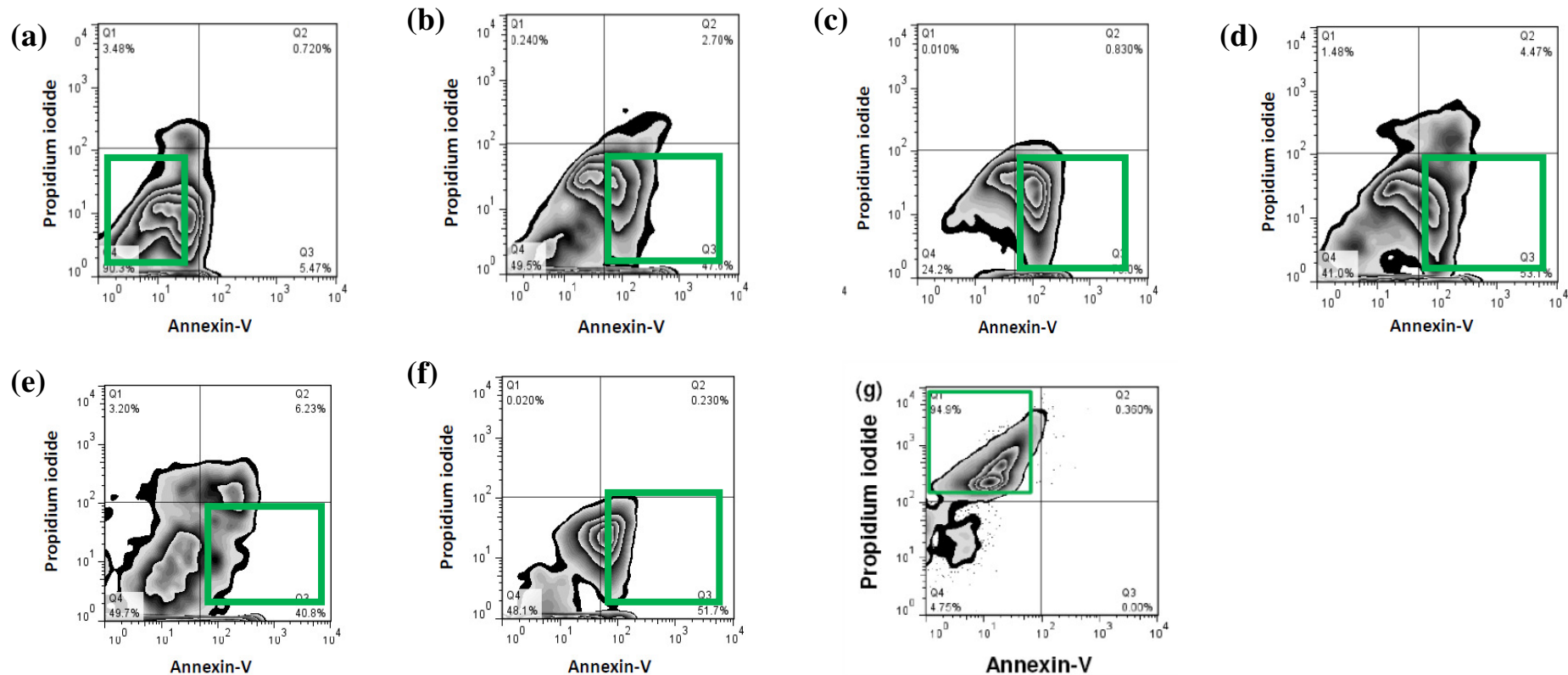
Fig. 7.4. Flow cytometry representative zebra plots of Vero cells: Induced cell death was measured with annexin-V and propidium iodide. (a) Viable cells remained unstained (annexin-V negative, propidium iodide negative). Quadrant Q4 was selected for sorting unstained viable cells. Each treatment's effect was measured after being treated with the 2 x CC_{50} concentrations (that was determined with XTT viability assay, Chapter 3). (b) Auranofin 2 x CC_{50} treated cells displayed 47% early apoptotic cells. (c) When the cells were exposed to AE 76 2 x CC_{50} there were 75% early apoptotic cells. (d) The compound, AE 125 leads to 53% early apoptotic cells. (e) Actinomycin D treated cells had 40% early apoptotic cells while cells treated with the (f) crude extract, *Plectranthus ciliatus* had 51% of the cell in the early apoptotic quadrant. Quadrant Q3 was used to sort apoptotic cells while (g) Q1 was selected to sort necrotic cells.

7.3.3 *Raman microspectroscopic investigation of viable, apoptotic and necrotic cells*

The sorted cells were analysed using Raman spectroscopy which resulted in a typical Raman spectra for the unstained HeLa and Vero cells that were classified as viable using flow cytometry and confirmed using TEM (Chapter 6). The spectra for both types of viable cells contained regions assigned to nucleic acids, proteins and lipids. Early apoptotic cells (annexin-V positive, propidium iodide negative) as well as necrotic cells (annexin-V negative, propidium iodide positive) did not show any irregularities in the spectra recorded that could be related to the staining of the cells. Brauchle *et al*. (2014) conducted a similar study where cell death was induced without the aid of chemicals. The cells were investigated using annexin-V and propidium iodide fluorescence microscopy combined with Raman spectroscopy and found that no significant changes were evident in stained cells versus unstained cells diagnosed in the same class of cell death [123]. Untreated HeLa and Vero cells had similar Raman spectra with only minor changes observed after the cells were treated with methanol (Fig. 7.5). Furthermore, the baselines for especially *P. ciliatus* treated cells were distorted, due to the additional fluorescence of the plant extract. The baseline distortion was overcome by calculating the second derivatives that were not influenced by the baseline. Another advantage of second derivatives was that small changes were visually enhanced. A peak was detected in the background CaF_2. The band was at 1555 cm^{-1} and associated with protein vibrations and tyrosine [211], which could be due to cell debris (since the cells were processed for Raman spectroscopy after being sorted). The fore mentioned peak was deliberately excluded from the analysis since the intensity of the band was consistently detected and also not significantly altered by treatments.
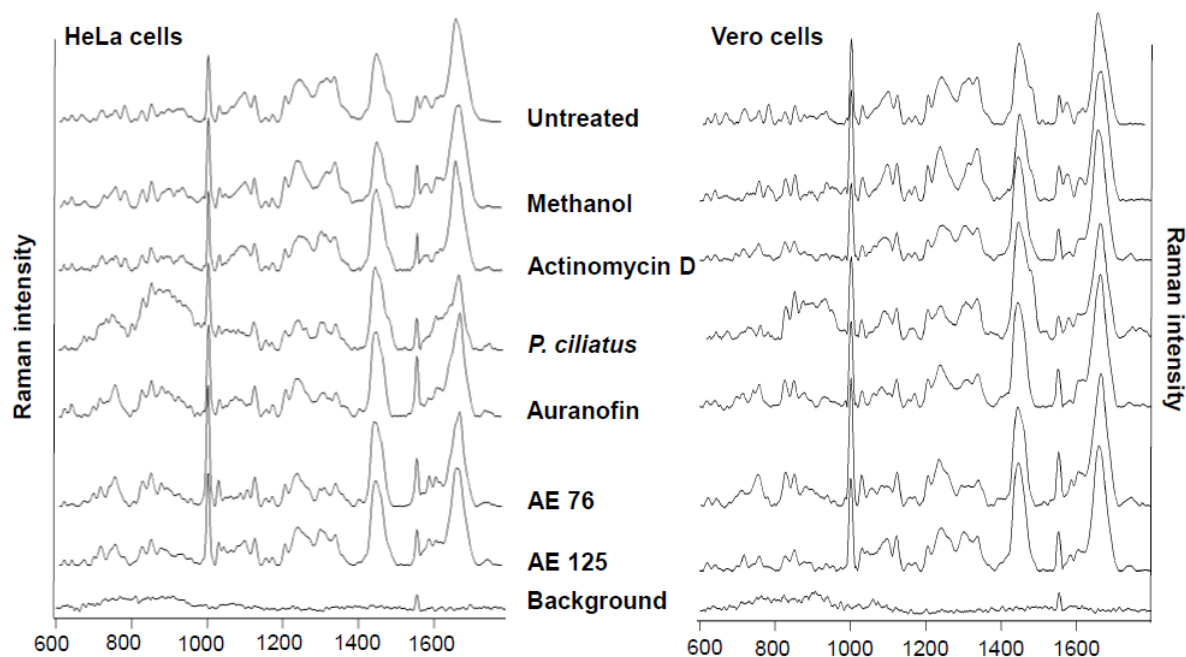
Fig. 7. 5. Average Raman spectra of untreated and treated HeLa (left) and Vero cells (right). Untreated HeLa and Vero cells' spectra are very similar, with only very minor changes in the spectra after the cells were treated with methanol (necrosis inducer). Background measurements showed the presence of a peak around 1555 cm^{-1} assigned to protein residue of cell debris.

Statistical analysis was done on the averages of the second derivatives of HeLa and Vero cells. Since HeLa cells were the cancerous cells, a full wavenumber statistical analysis was done. Twelve Raman peaks were identified to be significantly different (one way Anova, Tukey test, Bonferonni test, $p < 0.05$). Those bands were; 644 cm^{-1}, 755 cm^{-1}, 785 cm^{-1}, 800 cm^{-1}, 856 cm^{-1}, 932 cm^{-1}, 1099 cm^{-1}, 1226 cm^{-1}, 1300 cm^{-1}, 1486 cm^{-1} and 1642 cm^{-1} in HeLa cells. Alterations to amino acid molecules were evident in the peaks at 644 cm^{-1} (C-C vibrations of phenylalanine [211]) and 755 cm^{-1} (symmetric breathing of tryptophan [211]) and amide III protein peaks and trypthophan at 1226 cm^{-1} [211]. Nucleic acids decreased significantly at the peak of 785 cm^{-1} (thymine, uracil [183], adenine and guanine vibrations and phosphodiester backbone vibrations of DNA [11] and RNA) [154] and at 1485 cm^{-1} (thymine [151]) in HeLa and Vero cells (Fig. 7.2 and Fig. 7.3). A peak associated with phosphate backbone geometry and phosphate ion interactions (800 cm^{-1}) [211] were visibly evident in HeLa cells as well in most of the cells treated with apoptosis induced treatments as well as a significant decrease in phosphodioxy groups found in nucleic acids. Collagen associated protein and amino acids bands; 856 cm^{-1} (amino acid side chains of proline, hydroxyproline and C-C vibrations of collagen) [119] in Vero and HeLa cells, 932 cm^{-1} (C-C

- 142 -

and α-helix vibrations) and 966 cm^{-1} decreased in HeLa cells which were indicative of a decreasing protein content in the cells. A shoulder band appeared for some of the apoptotic cells. A significant increase in lipids was also seen at 1300 cm^{-1} in HeLa and Vero cells. A decrease in protein content and an increase in lipids have previously been linked to apoptosis [12,120,127,128].
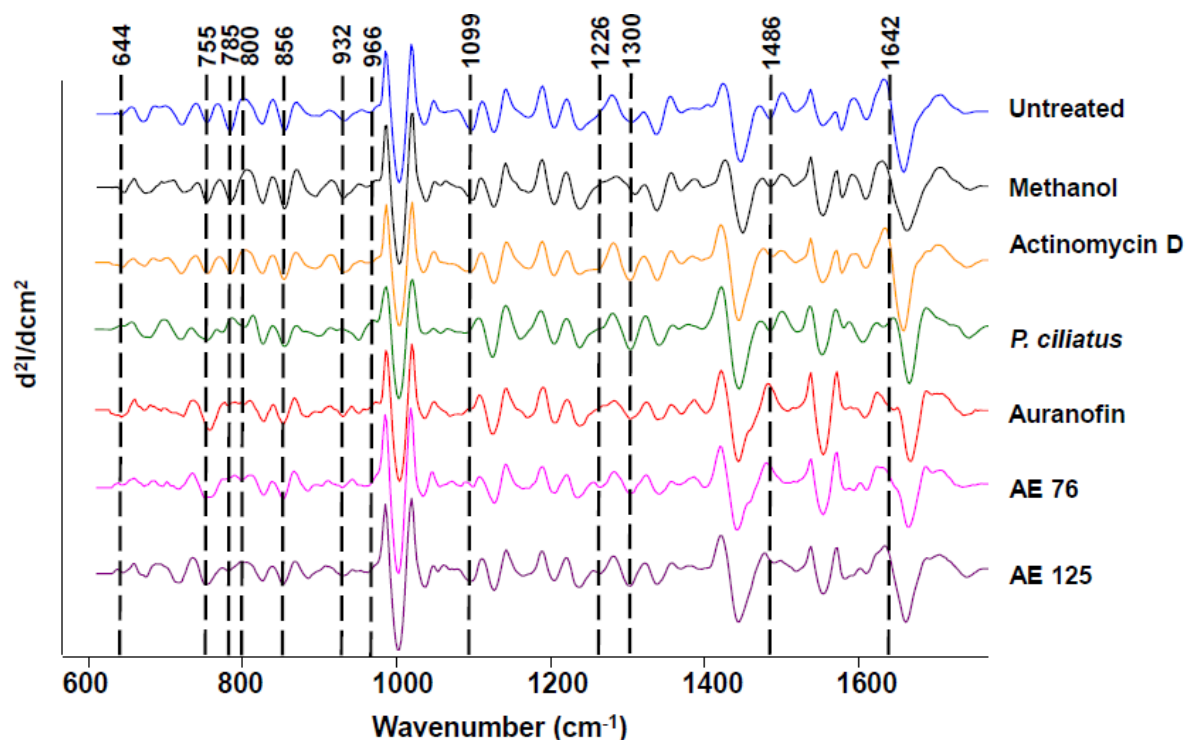
Fig. 7. 6. Average second derivatives of untreated and treated HeLa cells. The lines indicate significantly (one way ANOVA, Tukey, Bonferonni, p < 0.05) altered bands after treatment.
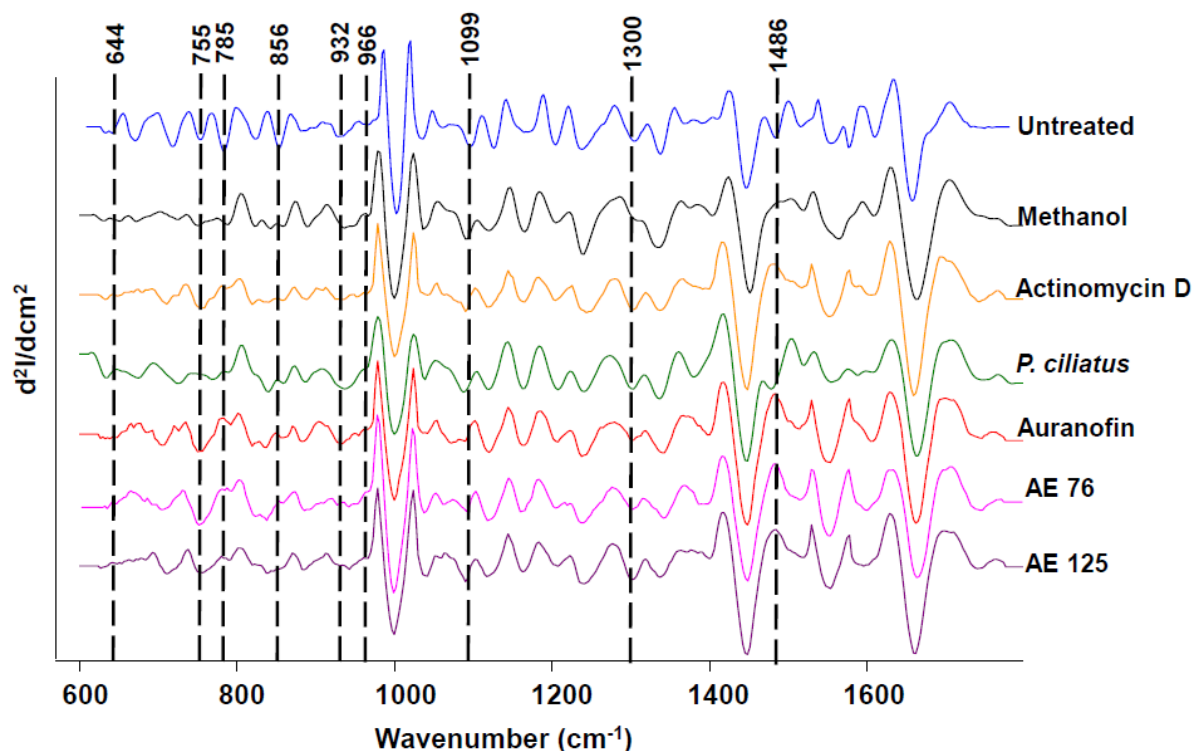
Fig. 7. 7. **Average second derivatives of viable and dead Vero cells treated with metallodrugs and naturally derived products.** Black dashed lines indicate significantly (one way ANOVA, Tukey, Bonferonni, $p < 0.05$) altered bands after treatment.

PCA plots were constructed (Fig. 7.8 to Fig. 7.13) to determine the trends in the data and also to determine what the major Raman peaks were that contributed to the distinction between viable and necrotic and viable and apoptotic cells. For necrotic cell death, only one death inducer was investigated. When PCA plots were constructed for HeLa and Vero cells to distinguish between viable and necrotic cells, good separation was observed for both cell lines in the regions between 600 - 1800 cm^{-1} (Fig. 7.8 and Fig. 7.9) and 2600 – 3200 cm^{-1} (Fig. 7.12 and Fig. 7.13). The second derivatives were used in the PCA analysis which then indicated that a positive score in the PCA plot translated to a negative loading and vice versa [138]. A negative loading in relation to second derivatives is indicative of increases in the peaks, whereas positive loadings were interpreted as decreased peaks. Therefore, viable HeLa cells had lower Raman intensities for 762 cm^{-1} as compared to necrotic cells (Fig. 7.8). The peak at 762 cm^{-1} was assigned to tryptophan and phosphatidylethanolamine [211]. Phosphatidylethanolamine is just as phosphatidylserine located on the inner plasma membrane of mammalian cells and consists up to 50% of the phospholipids of the membrane. Only when the membrane's integrity is compromised will the intensity of this peak increase,

as in the case of apoptosis, where this phospholipid is also externalised (Chapter 5) [194]. Therefore, 762 cm^{-1} is not only an indicator of apoptosis (Chapter 5, [126,194]) but also for necrosis. PC 1 negative loadings were associated with necrotic cells of which the most prominent peaks were 1025 cm^{-1} (glycogen / carbohydrates), 1093 cm^{-1} (phosphodiester stretching vibration of DNA backbone), 1464 cm^{-1} (CH$_2$ vibrations of lipids and proteins), 1486 cm^{-1} and 1573 cm^{-1} guanine and adenine and TRP protein) [121,211]. A slight increase in carbohydrates and glycogen in necrotic cells was due to methanol preserving the glycogen. Alcoholic fixatives are routinely used for the preservation of glycogen in cells and tissues. The increase in phosphodiester bonds of DNA and mixed alterations in purines were due to methanol causing DNA breaks prior to the induction of necrosis. DNA breaks had also been reported in cells that were treated with high concentrations of hydrogen peroxide [212] which is also a well documented inducer of necrosis.
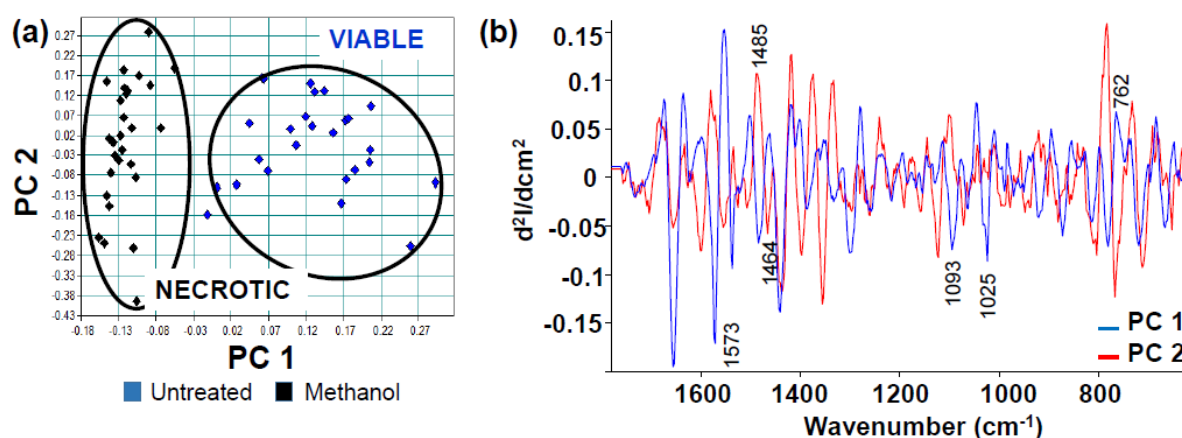
Fig. 7. 8. (a) PCA plot of viable and necrotic HeLa cells in the region of 600 cm^{-1} and 1800 cm^{-1}. Separation is observed in PC 1. **(b) Loading plot of PC 1 and PC 2 that was used for the PCA plot construction**. Major changes in the loadings are indicated which contributed to the separation of the two types of cell deaths investigated.

When viable and necrotic Vero cells were compared, PC 1 also contributed to the largest variability (Fig. 7.9). Viable cells had a negative score plot and was thus characterised by the positive peaks of loading of PC 1. A prominent peak 719 cm-1 was seen in the positive loading of PC 1 and thus associated with viable cells. The peak was assigned to choline stretching of phosphatidylcholine, which indicates that lower intensity was found in necrotic cells [119]. A decrease of phosphatidylcholine in necrotic cells was also detected by Matthews *et al.* and Ong *et al.* [121,128]. A decrease was also seen (as in the case with

necrotic HeLa cells, PC 1 loading) in 733 cm^{-1} assigned to phosphatidylserine. The disruption of phospholipids in the plasma membrane leads to the severe changes in phospholipid vibrations.
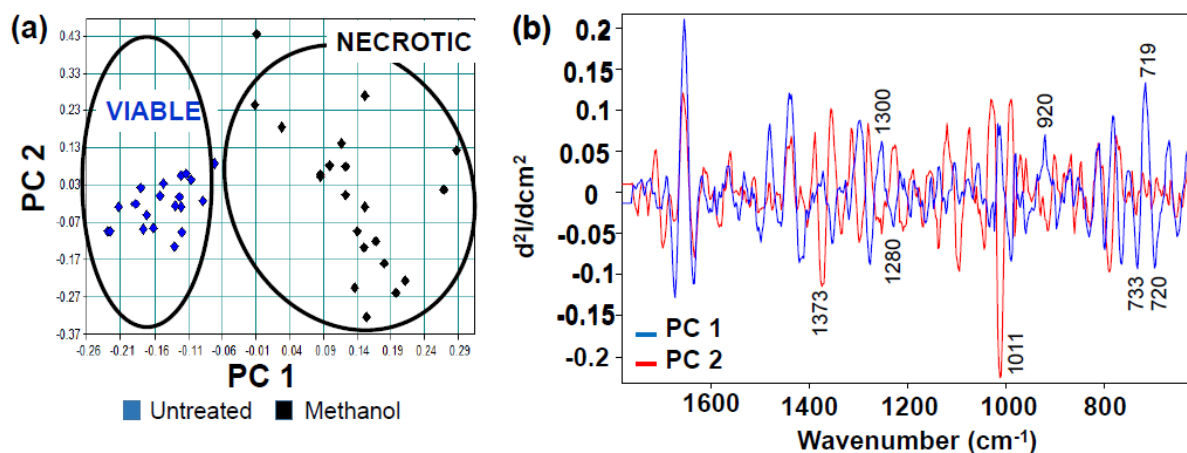
Fig. 7. 9. (a) PCA plot of viable and necrotic Vero cells. Separation is observed by PC 1. **(b) Loading plots of PC 1 and PC 2.** Major changes in the loadings are indicated which contributed to the separation of the two types of cell deaths investigated.

The differences between apoptotic and viable HeLa and Vero cells were best described in PC 1 (Fig 7.10 and Fig. 7.11). Only one apoptotic sample clustered with viable cells namely actinomycin D in HeLa cells but not in Vero cells. Since poor caspase activity was detected in those cells and autophagy (in TEM analysis, Chapter 6), it is no surprise that the cells clustered out of the norm. It should be kept in mind that HeLa cells are the cancerous cells and thus naturally more resistant to apoptotic signals. The rest of the sorted apoptotic HeLa and Vero cells had increased peaks at 762 cm^{-1} (phosphoethanolamine and tryptophan) which was also detected previously (Chapter 5) and in this study to also be lowered in necrotic cells. Apoptotic cells also had decreased peaks at 785 cm^{-1} and 1572 cm^{-1}. The DNA associated peak at 785 cm^{-1} was assigned to DNA in apoptotic cells and have been reported on various occasions [11,12,185]. The peak at 1572 cm^{-1} is assigned to C-N vibrations of proteins, adenine, and guanine and were also detected in both HeLa and Vero cells. The decrease in the band at 1572 cm^{-1} and had been previously detected [120,127]. No studies were evident where necrosis was associated with alterations in this peak.

Fig. 7. 10. (a) PCA plot of viable and apoptotic HeLa cells in the fingerprint region. Poor separation is observed by PC 1. All apoptotic cells clustered separately from the viable cells, except for some AE 125 and actinomycin D treated cells. **(b) Loading plots of PC 1 and PC 2 that were used for the PCA plot construction.** Major changes in the loadings were reported which contributed to the separati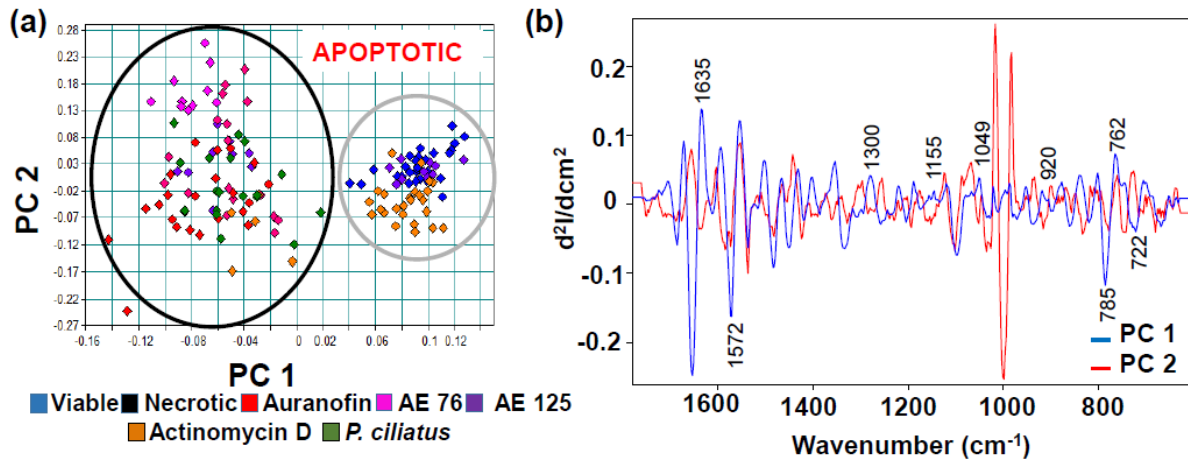on of the two types of cell death investigated, out of this loading it was possible to determine the remaining characteristics of AE 125 and actinomycin D sorted apoptotic cells.

Fig. 7. 11. PCA plot of viable and apoptotic Vero cells in the region of 600 cm^{-1} and 1800 cm^{-1}. Relatively good separation was observed by PC 1. The apoptotic cells clustered separately from the viable cells and sample heterogeneity was prominent in apoptotic cells seen in the scattered samples. The cells were still to some extend in various stages of apoptotic cell death stages and due to the Raman spectra recorded in the middle of the cells where nuclear heterogeneity can be very different due to the stage of nuclear fragmentation as discussed in Chapter 5 and elsewhere [123,128,194]. **(b) Loading plots** that were used for the PCA plot construction. Bands that contributed to the clustering are indicated.

The same trends were seen in the high wavenumbers of 2600-3200 cm^{-1} when viable cells were compared to necrotic HeLa or Vero cells (Fig. 7. 7 and Fig. 7. 8). Two peaks in PC 1 were responsible for the separate clustering of viable and necrotic cells. Those peaks were 2831 cm^{-1} and 2848 cm^{-1}. Basically in both cell lines the two peaks decreased in necrotic cells as compared to viable cells, since it was shown that viable cells had higher intensities in 2848 cm^{-1}. A decrease in high wavenumber regions had previously been reported in dead cells [124].
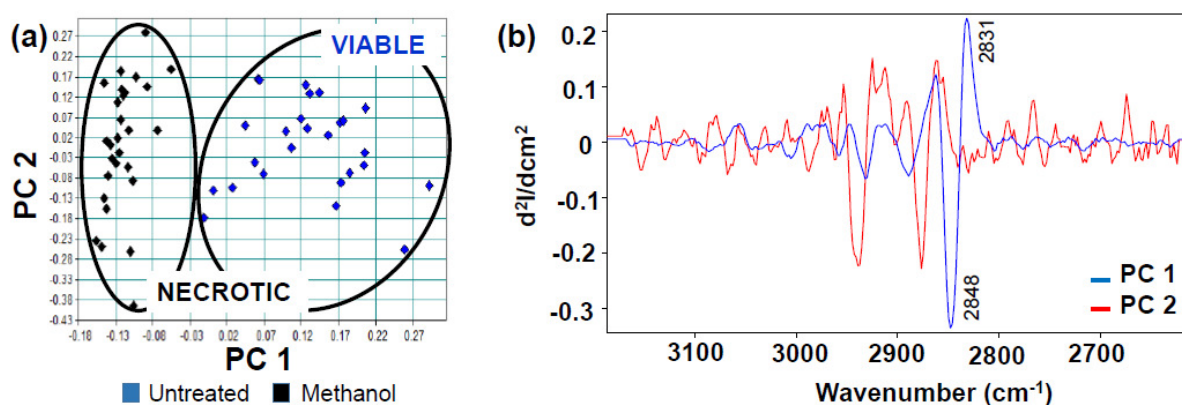
Fig. 7. 12. (a) PCA plot of viable and necrotic HeLa cells in the region of 2700 cm^{-1} and 3200 cm^{-1}. Separation was observed by PC 1. **(b) Loading plots of PC 1 and PC 2.** Major changes in the loadings were indicated which contributed to the separation of viable and necrotic cells**.**
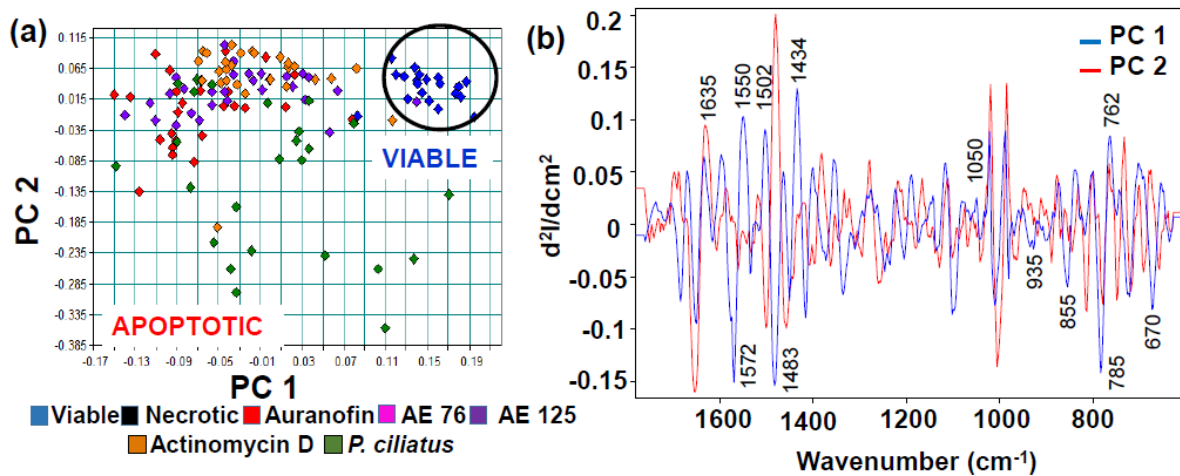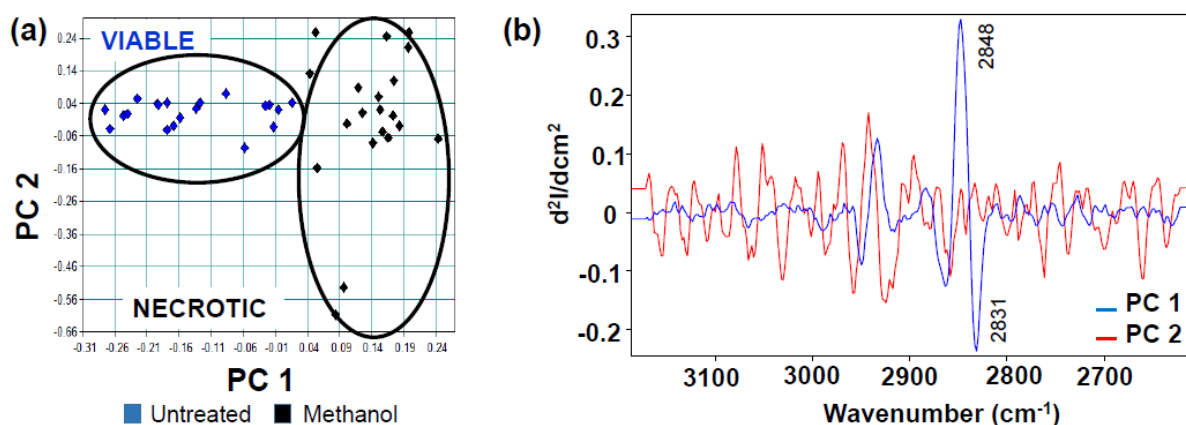

 Fig. 7. 13. (a) PCA plot of viable and necrotic Vero cells. Separation was observed by PC 1. **(b) Loading plots of PC 1 and PC 2 that were used for the PCA plot.** Major changes in the loadings are shown**.**

To summarize; caspase dependent apoptosis was detected in HeLa and Vero cells, although the activity was weak in actinomycin D treated cells. Further studies, to investigate whether RT-CES can be used for the detection of caspase 3 / 7 activity, should be explored since adherence and caspase activity are linked. Flow cytometric sorting of apoptotic and necrotic cells were an easy and rapid method for accurately purifying cell populations. Raman spectroscopy detected cell death biomarkers, some that were previously identified and also new bands that can be used to distinguish between viable and dead cells. Necrotic cells were had increased band absorbance at 762 cm^{-1} and increase in phosphodiester bonds. Necrotic cells were also associated with decreased absorbance bands for phosphatidylcholine and phosphatidylserine. Apoptotic cells had increased bands at 762 cm^{-1} assigned to phosphatidylethanolamine which was also detected previously (Chapter 5). A known apoptotic biomarker, 785 cm^{-1} was also prominent in this study, which also validated the sorting of the cells as valid. The band at 1572 cm^{-1} was identified in apoptotic cells and some necrotic cells which had not been previously described in the literature as a biomarker for necrosis. The relationship between necrosis and the band should still be investigated.

Chapter 8: Overall conclusion

This investigation was successful in demonstrating that label free biophysical techniques complemented conventional methodologies for the assessment of cell status, especially cell death.

8.1 Cytotoxicity of cell death inducers (Chapter 3)

The cytotoxicity of each selected treatment / compound was determined using one of the well-known viability dyes. The viability dye was user-friendly, cost effective and with acceptable reproducibility. The three metallodrugs and naturally derived products were cytotoxic at low concentrations. The cytotoxicities were summarized in Chapter 3, Table 3.2 for HeLa and Vero cells. Briefly, all metallodrugs had CC_{50} values lower than 11 µM against the proliferation of HeLa cells while natural derivied products had CC_{50} values lower than 10 µg/mL. All metallodrugs had CC_{50} values lower than 7 µM againt the proliferation of Vero cells while natural derived products had CC_{50} values lower than 20 µg/mL. Due to the very low selectivity indices of the metallodrugs, structural modifications could increase selectivity to produce compounds that are more effective against the proliferation of cancerous cells. The plant extract, *P. ciliatus* had a low selectivity index, but due to the diverse collection of secondary compounds in plant species, isolated compounds may show improved selectivity. In the complex mixture of phytochemicals, there may be compounds with more selective activity against the proliferation of cancer cells.

8.2 *Plectranthus ciliatus* – Impedance technology and FTIR spectroscopy (Chapter 4)

Real Time Cell Electronic Sensing and FTIR spectroscopy allowed for complementary conclusions. RT-CES determined whether the treatments were cytotoxic, cytostatic or nontoxic based on morphological changes during treatments. On the other hand, FTIR spectroscopy confirmed that the cytostatic behaviour of cells did not commit to the cell to death and it could still recover from the treatment. FTIR spectroscopy could also detect on a molecular level the early onset of stress responses before any morphological changes were

evident. Therefore, FTIR spectroscopy has the potential of becoming an invaluable tool to detect early responses of cells to stressors and for the detection of cytotoxic responses. FTIR spectroscopy which is economical, user-friendly and does not need specialized consumables to assist in the evaluation of cytotoxins. For future projects, a wider variety of cytotoxins should be tested at different concentrations and on different cell lines and primary cells to expand the field further.

8.3 Metallodrug apoptosis and Raman spectroscopy (Chapter 5)

In this chapter, metallodrugs induced early apoptosis. By utilising Raman spectroscopy, spectral signatures known to be evident in apoptotic cells were detected. Raman spectroscopy confirmed the mechanism of action of the metallodrugs. Flow cytometry and Raman spectroscopy detected that some metallodrugs were more effective in inducing apoptosis than others. Phosphatidyletaholamine was detected during the PCA analysis as the peak significantly increased in apoptotic cells. The detection of phosphatidylethanolamine should be confirmed further substantiated through the detection of fluorescent anti-phosphatidylethanolamine antibodies using enzyme-linked immunosorbent assay, fluorescent microscopy or flow cytometry. Correlations between flow cytometric data and Raman spectra were evident in the detection of indicators of apoptosis. The increase of glucose peak intensities was also unmistakeable and the important role this metabolite plays during cancer cell survival (high levels of glucose consumption involved in excreting chemotherapy), supported that observation. To confirm the results reported in this chapter the study was repeated with metallodrugs and naturally derived products in another cell line (including necrotic cells) to determine if the observed band was exclusively for apoptotic cells (Chapter 7). Testing whether this type of responses is found in other cell lines may give insight into the survival mechanism of cancer cells that have not been explored in Raman spectroscopic investigations yet and should be investigated in the future.

8.4 FTIR spectroscopy of sorted cells (Chapter 6)

Dead cells were sorted into early apoptotic and necrotic cells using flow cytometry. The sorted cells were investigated using TEM, which confirmed that the cells were either necrotic or apoptotic. TEM remains a very reliable and information rich technique to identify the type of cell death because of the visualization of characteristics of necrosis / apoptosis. FTIR

analysis was carried out on flow cytometrically sorted cells. A definite trend was seen in PCA plots where natural product treated apoptotic HeLa and Vero cells respectively, separated. This was also the case for metallodrug treated cells. Based on significant changes ($p < 0.05$, one-way Analysis of Variance) four bands were identified which could discriminate between viable and necrotic cells in both cell lines, these bands were 1022 cm^{-1}, 2852 cm^{-1}, 2875 cm^{-1} and 2923 cm^{-1}. Significantly altered bands were identified in the two different cell lines that distinguished viable from apoptotic, viable from necrotic and apoptotic from necrotic cells respectively. Using Principal Component Analysis, good separation was found between the different types of cell death and the loading plots indicated an increase in an additional band at 1623 cm^{-1} in dead cells.

8.5 Raman spectroscopy of sorted cells (Chapter 7)

Caspase dependent apoptosis was detected in HeLa and Vero cells but at different levels of magnitude. Further studies, to investigate whether RT-CES can be used for the detection of caspase 3 / 7 activity, should be explored since cell adherence to a surface (such as the culture flask) and caspase activity are linked. Flow cytometric sorting of apoptotic and necrotic cells were an easy and rapid method for accurately purifying cell populations. Raman spectroscopy detected cell death biomarkers, some that were previously identified and also new bands that can be used to distinguish between viable and dead cells. Necrotic cells had increased band absorbance at 762 cm^{-1} and increased in phosphodiester bonds. Necrotic cells were also associated with decreased absorbance bands for phosphatidylcholine and phosphatidylserine. Apoptotic cells had increased bands at 762 cm^{-1} assigned to phosphatidylethanolamine which was also detected previously (Chapter 5). A known apoptotic biomarker, 785 cm^{-1} was also prominent in this study, which validated the sorting of the cells. A new band at 1572 cm^{-1} was identified in dead cells which had not been previously described in the literature as a biomarker. The assignment of the band to a specific biomolecule associated with cell death should still be investigated.

8.6 Novel aspects of this research

1. Novel treatments were tested against cancer cells.
2. This was the first study to compare FTIR spectroscopy with RT-CES data.

3. Charactering cytostatic and early onset stress responses of cancer cells using FTIR spectroscopy.

4. Cytostatic cells were proven to be viable using FTIR spectroscopy.

5. Elucidating the mechanism of action of novel metallodrugs in terms of cell death induction.

6. Detecting phosphatidylethanolamine as a possible biomarker of apoptosis using Raman spectroscopy.

7. Confirming survival attempts of cancer cells under chemical stress using Raman spectroscopy.

8. Methodology development in terms of achieving pure cell populations for investigations using vibrational spectroscopy.

9. Emphasazing the importance of conducting studies on cancerous and noncancerous cells in spectroscopic studies and to take into account the type of treatment and concentration thereof.

8.7 Revisiting the hypothesis

Hypothesis: *The work undertaken here sought to investigate the hypothesis that vibrational spectroscopic assessment of cell death associated molecules should identify complementary markers as those reached using conventional biochemical methods.*

The hypothesis suggested that biochemical and biophysical techniques would provide complementary information on molecular components which should distinguish viable from dead cells. The hypothesis is accepted based on the fact that labelled biochemical techniques such as XTT, flow cytometry, caspase 3/7 fluorescence assays and TEM could be correlated to specific peaks in vibrational spectroscopy. In addition, it was found that using unlabelled real time analysis of cell (RT-CES) similar conclusions could be reached as those based on data collected with FTIR spectroscopy. It was also found that phosphatidylethanolamine could be developed into a cell death (apoptotic and necrotic) marker in unlabelled cells (data collected using Raman spectroscopy). Bands previously identified as being associated with cell death was detected in the FACS sorted cells. Therefore, flow cytometry results supported the findings of vibrational spectroscopy.

To conclude, cell death analysis using vibrational spectroscopy for understanding the underlying mechanisms and to detect different types of cell death is still relatively new but the potential for this type of spectroscopy to become a routine experimental setup in every laboratory investigating cellular behaviour in response to external stimuli is promising. This research broadens the knowledge base of biomarkers associated with specific types of cell death externally induced, in vitro. The approach presented here may be useful in the (*in vitro*) evaluation of diseases where cell death is induced as part of the pathology. Vibrational spectroscopy could be invaluable in broadening the knowledge of cell death induction due to specific cellular stresses such as microbial or parasite infestations, ischemic injury and neurological diseases and the underlying mechanisms of cell death pathways induced. Data produced in this investigation substantially supplemented vibrational spectroscopic knowledge into understanding cellular stress, cell death and potential cell death markers *in vitro*.

8.8 Future perspectives

The future direction of the work was provided as part of the separate chapter conclusions. Briefly, FTIR spectroscopy should be further developed into a tool for the detection of cytostatic and cytotoxic responses using a variety of treatments and different cell lines. The detection of Z-DNA in HeLa cells after treatment with the crude extract should be confirmed with conventional assays. Phosphatidylethanolamine externalisation should be confirmed using conventional biochemical assays. The glucose metabolism of cancer cells should be further investigated using vibrational spectroscopy. Sorting of the cells using FACS has the potential to investigated pure populations of diseased cells. The relationship between cell adherence and caspases activity should be further investigated using RT-CES and vibrational spectroscopy. The relationship of Raman bands at 762 cm^{-1} and 1572 cm^{-1}, as well as other identified and known bands, should be investigated for possible trends in dead cells.

Chapter 9: References

[1]   E. Solary, L. Dubrez, B. Eymin, The role of apoptosis in the pathogenesis and treatment of diseases, Eur. Respir. J., 9 (1996) 1293–1305.

[2]   M. Agostini, P. Tucci, G. Melino, Cell death pathology: Perspective for human diseases, Biochem. Biophys. Res. Commun., 414 (2011) 451–455.

[3]   P. Kapewangolo, Investigating plant species from the Lamiaceae family for activity against HIV/AIDS and immunomodulatory properties, University of Pretoria, 2013.

[4]   N.H. Gama, Bioactivity of metallodrugs, University of Pretoria, 2012.

[5]   C.W. Lukhoba, M.S.J. Simmonds, A.J. Paton, Plectranthus: A review of ethnobotanical uses, J. Ethnopharmacol., 103 (2006) 1–24.

[6]   Z.M. Chirenje, HIV and cancer of the cervix, Best Pract. Researh Clin. Obstet. Gynaecol., 19 (2005) 269–276.

[7]   N.W. Cummins, A.D. Badley, Mechanisms of HIV-associated lymphocyte apoptosis: 2010, Cell Death Dis., 1 (2010) e99–9.

[8]   M.J. Silverberg, C. Chao, W. a Leyden, L. Xu, M. a Horberg, D. Klein, W.J. Towner, R. Dubrow, C.P. Quesenberry, R.S. Neugebauer, D.I. Abrams, HIV infection, immunodeficiency, viral replication, and the risk of cancer, Cancer Epidemiol. Biomarkers Prev., 20 (2011) 2551–2559.

[9]   G. Mena-Rejon, E. Caamal-Fuentes, Z. Cantillo-Ciau, R. Cedillo-Rivera, J. Flores-Guido, R. Moo-Puc, In vitro cytotoxic activity of nine plants used in Mayan traditional medicine, J. Ethnopharmacol., 121 (2009) 462–465.

[10]   O. Kepp, L. Galluzzi, M. Lipinski, J. Yuan, G. Kroemer, Cell death assays for drug discovery, Nat. Rev. - Drug Discov., 10 (2011) 221–237.

[11]   S. Verrier, I. Notingher, J.M. Polak, L.L. Hench, In situ monitoring of cell death using Raman microspectroscopy, Biopolymers, 74 (2004) 157–162.

[12]   I. Notingher, S. Verrier, S. Haque, J. Polak, L. Hench, Spectroscopic study of human lung epithelial cells (A549) in culture: living cells versus dead cells, Biopolymers, 72 (2003) 230–240.

[13]   U. Zelig, J. Kapelushnik, R. Moreh, S. Mordechai, I. Nathan, Diagnosis of Cell Death by Means of Infrared Spectroscopy, Biophys. J., 97 (2009) 2107–2114.

[14]   G.E. Jamin, L. Miller, J. Moncuit, W. Fridman, P. Dumas, J. Teillaud, Chemical heterogeneity in cell death: Combined synchrotron IR and fluorescence microscopy studies of single apoptotic and necrotic cells, Biopolym., 72 (2003) 366–373.

[15]   P. Saikumar, M.A. Venkatachalam, Apoptosis and cell death, in: T.C. Allen, P.T. Cagle (Eds.), Basic Concepts Mol. Pathol., Springer US, Boston, MA, 2009: pp. 29–40.

[16]   S. Elmore, Apoptosis: A review of programmed cell death, Toxicol. Pathol., 35 (2007) 495–516.

[17]   P. Saikumar, Z. Dong, V. Mikhailov, M. Denton, J. Weinberg, M. Venkatachalam, Apoptosis: Definition, Mechanisms, and Relevance to Disease, Am. J. Med., 107 (1999) 489–506.

[18]   G. Kroemer, L. Galluzzi, P. Vandenabeele, J. Abrams, E. Almeri, E. Baehrecke, M. Blagosklonny, W. El-Deiry, P. Golstein, D. Green, M. Hengartner, R. Knight, S. Kumar, S. Lpipon, Classification of cell death, Cell Death Differ., 16 (2009) 3–11.

[19]   S.R. Dillon, M. Mancini, a. Rosen, M.S. Schlissel, Annexin V Binds to Viable B Cells and Colocalizes with a Marker of Lipid Rafts upon B Cell Receptor Activation, J. Immunol., 164 (2000) 1322–1332.

[20]   C. Ferraro-Peyret, L. Quemeneur, M. Flacher, J.-P. Revillard, L. Genestier, Caspase-Independent Phosphatidylserine Exposure During Apoptosis of Primary T Lymphocytes, J. Immunol., 169 (2002) 4805–4810.

[21]   G. Kung, K. Konstantinidis, R.N. Kitsis, Programmed necrosis, not apoptosis, in the heart, Circ. Res., 108 (2011) 1017–1036.

[22]   M. Lamkanfi, V.M. Dixit, Review Manipulation of Host Cell Death Pathways during Microbial Infections, Cell Host Microbe, 8 (2010) 44–54.

[23]   T. Van den Berghe, S. Grootjans, V. Goossens, Y. Dondelinger, D. V Krysko, N. Takahashi, P. Vandenabeele, Determination of apoptotic and necrotic cell death in vitro and in vivo, Methods, 61 (2013) 117–129.

[24]   M. V Jain, A.M. Paczulla, T. Klonisch, F.N. Dimgba, S.B. Rao, K. Roberg, F. Schweizer, C. Lengerke, P. Davoodpour, V.R. Palicharla, S. Maddika, M. Łos, Interconnections between apoptotic, autophagic and necrotic pathways: implications for cancer therapy development, J. Cell. Mol. Med., 17 (2013) 12–29.

[25]   B. Zhivotovsky, S. Orrenius, Cell death mechanisms: Cross-talk and role in disease, Exp. Cell Res., 316 (2010) 1374–1383.

[26]   W. Martinet, S. Verheye, G.R.Y. De Meyer, Selective depletion of macrophages in atherosclerotic plaques via macrophage-specific initiation of cell death, Trends Cardiovasc. Med., 17 (2007) 69–75.

[27]   D. Hanahan, R.A. Weinberg, The Hallmarks of Cancer Review, Cell, 100 (2000) 57–70.

[28]   D. Hanahan, R.A. Weinberg, Hallmarks of cancer: the next generation, Cell, 144 (2011) 646–674.

[29]   M.J. Brown, L.D. Attardi, The role of apoptosis in cancer development and treatment response, Nat. Rev. Cancer, 5 (2005) 231–237.

[30]   A.-M. Florea, D. Busselberg, Cisplatin as an Anti-Tumor Drug: Cellular Mechanisms of Activity, Drug Resistance and Induced Side Effects, Cancers (Basel)., 3 (2011) 1351–1371.

[31]   S. Romero-Garcia, J.S. Lopez-Gonzalez, J.L. Báez-Viveros, D. Aguilar-Cazares, H. Prado-Garcia, Tumor cell metabolism An integral view, Cancer Biol. Thearpy, 12 (2011) 939–948.

[32]   World Health Organisation Cancer Fact Sheet Number 297, (2014). [Online]. Available: http://www.who.int/mediacentre/factsheets/fs297/en/ Accessed: 15/05/2014.

[33]   World Health Organisation, Human papillomavirus (HPV) and cervical cancer, Fact Sheet Number 380, (2013). [Online]. Available: http://www.who.int/mediacentre/factsheets/fs380/en/ Accessed:10/05/2014.

[34]   J. Ferlay, I. Soerjomataram, M. Ervik, R. Dikshit, S. Eser, S. Mathers, M. Rebelo, D. Parkin, D. Forman, F. Bray, Cancer Incidence and Mortality Worldwide: IARC CancerBase No 11 [Internet] Lyon, France: International Agency for Research on Cancer, GLOBOCAN 2012 v1.0, (2013).

[35]   S.E. Waggoner, Cervical cancer, Lancet, 361 (2003) 2217–2225.

[36]   L.C. Snyman, Prevention of cervical cancer - how long before we get it right?, S. Afr. J. Obstet. Gynaecol., 19 (2012) 2–3.

[37]   L. Denny, Cervical cancer in South Africa: an overview of current status and prevention strategies, Contin. Med. Educ., 28 (2010) 70–73.

[38]   Food and Drug Administration, Cervarix, (2014). [Online]. Available: http://www.fda.gov/biologicsbloodvaccines/vaccines/approvedproducts/ucm186957.htm Accessed: 13/09/2014.

[39]   Food and Drug Administration, Gardasil, (2014). [Online]. Available: http://www.fda.gov/BiologicsBloodVaccines/Vaccines/ApprovedProducts/UCM094042 Accessed: 13/09/2014

[40]   R.I. Anorlu, Cervical cancer: the sub-Saharan African perspective, Reprod. Health Matters, 16 (2008) 41–49.

[41]   V. Milacic, D. Fregona, Q.P. Dou, Gold complexes as prospective metal-based anticancer drugs, Histol. Histopathol., 23 (2008) 101–108.

[42]   F. Guidi, I. Landini, M. Puglia, F. Magherini, C. Gabbiani, M.A. Cinellu, S. Nobili, T. Fiaschi, L. Bini, E. Mini, L. Messori, A. Modesti, Proteomic analysis of ovarian cancer cell responses to cytotoxic gold compounds, Metallomics, 4 (2012) 307–314.

[43]   M.W.M. van Ruijven, J.C.M.J. de Groot, F. Hendriksen, G.F. Smoorenburg, Immunohistochemical detection of platinated DNA in the cochlea of cisplatin-treated guinea pigs, Hear. Res., 203 (2005) 112–121.

[44]   S. Medici, M. Peana, V.M. Nurchi, J.I. Lachowicz, G. Crisponi, M.A. Zoroddu, Noble metals in medicine: latest advances, Coord. Chem. Rev., (2014) 1–22.

[45]   G.J. Higby, Gold in medicine: a review of its use in the West before 1900, Gold Bull., 15 (1982) 130–140.

[46]   A. De Luca, C.G. Hartinger, P.J. Dyson, M. Lo Bello, A. Casini, A new target for gold(I) compounds: glutathione-S-transferase inhibition by auranofin, J. Inorg. Biochem., 119 (2013) 38–42.

[47]   L. Oehninger, R. Rubbiani, I. Ott, N-Heterocyclic carbene metal complexes in medicinal chemistry, Dalt. Trans., 42 (2013) 3269–3284.

[48]   A.Y.F. Elkhadir, Phosphorous-nitrogen gold (I), palladium (II) and platinum (II) bimetallic complexes as potential antimalaria, antiHIV, antimycobateria, and anticancer agents, University of Johannesburg, 2014.

[49]   G.M. Cragg, D.J. Newman, Natural products: a continuing source of novel drug leads, Biochim. Biophys. Acta, 1830 (2013) 3670–3695.

[50]   Y. Liu, Z. Yang, J. Du, X. Yao, X. Zheng, R. Lei, J. Liu, H. Hu, H. Li, Interaction of Taxol with intravenous immunoglobulin: an inhibition of Taxol from crystallizing in aqueous solution, Int. Immunopharmacol., 8 (2008) 390–400.

[51]   B.S. Aswal, D.S. Bhakuni, A.K. Goel, K. Kar, B.N. Mehrotra, K.C. Mukherjee, Screening of Indian plants for biological activity: Part X, Indian J. Exp. Biol., 22 (1984) 312–332.

[52]   S.S. El-Hawary, R.H. El-Sofany, A.R. Abdel-Monem, R.S. Ashour, A.A. Sleem, Polyphenolics content and biological activity of Plectranthus amboinicus (Lour) spreng growing in Egypt (Lamiaceae), Pharmacogn. J., 4 (2012) 45–54.

[53]   L.J. Rice, G.J. Brits, C.J. Potgieter, J. Van Staden, Plectranthus: A plant for the future?, South African J. Bot., 77 (2011) 947–959.

[54]   M. Abdel-Mogib, H.A. Albar, S.M. Batterjee, Chemistry of the Genus Plectranthus, Molecules, 7 (2002) 271–301.

[55]   A. M. Viljoen, B. Demirci, K.H.C. Başer, C.J. Potgieter, T.J. Edwards, Microdistillation and essential oil chemistry—a useful tool for detecting hybridisation in Plectranthus (Lamiaceae), South African J. Bot., 72 (2006) 99–104.

[56]   F. Bakkali, D. Averbeck, S. Averbeck, M. AIdaomar, Biological effects of essential oils – A review, Food Chem. Toxicol., 46 (2008) 446–475.

[57]   R.J. Thoppil, A. Bishayee, Terpenoids as potential chemopreventive and therapeutic agents in liver cancer, World J. Hepatol., 3 (2011) 228–49.

[58]   Y. Yang, Z. Zhang, S. Li, X. Ye, X. Li, K. He, Synergy effects of herb extracts: pharmacokinetics and pharmacodynamic basis, Fitoterapia, 92 (2014) 133–147.

[59]   H. Wagner, G. Ulrich-Merzenich, Synergy research: approaching a new generation of phytopharmaceuticals, Phytomedicine, 16 (2009) 97–110.

[60]   E.M. Williamson, Synergy and other interactions in phytomedicines, Phytomedicine, 8 (2001) 401–9.

[61]   K. Le Roux, A.A. Hussein, N. Lall, In vitro chemo-preventative activity of Crotalaria agatiflora subspecies agatiflora Schweinf, J. Ethnopharmacol., 138 (2011) 748–755.

[62]   The Scott Hamilton CARES Initiative, Actinomycin D, (2014). [Online]. Available: http://chemocare.com/chemotherapy/drug-info/actinomycin-d.aspx#.VCLb7ZVxnIU Accessed: 24/09/2014.

[63]   K. Kleeff, M. Kornmann, H. Sawhney, M. Korc, Actinomycin D induces apoptosis and inhibits growth of pancreatic cancer cells, Int. J. Cancer, 86 (2000) 399–407.

[64]   S.G. Sawicki, G.C. Godman, On the differential cytotoxicity of actinomycin D, J. Cell Biol., 50 (1971) 746–761.

[65]   D. Drygin, A. Lin, J. Bliesath, C.B. Ho, S.E. O'Brien, C. Proffitt, M. Omori, M. Haddach, M.K. Schwaebe, A. Siddiqui-Jain, N. Streiner, J.E. Quin, E. Sanij, M.J. Bywater, R.D. Hannan, D. Ryckman, K. Anderes, W.G. Rice, Targeting RNA polymerase I with an oral small molecule CX-5461 inhibits ribosomal RNA synthesis and solid tumor growth, Cancer Res., 71 (2011) 1418–1430.

[66]   G.J. Veal, J. Errington, J. Sludden, M.J. Griffin, L. Price, A. Parry, J. Hale, A.D.J. Pearson, A. V Boddy, Determination of anti-cancer drug actinomycin D in human plasma by liquid chromatography–mass spectrometry, J. Chromatogr. B, 795 (2003) 237–243.

[67]   O. Rixe, T. Fojo, Is cell death a critical end point for anticancer therapies or is cytostasis sufficient?, Clin. Cancer Res., 13 (2007) 7280–7287.

[68]   B.P. Lucey, W.A. Nelson-Rees, G.M. Hutchins, Henrietta Lacks, HeLa cells, and cell culture contamination, Arch. Pathol. Lab. Med., 133 (2009) 1463–1467.

[69]   American Tissue Culture Collection - Cell lines and hybridomas. [Online]. Available: http://www.atcc.org/~/media/Attachments/E/7/3/C/1765.ashx Accessed: 10/09/2014.

[70]   V.A. McKusick, P.S. Harper, History of medical genetics, in: Emery Rimoin's Princ. Pract. Med. Genet., Sixth Edit, Elsevier, 2013: pp. 1–39.

[71]   Scopus Search Results - HeLa and Vero cells (2014). [Online]. Available: www.scopus.com Accessed: 24/09/2014.

[72]   B. Trivedi, The primate connection, Nature, 466 (2010) S5.

[73]   A. Stander, S. Marais, V. Stivaktas, C. Vorster, C. Albrecht, M. Lottering, A.M. Joubert, In vitro effects of Sutherlandia frutescens water extracts on cell numbers , morphology , cell cycle progression and cell death in a tumorigenic and a non-tumorigenic epithelial breast cell line, J. Ethnopharmacol., 124 (2009) 45–60.

[74]   M.V. Berridge, A.S. Tan, K.D. McCoy, R. Wang, The biochemical and cellular basis of cell proliferation assays that use tetrazolium salts, Biochemica, 4 (1996) 14–19.

[75]   N. Mbaveng, A.T., Kuete, V., Mapunya, B.M., Beng, V.P., Nkengfack, A.E., Meyer, J.J.M. and Lall, Evaluation of four Cameroonian medicinal plants for anticancer, antigonorrheal and antireverse transcriptase activities, Environ. Toxicol. Pharmacol., (2011).

[76]   B.P. Raval, M.P. Suthar, R.K. Patel, Potent in vitro anti-tumor activity of Symplocos racemosa against leukeaemia and cervical cancerle, Electron. J. Biol., 5 (2009) 89–91.

[77]   R.R. Patel, A.A. Nagar, R.C. Patel, D.K. Rathod, V.R. Patel, In vitro anticancer activity of Rubicia cordifolia against HeLa and HEP-2 cell lines, Int. J. Pharm. Pharm. Sci., 3 (2011) 70–71.

[78]   O. Brenes, E. Munoz, R. Roldan-Rodriguez, C. Diaz, Cell death induced by Bothrops asper snake venom metalloproteinase on endothelial and other cell lines, Exp. Mol. Pathol., 88 (2010) 424–432.

[79]   E. Urcan, U. Haertel, M. Styllou, R. Hickel, H. Scherthan, F.X. Reichl, Real-time xCELLigence impedance analysis of the cytotoxicity of dental composite components on human gingival fibroblasts, Dent. Mater., 26 (2010) 51–58.

[80]   P.N. Fonteh, F.K. Keter, D. Meyer, New bis (thiosemicarbazonate) gold (III) complexes inhibit HIV replication at cytostatic concentrations: Potential for incorporation into virostatic cocktails, J. Inorg. Biochem., 105 (2011) 1173–1180.

[81]   A. Ehlers, S. Stempin, R. Al-Hamwi, A. Lampen, Toxicon Embryotoxic effects of the marine biotoxin okadaic acid on murine embryonic stem cells, Toxicon, 55 (2010) 855–863.

[82]   P. Kapewangolo, A.A. Hussein, D. Meyer, Inhibition of HIV-1 enzymes, antioxidant and anti-inflammatory activities of Plectranthus barbatus, J. Ethnopharmacol., 149 (2013) 184–190.

[83]   Z. Darzynkiewicz, X. Li, E. Bedner, Use of Flow and Laser-Scanning Cytometry in Analysis of Cell Death, 66 (2001) 69–109.

[84]   I. Vermes, C. Haanen, C. Reutelingsperger, Flow cytometry of apoptotic cell death, J. Immunol. Methods, 243 (2000) 167–190.

[85]   St Michael's Hospital Core Facilities - Flow cytometry and sorting (2015). [Online]. Available: http://www.stmichaelshospital.com/research/facilities/flow-Cytometry-Viability-Apoptosis.php Accessed: 9/01/2015.

[86]   N.S. Barteneva, K. Ketman, E. Fasler-Kan, D. Potashnikova, I.A. Vorobjev, Cell sorting in cancer research--diminishing degree of cell heterogeneity, Biochim. Biophys. Acta, 1836 (2013) 105–122.

[87]   M.J. Wilkerson, Principles and applications of flow cytometry and cell sorting in companion animal medicine, Vet. Clin. North Am. Small Anim. Pract., 42 (2012) 53–71.

[88]   F.C. Cruz, E. Koya, D.H. Guez-Barber, J.M. Bossert, C.R. Lupica, Y. Shaham, B.T. Hope, New technologies for examining the role of neuronal ensembles in drug addiction and fear, Nat. Rev. Neurosci., 14 (2013) 743–754.

[89]   Transmission electron microscope (TEM), Online, Encycl. Br., (2014). [Online]. Available: http://www.britannica.com/EBchecked/topic/602949/transmission-electron-microscope. Accessed: 8/10/2014.

[90]   T. Klein, E. Buhr, C.G. Frase, TSEM: A Review of Scanning Electron Microscopy in Transmission Mode and Its Applications, in: J.T.J. Cremer (Ed.), Adv. Imaging Electron Phys., 172nd ed., Elsevier Inc., 2012: pp. 297–356.

[91]   A. Tinari, A.M. Giammarioli, V. Manganelli, L. Ciarlo, W. Malorni, Analyzing Morphological and Ultrastructural Features in Cell Death, Methods in Emzymology, 442 (2008) 1–26.

[92]   Y. Otsuki, Z. Li, M. Shibata, Apoptotic Detection Methods - from Morphology to Gene, Prog. Histochem. Cytochem., 38 (2003) 275–340.

[93]   D.R. McIlwain, T. Berger, T.W. Mak, Caspase functions in cell death and disease, Cold Spring Harb. Perspect. Biol., 5 (2013) a008656.

[94]   J.G. Walsh, S.P. Cullen, C. Sheridan, U.L. Alexander, C. Gerner, S.J. Martin, Executioner caspase-3 and caspase-7 are functionally distinct proteases, PNAS, 105 (2008) 12815–12819.

[95]   T. Sundquist, R. Moravec, A. Niles, T. Riss, Timing your apoptosis assays: Timeline of Biochemical Events During Apoptosis, Cell Notes, (2006) 18–21.

[96]   Promega Corporation, Apo-ONE ® Homogeneous Caspase-3 / 7 Assay Protocol. (2009).

[97]   D.W. Straughan, J.H. Fentem, M. Balls, Replacement alternative and complementary in vitro methods in pharmaceutical research, in: Vitr. Methods Pharm. Res., Academic Press Ltd., 1997: pp. 1–13.

[98]   S. Diemert, A.M. Dolga, S. Tobaben, J. Grohm, S. Pfeifer, E. Oexler, C. Culmsee, Impedance measurement for real time detection of neuronal cell death, J. Neurosci. Methods, 203 (2012) 69–77.

[99]   D. Wlodkowic, W. Telford, J. Skommer, Z. Darzynkiewicz, Apoptosis and Beyond: Cytometry in Studies of Programmed Cell Death, in: Methods Cell Biol., Elsevier Inc., 2011: pp. 55–98.

[100]   Z. Movasaghi, S. Rehman, D.I. ur Rehman, I. Rehman, Fourier Transform Infrared (FTIR) Spectroscopy of Biological Tissues, Appl. Spectrosc. Rev., 43 (2008) 134–179.

[101]   D.I. Ellis, R. Goodacre, Metabolic fingerprinting in disease diagnosis: biomedical applications of infrared and Raman spectroscopy, Analyst, 131 (2006) 875–885.

[102]   S. Petit, J. Madejova, Fourier Transform Infrared Spectroscopy, in: Handb. Clay Sci., 2nd ed., Elsevier Ltd., 2013: pp. 213–231.

[103]   W. Petrich, Mid-infrared and Raman spectroscopy for medical diagnostics, Appl. Spectrosc. Rev., 36 (2001) 181–237.

[104]   C.M. Krishna, G.D. Sockalingum, R.A. Bhat, L. Venteo, P. Kushtagi, M. Pluot, M. Manfait, FTIR and Raman microspectroscopy of normal, benign, and malignant formalin-fixed ovarian tissues, Anal. Bioanal. Chem., 387 (2007) 1649–1656.

[105]   S. Boydston-White, T. Chernenko, A. Regina, M. Miljkovic, C. Matthaus, M. Diem, Microspectroscopy of single proliferating HeLa cells, Vib. Spectrosc., 38 (2005) 169–177.

[106]   R. Gasper, J. Dewelle, R. Kiss, T. Mijatovic, E. Goormaghtigh, IR spectroscopy as a new tool for evidencing antitumor drug signatures, Biochim. Biophys. Acta - Biomembr., 1788 (2009) 1263–1270.

[107] A. Derenne, R. Gasper, E. Goormaghtigh, The FTIR spectrum of prostate cancer cells allows the classification of anticancer drugs according to their mode of action, Analyst, 136 (2011) 1134–1141.

[108] S. Machana, N. Weerapreeyakul, S. Barusrux, T. Kanjana, W. Tanthanuch, FTIR microspectroscopy discriminates anticancer action on human leukemic cells by extracts of Pinus kesiya; Cratoxylum formosum ssp pruniflorum and melphalan, Talanta, 93 (2012) 371–382.

[109] M.J. Baker, J. Trevisan, P. Bassan, R. Bhargava, H.J. Butler, K.M. Dorling, P.R. Fielden, S.W. Fogarty, N.J. Fullwood, K.A. Heys, C. Hughes, P. Lasch, P.L. Martin-Hirsch, B. Obinaju, G.D. Sockalingum, J. Sulé-Suso, R.J. Strong, M.J. Walsh, B.R. Wood, P. Gardner, et al., Using Fourier transform IR spectroscopy to analyze biological materials, Nat. Protoc., 9 (2014) 1771–1791.

[110] K.-Z. Liu, H.. Mantsch, Apoptosis-induced structural changes in leukemia cells identified by IR spectroscopy, J. Mol. Struct., 565-566 (2001) 299–304.

[111] S. Gaudenzi, D. Pozzi, P. Toro, I. Silvestri, S. Morrone, A.C. Castellano, Cell apoptosis specific marker found by Fourier Transform Infrared Spectroscopy, Spectroscopy, 18 (2004) 415–422.

[112] R. Yamaguchi, A. Hirano-Iwata, Y. Kimura, M. Niwano, K. Miyamoto, Real-time monitoring of cell death by surface infrared spectroscopy, Appl. Phys. Lett., 91 (2007) 203902.

[113] P. Buriankova, L., Nadova, Z., Jancura, D., Refregiers, M., Yousef, I., Mikes, J., Miskovsky, Synchrotron based Fourier-transform infrared microspectroscopy as sensitive technique for the detection of early apoptosis in U-87 MG cells, Laser Phys. Lett., 7 (2010) 613–620.

[114] L. Di Giambattista, D. Pozzi, P. Grimaldi, S. Gaudenzi, S. Morrone, A.C. Castellano, New marker of tumor cell death revealed by ATR-FTIR spectroscopy, Anal Biioanal Chem, 399 (2011) 2771–2778.

[115] K.L. Brown, O.Y. Palyvoda, S.L. Thakur, J.S., Nehlsen-Cannarella, O.R. Fagoaga, S.A. Gruber, G.W. Aumer, Raman spectroscopic differentiation of activated versus non-activated T lymphocytes: An in vitro study of an acute allograft rejection model, J. Immunol. Methods, 340 (2009) 48–54.

[116] G. Pyrgiotakis, O. Kundakcioglu, K. Finton, P.M. Pardalos, K. Powers, B.M. Moudgil, Cell death discrimination with Raman spectroscopy and support vector machines, Ann. Biomed. Eng., 37 (2009) 1464–1473.

[117] E. Brauchle, K. Schenke-Layland, Raman spectroscopy in biomedicine – non-invasive in vitro analysis of cells and extracellular matrix components in tissues, Biotechnol. J., 8 (2013) 288–297.

[118] J. Guo, W. Cai, B. Du, M. Qian, Z. Sun, Raman spectroscopic investigation on the interaction of malignant hepatocytes with doxorubicin, Biophys. Chem., 140 (2009) 57–61.

[119]   Z. Movasaghi, S. Rehman, I.U. Rehman, Raman Spectroscopy of Biological Tissues, Appl. Spectrosc. Rev., 42 (2007) 493–541.

[120]   H. Yao, Z. Tao, M. Ai, L. Peng, G. Wang, B. He, Y. Li, Raman spectroscopic analysis of apoptosis of single human gastric cancer cells, Vib. Spectrosc., 50 (2009) 193–197.

[121]   Y.H. Ong, M. Lim, Q. Liu, Comparison of principal component analysis and biochemical component analysis in Raman spectroscopy for the discrimination of apoptosis and necrosis in K562 leukemia cells, Opt. Express, 20 (2012) 22158–22171.

[122]   M. Isabelle, V.I. Poon, Z. V Petropoulos, S.J. Harder, J.J. Lum, Exploring new strategies to monitor autophagy and related cell death pathways using Raman spectroscopy, J. Cancer Res. Ther. Oncol., 1 (2013) 1–5.

[123]   E. Brauchle, S. Thude, S.Y. Brucker, K. Schenke-Layland, Cell death stages in single apoptotic and necrotic cells monitored by Raman microspectroscopy, Sci. Rep., 4 (2014) 4698–4707.

[124]   S. Caponi, L. Liguori, A. Giugliarelli, M. Mattarelli, A. Morresi, P. Sassi, L. Urbanelli, C. Musio, Biophysical Chemistry Raman micro-spectroscopy: A powerful tool for the monitoring of dynamic supramolecular changes in living cells, Biophys. Chem., 182 (2013) 58–63.

[125]   A. Zoladek, F. Pascut, P. Patel, I. Notingher, Non-invasive time-course imaging of apoptotic cells by confocal Raman micro-spectroscopy, J. Raman Spectrosc., 42 (2011) 251–258.

[126]   C.A. Owen, J. Selvakumaran, I. Notingher, G. Jell, L.L. Hench, M.M. Stevens, In Vitro Toxicology Evaluation of Pharmaceuticals Using Raman Micro-Spectroscopy, J. Cell. Biochem., 99 (2006) 178–186.

[127]   T.J. Moritz, D.S. Taylor, D.M. Krol, J. Fritch, J.W. Chan, Detection of doxorubicin-induced apoptosis of leukemic T-lymphocytes by laser tweezers Raman spectroscopy, Biomed. Opt. Express, 1 (2010) 1138–1147.

[128]   Q. Matthews, A. Jirasek, J. Lum, X. Duan, A.G. Brolo, Variability in Raman Spectra of Single Human Tumor Cells Cultured in Vitro: Correlation with Cell Cycle and Culture Confluency, Appl. Spectrosc., 64 (2010) 871–887.

[129]   M.J. Walsh, M.N. Singh, H.M. Pollock, L.J. Cooper, M.J. German, H.F. Stringfellow, N.J. Fullwood, E. Paraskevaidis, P.L. Martin-hirsch, F.L. Martin, ATR microspectroscopy with multivariate analysis segregates grades of exfoliative cervical cytology, Biochem. Biophys. Res. Commun., 352 (2007) 213–219.

[130] A.R. Timerbaev, C.G. Hartinger, S.S. Aleksenko, B.K. Keppler, Interactions of Antitumor Metallodrugs with Serum Proteins: Advances in Characterization Using Modern Analytical Methodology, Chem. Rev., 106 (2006) 2224–2249.

[131] E.R.T. Tiekink, Anti-cancer potential of gold complexes, Inflammopharmacology, 16 (2008) 138–142.

[132] R. Sammons, A. Thackray, H. Ledo, P. Marquis, I. Jones, P. Yong, L. Macaskie, Characterisation and sintering of nanophase hydroxyapatite synthesised by a species of Serratia, Funct. Mater. Nanotechnologies, 93 (2007) 1–7.

[133] A. Barth, Infrared spectroscopy of proteins, Biochim. Biophys. Acta, 1767 (2007) 1073–1101.

[134] P.I. Haris, F. Severcan, FTIR spectroscopic characterization of protein structure in aqueous and non-aqueous media, J. Mol. Catal. B Enzym., 7 (1999) 207–221.

[135] Y. Wang, Q. Zhou, B. Li, B. Liu, G. Wu, M. Ibrahim, G. Xie, H. Li, G. Sun, Differentiation in MALDI-TOF MS and FTIR spectra between two closely related species Acidovorax oryzae and Acidovorax citrulli, BMC Microbiol., 12 (2012) 182–197.

[136] H.H. Mantsch, L.-P. Choo-Smith, R.A. Shaw, Vibrational spectroscopy and medicine: an alliance in the making, Vib. Spectrosc., 30 (2002) 31–41.

[137] X. Lu, B. Rasco, J. Jabal, D. Aston, M. Lin, M. Konkel, Investigating antibacterial effects of garlic (Allium sativum) concentrate and garlic-derived organosulfur compounds on Campylobacter jejuni by using Fourier Transform infrared spectroscopy, Raman spectroscopy, and electrom microscopy, Appl. Environ. Microbiol., 77 (2011) 5257–5269.

[138] K.L. Munro, K.R. Bambery, E.A. Carter, L. Puskar, M.J. Tobin, B.R. Wood, C.T. Dillon, Synchrotron radiation infrared microspectroscopy of arsenic-induced changes to intracellular biomolecules in live leukemia cells, Vib. Spectrosc., 53 (2010) 39–44.

[139] A. Derenne, V. Van Hemelryck, D. Lamoral-Theys, R. Kiss, E. Goormaghtigh, FTIR spectroscopy: A new valuable tool to classify the effects of polyphenolic compounds on cancer cells, Biochim. Biophys. Acta - Mol. Basis Dis., 1832 (2013) 46–56.

[140] S. Kustermann, F. Boess, A. Buness, M. Schmitz, M. Watzele, T. Weiser, T. Singer, L. Suter, A. Roth, A label-free, impedance-based real time assay to identify drug-induced toxicities and differentiate cytostatic from cytotoxic effects, Toxicol. Vitr., 27 (2013) 1589–1595.

[141] Y.A. Abassi, B. Xi, W. Zhang, P. Ye, S.L. Kirstein, M.R. Gaylord, S.C. Feinstein, X. Wang, X. Xu, Kinetic cell-based morphological screening: prediction of mechanism of compound action and off-target effects, Chem. Biol., 16 (2009) 712–723.

[142] E. Çetinus, T. Temiz, M. Ergül, A. Altun, Ş. Çetinus, T. Kaya, Thyme essential oil inhibits proliferation of DLD-1 colorectal cancer cells through antioxidant effect, Cumhur. Med. J., 35 (2013) 14–24.

[143] K. Le Roux, L.C. Prinsloo, A.A. Hussein, N. Lall, A micro-Raman spectroscopic investigation of leukemic U-937 cells treated with Crotalaria agatiflora Schweinf and the isolated compound madurensine, Spectrochim. Acta Part A Mol. Biomol. Spectrosc., 95 (2012) 547–554.

[144] K. Flower, I. Khalifa, P. Bassan, D. Démoulin, E. Jackson, N. Lockyer, A. McGown, P. Miles, L. Vaccari, P. Gardner, Synchrotron FTIR analysis of drug treated ovarian A2780 cells: an ability to differentiate cell response to different drugs?, Analyst, 136 (2011) 498–507.

[145] T. Gao, Y. Ci, H. Jian, C. An, FTIR investigation of the interaction of tumor cells treated with caffeic acid and chlorogenic acid, Vib. Spectrosc., 24 (2000) 225–231.

[146] C. Gaspar-Marques, M.F. Simões, M.L. Valdeira, B. Rodriguez, Terpenoids and phenolics from Plectranthus strigosus, bioactivity screening, Nat. Prod. Res., 22 (2008) 167–177.

[147] S. Huang, R. Zheng, Rosmarinic acid inhibits angiogenesis and its mechanism of action in vitro, Cancer Lett., 239 (2006) 271–280.

[148] C.H. Wu, J.S. Pan, W.C. Chang, J.S. Hung, S.J.T. Mao, The molecular mechanism of actinomycin D in preventing neointimal formation in rat carotid arteries after balloon injury, J. Biomed. Sci., 12 (2005) 503–512.

[149] C. Matthaus, T. Chernenko, J.A. Newmark, C.M. Warner, M. Diem, Label-free detection of mitochondrial distribution in cells by nonresonant Raman microspectroscopy, Biophys. J., 93 (2007) 668–673.

[150] M. Jackson, H.H. Mantsch, The use and misuse of FTIR spectroscopy in the determination of protein structure, Crit. Rev. Biochem. Mol. Biol., 30 (1995) 95–120.

[151] M. Banyay, M. Sarkar, A. Graslund, A library of IR bands of nucleic acids in solution, Biophys. Chem., 104 (2003) 477–488.

[152] J. Liquier, A. Akhebat, E. Taillandier, Characterization by FTIR spectroscopy of the oligoribonucleotide duplexes r (A-U)6, and r (A-U)8, Spectrochim. Acta, 47A (1991) 177–186.

[153] M. Tsuboi, Applied Spectroscopy Reviews, Volume III, John Wiley and Sons, New York, NY, 1970.

[154] M. Ghomi, R. Leterllier, J. Liquier, E. Taillandier, Interpretation of DNA vibrational spetra by normal coordinate analysis, Int. J. Biochem., 22 (1990) 691–699.

[155]   M. de la Fuente, A. Hernanz, R. Navarro, IR and Raman study on the interactions of the 5'-GMP and 5'-CMP phosphate groups with Mg(II), Ca(II), Sr(II), Ba(II), Cr(III), Co(II), Cu(II), Zn(II), Cd(II), Al(III) and Ga(III), J. Biol. Inorg. Chem., 9 (2004) 973–986.

[156]   A. Barth, K. Hauser, W. Mantele, J.J.E.T. Corrie, D.R. Trenthams, Photochemical Release of ATP from "Caged ATP" Studied by Time-Resolved Infrared Spectroscopy, J. Am. Chem. Soc., 117 (1995) 10311–10316.

[157]   S.-Y. Lin, H.-L. Chu, Fourier transform infrared spectroscopy used to evidence the prevention of β-sheet formation of amyloid β(1–40) peptide by a short amyloid fragment, Int. J. Biol. Macromol., 32 (2003) 173–177.

[158]   Z. Movasaghi, S. Rehman, D.I. ur Rehman, I. Rehman, Fourier Transform Infrared (FTIR) spectroscopy of biological tissues, Appl. Spectrosc. Rev., 43 (2008) 134–179.

[159]   M. Jackson, P.I. Haris, D. Chapman, Fourier Transform Infrared spectroscopic studies of lipids, polypeptides and proteins, J. Mol. Struct., 214 (1989) 329–355.

[160]   S.-Y. Lin, H.-L. Chu, Y.-S. Wei, Pressure-induced transformation of alpha-helix to beta-sheet in the secondary structures of amyloid beta (1-40) peptide exacerbated by temperature, J. Biomol. Struct. Dyn., 19 (2002) 619–625.

[161]   E. Gazi, P. Gardner, N.P. Lockyer, C. a Hart, M.D. Brown, N.W. Clarke, Direct evidence of lipid translocation between adipocytes and prostate cancer cells with imaging FTIR microspectroscopy, J. Lipid Res., 48 (2007) 1846–56.

[162]   L.M. Miller, P. Dumas, From structure to cellular mechanism with infrared microspectroscopy, Curr. Opin. Struct. Biol., 20 (2010) 649–656.

[163]   J. Cao, E.S. Ng, D. McNaughton, E.G. Stanley, A.G. Elefanty, M.J. Tobin, P. Heraud, The characterisation of pluripotent and multipotent stem cells using Fourier transform infrared microspectroscopy, Int. J. Mol. Sci., 14 (2013) 17453–17476.

[164]   D. Ami, P. Mereghetti, A. Natalello, S.M. Doglia, Fourier Transform Infrared microspectroscopy as a tool for embryonic stem cell studies, methodological advances in the culture, manupulation and utalization of embryonic stem cells for basic and practical applications, InTech, 2011. Prof. Craig Atwood (Ed.), ISBN: 978-953-307-197-8, InTech, Available from: http://www.intechopen.com/books/methodological- advances-in-the-culture-manipulation-and-utilization-of-embryonic-stem-cells-for-basic-and-practical- applications/fourier-transform-infrared-microspectroscopy-as-a-tool-for-embryonic-stem-cell-studies

[165] E. Benedetti, E. Bramanti, F. Papineschi, I. Rossi, E. Benedetti, Determination of the relative amount of nucleic acids and proteins in leukemic and normal lymphocytes by means of Fourier Transform Infrared Microspectroscopy, Appl. Spectrosc., 51 (1997) 792–797.

[166] B.R. Wood, B. Tait, D. McNaughton, Fourier Transform Infrared Spectroscopy as a Method for Monitoring the Molecular Dynamics of Lymphocyte Activation, Appl. Spectrosc., 54 (2000) 353–359.

[167] M. Filimonova, V. Gubskaya, R. Davidov, A. Garusov, I. Nuretdinov, Metal binding induces conversion of B- to the hybrid B-Z-form in natural DNA, Int. J. Biol. Macromol., 43 (2008) 289–294.

[168] I. Lampronti, M.T. Hassan Khan, N. Bianchi, G. Feriotto, C. Mischiati, M. Borgatti, R. Gambari, M.H. Khan, Effects of medicinal plant extracts on molecular interactions between DNA and transcription factors, Adv. Phytomedicine, 2 (2006) 35–43.

[169] M.M. Garner, G. Felsenfeld, Effect of Z-DNA on nucleosome placement, J. Mol. Biol., 196 (1987) 581–590.

[170] F. Azorin, A. Nordheim, A. Rich, Formation of Z-DNA in negatively supercoiled plasmids is sensitive to small changes in salt concentration within the physiological range, EMBO J., 2 (1983) 649–655.

[171] E.A.C. MacRobbie, Ionic relations of guard cells, in: E. Zeiger, G.D. Farquha, I.R. Cowan (Eds.), Stomatal Funct., Stanford University Press, California, 1987: pp. 125–162.

[172] N. Zaidi, L. Lupien, N.B. Kuemmerle, W.B. Kinlaw, J. V Swinnen, K. Smans, Lipogenesis and lipolysis: the pathways exploited by the cancer cells to acquire fatty acids, Prog. Lipid Res., 52 (2013) 585–589.

[173] M. Di Vito, L. Lenti, A. Knijn, E. Iorio, F. D'Agostino, A. Molinari, A. Calcabrini, A. Stringaro, S. Meschini, G. Arancia, A. Bozzi, R. Strom, F. Podo, 1H NMR-visible mobile lipid domains correlate with cytoplasmic lipid bodies in apoptotic T-lymphoblastoid cells, Biochim. Biophys. Acta, 1530 (2001) 47–66.

[174] G. Birarda, D. Bedolla, E. Mitri, S. Pacor, G. Grenci, L. Vaccari, Apoptotic pathways of U937 leukemic monocytes investigated by infrared microspectroscopy and flow cytometry, Analyst, In press (2014).

[175] A. Amit, C.L. Edwards, P. Athey, A.L. Kaplan, Extensive subcutaneous metastases from squamous cell carcinoma of the cervix in patient with HIV, Int J Gyneocol Cancer, 11 (2001) 78–80.

[176] C. Wetzel, P.C. Kunz, M.U. Kassack, A. Hamacher, P. Böhler, W. Watjen, I. Ott, R. Rubbiani, B. Spingler, Gold(I) complexes of water-soluble diphos-type ligands: synthesis, anticancer activity, apoptosis and thioredoxin reductase inhibition, Dalt. Trans., 40 (2011) 9212–9220.

[177]   C.-M. Che, R.W.-Y. Sun, W.-Y. Yu, C.-B. Ko, N. Zhu, H. Sun, Gold(III) porphyrins as a new class of anticancer drugs: cytotoxicity, DNA binding and induction of apoptosis in human cervix epitheloid cancer cells, Chem. Commun., 14 (2003) 1718–1719.

[178]   N.W. Alcock, P. Moore, P.A. Lampe, K.F. Mok, Crystal and Molecular Structures of Two Complexes of Diphenyl(2- pyridy1)phosphine (L): [AuCIL] and [Ag2C12L,], Dalt. Trans., (1982) 207–210.

[179]   M.J. Calhorda, C. Ceamanos, O. Crespo, M.C. Gimeno, A. Laguna, C. Larraz, P.D. Vaz, M.D. Villacampa, Heteropolynuclear gold complexes with metallophilic interactions: modulation of the luminescent properties, Inorg. Chem., 49 (2010) 8255–8269.

[180]   A.B. Mullick, Y.M. Chang, I. Ghiviriga, K.A. Abboud, W. Tan, A.S. Veige, Human cancerous and healthy cell cytotoxicity studies of a chiral µ-dicarbene–digold(I) metallamacrocycle, Dalt. Trans., 42 (2013) 7440–7446.

[181]   See supplementary material at Appendix for details on the metallodrugs, flow cytometry dot plots, raw Raman data, one way ANOVA analysis and the Tukey multicomparison test (2014).

[182]   A. Fujioka, K. Terai, R.E. Itoh, K. Aoki, T. Nakamura, S. Kuroda, E. Nishida, M. Matsuda, Dynamics of the Ras/ERK MAPK cascade as monitored by fluorescent probes, J. Biol. Chem., 281 (2006) 8917–26.

[183]   C. Matthaus, S. Boydston-White, M. Miljkovic, M. Romeo, M. Diem, Raman and Infrared Microspectral Imaging of Mitotic Cells, Appl. Spectrosc., 60 (2006) 1–8.

[184]   G. Perna, M. Lasalvia, P. D'Antonio, N. L'Abbate, V. Capozzi, Identification of chemical modification in single human keratinocyte cells exposed to low doses of chlorpyriphos by Raman micro-spectroscopy, J. Raman Spectrosc., 42 (2011) 603–611.

[185]   I. Notingher, J. Selvakumaran, L.L. Hench, New detection system for toxic agents based on continuous spectroscopic monitoring of living cells, Biosens. Bioelectron., 20 (2004) 780–789.

[186]   A. Salman, E. Shufan, L. Zeiri, M. Huleihel, Detection and identification of cancerous murine fibroblasts, transformed by murine sarcoma virus in culture, using Raman spectroscopy and advanced statistical methods, Biochim. Biophys. Acta - Gen. Subj., 1830 (2013) 2720–2727.

[187]   C. Krafft, L. Neudert, T. Simat, R. Salzer, Near infrared Raman spectra of human brain lipids, Spectrochim. Acta Part A, 61 (2005) 1529–1535.

[188]   R. Chaurio, C. Janko, L.E. Munoz, B. Frey, M. Herrmann, U.S. Gaipl, Phospholipids: Key Players in Apoptosis and Immune Regulation, Molecules, 14 (2009) 4892–4914.

[189] J.H. Stafford, P.E. Thorpe, Increased Exposure of Phosphatidylethanolamine on the Surface of Tumor vascular endothelium, Neoplasia, 13 (2011) 299–308.

[190] K. Emoto, N. Toyama-Sorimachi, H. Karasuyama, K. Inoue, M. Umeda, Exposure of phosphatidylethanolamine on the surface of apoptotic cells, Exp. Cell Res., 232 (1997) 430–434.

[191] M. Sanmarco, M.-C. Boffa, Antiphosphatidylethanolamine antibodies and the antiphospholipid syndrome, Lupus, 18 (2009) 920–923.

[192] M. Diem, M. Miljkovic, B. Bird, T. Chernenko, J. Schubert, E. Marcsisin, A. Mazur, E. Kingston, E. Zuser, K. Papamarkakis, N. Laver, Applications of Infrared and Raman Microspectroscopy of Cells and Tissue in Medical Diagnostics : Present Status and Future Promises, Spectrosc. An Int. J., 27 (2012) 463–496.

[193] H. Holman, M. Martin, E. Blakely, K. Bjornstad, W. McKinney, IR spectroscopic characteristics of cell cycle and cell death probed by synchrotron radiation based Fourier transform IR spectromicroscopy, Biopolym., 57 (2000) 329–335.

[194] K. le Roux, L.C. Prinsloo, D. Meyer, Metallodrug induced apoptotic cell death and survival attempts are characterizable by Raman spectroscopy, Appl. Phys. Lett., 105 (2014) 123702.

[195] K. le Roux, L.C. Prinsloo, D. Meyer, Cellular injury evidenced by impedance technology and infrared microspectroscopy, Spectrochim. Acta Part A Mol. Biomol. Spectrosc., 138 (2015) 321–330.

[196] C. Jin, S. Wu, X. Lu, Q. Liu, M. Qi, S. Lu, Q. Xi, Y. Cai, Induction of the bystander effect in Chinese hamster V79 cells by actinomycin D, Toxicol. Lett., 202 (2011) 178–185.

[197] C.F. Van der Merwe, J. Coetzee, Quetol 651 for general use: a revised formulation, Commun. Electron Microsc. Soc. South. Africa, 22 (1992) 31–32.

[198] E. Venter, C.F. Van Der Merwe, A. V Buys, H. Huismans, V. Van Staden, Comparative ultrastructural characterization of African horse sickness virus-infected mammalian and insect cells reveals a novel potential virus release mechanism from insect cells, J. Gen. Virol., 95 (2014) 642–651.

[199] B. Mohlenhoff, M. Romeo, M. Diem, B.R. Wood, Mie-Type Scattering and Non-Beer-Lambert Absorption Behavior of Human Cells in Infrared Microspectroscopy, Biophys. J., 88 (2005) 3635–3640.

[200] A. Rich, S. Zhang, Z-DNA: the long road to biological function, Nat. Rev. Genet., 4 (2003) 566–573.

[201] V. V Didenko, H. Ngo, D.S. Baskin, Early Necrotic DNA Degradation, Am. J. Pathol., 162 (2003) 1571–1578.

[202]   K.C. Summers, F. Shen, E.A. Sierra Potchanant, E.A. Phipps, R.J. Hickey, L.H. Malkas, Phosphorylation: the molecular switch of double-strand break repair, Int. J. Proteomics, (2011) 373816–373824.

[203]   S.M. Doglia, D. Ami, A. Natalello, P. Gatti-Lafranconi, M. Lotti, Fourier transform infrared spectroscopy analysis of the conformational quality of recombinant proteins within inclusion bodies, Biotechnol. J., 3 (2008) 193–201.

[204]   N. Yadav, a Pliss, a Kuzmin, P. Rapali, L. Sun, P. Prasad, D. Chandra, Transformations of the macromolecular landscape at mitochondria during DNA-damage-induced apoptotic cell death, Cell Death Dis., 5 (2014) e1453.

[205]   G.I. Dovbeshko, N.Y. Gridina, E.B. Kruglova, O.P. Pashchuk, FTIR spectroscopy studies of nucleic acid damage, Talanta, 53 (2000) 233–246.

[206]   G. Hastings, R. Wang, P. Krug, D. Katz, J. Hilliard, Infrared microscopy for the study of biological cell monolayers I Spectral effects of acetone and formalin fixation, Biopolymers, 89 (2008) 921–930.

[207]   Y. Ling, Y.U.N. Zhong, R. Perez-Soler, Disruption of Cell Adhesion and Caspase-Mediated Proteolysis of beta and gamma Catenins and APC Protein in Paclitaxel-Induced Apoptosis, Mol. Pharmacol., 59 (2001) 593–603.

[208]   L.-P. Wen, J.A. Fahrni, S. Troie, J.-L. Guan, K. Orth, G.D. Rosen, Cleavage of Focal Adhesion Kinase by Caspases during Apoptosis, J. Biol. Chem., 272 (1997) 26056–26061.

[209]   S. Magali, S. Hermann, Letting go: modification of cell adhesion during apoptosis, J. Biol., 8 (2009) 49.

[210]   M. Brentnall, D.B. Weir, A. Rongvaux, A.I. Marcus, L.H. Boise, Procaspase-3 regulates fibronectin secretion and influences adhesion, migration and survival independently of catalytic function, J. Cell Sci., 127 (2014) 2217–2226.

[211]   A.C.S. Talari, Z. Movasaghi, S. Rehman, I.U. Rehman, Raman Spectroscopy of Biological Tissues, Appl. Spectrosc. Rev., 50 (2014) 46–111.

[212]   D.W. Fairbairn, K.L.O. Neill, Necrotic DNA degradation mimics apoptotic nucleosomal fragmentation comet tail lenght, Vitr. Cell. Dev. Biol., 31 (1995) 171–173.

[213]   P. Fonteh, D. Meyer, Novel gold(I) phosphine compounds inhibit HIV-1 enzymes, Metallomics, 1 (2009) 427–433.

[214]   P.J. Larkin, Infrared and Raman spectroscopy; Principles and spectral interpretation, Elsevier, 2011.

Appendix

In this section, all results will be presented that were supportive to the different chapters of this thesis, but were not essential to prove the conclusions. Firstly for the published chapters (Chapter 4 and Chapter 5) the supplementary data is unchanged and was published online while supporting data were placed in the appendix due to the multitude data obtained during this investigation.
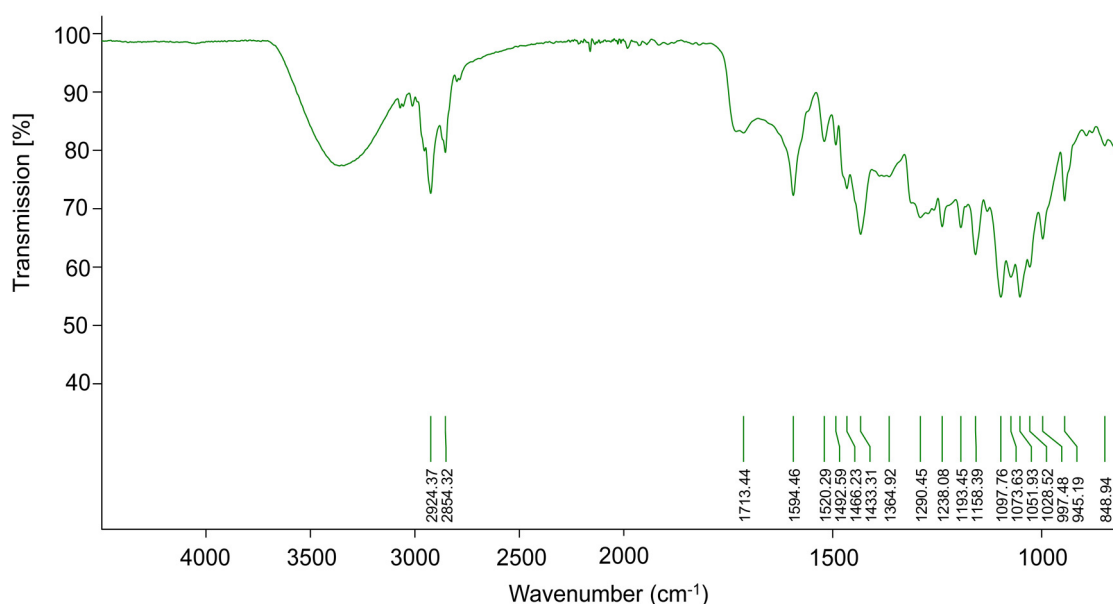
A.1. Supplementary data for Chapter 4

Fig. A- 1. The FTIR spectrum of the crude extract, *P. ciliatus*. In the region of 1800-2000 cm^{-1} noise is evident which could be due to the plant extract containing numerous components.

## A.2. Supporting data for Chapter 4

To support the findings in Chapter 4, another analysis was carried out concurrently with the previously described metallodrugs to serve as a validation. The results will briefly be discussed in terms of correlation with the discoveries of Chapter 4. Validation of findings is imperative since the type of treatment may largely influence the conclusions made.

Experiments were carried out as described in Chapter 4, in this segment details will be given on what concentrations were used. HeLa cells were grown as previously described. The RT-CES analysis was carried out as set out in Section A. The three different concentrations that were tested against HeLa cells were in relation to the XTT results presented in Chapter 3 (Table 3.2) and is listed below for clarity (Table A-1). FTIR microscopectroscopic analyses were conducted on HeLa cells to determine whether cytostatic, early stress responses and cytotoxic cellular responses could be distinguished.

Table A- 1. Concentrations of the cell death inducers used in the RT-CES experiments on HeLa cells

Treatment	Cytotoxic concentration		
	0.5 x CC$_{50}$	CC$_{50}$	2 x CC$_{50}$
Auranofin	1.4 µM	2.8 µM	5.6 µM
AE 76	5.2 µM	10.4 µM	20.5 µM
AE 125	4.5 µM	8.9 µM	17.9 µM

Auranofin had a different RT-CES profile than AE 76 and AE 125 treated HeLa cells (Fig.A-2). It was observed that the highest concentration of all metallodrugs produced the quicker result with the immediate decrease in the CI in all three cases. The CI decrease was less severe for AE 125 treated cells than auranofin and AE 76 treated cells. Auranofin treated cells (2.8 µM and 5.6 µM) displayed identical CI profiles, which indicated that auranofin was highly effective at killing the cells at both concentrations. On the other hand, both AE 76 and AE 125 treated cells showed minor symptoms of cytotoxicity with both the treatments at 0.5 x CC$_{50}$ and CC$_{50}$ concentrations. Using the RTCA software the CC$_{50}$ values, as measured with the RT-CES system, were as follows; auranofin 1.6 µM, AE 76 11.9 µM and AE 125 8.9 µM. Comparing the CC$_{50}$ values obtained with XTT and RT-CES, in the case of auranofin the CC$_{50}$ value was lower than the XTT determined value (Table 3.2), while the CC$_{50}$ values for AE 76 and AE 125 were similar. Dissimilar CC50 values were seen for auranofin and *P. ciliatus* due to the different mechanism of measuring cell death, with RT-CES being generally more sensitive than the XTT assay.
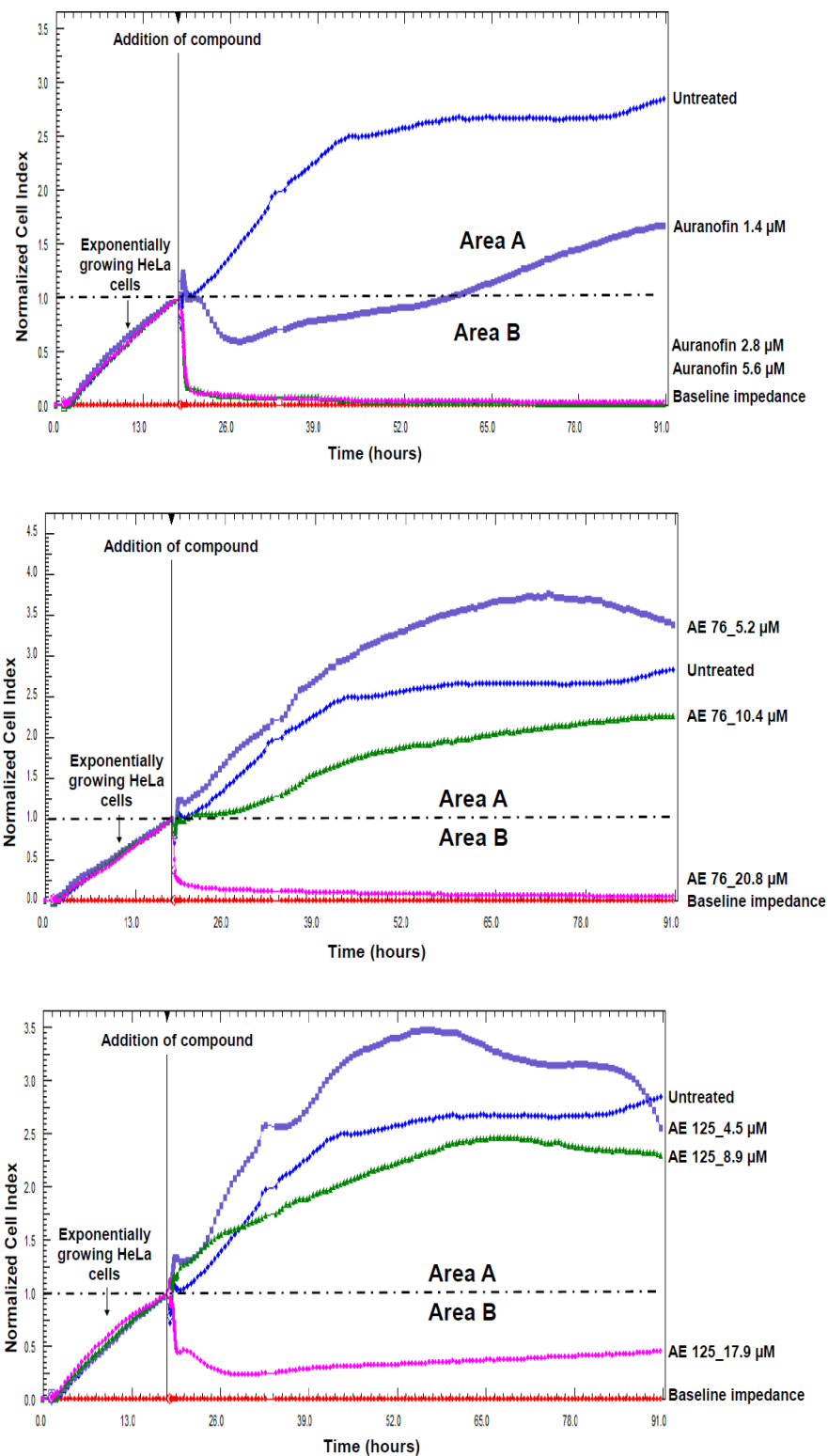
Fig. A- 2. The effect on proliferation of (a) auranofin (positive cell death inducer), (b) AE 76 and (c) AE 125 treated HeLa cells using RT-CES. Cells were incubated for approximately 18 hours after which the treatments at three different concentrations were added.

RT-CES curves were used to predict the cellular response to the metallodrugs using the guidelines of Kustermann *et al.* (2013) described in Chapter 4. A summary of the findings was given in Table A-2. It was found that auranofin elicited cytostatic cellular responses at low concentrations while severe cytotoxicity was seen when the concentration of the treatment increased. The minor changes in the CI curves during AE 76 and AE 125 treatments (low concentrations) were classified as nontoxic.

Table A- 2. Summary of cellular responses of HeLa cells after metallodrug treatment.

Treatment	Assignment
Untreated	-
Auranofin 1.4 µM	Cytostatic
Auranofin 2.8 µM	Cytotoxic
Auranofin 5.6 µM	Cytotoxic
AE 76_5.2 µM	Nontoxic
AE 76_10.4 µM	Nontoxic
AE 76_20.8 µM	Cytotoxic
AE 125_4.5 µM	Nontoxic
AE 125_8.9 µM	Nontoxic
AE 125_17.9 µM	Cytotoxic

Spectral data collected for the cells treated with the metallodrugs were processed in the same manner as described in Chapter 4. The raw spectra showed small differences within the data (Fig. A-3), but as with the case of the data in Section, the second derivatives were used for interpretation of the data. Vibrational peaks discussed in Chapter 4 were highlighted for metallodrug treated cells Fig. A-4, Fig. A-5, Fig. A-6 and summarized in Table 4.4, Chapter 4.
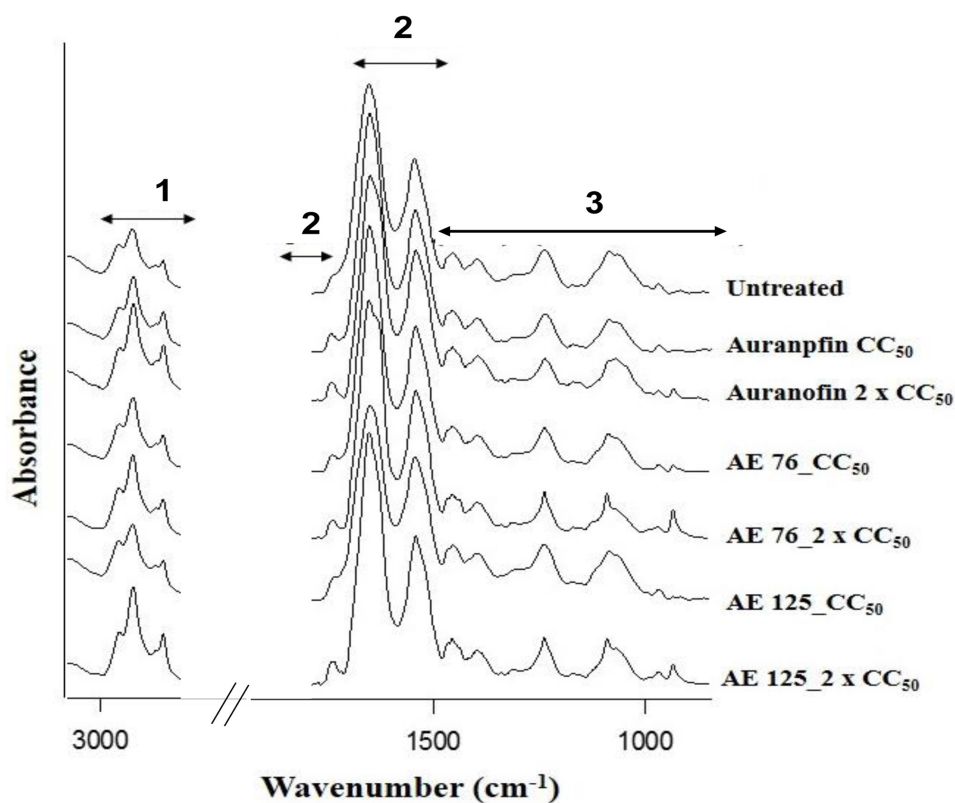
Fig. A- 3. Average FTIR spectra in the regions between 850 – 1800 cm^{-1} and 2800 - 3000 cm^{-1} of untreated and treated HeLa cells. The interaction between HeLa cells and the treatments *Plectranthus ciliatus* and actinomycin D at two different concentrations. Major vibrations assigned to biological molecules are indicated. Region 1 represents lipid acyl chains, 2, an ester bond of phospholipids, amide I and amide II while in region 3 carbohydrates and phosphates associated with nucleic acids vibrate (See Table 4.4, Chapter 4).
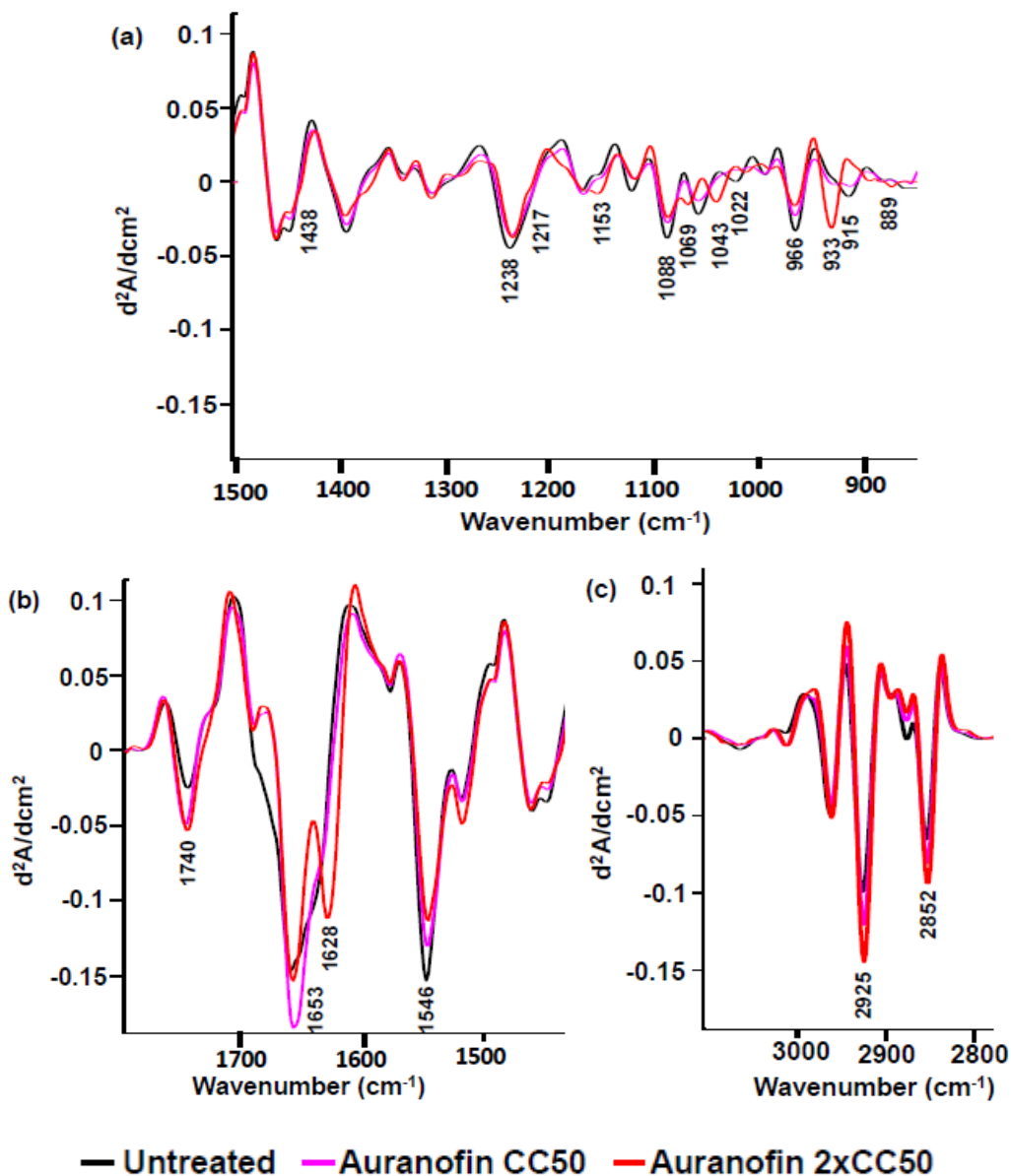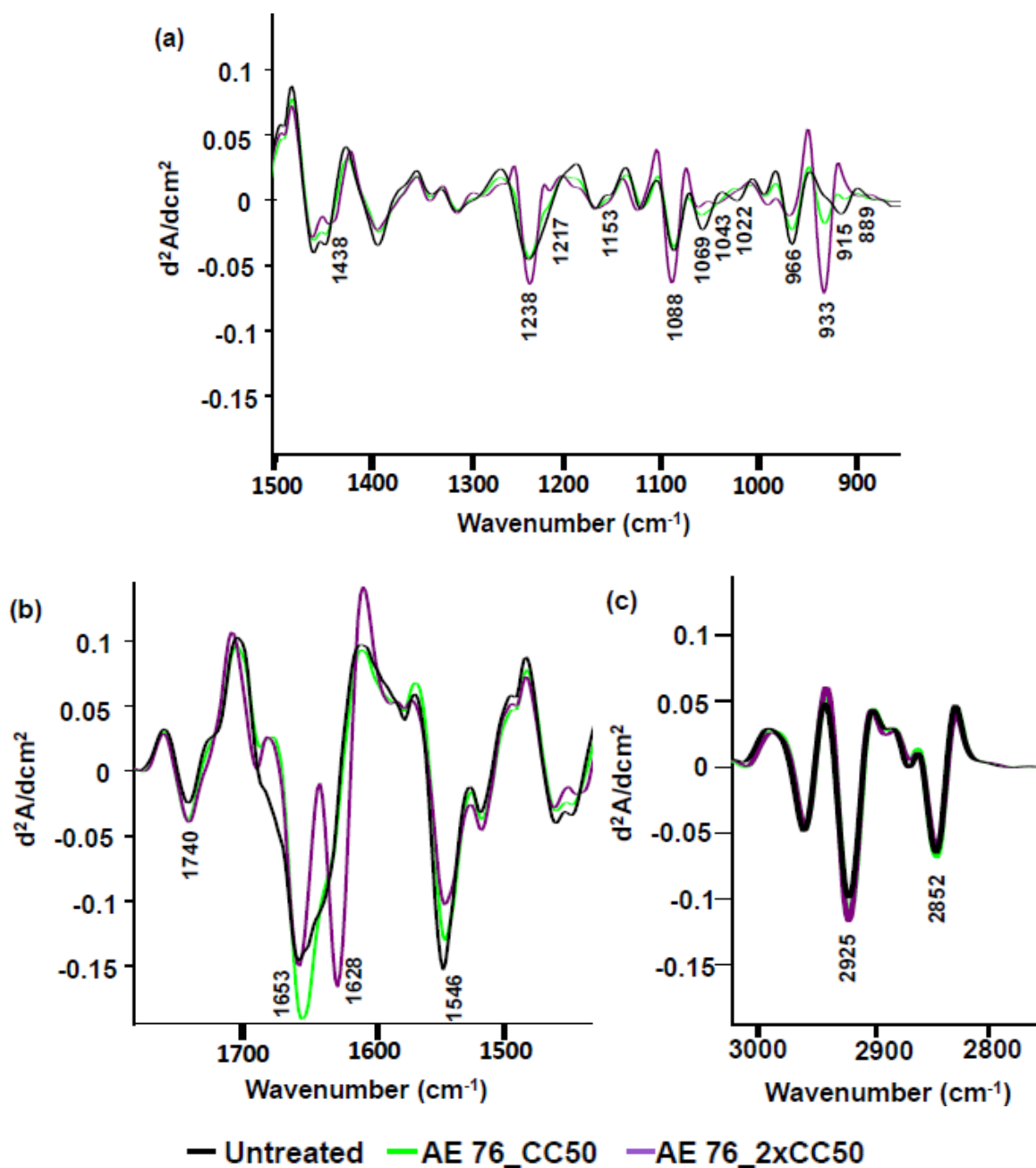
Fig. A- 4. **Average second derivatives in the regions of (a) 850 - 1500 cm^{-1}, (b) 1450 – 1800 cm^{-1} and (c) 2800-3000 cm^{-1} of untreated and auranofin treated HeLa cells.   The interaction between HeLa cells and auranofin is illustrated at two different concentrations. The most prominent spectral changes were seen when cells were treated with the highest concentration (2 x CC$_{50}$ = 5.6 μM) of auranofin.**

Fig. A- 5. Average second derivatives in the regions of (a) 850 - 1500 cm⁻¹, (b) 1450 – 1800 cm⁻¹ and (c)
2800-3000 cm⁻¹ of untreated and AE 76 treated HeLa cells. The interaction between HeLa cells and the
AE 76 is illustrated at two different concentrations based on XTT data. The most prominent spectral
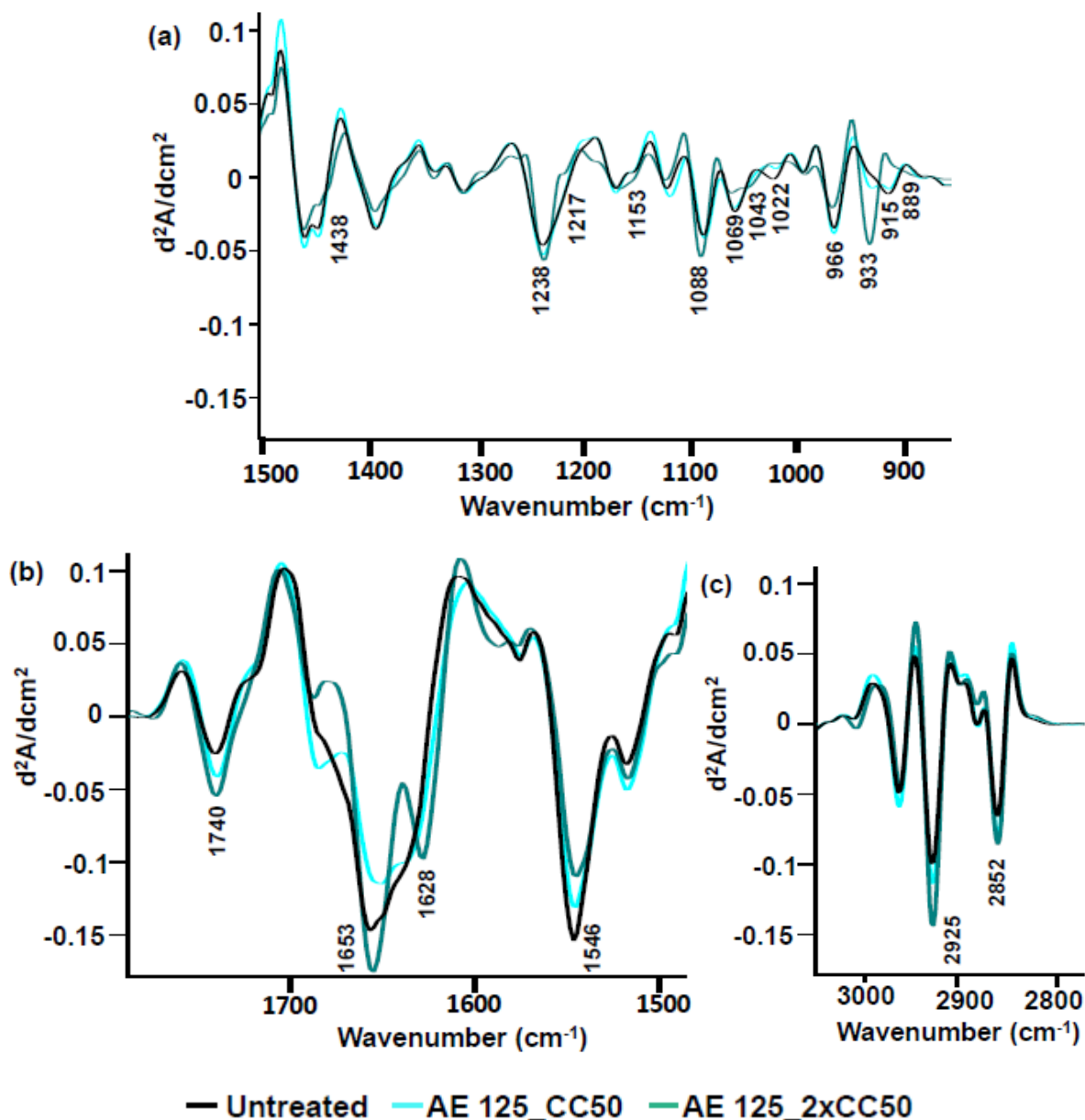**changes were seen when cells were treated with the highest concentration (2 x CC₅₀ = 20.8 µM) of AE 76.**

Fig. A- 6. **Average second derivatives in the regions of (a) 850 - 1500 cm⁻¹, (b) 1450 – 1800 cm⁻¹ and (c) 2800-3000 cm⁻¹ of untreated and AE 125 treated HeLa cells. The interaction between HeLa cells and the AE 125 is illustrated at two different concentrations based on XTT data. The most prominent spectral changes are seen when cells were treated with the highest concentration (2 x CC₅₀ = 17.9 μM) of AE 125.**

Statistical analyses were carried out on the same bands that were found to be significantly different when the crude plant extract and actinomycin D were investigated. Nine out of the thirteen bands were significantly altered after the treatments and listed in Table A-3.

Table A- 3. FTIR vibrational peak assignments are showing modifications after HeLa cells were treated with the metallodrugs.

FTIR frequency (cm^{-1})	One way ANOVA p-value	Multiple comparison outcomes
915	0.001	Nontoxic vs. cytotoxic
933	0.004	Nontoxic vs. cytotoxic
989	0.003	Nontoxic vs. cytotoxic
1192	0	Nontoxic vs. cytotoxic
		Nontoxic vs. AE 76 CC_{50}
1437	0	Nontoxic vs. cytotoxic
		Nontoxic vs. AE 76 CC_{50}
		Cytotoxic vs. AE 76 CC_{50}
1450	0	Nontoxic vs. cytotoxic
		Cytotoxic vs. AE 76 CC_{50}
1546	0	Nontoxic vs. cytotoxic
1679	0	Nontoxic vs. cytotoxic
2874	0	Nontoxic vs. cytotoxic
		Cytotoxic vs. AE 76 CC_{50}

Principal component analysis (PCA) was also conducted this set of spectra. Untreated and treated cells at different concentrations of auranofin, AE 76 and AE 125 showed spectral variance which could be described by the first two principal components (PC). The total percentage variance per PC was indicated in brackets (Fig. A-7). Forty seven percent of the spectral variance was explained by the data reported. It was found that PC 1 separated the spectra based on cytotoxic (auranofin, AE 76 and AE 125 at the highest concentration tested) from nontoxic representative data (untreated, AE 125 at the lowest treated concentration). Cells treated with AE 76 (CC_{50}) were also classified as nontoxic by the results of RT-CES, but clustered closer to the cytotoxic cells. Table A-3 lists vibrational bands that could have led to the clustering of the group further away from the nontoxic group. Cells treated with AE 76 (CC_{50}) could also have shown similar behaviour than *P. ciliatus* CC_{50} treated cells that were ultimately described as showing signs of early stress related responses due to treatment.
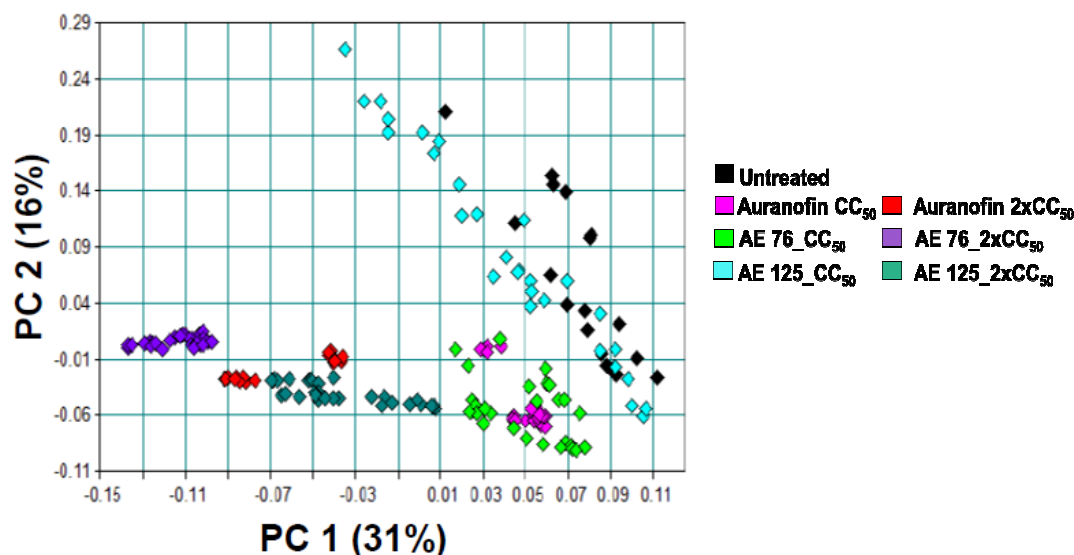
Fig. A-7. Principal component analysis of the spectral variance of the metallodrug treated HeLa cells in the regions of 850-1800 cm^{-1} and 2800-3000 cm^{-1}. It can be seen that untreated cells and AE 125 (CC$_{50}$) clustered separately, indicating that the spectra of those two groups were the most similar. Auranofin CC$_{50}$ and AE 76 CC$_{50}$ cells clustered together and was in the middle of the two groups representing viable and cytotoxic groups. This indicated that auranofin / AE 76 (CC$_{50}$) were showing signs of early stress related responses. HeLa cells treated with the higher concentrations of metallodrugs clustered together indicative of cytotoxicity and thus the most spectral differences were identified in those samples.

A.3. Supporting data: Vero cell cytotoxicity and RT-CES

Vero cells that were investigated in Chapters 6 and 7 were also analysed with RT-CES; firstly to confirm that the CC$_{50}$ values calculated with XTT were accurate and secondly to determine the types of cellular responses described by RT-CES. The method that was used was the same as the one that was followed for HeLa cells. In Table A.4, the concentrations that were tested were listed. The optimal cell number were first determined and it was found that 10 000 cells per well were optimal to reach a CI value of 1 at 24 hours (Fig. A-8). After the cells had been monitored using RT-CES (Fig. A-9), the CC$_{50}$ values were calculated and tabulated in Table A-5. The CC$_{50}$ values calculated using RT-CES was similar to XTT in the case of auranofin, AE 76 and AE 125 but differed for *P. ciliatus* and actinomycin D.

Table A-4. Vero cytotoxicity determined with RT-CES (confirmation of CC$_{50}$ values determined by XTT).

|	Cytotoxic concentration		
Treatment	**0.5 x CC$_{50}$**	**CC$_{50}$**	**2 x CC$_{50}$**
Plectranthus ciliatus	9.95 µg/mL	19.9 µg/mL	39.8 µg/mL
Actinomycin D	0.06 µg/mL	0.11 µg/mL	0.22 µg/mL
Auranofin	0.75 µM	1.5 µM	3 µM
AE 76	3.3 µM	6.6 µM	13.2 µM
AE 125	3.5 µM	6.9 µM	13.8 µM
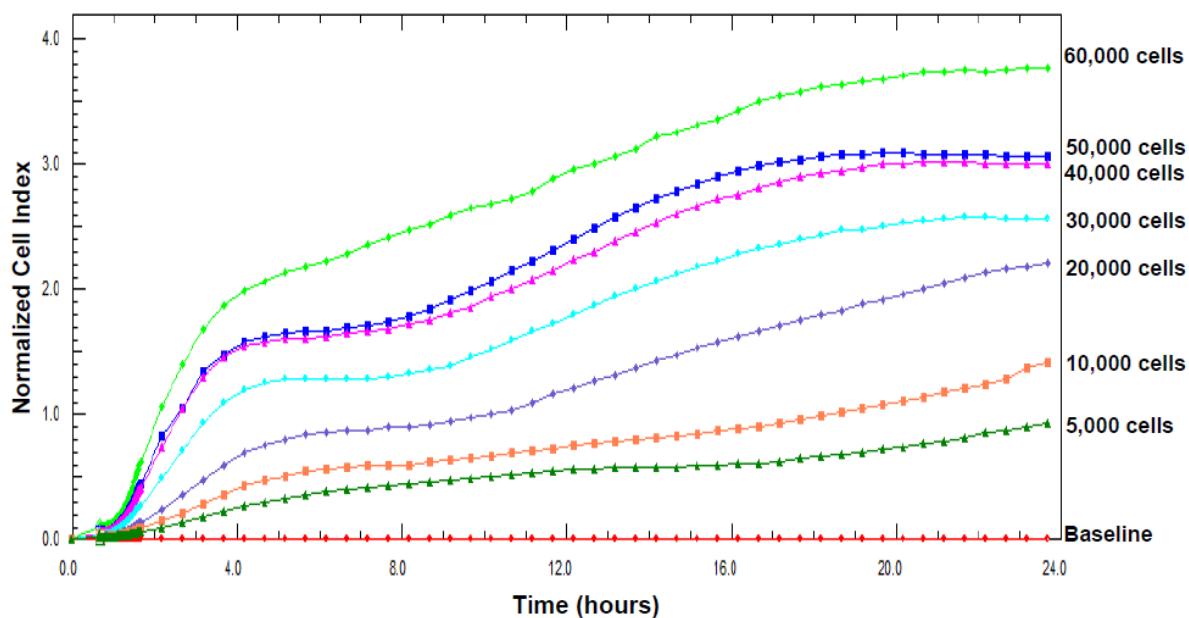
Fig. A-8. Representative Vero cell titration to determine the optimal amount of cells to be used in the RT-CES experiment. The optimal CI value is around 1, between 18-24 hours after the cells were seeded.
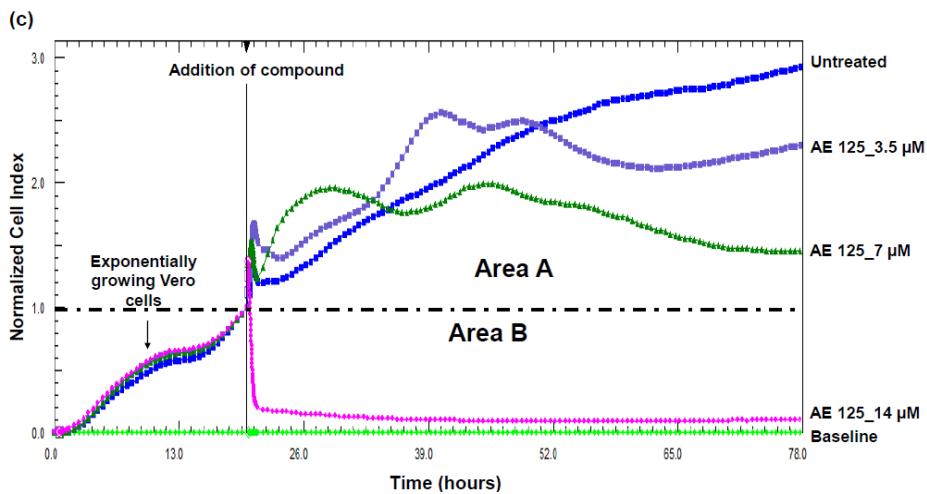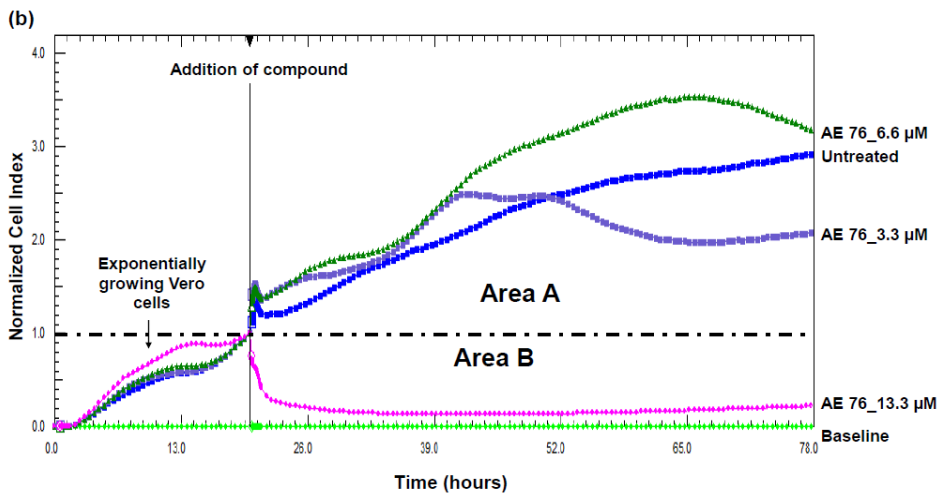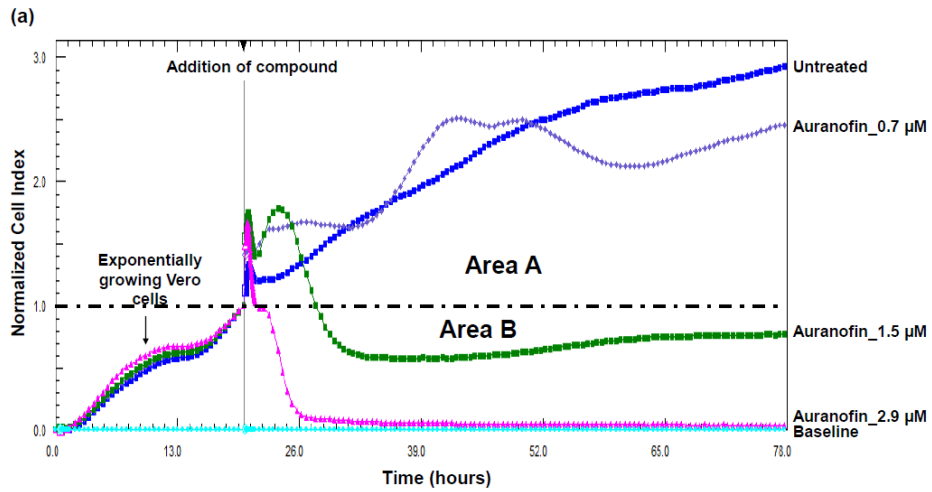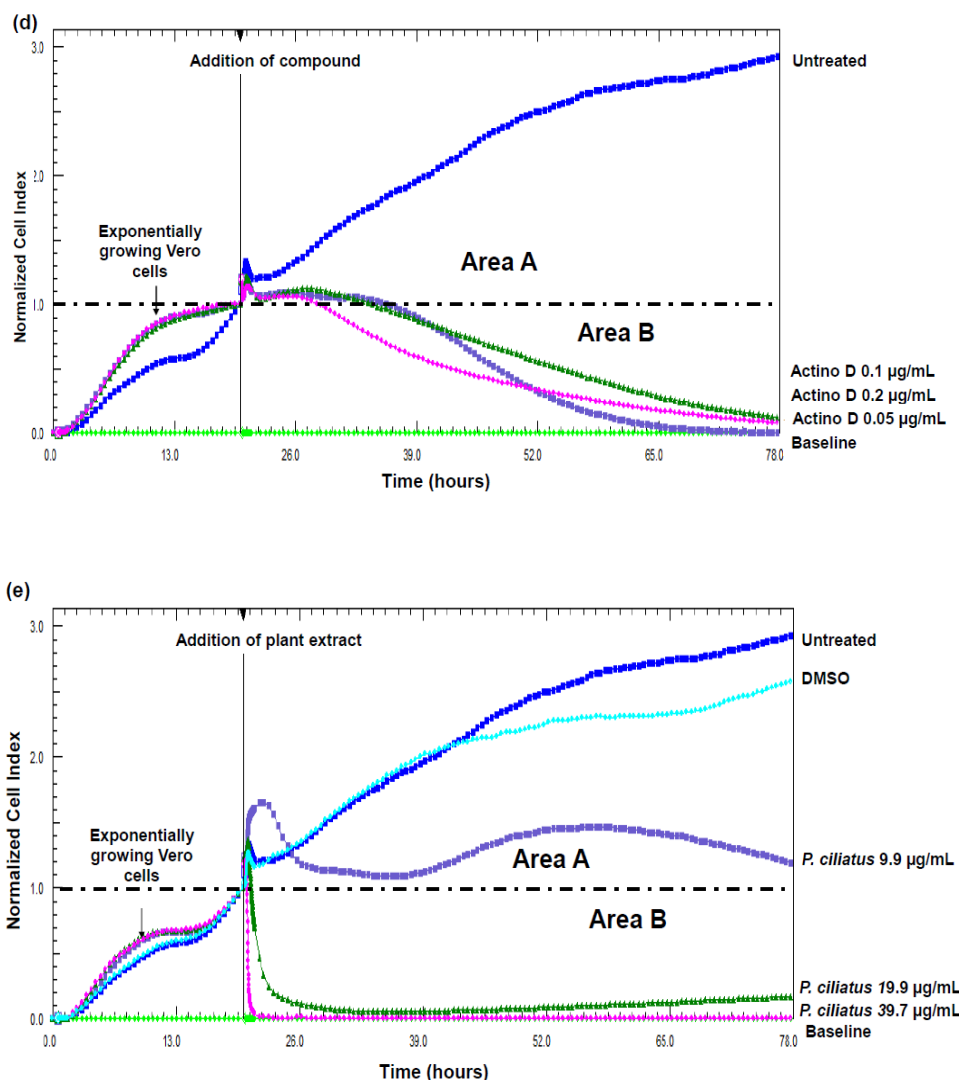
Fig. A-9. Representative graphs of the effect on proliferation of; (a) Auranofin, (b) AE 76, (c) AE 125 (d) actinomycin D and (e) *Plectranthus ciliatus* extract treated Vero cells using RT-CES. Cells were incubated for approximately 20 hours after which the treatments at three different concentrations were performed. In (a) – (c) the metallodrugs showed similar trends where the highest concentration of the compound led to the immediate drop in the CI value. Actinomycin D treated cells (d) represented an entirely different trend in the cellular response, where all three different concentrations had the same effect on the CI. This could be due to the inhibition of protein synthesis (as discussed in Chapter 2). *Plectranthus ciliatus* treated cells (e) were most severely affected by the treatment at the CC50 and 2 x CC50 values while, at the lowest concentration, the CI decreased by half.

Table A- 5. The CC$_{50}$ values of the treatments against the proliferation of Vero cells as determined by RT-CES (n=3, CC$_{50}$ ± SEM).

| Cell death inducers	Vero cells
Auranofin	1.4 ± 0.2 µM
AE 76	7.5 ± 0.2 µM
AE 125	7.8 ± 0.3 µM
Actinomycin D	0.06 ± 0.0002 µg/mL
Plectranthus ciliatus	13.5 ± 1 µg/mL

Using the Kustermann *et al*. (2013) guidelines to determine the cellular response to treatment, it was found that the compounds were either nontoxic or cytotoxic, cytostatic responses (Table A-6).

**Table A-6. Summary of cellular responses after metallodrug treatment.**

Treatment	Assignment
Untreated	-
Auranofin 1.4 µM	Cytostatic
Auranofin 2.8 µM	Cytotoxic
Auranofin 5.6 µM	Cytotoxic
AE 76_5.2 µM	Nontoxic
AE 76_10.4 µM	Nontoxic
AE 76_20.8 µM	Cytotoxic
AE 125_4.5 µM	Nontoxic
AE 125_8.9 µM	Nontoxic
AE 125_17.9 µM	Cytotoxic
Actinomycin D 0.05 µg/mL	Cytotoxic
Actinomycin D 0.1 µg/mL	Cytotoxic
Actinomycin D 0.2 µg/mL	Cytotoxic
P. ciliatus **9.9 µg/mL**	Cytostatic
P. ciliatus **19.9 µg/mL**	Cytotoxic
P. ciliatus **39.7 µg/mL**	Cytotoxic

A.4. Supplementary data for Chapter 5

Chapter 5 is a published manuscript and due to the word limit of the journal, some of the data had to be presented in the supplementary material. The data in Section A.4 is, therefore, unchanged as found online for the manuscript.
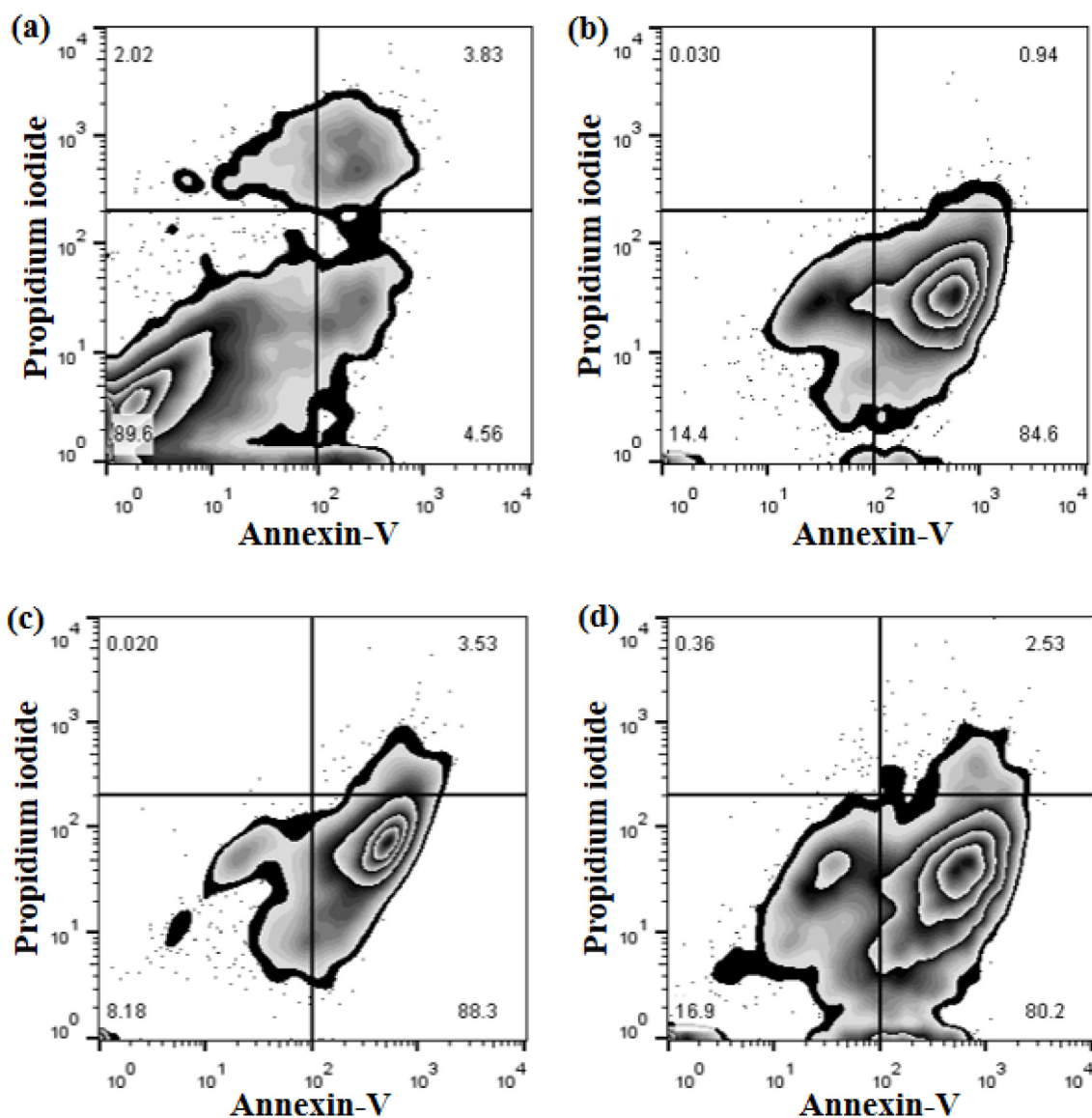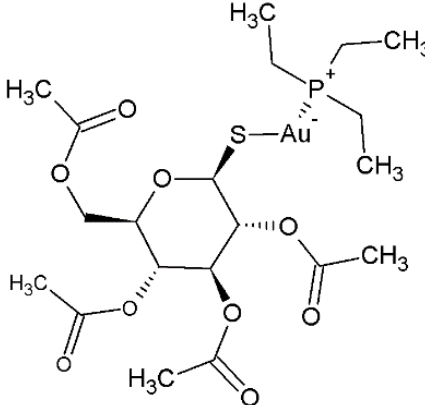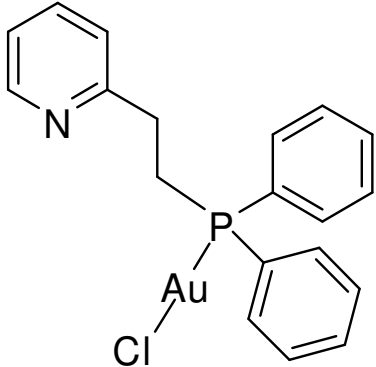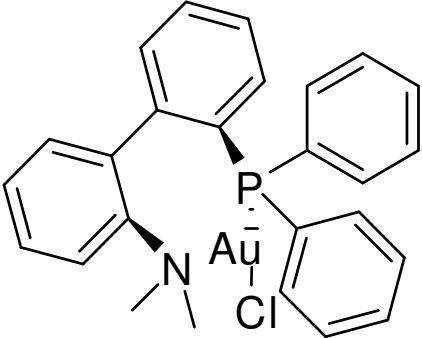

Fig. A- 10. Flow cytometry: Representative Zebra plots of annexin-V and propidium iodide staining of (a) untreated, (b) auranofin treated, (c) AE 76 treated and (d) AE 125 treated HeLa cells. Metallodrugs induced primarily early apoptosis (annexin-V positive, propidium iodide negative – bottom right quadrant), while minimal late apoptosis (annexin-V positive, propidium iodide positive – top right quadrant) were induced and necrotic events (annexin-V negative, propidium iodide positive – top left quadrant) were negligible.
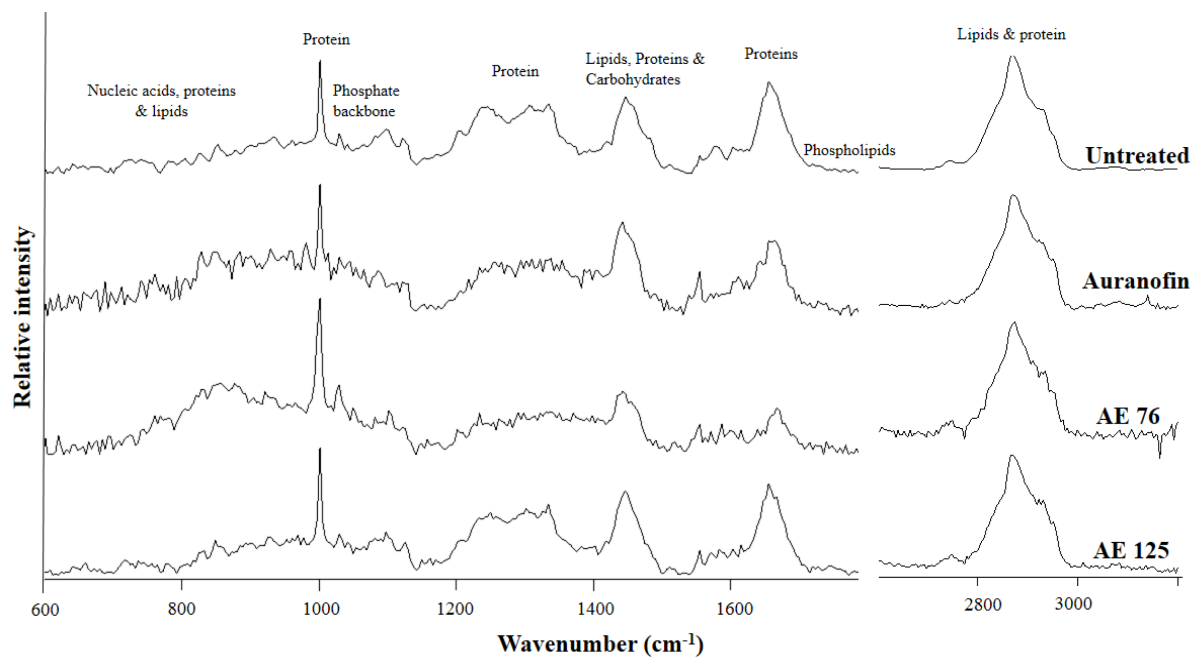
Fig. A-11. Representative Raman spectra of untreated and metallodrug treated HeLa cells in the regions between 600 – 1800 cm^{-1} and 2600 – 3200 cm^{-1}. On the figure, major biomolecular vibrations are indicated where nucleic acids, carbohydrates, proteins and lipids are found.

Table A-7. List of metallodrugs with full names, molecular weights and the chemical structures.

Metallodrug	Full Name	Molecular weight (g/mol)	Structure
Auranofin	1-Thio-β-D- glucopyrano satotriethylphosphine gold-2,3,4,6-tetraacetate, 3,4,5- Triacetyloxy-6-(acetyloxy-methyl) oxane-2-thiolate triethylphosphanium	678.48	
AE 76	2-(2-(diphenylphosphino)-ethyl)pyridyl-gold(I) chloride	523.75	
AE 125	2-(diphenylphosphino)-2'-(N,N-dimethylamino)biphenyl-gold(I) chloride	613.87	

Table A-8. Statistical significance of the peaks using one way ANOVA and Tukey's post test

Raman shift	One way ANOVA p-value	Tukey's multiple comparisons	Significant
733	0.004	Untreated vs Auranofin	Yes
		Untreated vs AE 76	No
		Untreated vs AE 125	No
		Auranofin vs. AE 76	Yes
		Auranofin vs AE 125	No
		AE 76 vs AE 125	No
750	0.0002	Untreated vs Auranofin	Yes
		Untreated vs AE 76	Yes
		Untreated vs AE 125	No
		Auranofin vs AE 76	No
		Auranofin vs AE 125	Yes
		AE 76 vs AE 125	Yes
761	0.033	Untreated vs Auranofin	No
		Untreated vs AE 76	No
		Untreated vs AE 125	Yes
		Auranofin vs AE 76	No
		Auranofin vs AE 125	No
		AE 76 vs AE 125	No
787	0.002	Untreated vs Auranofin	Yes
		Untreated vs AE 76	Yes
		Untreated vs AE 125	Yes
		Auranofin vs AE 76	No
		Auranofin vs AE 125	No
		AE 76 vs AE 125	No

Raman shift	One way ANOVA p-value	Tukey's multiple comparison	Significant
968	<0.0001	Untreated vs Auranofin	No
		Untreated vs AE 76	Yes
		Untreated vs AE 125	No
		Auranofin vs AE 76	Yes
		Auranofin vs AE 125	No
		AE 76 vs AE 125	Yes
1004	<0.0001	Untreated vs Auranofin	No
		Untreated vs AE 76	Yes
		Untreated vs AE 125	No
		Auranofin vs AE 76	Yes
		Auranofin vs AE 125	No
		AE 76 vs AE 125	Yes
1028	0.001	Untreated vs Auranofin	No
		Untreated vs AE 76	Yes
		Untreated vs AE 125	No
		Auranofin vs AE 76	Yes
		Auranofin vs AE 125	No
		AE 76 vs AE 125	Yes
1072	0.004	Untreated vs Auranofin	No
		Untreated vs AE 76	No
		Untreated vs AE 125	No
		Auranofin vs AE 76	Yes
		Auranofin vs AE 125	No
		AE 76 vs AE 125	No

Raman shift	One way ANOVA p-value	Tukey's multiple comparison	Significant
1112	0.013	Untreated vs Auranofin	No
		Untreated vs AE 76	No
		Untreated vs AE 125	No
		Auranofin vs AE 76	Yes
		Auranofin vs AE 125	No
		AE 76 vs AE 125	No
1155	0.005	Untreated vs Auranofin	No
		Untreated vs AE 76	No
		Untreated vs AE 125	No
		Auranofin vs AE 76	Yes
		Auranofin vs AE 125	No
		AE 76 vs AE 125	No
1278	<0.0001	Untreated vs Auranofin	Yes
		Untreated vs AE 76	Yes
		Untreated vs AE 125	Yes
		Auranofin vs AE 76	No
		Auranofin vs AE 125	No
		AE 76 vs AE 125	Yes
1300	0.002	Untreated vs Auranofin	Yes
		Untreated vs AE 76	Yes
		Untreated vs AE 125	No
		Auranofin vs AE 76	No
		Auranofin vs AE 125	No
		AE 76 vs AE 125	No

Raman shift	One way ANOVA p-value	Tukey's multiple comparison	Significant
1513	0.029	Untreated vs Auranofin	No
		Untreated vs AE 76	No
		Untreated vs AE 125	No
		Auranofin vs AE 76	No
		Auranofin vs AE 125	No
		AE 76 vs AE 125	No
1543	<0.0001	Untreated vs Auranofin	Yes
		Untreated vs AE 76	No
		Untreated vs AE 125	No
		Auranofin vs AE 76	Yes
		Auranofin vs AE 125	Yes
		AE 76 vs AE 125	No
1584	0.015	Untreated vs Auranofin	Yes
		Untreated vs AE 76	No
		Untreated vs AE 125	No
		Auranofin vs AE 76	No
		Auranofin vs AE 125	No
		AE 76 vs AE 125	No
1614	<0.0001	Untreated vs Auranofin	Yes
		Untreated vs AE 76	Yes
		Untreated vs AE 125	No
		Auranofin vs AE 76	No
		Auranofin vs AE 125	Yes
		AE 76 vs AE 125	Yes

| Raman shift	One way ANOVA p-value	Tukey's multiple comparison	Significant
1653	0.0003	Untreated vs Auranofin	No
		Untreated vs AE 76	Yes
		Untreated vs AE 125	No
		Auranofin vs AE 76	No
		Auranofin vs AE 125	No
		AE 76 vs AE 125	Yes
1720	<0.0001	Untreated vs Auranofin	Yes
		Untreated vs AE 76	Yes
		Untreated vs AE 125	No
		Auranofin vs AE 76	Yes
		Auranofin vs AE 125	Yes
		AE 76 vs AE 125	Yes

A.5. Supporting data for Chapter 5

Cytotoxicity could be positively identified using FTIR spectroscopy in HeLa cells treated with 18.5 µg/mL crude plant extract while cells treated with 0.4 µg/mL actinomycin D were cytostatic as determined with RT-CES. Flow cytometric and Raman spectroscopy were done on actinomycin D and *P. ciliatus* to determine if the findings in Chapter 5 was specifically applicable to metallodrug treated HeLa cells or if the same trends could be seen after cells were treated with naturally derived products. The methodology was the same as reported in Chapter 5 but instead of one concentration of treatments both the CC_{50} and 2 CC50 concentrations effects were measured.   The respective treatments were untreated cells, vehicle treated (DMSO 0.09%), 0.4 µg/mL actinomycin D and 18.5 µg/mL crude plant extract. After 72 hours, incubation measurements were taken using the Raman spectrometer. Vero cells were also analysed in the same manner using flow cytometry.
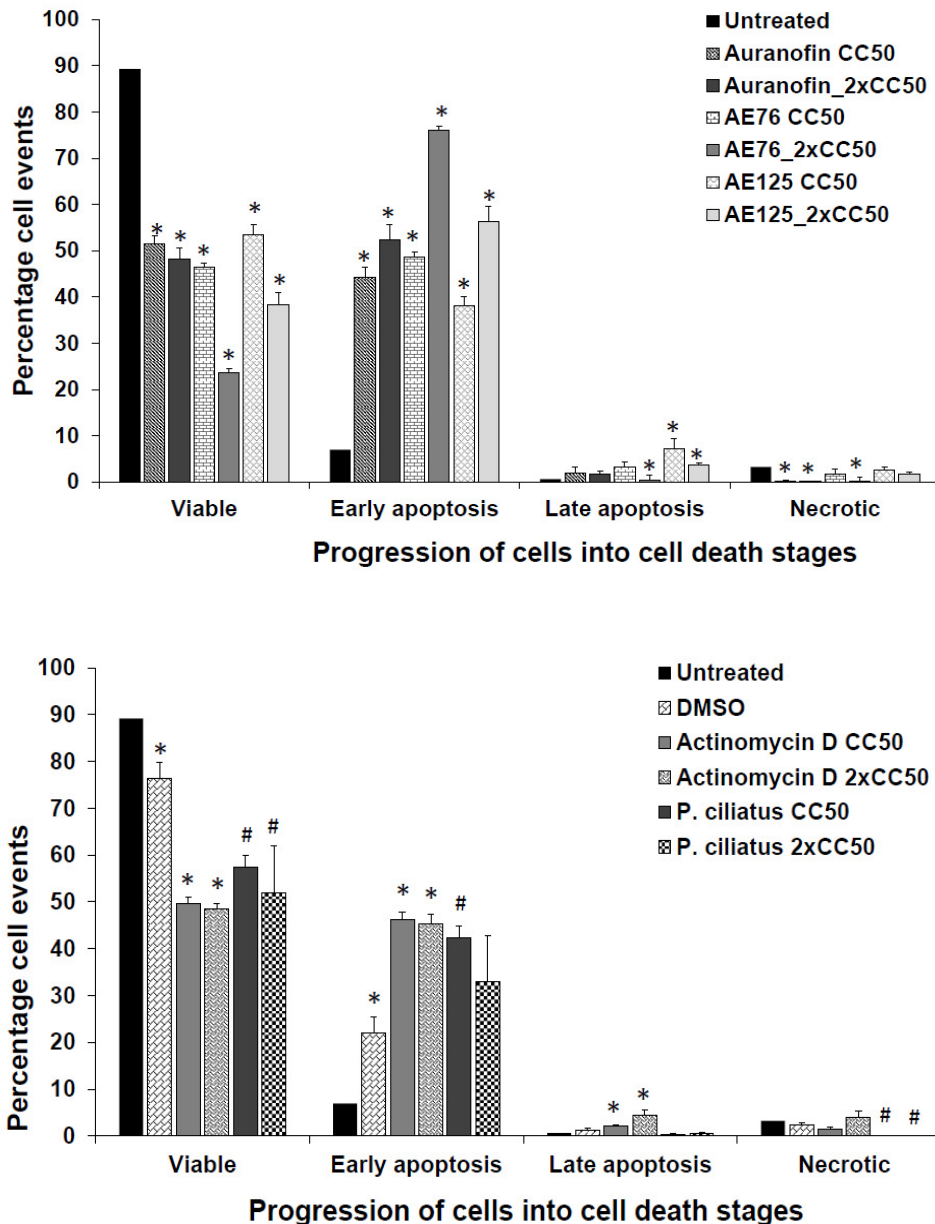
HeLa cells treated with the cell death inducers were investigated using flow cytometry to determine the type of cell death induced, after which Raman spectroscopy was utilised to determine what molecular changes could be detected. Annexin-V and propidium iodide is

well-characterized fluorochromes and depending on the manner in which they bind, the quantity of apoptotic or necrotic cells can be determined [61,73,213]. Annexin-V binds to phosphatidylserine, a phospholipid which is externalized during apoptotic cell death[16]. The "eat me" phospholipid is usually found on the inner leaflet of viable cells and is only externalised during membrane reorganisation during apoptosis. Phosphotadylserine is recognised by phagocytic cells which will then engulf the cells [188]. Propidium iodide is a DNA intercalator which can only enter membrane compromised dead cells. When cells undergo necrosis, known as chaotic cell death, plasma membrane damage leads to cells leaking. This leakage causes cytoplasm and organelles to ooze out of the cells. Propidium iodide is then able to intercalate easily into the DNA. When cells undergo apoptotic cell death and are not engulfed by phagocytic cells, the cells will start to degrade which could also lead to apoptotic cells taking up propidium iodide. This type of cell death is then classified as late apoptosis or secondary necrosis [84].

In Fig. A-12 and Fig. A-13, the average induced cell death in HeLa and Vero cells are illustrated. Accompanying the bar graphs, representative zebra plots were also included (Fig. A-14 and Fig. A-15). It was found that viable cells, as well as DMSO, treated cells showed low percentages of cell death (Fig. A-12 and Fig. A-13). The small percentage of dead cells found in the untreated and DMSO treated populations could be due to loss of cell viability during cell processing. The largest percentage dead cells after treatment were found to be early apoptotic. The induction of apoptosis was also seen to be concentration dependent. Between 30-50% of the cells, in both treatments (2 x CC_{50}) had exposed phosphatidylserine and thus annexin-V bound to the phospholipid could be detected. Very low percentages late apoptosis and necrosis were detected after both actinomycin D and *P. cilatus* treatments.
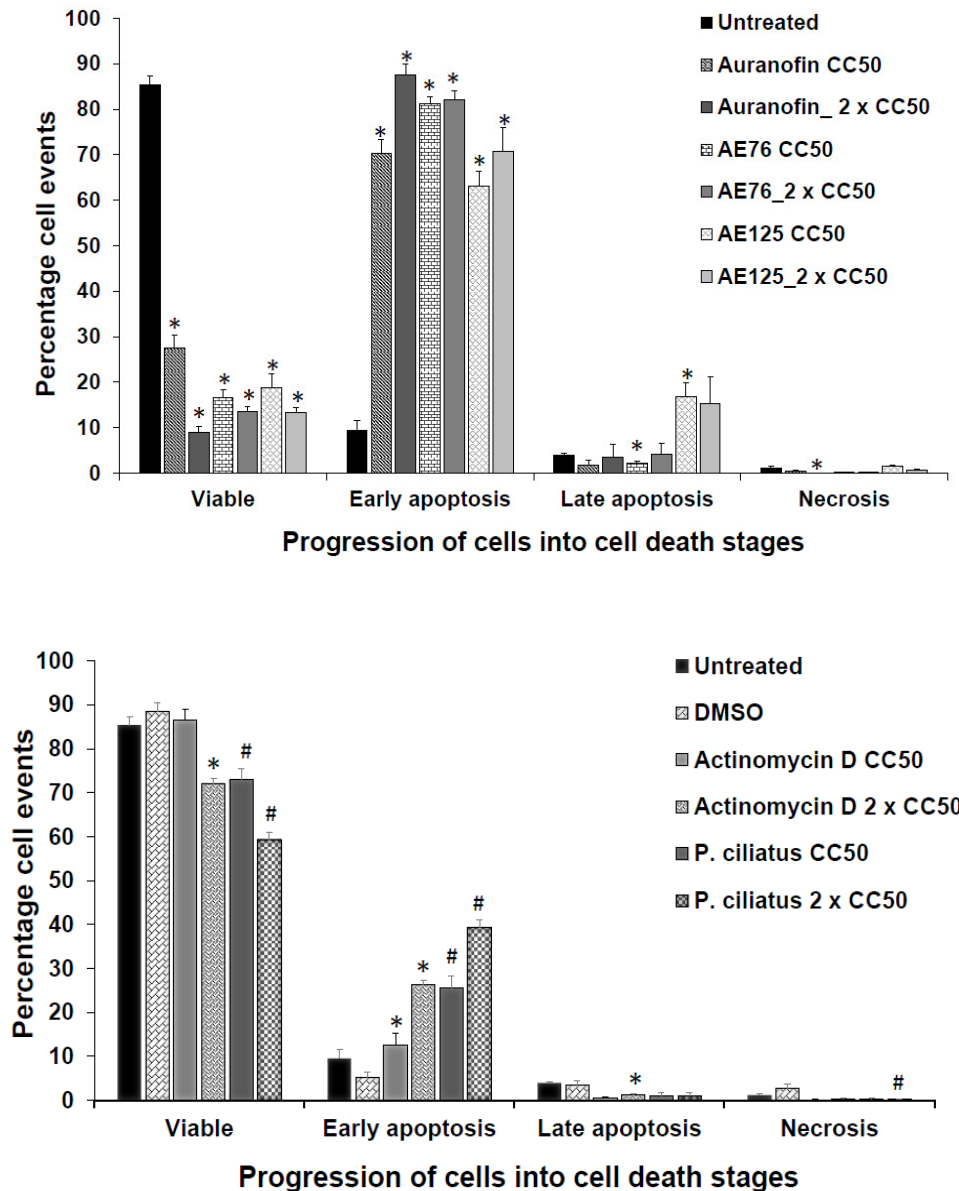
Fig. A-12. Bar graphs illustrating the average percentages viable and induced cell death in HeLa cells treated with (a) different concentrations of metallodrugs and (b) different concentrations of natural derived products, determined by flow cytometry using annexin-V and propidium iodide dyes. It was found that the induction of early apoptosis was significant (*$p < 0.05$, One way ANOVA) for all treatments especially in the case of early apoptosis where all the metallodrug treatments at different concentrations induced large percentages of apoptosis. Very low percentages of late apoptosis and necrotic events were evident. The natural dervied products induced significant percentages of early apoptosis although the yield of the populations were not as high as compared to the metallodrug treated cells. Further studies were only conducted using the 2 x CC_{50} concentrations of the cell death inducers (n=4).

Fig. A-13. Bar graphs illustrating the average percentages viable and induced cell death in Vero cells treated with different concentrations of (a) metallodrugs and (b) naturally derived products determined by flow cytometry using annexin-V and propidium iodide dyes. It was found that the induction of early apoptosis was significant (*$p < 0.05$, One way ANOVA) for all treatments although the yield of early apoptotic cells were lower than in the case of HeLa cell. Very low percentages of late apoptosis and necrotic events were evident. Further studies were conducted by only using 2 x CC_{50} to induce cell death (n=3).
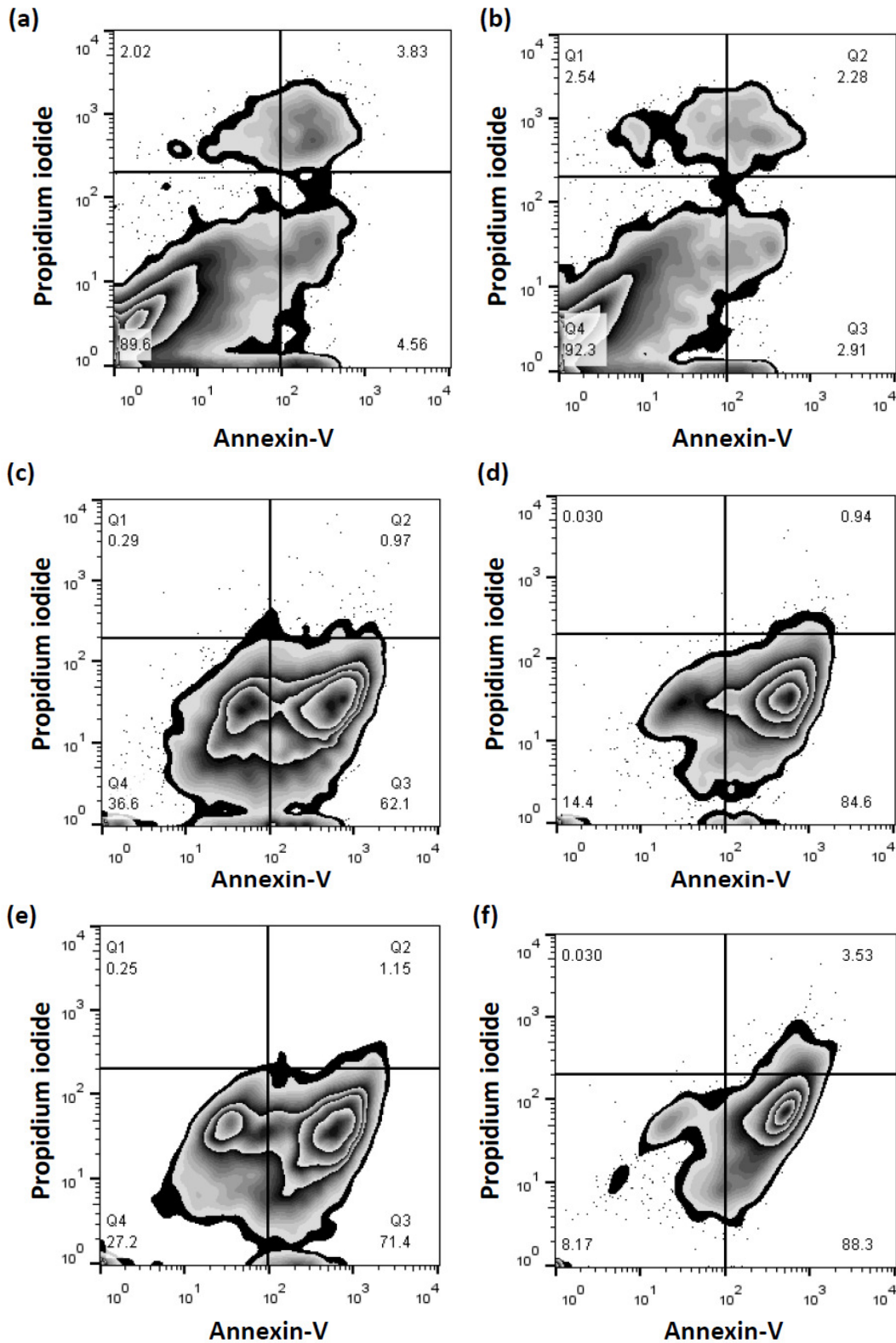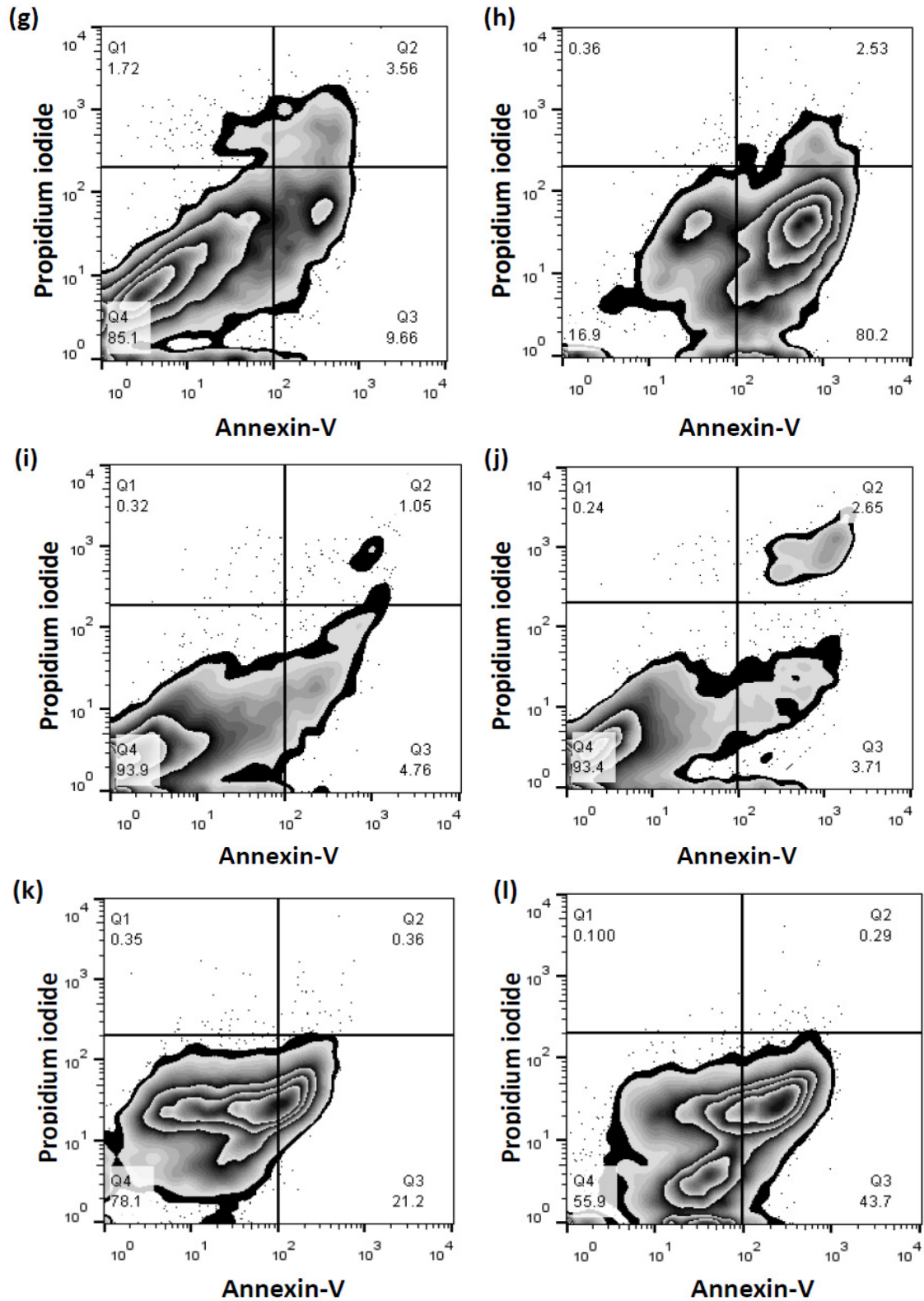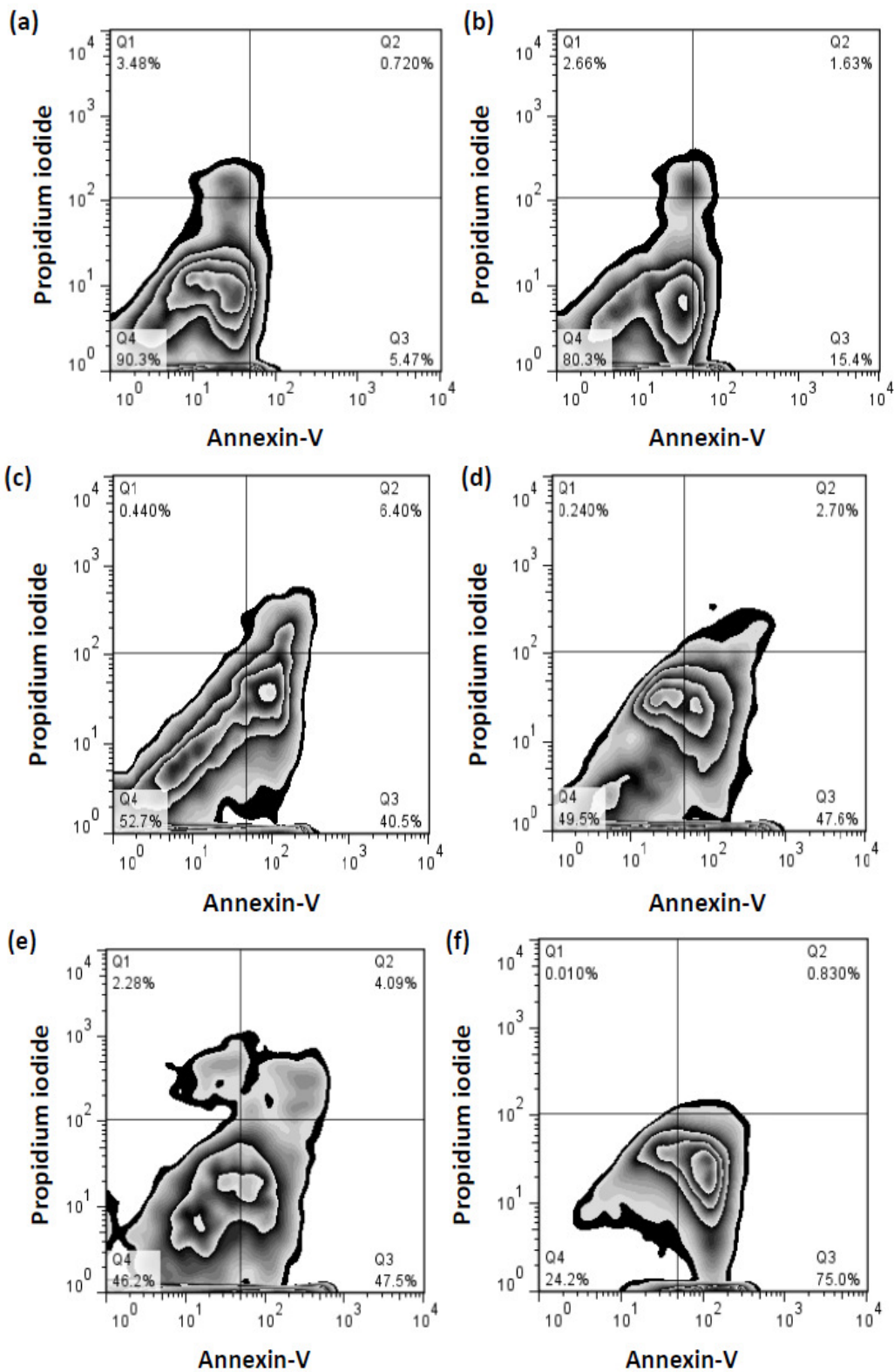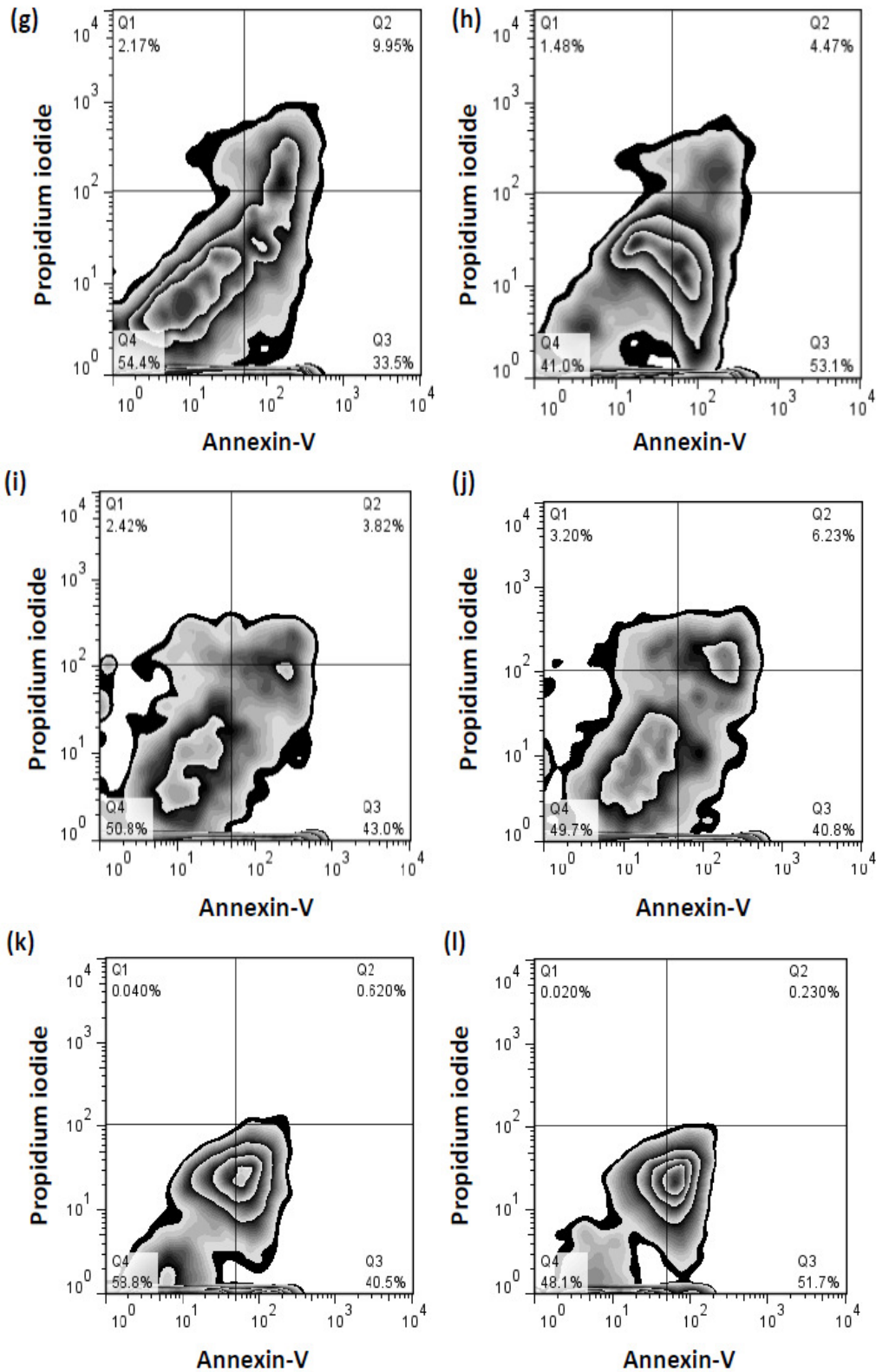
Fig. S5. 1. Flow cytometry representative zebra plots: Treatments induced cell death of HeLa cells and were measured with annexin-V and propidium iodide. Metallodrugs and naturally derived products were used as cell death inducers. It was found that (a) untreated and (b) DMSO (0.009%) treated HeLa cells were viable with the cells not staining (annexin-V negative, propidium iodide negative). Each treatment's effect was measured at two different concentrations, CC_{50} and 2 x CC_{50} (that was determined with an XTT viability assay). Auranofin (c) CC_{50} displayed two visible populations of which 62% were classified as early apoptotic (annexin-V positive, propium iodide negative) and (d) 2 x CC50 presented one population that consisted of 85% apoptotic cells. A similar trend was seen when the cells were treated with AE 76 (e) CC50 and (f) 2 x CC_{50} where an apoptotic population of cells were 71% at the lowest treatment concentration and increased to 88% in the case of the highest concentration. The third metallodrug, AE 125 (g) at CC_{50} concentration lead to a very small change in the viability of the cells with around 90% viable cell, while an apoptotic cell death was 80% when the cells were treated with double the concentration of AE 125. The naturally derived products in this experiment did not show very good results for the (i -j) actinomycin D treated cells. Less than 10% apoptosis was induced. When the cells were treated with the crude extract, *Plectranthus ciliatus*, 21% of the cell were apoptotic (k) with an increase to 43% apoptotic cells at the highest concentration tested (l).

Fig. S5.2. Flow cytometry representative zebra plots: Induced cell death of Vero cells was measured with annexin-V and propidium iodide. Metallodrugs and naturally derived products were used as cell death inducers. It was found that (a) untreated and (b) DMSO (0.02%) treated HeLa cells were viable with the cells not staining (annexin-V negative, propidium iodide negative), although there was a slight decrease in cell viability when the cells were treated with the vehicle control. Each treatment's effect was measured at two different concentrations, CC_{50} and 2 x CC_{50} (that was determined with XTT viability assay). Auranofin (c) CC50 displayed 40% early apoptotic cells (annexin-V positive, propidium iodide negative) and (d) 2 x CC50 treated cells displayed 47% early apoptotic cells. When the cells were exposed to AE 76 (e) CC50 and (f) 2 x CC50 there were 48% and 75% early apoptotic cells respectively. The compound, AE 125 (g) at CC50 concentration lead to 33% early apoptotic cells while 53% early apoptotic cells were detected treated with double the concentration of AE 125. Actinomycin D treated cells (i) had similar percentages early apoptotic cells approximately 40%, irrespective of the concentrations tested. When the cells were treated with the crude extract, *Plectranthus ciliatus*, 41% of the cell were detected in the early apoptotic quadrant (k) and 52% of the treated cells were early apoptotic at the highest concentration tested (l).

The average Raman spectra of HeLa cells treated with actinomycin D and *P. ciliatus* showed very small spectral changes and due to less effective baseline correction of *P. ciliatus* treated cells the second derivatives were used to interpret the data (Fig. S5.7). The vibrational bands are discussed in Chapter 5.
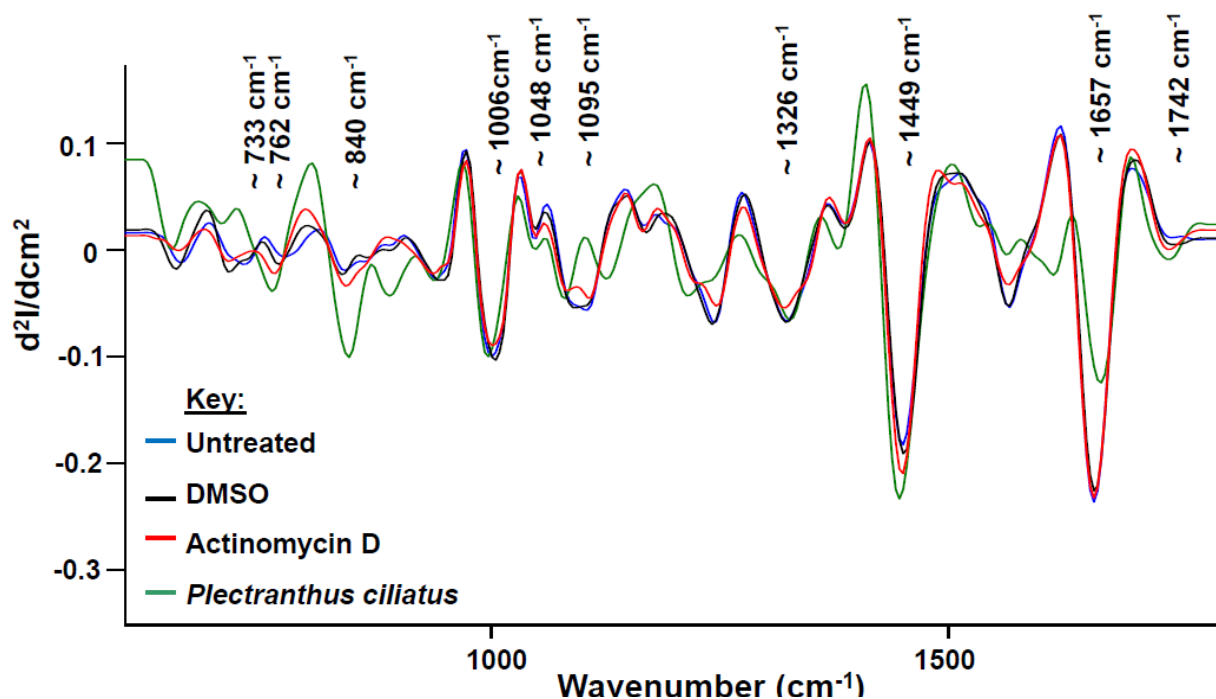

Fig. A- 14. **The second derivatives of untreated, DMSO treated, actinomycin D and *P. ciliatus* treated HeLa cells in the regions between 600 to 1800 cm^{-1}. Major spectral differences are visible indicating aspects of the mechanism of action of these metallodrugs and also induction of apoptotic cell death.**

Similar vibrational peak changes were seen in actinomycin D treated and *P. ciliatus*. Apoptosis was induced to a lesser extent in the naturally derived products as compared to the metallodrugs, but still very good indicators were present that the cells were under chemical stress. Cancer cells do not die easily and accordingly will do anything to keep them alive. These analyses were done on mixed populations of cells that were individually affected to different degrees. In the next chapter, cells are sorted into very pure populations of either apoptotic cells or necrotic cells. With highly pure populations, it was possible to find biomarkers for specifically apoptosis and necrosis.